frontiers | Research Topics

Investigating connectivity to advance the predictive understanding of watershed processes and the Earth's critical zone

Edited by
Dipankar Dwivedi, Ronald Erwin Pöppl and Ellen Wohl

Published in
Frontiers in Water

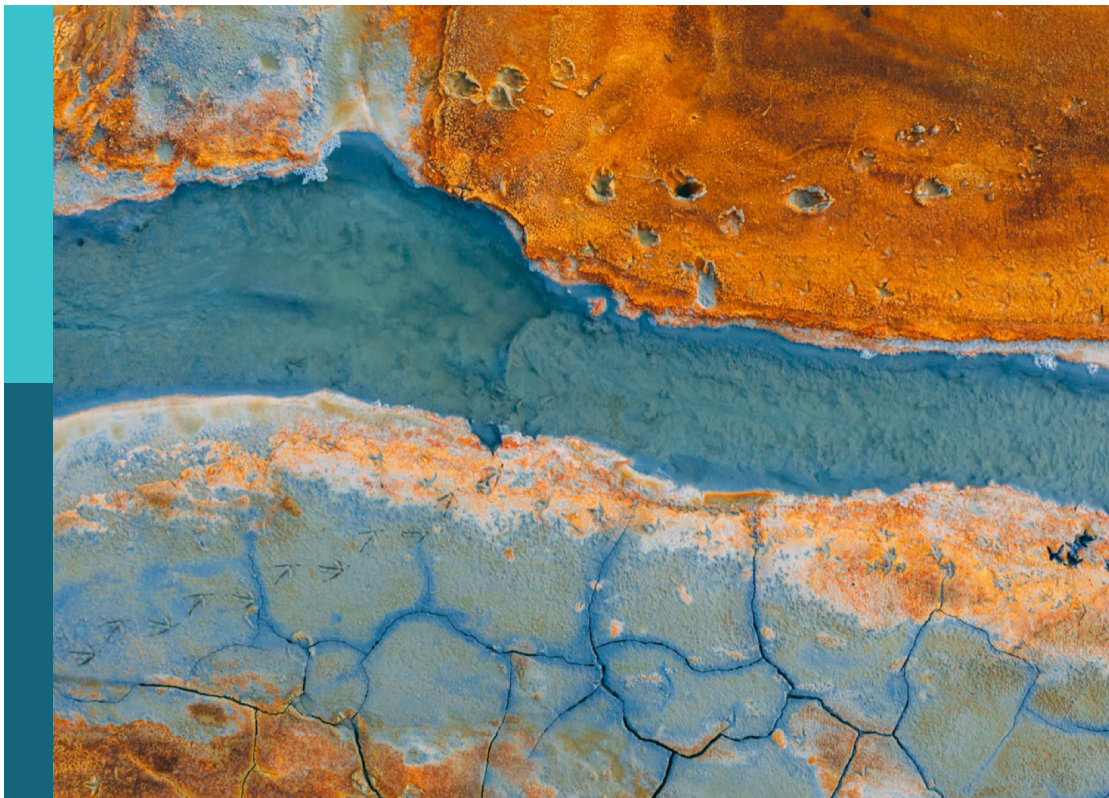

ISSN 1664-8714
ISBN 978-2-8325-6311-3
DOI 10.3389/978-2-8325-6311-3

About Frontiers

Frontiers is more than just an open access publisher of scholarly articles: it is a pioneering approach to the world of academia, radically improving the way scholarly research is managed. The grand vision of Frontiers is a world where all people have an equal opportunity to seek, share and generate knowledge. Frontiers provides immediate and permanent online open access to all its publications, but this alone is not enough to realize our grand goals.

Frontiers journal series

The Frontiers journal series is a multi-tier and interdisciplinary set of open-access, online journals, promising a paradigm shift from the current review, selection and dissemination processes in academic publishing. All Frontiers journals are driven by researchers for researchers; therefore, they constitute a service to the scholarly community. At the same time, the *Frontiers journal series* operates on a revolutionary invention, the tiered publishing system, initially addressing specific communities of scholars, and gradually climbing up to broader public understanding, thus serving the interests of the lay society, too.

Dedication to quality

Each Frontiers article is a landmark of the highest quality, thanks to genuinely collaborative interactions between authors and review editors, who include some of the world's best academicians. Research must be certified by peers before entering a stream of knowledge that may eventually reach the public - and shape society; therefore, Frontiers only applies the most rigorous and unbiased reviews. Frontiers revolutionizes research publishing by freely delivering the most outstanding research, evaluated with no bias from both the academic and social point of view. By applying the most advanced information technologies, Frontiers is catapulting scholarly publishing into a new generation.

What are Frontiers Research Topics?

Frontiers Research Topics are very popular trademarks of the *Frontiers journals series*: they are collections of at least ten articles, all centered on a particular subject. With their unique mix of varied contributions from Original Research to Review Articles, Frontiers Research Topics unify the most influential researchers, the latest key findings and historical advances in a hot research area.

Find out more on how to host your own Frontiers Research Topic or contribute to one as an author by contacting the Frontiers editorial office: frontiersin.org/about/contact

Investigating connectivity to advance the predictive understanding of watershed processes and the Earth's critical zone

Topic editors

Dipankar Dwivedi — Berkeley Lab (DOE), United States

Ronald Erwin Pöppl — University of Vienna, Austria

Ellen Wohl — Colorado State University, United States

Citation

Dwivedi, D., Pöppl, R. E., Wohl, E., eds. (2025). *Investigating connectivity to advance the predictive understanding of watershed processes and the Earth's critical zone*. Lausanne: Frontiers Media SA. doi: 10.3389/978-2-8325-6311-3

Table of contents

frontiers | Frontiers in Water

TYPE Editorial
PUBLISHED 09 May 2025
DOI 10.3389/frwa.2025.1589792

OPEN ACCESS

EDITED BY
Mohammad Safeeq,
University of California, Merced, United States

REVIEWED BY
Julien Ackerer,
University of California, Merced, United States
Yang Yang,
Western Carolina University, United States

*CORRESPONDENCE
Dipankar Dwivedi
✉ DDwivedi@lbl.gov

RECEIVED 08 March 2025
ACCEPTED 15 April 2025
PUBLISHED 09 May 2025

CITATION
Dwivedi D, Pöppl RE and Wohl E (2025) Editorial: Investigating connectivity to advance the predictive understanding of watershed processes and the Earth's critical zone. *Front. Water* 7:1589792. doi: 10.3389/frwa.2025.1589792

Editorial: Investigating connectivity to advance the predictive understanding of watershed processes and the Earth's critical zone

Dipankar Dwivedi[1]*, Ronald E. Pöppl[2] and Ellen Wohl[3]

[1]Earth and Environmental Sciences, Lawrence Berkeley National Laboratory, Berkeley, CA, United States, [2]Institute of Hydrobiology and Aquatic Ecosystems Management, BOKU University, Vienna, Austria, [3]Department of Geosciences, Colorado State University, Fort Collins, CO, United States

KEYWORDS

hydrologic connectivity, watershed processes, critical zone, wildfire, drought, integrated water resources management, electric circuit analogy

Editorial on the Research Topic
Investigating connectivity to advance the predictive understanding of watershed processes and the Earth's critical zone

Hydrologic connectivity shapes watershed processes by regulating water, sediment, and nutrient movement, integrating the Earth's critical zone processes, and linking the hydrosphere with other physical and ecological "landscape" compartments. However, connectivity has traditionally been studied independently in hydrology, biogeochemistry, and geomorphology; as a result, these efforts have lacked a unified framework. Recognizing this challenge, the 2015 Geomorphology Symposium on Connectivity (Wohl et al., 2017) was not just another discussion on connectivity, but also one of the pivotal moments fostering interdisciplinary dialogue that emphasized the need for a more integrated approach. The 2015 Geomorphology Symposium on Connectivity highlighted key themes such as *sediment*, *hydrologic*, *geochemical*, *riverine*, and *landscape connectivity* as well as *connectivity modeling*—concepts that have often remained siloed within their respective disciplines. Since this symposium, significant progress in modeling, observations, and technologies has expanded the scope and depth of hydrologic connectivity research across scales. However, its full potential remains underutilized in catchment science, emphasizing the need to synthesize existing research and bridge critical knowledge gaps (see Wohl et al., 2019 and references therein). This Research Topic in *Frontiers in Water* addresses challenges in hydrologic connectivity by integrating key developments, theoretical innovations, data-driven methods, and interdisciplinary perspectives. The contributions span four key themes, as outlined in the following paragraphs.

Conceptual and theoretical frameworks

The studies presented here examine the conceptual framework of hydrologic connectivity by integrating interdisciplinary perspectives, refining models, and incorporating emerging technologies to enhance predictability and management strategies. Dwivedi et al. synthesized current knowledge from hydrology, ecology, biogeochemistry, and geomorphology, offering a more comprehensive framework for connectivity research. Their study categorized connectivity according to spatial domains (surface, subsurface, and surface-subsurface) and connectivity dimensions (longitudinal, lateral, and vertical). They argued that, although analyzing connectivity by spatial domains, connectivity dimensions, or temporal scale is practical, its full impact on catchment dynamics is best understood holistically, yet many resource management strategies fail to incorporate this integrated perspective. They further emphasized that incorporating emerging technologies such as artificial intelligence, graph theory, and entropy-based metrics into improved measurement and modeling approaches can address critical gaps in understanding connectivity dynamics, particularly the inadequate spatial and temporal coverage.

These researchers proposed an integrated, system-based approach to hydrologic connectivity, linking key processes across disciplines. They suggested that simple analogies, such as the electric circuit analogy, can help interdisciplinary integration, illustrating how water flow, resistance, and storage interact within a system. In this analogy, gravitational potential drives water movement like voltage in an electrical circuit (Figure 1). At the same time, obstacles such as vegetation and rocks act as resistors; meanwhile, wetlands function as capacitors for temporary water storage, and groundwater flow represents inductance, highlighting subsurface interactions. Such simplified representations provide intuitive ways to bridge disciplinary perspectives and enhance integrated water management approaches. Table 1 expands on this analogy by contextualizing them within the effects of disturbances (e.g., wildfire, drought) and management practices (e.g., thinning, prescribed fire). While this analogy is intended to inspire a unified framework for understanding hydrologic connectivity, further research is necessary to enable its practical implementation in watershed management. Ultimately, the researchers recommended

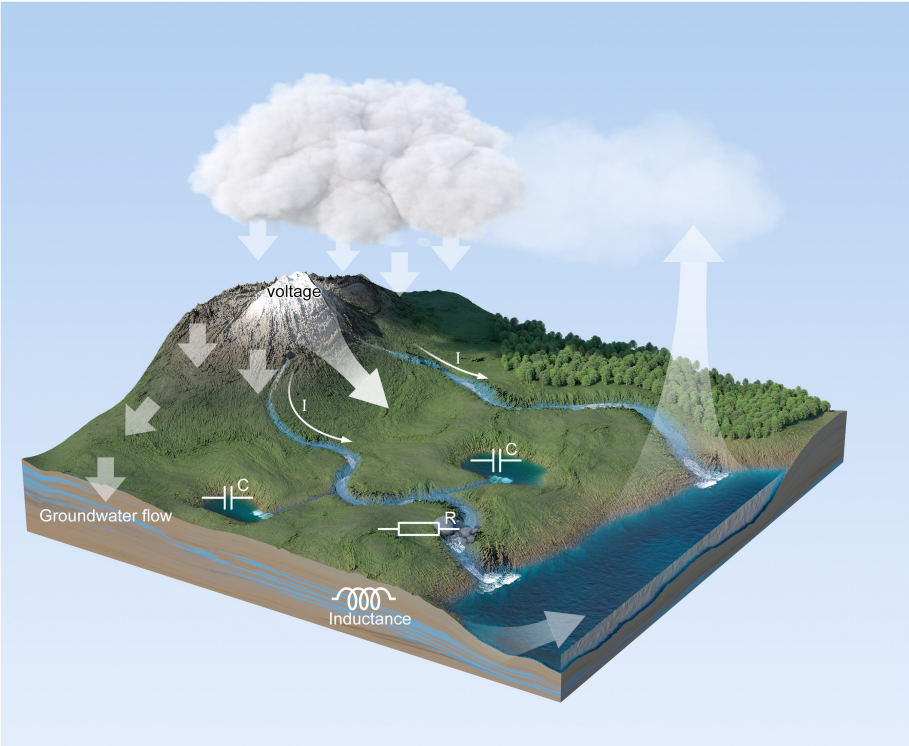

FIGURE 1
Conceptual analogy of hydrologic connectivity as an electric circuit. In this analogy, Voltage (V) represents the driving force, analogous to the gravitational potential that propels water flow; Current (I) corresponds to the rate of water flux through surface and subsurface pathways; Capacitor (C) symbolizes temporary water storage, such as wetlands, soil moisture, or aquifers that buffer and release water over time; Resistor (R) represents the resistance to flow imposed by features like vegetation, soil texture, compaction, or bedrock; and Inductor (L) captures system memory or lag effects, reflecting delayed hydrologic responses due to subsurface processes. While this illustration emphasizes surface processes for clarity, groundwater plays a critical role in shaping hydrologic connectivity. Specifically, aquifers act as capacitors by storing and slowly releasing water; confining layers or low-permeability zones function as resistors by limiting flow; and the slow movement and delayed discharge of groundwater contribute to the system's inductance, introducing lags in hydrologic response to climate or management interventions.

TABLE 1 Comparison of electric circuit concepts and hydrologic analogs, including implications for disturbance and watershed management.

Electric circuit concept	Hydrologic analog	Explanation and role in disturbance/management context
Voltage	Hydraulic head/pressure gradient	Represents the energy that drives water flow; drought lowers this gradient, while post-fire conditions can temporarily increase it via preferential flow and reduced vegetation uptake, steepening gradients.
Current	Water flux/discharge	Represents water flow rate through soils or channels; it can increase after thinning or fire due to reduced vegetation water uptake.
Resistance	Low-permeability layers, soil compaction	Controls the extent to which water movement is impeded; fire may reduce resistance through hydrophobicity, while compaction increases it.
Inductance	Delayed system response/memory effects	Represents delays in hydrologic response, such as soil wetting or vegetation regrowth. Management interventions can either shorten or prolong these response times.
Capacitance	Soil moisture storage/specific yield	Represents the capacity to store water; thinning can increase it by reducing interception, while wildfire may decrease it by consuming surface organic layers.
Conductance	Hydraulic conductivity	Indicates how easily water can move through the system; enhanced by preferential flow paths but may decline if soils seal after disturbance.
Power source/battery	Precipitation & recharge zones	Supplies energy to the system through water input; climate change can shift this supply, and management can alter recharge dynamics.
Circuit topology	Watershed structure, flow paths, landscape features	Defines the pathways through which water moves across the landscape. Fire can alter or disrupt these routes, while management practices such as restoration can reshape and enhance connectivity.
Load/energy use	Evapotranspiration, pumping, seepage	Represents water losses from the system. Thinning or drought can reduce evapotranspiration, while pumping increases demand and disrupts hydrologic balance.
Open circuit	Disconnected patches, perched water tables	Restricts or prevents water flow. This can result from soil sealing, drought-induced disconnection, or the presence of artificial barriers.
Conductive pathways	Fractures, macropores, channel networks	Facilitates rapid water movement. Wildfire can generate new preferential flow paths, while compaction may eliminate them.
Time-varying input (Alternating current; AC)	Seasonal or event-driven changes (e.g., storms)	Represents fluctuating hydrologic inputs. Management actions, such as prescribed burns, can alter the timing or intensity of seasonal flows.

better interdisciplinary collaboration and adaptive management approaches to incorporate hydrologic connectivity into ecosystem restoration and resource management.

Cho et al. expanded this conceptual foundation by introducing a sediment connectivity model that links hydrologic pathways and geomorphic processes. Their framework emphasized the role of spatial-temporal feedback between hydrologic processes (e.g., runoff, infiltration, return flow, percolation, and groundwater flow) and geomorphic drivers (e.g., runoff depth, soil conditions) in sediment transport, storage, and connectivity at multiple scales. Although to date their work remains theoretical and requires empirical validation for practical application, it demonstrated the value of incorporating geomorphic drivers into hydrologic connectivity studies to predict sediment flux and inform watershed management strategies. Considered together, the studies discussed in this section strengthen the conceptual foundation of hydrologic connectivity by integrating interdisciplinary perspectives, refining models, utilizing real-time data, and standardizing approaches to enhance predictability and inform sustainable water management in catchment systems.

Drivers and mechanisms of hydrologic connectivity

Several studies have explored key aspects of hydrologic connectivity—namely, topographic influence, wood accumulation, and tectonic impacts—that shape water movement, sediment transport, and landscape evolution across different timescales. Tull et al. investigated how topographic bluffs influence river–floodplain connectivity and residence times. According to their findings, bluff topography directs flow from the floodplain to the river. In contrast, levee-channels (i.e., the portion of a river confined between levees and engineered embankments) flow to the floodplain, with bluffs altering inundation patterns, creating exchange zones, and affecting residence times, nutrient transport, and sediment dynamics. Tull et al. ultimately emphasized the importance of integrating topographic features into floodplain restoration and management efforts, bolstering ecosystem functions such as solute sequestration and nutrient cycling.

Marshall and Wohl focused on the role of wood accumulation in driving channel bifurcations and altering flow paths within river systems. Their study challenged traditional bifurcation classifications by proposing a continuum model that links the ratio of erosive force to erosional resistance (F/R) with bifurcation type. The authors demonstrated that higher F/R values lead to lateral bifurcations and increased channel avulsion whereas lower values result in more stable banks and longitudinal bifurcations. These findings have significant implications for river restoration and sediment transport modeling.

Similarly, Han and Wilson examined the long-term evolution of hydrologic connectivity under tectonic and climatic influences in rift basins. Employing simulation models, they assessed how tectonic extension and climate change shape water storage,

connectivity, and flow dynamics over geological timescales. Their work emphasized the need to integrate tectonic processes into hydrologic models to improve predictions of landscape evolution and promote sustainable water resource management, particularly in tectonically active regions. These two studies demonstrate how topography, wood accumulation, and tectonic forces shape hydrologic connectivity across scales, providing insights for predictive modeling and sustainable watershed management.

Hydrologic connectivity and nutrient cycling

Research has also examined storm-driven, sediment-mediated nitrogen connectivity and the geomorphic control of coarse particulate organic matter (CPOM), highlighting their combined influence on nutrient fluxes and sustainable stream management. Joshi et al. investigated the dual role of suspended sediments as nitrogen exporters and reactors for denitrification and assimilatory nitrogen uptake during storms while quantifying the proportions of assimilatory nitrogen uptake and denitrification losses relative to the suspended-sediment-bound nitrogen load and examining how these vary across drainage areas, storm sizes, and the rising and falling limbs of the storm hydrograph. Their study demonstrated how storm-driven sediment transport enhances nitrogen connectivity by increasing denitrification rates and nutrient uptake, significantly altering watershed nutrient cycling. By linking sediment transport to nitrogen removal processes, the findings inform watershed management strategies to mitigate nitrogen pollution and improve water quality, particularly in response to extreme hydrological events.

Fogel and Lininger examined how geomorphic complexity influences CPOM transport and storage in headwater streams. Their study revealed that stream reaches with more retentive features, such as wood and cobbles, store greater amounts of CPOM while valley geometry influences transport at broader spatial scales. These findings underscore the need to consider geomorphic complexity in stream management and habitat restoration, as both direct alterations (e.g., dam construction, water diversions, wood removal, logging) and indirect changes (e.g., shifts in precipitation patterns and snowpack conditions) can substantially modify peak flow magnitude and frequency, valley bottom geometry, lateral connectivity, and in-stream wood and woody CPOM loads. Taken together, these studies emphasize how hydrologic and geomorphic processes regulate nutrient and organic matter fluxes in stream ecosystems, with storm-driven sediment transport enhancing nitrogen removal and geomorphic complexity shaping nutrient and CPOM retention.

Hydrologic connectivity and catchment dynamics

Understanding key aspects of climate-driven river evolution–investigating drainage system changes over geological timescales, evaluating discrepancies between predicted and observed network development, and identifying additional geomorphic and hydrologic feedbacks–can inform the refinement of predictive models for river network evolution. Hunt et al. developed a predictive model for river network evolution under climatic influences, assessing drainage system changes over geological timescales. Although some rivers align with theoretical expectations, such as groundwater–river interactions following a non-linear spatio-temporal scaling relationship, others deviate, like the Rio Grande and Pecos, suggesting additional geomorphic and hydrologic feedbacks. Importantly, the findings from this study revealed that connectivity patterns within river networks critically influence these dynamics, underscoring the need to refine climate-driven river evolution models by incorporating a broader range of hydrologic, geomorphic, and climatic variables while addressing theoretical assumptions and limited long-term data through expanded geographic coverage and improved modeling approaches.

Conclusion: bridging hydrologic connectivity research with practical applications

This Research Topic advances hydrologic connectivity by integrating interdisciplinary frameworks, refining sediment connectivity models, and examining key drivers such as topography, wood accumulation, and tectonic forces across different timescales. Biogeochemical processes and nutrient cycling underscore the importance of connectivity for sustainable water management, particularly through storm-driven sediment transport in nitrogen connectivity and the influence of geomorphic complexity on CPOM retention. In addition, research on climate-driven river evolution provides critical insights for refining predictive models. Future research should address critical gaps by advancing process-based and percolation theory-based models, graph theory, and entropy-based metrics to improve the precision of connectivity dynamics analysis (e.g., Matheus Carnevali et al., 2021; Dwivedi and Mohanty, 2016; Arora et al., 2019; Dwivedi et al., 2022; Dewey et al., 2022; Arora et al., 2022; Wohl et al., 2019; Wohl, 2019; Pöppl et al., 2024) to enhance the analysis of connectivity dynamics and improve model precision. Concentration–discharge (C–Q) relationships also offer valuable insights into hydrologic connectivity by linking critical zone structure, biogeochemical processes, and landscape heterogeneity (Herndon et al., 2015; Ackerer et al., 2020; Arora et al., 2020). These metrics can be leveraged to infer various dimensions of hydrologic connectivity–including vertical, lateral, and horizontal linkages–and warrant further exploration to uncover additional spatial and temporal patterns across watershed systems. Furthermore, addressing data limitations, implementing modeling approaches, and integrating machine learning techniques will be critical for strengthening hydrologic connectivity applications in environmental management (e.g., Varadharajan et al., 2019; Faybishenko et al., 2022). Ultimately, interdisciplinary collaboration and adaptive management strategies are vital for effectively integrating hydrologic connectivity into ecosystem restoration and resource management.

Author contributions

DD: Writing – original draft, Writing – review & editing. RP: Writing – review & editing. EW: Writing – review & editing.

Funding

The author(s) declare that financial support was received for the research and/or publication of this article. This research was supported by the U.S. Department of Energy (DOE), Office of Biological and Environmental Research (BER), as part of BER's Environmental System Science (ESS) Program through the Watershed Function Scientific Focus Area (SFA) at Lawrence Berkeley National Laboratory (LBNL). The Watershed Function SFA specifically supported DD's work at LBNL, funded by the DOE Office of Science, BER, under Award No. DE-AC02-05CH11231.

Conflict of interest

The authors declare that the research was conducted in the absence of any commercial or financial relationships that could be construed as a potential conflict of interest.

The author(s) declared that they were an editorial board member of Frontiers, at the time of submission. This had no impact on the peer review process and the final decision.

Generative AI statement

The author(s) declare that Gen AI was used in the creation of this manuscript. This work utilized generative AI tools solely for minor editorial refinements and formatting assistance. No original content was generated using AI.

Publisher's note

References

Ackerer, J., Steefel, C., Liu, F., Bart, R., Safeeq, M., O'Geen, A., et al. (2020). Determining how critical zone structure constrains hydrogeochemical behavior of watersheds: learning from an elevation gradient in california's sierra nevada. *Front. Water* 2:23. doi: 10.3389/frwa.2020.00023

Arora, B., Briggs, M. A., Zarnetske, J. P., Stegen, J., Gomez-Velez, J. D., Dwivedi, D., et al. (2022). "Hot spots and hot moments in the critical zone: identification of and incorporation into reactive transport models," in *Biogeochemistry of the Critical Zone* (Springer), 9–47. doi: 10.1007/978-3-030-95921-0_2

Arora, B., Burrus, M., Newcomer, M., Steefel, C. I., Carroll, R. W., Dwivedi, D., et al. (2020). Differential cq analysis: a new approach to inferring lateral transport and hydrologic transients within multiple reaches of a mountainous headwater catchment. *Front. Water* 2:24. doi: 10.3389/frwa.2020.00024

Arora, B., Wainwright, H. M., Dwivedi, D., Vaughn, L. J., Curtis, J. B., Torn, M. S., et al. (2019). Evaluating temporal controls on greenhouse gas (ghg) fluxes in an arctic tundra environment: An entropy-based approach. *Sci. Total Environ.* 649, 284–299. doi: 10.1016/j.scitotenv.2018.08.251

Dewey, C., Fox, P. M., Bouskill, N. J., Dwivedi, D., Nico, P., and Fendorf, S. (2022). Beaver dams overshadow climate extremes in controlling riparian hydrology and water quality. *Nat. Commun.* 13:6509. doi: 10.1038/s41467-022-34022-0

Dwivedi, D., and Mohanty, B. P. (2016). Hot spots and persistence of nitrate in aquifers across scales. *Entropy* 18:25. doi: 10.3390/e18010025

Dwivedi, D., Steefel, C. I., Arora, B., Banfield, J., Bargar, J., Boyanov, M. I., et al. (2022). From legacy contamination to watershed systems science: a review of scientific insights and technologies developed through doe-supported research in water and energy security. *Environ. Res. Lett.* 17:043004. doi: 10.1088/1748-9326/ac59a9

Faybishenko, B., Versteeg, R., Pastorello, G., Dwivedi, D., Varadharajan, C., and Agarwal, D. (2022). Challenging problems of quality assurance and quality control (QA/QC) of meteorological time series data. *Stoch. Environ. Res. Risk Assess.* 36, 1049–1062. doi: 10.1007/s00477-021-02106-w

Herndon, E. M., Dere, A. L., Sullivan, P. L., Norris, D., Reynolds, B., and Brantley, S. L. (2015). Landscape heterogeneity drives contrasting concentration-discharge relationships in shale headwater catchments. *Hydrol. Earth Syst. Sci.* 19, 3333–3347. doi: 10.5194/hess-19-3333-2015

Matheus Carnevali, P. B., Lavy, A., Thomas, A. D., Crits-Christoph, A., Diamond, S., Méheust, R., et al. (2021). Meanders as a scaling motif for understanding of floodplain soil microbiome and biogeochemical potential at the watershed scale. *Microbiome* 9:121. doi: 10.1186/s40168-020-00957-z

Pöppl, R. E., Parsons, A. J., and Keesstra, S. D. (2024). *Connectivity in Geomorphology*. Cambridge, New York: Cambridge University Press.

Varadharajan, C., Agarwal, D. A., Brown, W., Burrus, M., Carroll, R. W., Christianson, D. S., et al. (2019). Challenges in building an end-to-end system for acquisition, management, and integration of diverse data from sensor networks in watersheds: lessons from a mountainous community observatory in east river, colorado. *IEEE Access* 7, 182796–182813. doi: 10.1109/ACCESS.2019.2957793

Wohl, E. (2019). Forgotten legacies: Understanding and mitigating historical human alterations of river corridors. *Water Resour. Res.* 55, 5181–5201. doi: 10.1029/2018WR024433

Wohl, E., Brierley, G., Cadol, D., Coulthard, T. J., Covino, T., Fryirs, K., et al. (2019). A connectivity as an emergent property of geomorphic systems. *Earth Surface Proc. Landf.* 44, 4–26. doi: 10.1002/esp.4434

Wohl, E., Magilligan, F. J., and Rathburn, S. L. (2017). Introduction to the special issue: Connectivity in Geomorphology. *Geomorphology* 277, 1–5.

frontiers | Frontiers in Water

TYPE Original Research
PUBLISHED 11 April 2023
DOI 10.3389/frwa.2023.1155623

OPEN ACCESS

EDITED BY
Mohammad Safeeq,
University of California, Merced, United States

REVIEWED BY
Masato Kobiyama,
Federal University of Rio Grande do Sul, Brazil
David E. Rheinheimer,
California Natural Resources Agency,
United States

*CORRESPONDENCE
Anna Marshall
✉ amarsh01@colostate.edu

SPECIALTY SECTION
This article was submitted to Water and Critical Zone, a section of the journal Frontiers in Water

RECEIVED 31 January 2023
ACCEPTED 20 March 2023
PUBLISHED 11 April 2023

CITATION
Marshall A and Wohl E (2023) The continuum of wood-induced channel bifurcations. *Front. Water* 5:1155623. doi: 10.3389/frwa.2023.1155623

The continuum of wood-induced channel bifurcations

Anna Marshall* and Ellen Wohl

Department of Geosciences, Colorado State University, Fort Collins, CO, United States

Accumulations of wood in rivers can alter three-dimensional connectivity and facilitate channel bifurcations. Bifurcations divide the flow of water and sediment into secondary channels and are a key component of anastomosing rivers. While past studies illustrate the basic scenarios in which bifurcations can occur in anastomosing rivers, understanding of the mechanisms of bifurcations remains limited. We evaluate wood-induced bifurcations across thirteen anastomosing reaches in nine different streams and rivers in the U.S. Rocky Mountains to address conditions that favor different bifurcation types. We hypothesize that (1) wood-induced bifurcations exist as a continuum of different patterns in anastomosing rivers and (2) the position of a river segment along this continuum correlates with the ratio of erosive force to erosional resistance (F/R). We use field data to quantify F/R and compare varying F/R to bifurcation types across sites. Our results support these hypotheses and suggest that bifurcation types exist as a continuum based on F/R. At higher values of F/R, more channel avulsion is occurring and predominantly lateral bifurcations form. At lower values of F/R, banks are more resistant to erosive forces and wood-induced bifurcations are transitional or longitudinal with limited lateral extent. The relationship between F/R and bifurcation types is not linear, but it is progressive. Given the geomorphic and ecological functions associated with large wood and wood-induced channel bifurcations, it becomes important to understand the conditions under which wood accumulations can facilitate different types of bifurcations and the processes involved in these bifurcations. This understanding can inform river corridor restoration designed to enhance the formation of secondary channels, increase lateral and vertical connectivity, and promote an anastomosing planform.

KEYWORDS

large wood, channel planform, bifurcations, anastomosing, river restoration, resilience, connectivity

1. Introduction

River channels can split and merge at various spatiotemporal scales, creating and abandoning bifurcations as they migrate. Some of the earliest documentation of rivers depicts channels bifurcating (Carling et al., 2014, Figures 1, 2) and an extensive literature characterizes bifurcations (e.g., Bolla Pittaluga et al., 2003, 2015; Kleinhans et al., 2013). Bifurcations divide the flow of water and sediment into secondary channels and are a key component of delta distributary networks, braided planform, and anastomosing planform (Schumm, 1968; Knighton and Nanson, 1993; Burge, 2006). We consider anastomosing rivers to include at least two active parallel or sub parallel channels where flow rejoins downstream and vegetated islands or interfluves (≥ secondary channel width) are present between secondary channels. This description distinguishes anastomosing systems from distributary networks and braided planforms. Past work has described processes facilitating an anastomosing planform and planform distinctions

(Schumm, 1968; Smith, 1973; Smith and Smith, 1980; Rust, 1981; Nanson et al., 1986; Schumann, 1989; Knighton and Nanson, 1993; Schumm et al., 1996; Makaske, 1998, 2001; Burge, 2006; Carling et al., 2014), as well as the characteristics of anastomosing rivers across diverse settings (e.g., Schumm, 1968; Baker, 1978; Smith and Smith, 1980; Nanson et al., 1986; Schumann, 1989; Harwood and Brown, 1993; Wohl et al., 2022). While these studies illustrate the basic scenarios in which bifurcation can occur, understanding of some of the mechanisms of bifurcations in anastomosing systems remains limited. We briefly review the conditions facilitating the formation of anastomosing channels and the role of logjams in creating channel bifurcations.

1.1. Conditions facilitating anastomosing planform

Anastomosing planforms have been attributed to diverse influences, including:

- Vegetation (e.g., Smith, 1976; Gradziński et al., 2003; Larsen, 2019)
- Sediment supply and bank cohesion (e.g., Rust, 1981; Smith, 1983; Gibling et al., 1998; Makaske, 1998)
- Tectonic uplift and basin subsidence (e.g., Rust et al., 1985; Smith, 1986)
- Increased flow magnitude (e.g., Smith and Smith, 1980; Knighton and Nanson, 1993)
- Channel obstructions such as large wood (e.g., Burge and Lapointe, 2005; Wohl, 2011; Collins et al., 2012), ice dams (e.g., King and Martini, 1984), and beaver dams (e.g., Woo and Waddington, 1990; Gurnell, 1998; Burchsted et al., 2010; Polvi and Wohl, 2012; Laurel and Wohl, 2019).

The combination underlying every scenario of anastomosing is (i) limited lateral migration due to either bank stability and/or limited stream power, which prevents the channel(s) from being sufficiently laterally mobile to create a braided planform and (ii) sufficient discharge and stream power to, at least episodically, overtop the banks and erode persistent secondary channels into the floodplain (Smith and Smith, 1980; Harwood and Brown, 1993; Makaske, 2001).

The distinction between anastomosing and other channel planforms is, to some extent, arbitrary because natural channel planforms occur along continua such as those between anastomosing and braided, anastomosing and meandering, or braided and meandering. Different positions along these channel-planform continua can represent differences in either the underlying processes driving bifurcation or the balance between hydraulic erosive force and erosional resistance. Carling et al. (2014), for example, described differences in bifurcations based on accretionary-bar flow splitting processes vs. avulsive processes. Accretionary alluvial islands can cause channel splitting as can avulsion across the floodplain (Carling et al., 2014).

A single piece of large wood or a logjam can facilitate differences in bifurcations based on accretionary-bar flow splitting or avulsive processes. A logjam can force overbank flow, bank erosion, and lateral bifurcation *via* avulsion (Wohl, 2011; Wohl and Cadol, 2011; Collins et al., 2012). A logjam can also create lee deposition that is then stabilized by woody vegetation, forming a relatively short segment of split flow and a longitudinal bifurcation *via* accretionary-bar flow splitting processes (Gurnell and Bertoldi, 2020) (Figure 1). Here, we build on this process-based understanding by examining the conditions under which logjams obstructing a channel can facilitate avulsive lateral channel bifurcations vs. accretionary-bar flow splitting longitudinal bifurcations.

1.2. Logjams and channel bifurcations

Wood accumulations can alter the three-dimensional connectivity of a river corridor. Here, connectivity refers to the degree to which matter (water, solutes, sediment, organic matter) and organisms can move among components of a landscape or ecosystem (Wohl, 2017). Accumulations of large wood can obstruct flow and facilitate channel bifurcations. We propose that the occurrence and characteristics of wood-induced bifurcations are influenced by (i) the hydrologically connected width, (ii) wood blockage, and (iii) the ratio of erosive force to erosional resistance (F/R) (Figure 2).

Hydrologically connected width is governed by valley-floor topography and the magnitude of overbank flow, which together limit the maximum possible lateral extent of channel bifurcations and whether there is sufficient space to form a multichannel (braided or anastomosing) planform. As suggested in Figure 2, a narrow valley floor will support only a single channel.

Wood blockage refers to the ratio of logjam frontal area to channel cross-sectional area. Even a logjam that does not span the entire channel can create sufficient blockage and enough hydraulic roughness to enhance overbank flow and initiate splays or avulsion channels (Brummer et al., 2006; Collins et al., 2012), although channel-spanning jams are more likely to deflect flow overbank and create backwater effects (Jeffries et al., 2003; Livers and Wohl, 2021). Even though multichannel planforms can occur in the absence of wood obstructions, they are more likely to occur where these obstructions are present (Collins et al., 2012).

F/R values can control whether overbank flow creates a new channel, as well as the spatial and longitudinal extent and cross-sectional area of secondary channels. Erosive forces exerted against the channel banks and floodplain surface, including shear stress, thermal erosion, and abrasion by ice, typically increase with discharge. Erosional resistance or bank erodibility results from the frictional properties of sediments, the effective normal stress of the bank, and effective cohesion (i.e., cohesion added from vegetation roots; Simon et al., 2000). Banks erode as individual grains detach from the bank or a mass failure occurs. Erosional resistance is commonly influenced by grain size distribution, stratigraphy, moisture level, vegetation (Järvelä, 2004; Pollen-Bankhead and Simon, 2010), large wood (Wohl, 2013), and topographic heterogeneity (Güneralp and Rhoads, 2011). The ratio of erosive force to erosional resistance, as originally conceptualized by Schumm (1985) based on gradient, sediment load, and bank composition, correlates with channel planform along a spectrum

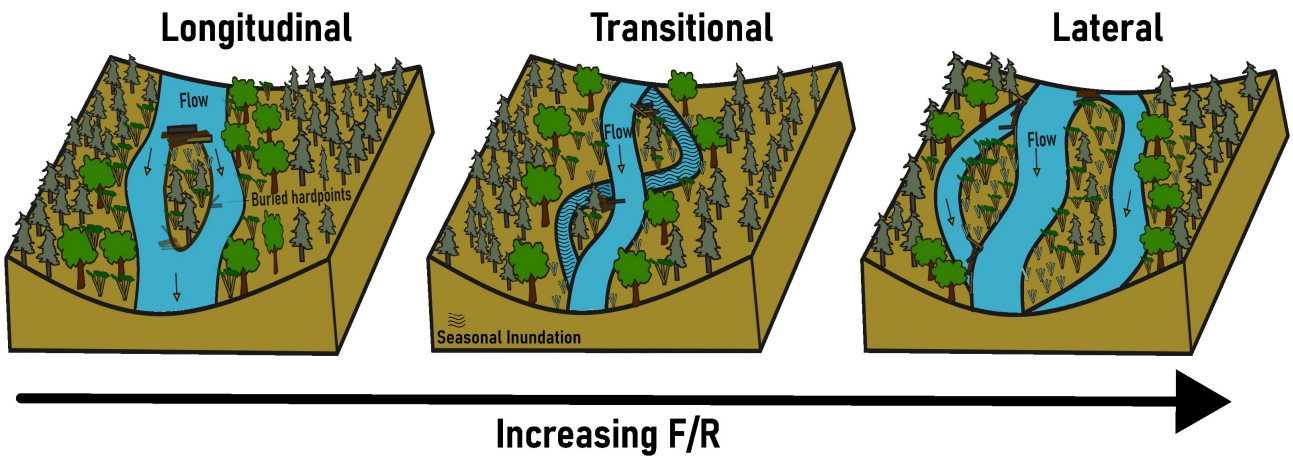

FIGURE 1
Conceptual illustration of jam-induced channel bifurcations. Lateral bifurcations (avulsive) form as a logjam forces overbank flow and bank erosion and the channel avulses laterally around the logjam. Longitudinal bifurcations (accretionary-bar splitting) form as a logjam creates lee deposition that is then stabilized by woody vegetation, forming a relatively short segment of split flow. Transitional bifurcations can have lateral and/or longitudinal bifurcations and depend on seasonal persistence of flow in secondary channels. An arrow showing increasing F/R with lateral bifurcation formation illustrates hypothesis 2.

from a single, straight channel (low F/R) to a braided channel (high F/R).

Both dispersed pieces of large wood and logjams can have varying influences on erosive force and erosional resistance depending on the location, movement, and characteristics of the wood. Dispersed pieces of large wood within a channel can increase hydraulic roughness and thus reduce velocity and erosive force exerted against the banks (Manga and Kirchner, 2000; Brooks et al., 2003; Daniels and Rhoads, 2004). A jam can have the same effect and create a backwater that reduces bank erosion upstream (Triska, 1984; Le Lay et al., 2013). A jam or large wood piece can also deflect flow toward the bank, which promotes bar growth and lateral channel movement, and over the bank across the floodplain in a manner that promotes formation of secondary channels that branch from and then rejoin the main channel downstream (O'Connor et al., 2003; Collins et al., 2012; Martín-Vide et al., 2014). The movement of wood can increase erosional force as a jam moves in congested transport (Piegay, 1993) or the lack of movement can increase erosional resistance as jams remain stable for long periods of time, forming buried hard points (Collins et al., 2012).

1.3. Objective and hypotheses

Our primary objective is to compare types of wood-induced channel bifurcations on multiple rivers and streams of differing size to address the conditions that favor one scenario over the other. We focus on systems where valley confinement, and thus hydrologically connected width, is not limited and where wood obstructions are abundant. We hypothesize that (1) wood-induced bifurcations exist as a continuum of different patterns in anastomosing rivers, as illustrated in Figures 1, 2, and the position of a river segment along this continuum correlates with F/R.

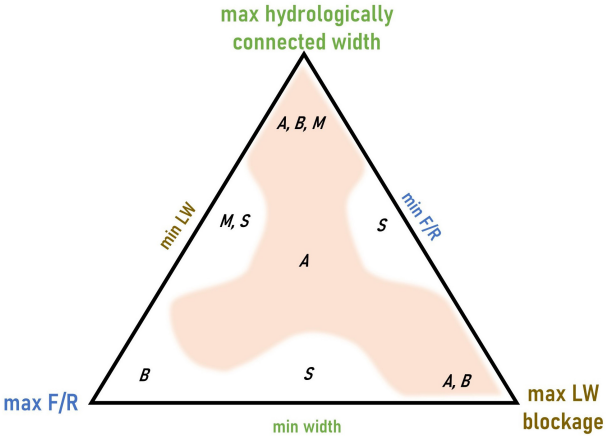

FIGURE 2
A ternary diagram illustrating how we conceptualize the interactions among three primary controls influencing wood-induced channel bifurcations. The maximum value of each of these controls occurs at a triangle vertex and the minimum at the mid-point of the opposite side of the triangle. Letters indicate channel planforms (A anastomosing, B braided, M meandering, S straight) and the shading indicates the range of conditions in which anastomosing channel planform can occur. Multiple letters separated by commas indicate that more than one channel planform is possible in that portion of the diagram.

2. Study area

We focus our work across nine rivers and streams of diverse size within the montane and mesic montane zone of the Rocky Mountains in Colorado and Montana, USA. We have thirteen study reaches across the nine study sites. Each river or stream reach has sufficient lateral space to create multiple channels (at least two) within the study areas.

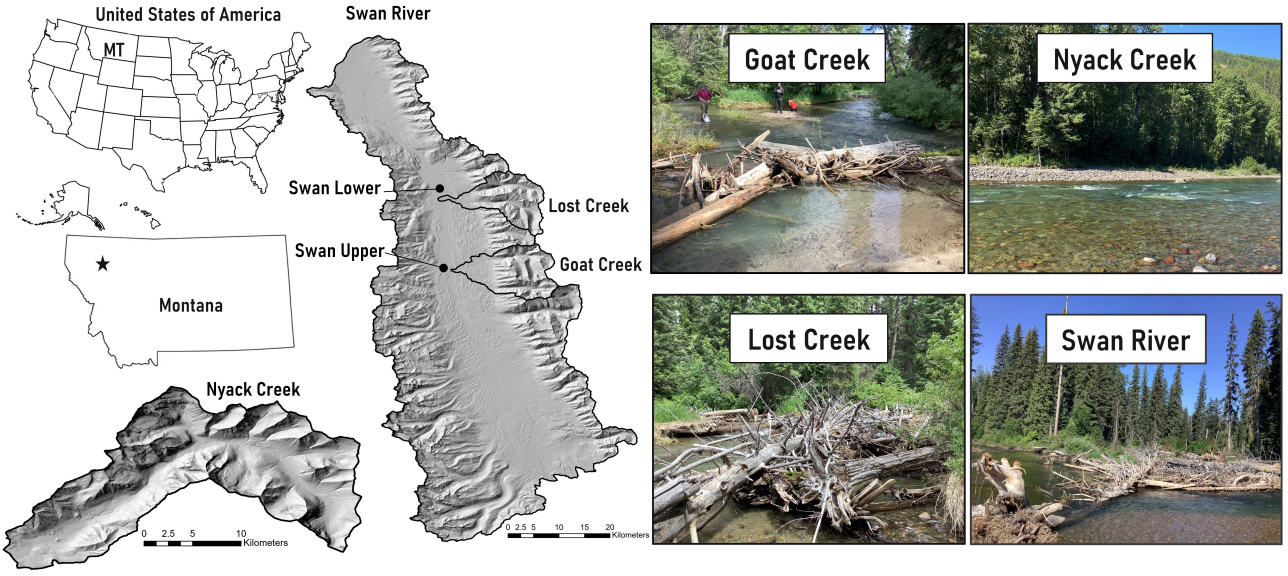

FIGURE 3
Montana field sites (Goat Creek, Lost Creek, Nyack Creek, Swan River). Note the different scale bars for the Nyack Creek and the Swan River watershed maps. Photos depict representative reach characteristics. We include two sites at Lost Creek, Goat Creek, and the Swan River in our results, but only show a photo of the upper reach for each site here.

2.1. Montana field sites

Study sites in Montana include Nyack Creek, the Swan River and two tributaries, Lost Creek and Goat Creek (Figure 3). We distinguish between upper and lower sites along the Swan River, Lost Creek, and Goat Creek. The Swan River (1,676 km^2 drainage area) runs north along a valley bounded by the Mission Range to the west and the Swan Range to the east before draining into the Flathead River. Both Goat Creek (~94 km^2 drainage area) and Lost Creek (~85 km^2 drainage area) are within the Swan River Basin. Nyack Creek (~200 km^2 drainage area) flows west into the Middle Fork Flathead River before draining into the Flathead River.

The Swan basin receives ~750 mm of mean annual precipitation and the Nyack receives ~1500 mm of mean annual precipitation. Precipitation varies significantly with topography and rain shadow effect from the Rocky Mountains. Rainfall, snowmelt, and rain-on-snow precipitation can all produce peak flows, but the largest annual peak flow is typically associated with spring snowmelt (MacDonald and Hoffman, 1995). The hydrology of the region is dominated by the accumulation and melting of seasonal snowpack, with high flow occurring during the spring and low flow occurring during the late summer, autumn, and winter months.

The region is underlain by the Proterozoic-age Belt Supergroup, which mostly consists of weakly metamorphosed, fine-grained sedimentary rocks. The area is within the Intermountain Seismic Belt, a seismically active zone characterized by range-bounding normal faults (Hofmann and Hendrix, 2010). In addition to continuing uplift, topography in the region was shaped by Pleistocene glaciations. Lacustrine glacial lake deposits along with volcanic ash layers overlie rocky glacial till (Locke, 1995; Hofmann and Hendrix, 2010). Soils are thin, have poorly developed profiles (Antos and James, 1981), and are mostly gravelly loamy sand (USDA, 2022). Channels primarily have cobble- to boulder-bed substrate with pool-riffle sequences. Valley width along the Swan is ~1–2 km with an average channel gradient of 0.5%. Valley width along Nyack Creek averages 400–500 m with an average channel gradient of 0.2%.

Valley floors in the region are primarily covered with mesic montane conifer forests and wetlands, with some areas of subalpine forest. Shade-intolerant species include western larch (*Larix occidentalis*), western white pine (*Pinus monticola*), and Douglas-fir (*Pseudotsuga menziesii*). Climax, shade-tolerant species include grand fir (*Abies grandis*) and western redcedar (*Thuja plicata*) (Antos, 1977). Despite a history of patch timber harvest and stand-replacing fires in the upland portions of the valley (Antos and James, 1981; Parks et al., 2015), substantial portions of old-growth forest remain (Lesica, 1996) and the floodplain has experienced little development. The Swan River and Nyack Creek corridors have a high volume of downed wood within the channel and floodplain (Wohl et al., 2018).

2.2. Colorado field sites

Study sites in Colorado include a site along Little Beaver Creek (LBC), two sites along North Saint Vrain Creek (NSV), and one site along each of three NSV tributaries, Cony Creek, Ouzel Creek, and Hunters Creek (Figure 4). Cony Creek (~ 20 km^2 drainage area), Ouzel Creek (~15 km^2 drainage area), and Hunters Creek (~12 km^2 drainage area) are all within the NSV drainage. NSV (drainage area 345 km^2) and LBC (drainage area 40 km^2) lie within the watershed of the South Platte River in the Colorado Front

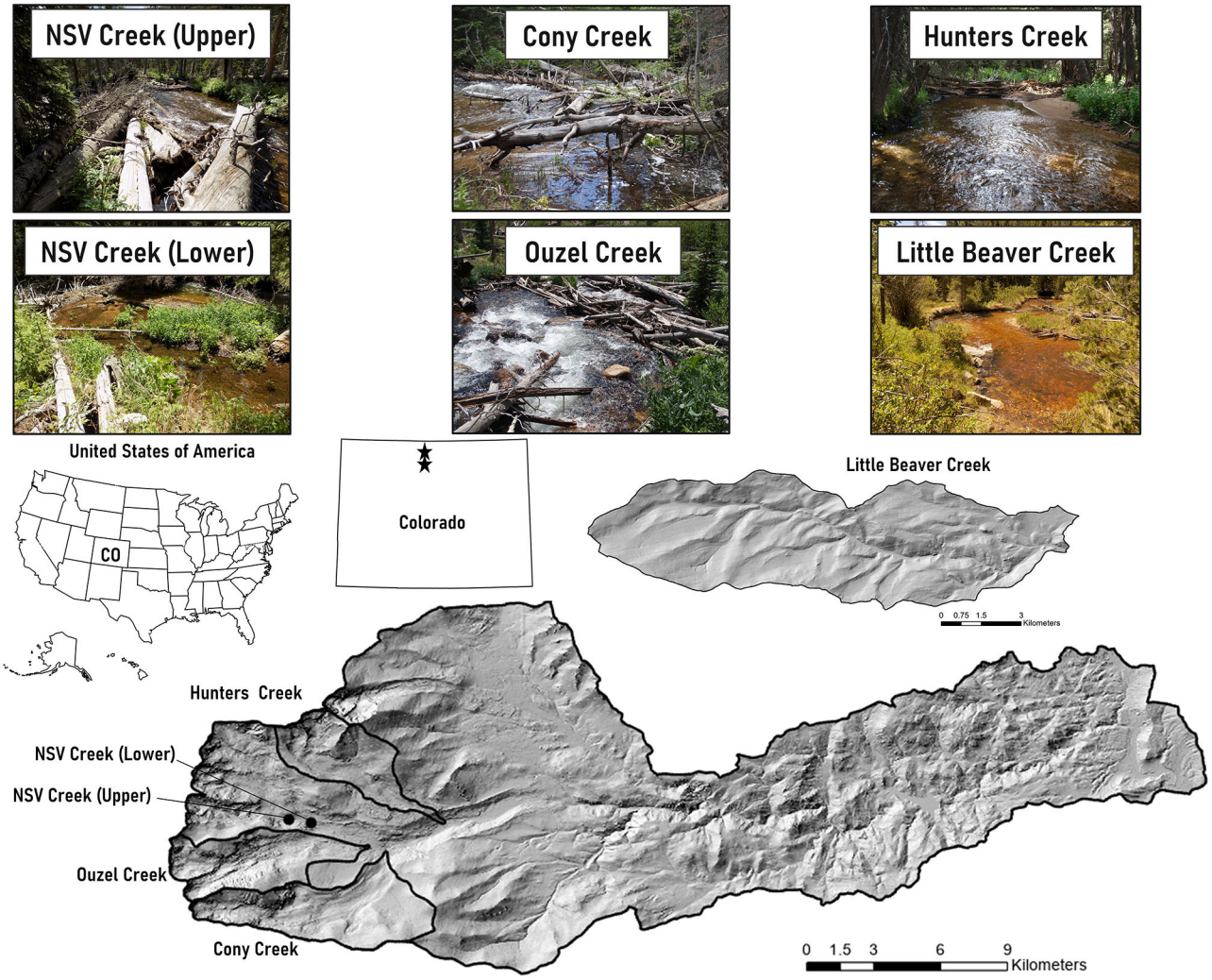

FIGURE 4
Colorado field sites (Cony Creek, Hunters Creek, Ouzel Creek, North Saint Vrain Creek, and Little Beaver Creek). Note different scale bars for Little Beaver Creek and the sites within the North Saint Vrain Creek watershed. Photos depict representative reach characteristics.

Range. The region receives ~550 mm of precipitation per year with variation based on elevation and has a mean annual temperature of 8.3°C (Barry, 1973). These sites are snowmelt dominated with a sustained seasonal peak, but summer convective storms can produce brief floods of higher magnitude (Jarrett, 1990).

Front Range catchments are underlain by Precambrian Silver Plume granite (Braddock and Cole, 1990; Cole et al., 2010). Valley geometry is highly variable longitudinally (Wohl et al., 2017), largely as a result of variations in bedrock joint density (Ehlen and Wohl, 2002). Fracture patterns in the granite create downstream alternations between relatively steep, narrowly confined valley segments and lower-gradient, less confined segments at lengths of 10^1-10^2 m. Channel planforms typically alternates between step-pool channels with boulder substrate in the most confined sections to anastomosing channels with pool-riffle bedforms or wood-forced steps and pools, and a cobble substrate, in the wider valley segments. Average channel gradient varies from 6 (upper portion NSV site) to 2% (Cony Creek) and channel substrate averages 45–60 mm diameter clasts, except in logjam backwaters where sand and fine gravel are present. Lower gradient and less confined reaches have anastomosing planforms with abundant channel-spanning logjams (Wohl, 2011) or beaver dams (John and Klein, 2004; Polvi and Wohl, 2012).

The region has old-growth montane forest. Dominant species include ponderosa pine (*Pinus ponderosa*), Engelmann spruce (*Picea engelmannii*), Douglas-fir (*Pseudotsuga menziesii*), aspen (*Populus tremuloides*), and willows (*Salix spp.*). Large wood is recruited to channels primarily from bank erosion and individual tree fall and channel-spanning logjams are abundant in the channels (Jackson and Wohl, 2015). Both watersheds have experienced recent disturbances by fire, flooding, and mass movements that significantly altered the watersheds and river corridors (Sibold et al., 2006; Rathburn et al., 2017; Sutfin and Wohl, 2019; Wohl et al., 2022). Most recently, the 2020

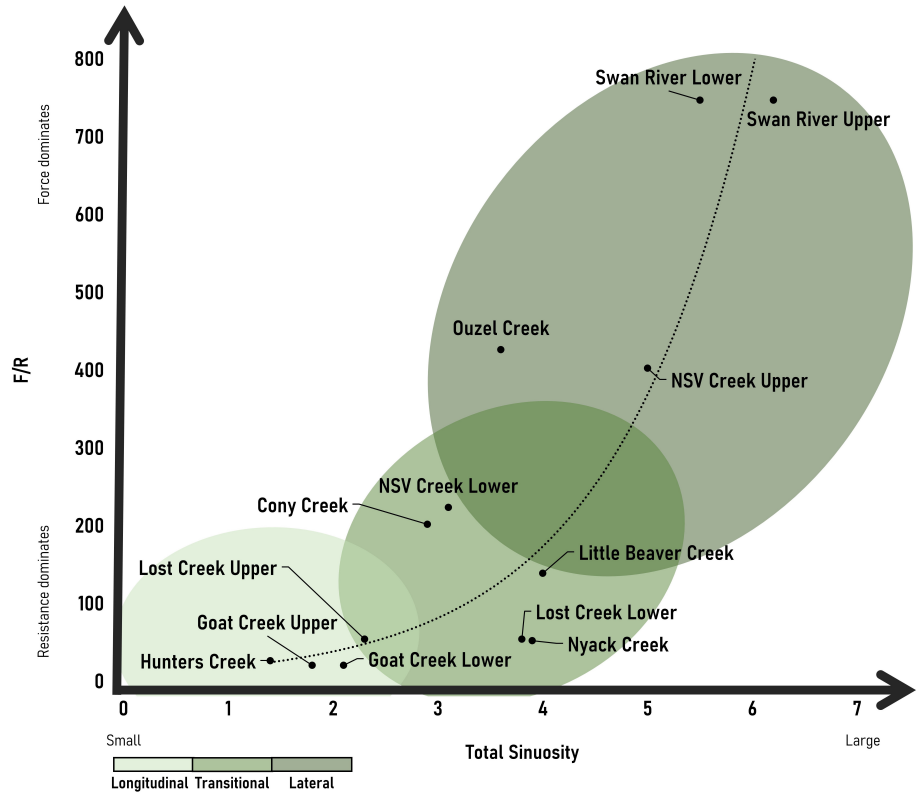

FIGURE 5
Observed continuum of channel bifurcations based on total sinuosity and F/R with an exponential line of best fit.

Cameron Peak fire burned substantial portions of the LBC watershed. New anastomosing reaches were created in both burned and unburned portions of the watershed during post-fire flash floods.

3. Methods

At each of our study sites, we characterized channel bifurcations and associated jams. We measured bank height, root depth/organic layer thickness, and coarse layer thickness, and collected one representative bank sample for organic layers and one for coarse layers to use in grain size analysis at locations where bifurcations occurred. Bank samples were sieved for grain size distribution. We measured the width of logjams relative to the width of the channel to calculate blockage ratios and used the most up-to-date Google Earth imagery at each site (spanning 2014–2022) to measure hydrologically connected width using the built-in measure tool (https://earth.google.com/web/).

We used our field data to quantify metrics of F and R. Our primary indicator of F is total stream power, which is the product of discharge, channel gradient, and the specific weight of water. Stream power is a useful predictor of channel form and dynamics because it quantifies the amount of geomorphic work that can be done by a stream, such as moving sediment on the bed or in the banks of the river (i.e., erosion or sediment transport). More specifically, stream power is commonly used as a tool to investigate the lateral stability of river channels (e.g., Chang, 1979; Nanson and Croke, 1992; Makaske, 1998). We used USGS StreamStats (https://streamstats.usgs.gov/ss/) to determine average snowmelt peak flow as a discharge value at which we expect wood can move. We used field measurements and LiDAR data to extract reach-scale channel gradient for each study site. We used the bank stability and toe erosion model (BSTEM; https://www.ars.usda.gov/southeast-area/oxford-ms/national-sedimentation-laboratory/watershed-physical-processes-research/research/bstem/) from the National Sedimentation Laboratory to provide comparative estimates of R (Simon et al., 2011). BSTEM integrates grain size, bank height and angle, sediment layer thicknesses, and vegetation data and is a commonly used tool for modeling streambank erosion and failure (Simon et al., 2000, 2011; Curran and Hession, 2013; Rinaldi and Nardi, 2013; Klavon et al., 2017). We use F/R to determine how much force relative to resistance is acting at each site and to compare the relative ratios across sites. We did not attempt to calculate a dimensionally correct ratio with respect to units. Rather, we use this ratio as an indicator of potential excess energy available for bank and floodplain erosion associated with channel bifurcations.

We manually measured total sinuosity and the ratio of channel migration width to average channel width as river corridor geometric variables using the built-in measure tool in Google Earth (https://earth.google.com/web/). Measurements were

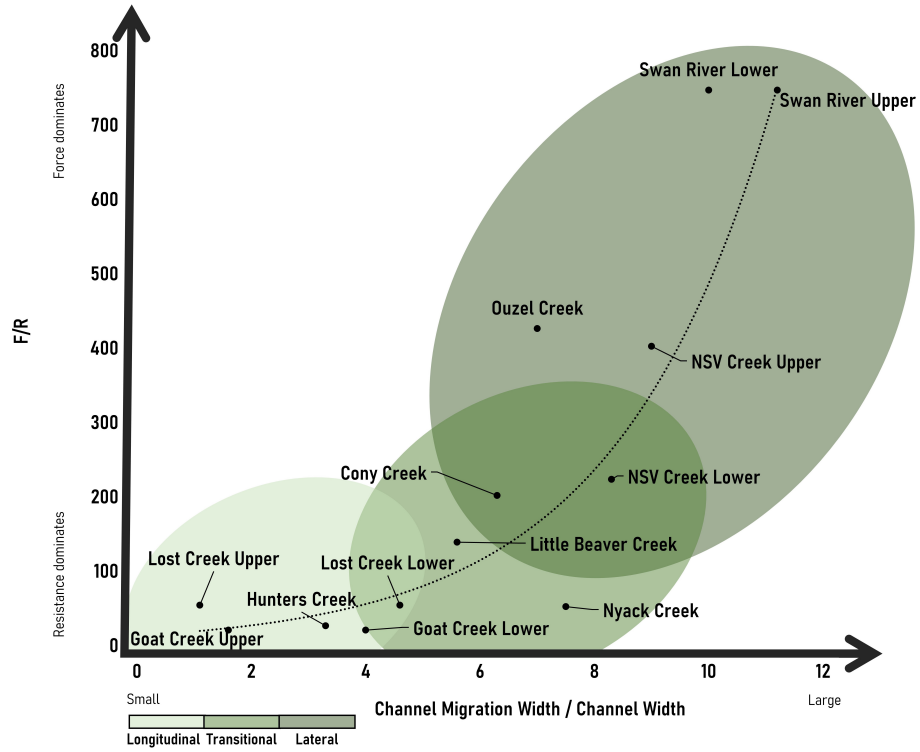

FIGURE 6
Observed continuum of channel bifurcations based on channel migration width/channel width and F/R with an exponential line of best fit.

averaged across 500-m reaches at our study sites. Total sinuosity is the ratio of total channel length of all active channels/valley length (Hong and Davies, 1979; Egozi and Ashmore, 2008). Channel migration width is measured as the meander belt or total width between the outermost active channel edges in a multi-channel system. The ratio of this value to main channel bankfull width provides a dimensionless indicator of the lateral extent of active channel bifurcations. We used both total sinuosity and channel migration width/channel width as metrics for the degree to which a river has bifurcated. The larger the value of either metric, the more the river approaches the lateral bifurcation endmember in Figure 1; smaller values indicate the longitudinal bifurcation endmember.

Given our small dataset, we ran both parametric and non-parametric statistical analyses to assess the relationship between F/R and bifurcations. We used RStudio to perform the statistical analyses (R Core Team., 2022). We ran a simple linear regression and calculate the Pearson correlation coefficient (r) from the multiple R-squared. We calculated the Spearman rank correlation coefficient (ρ) as a non-parametric measure of the relationship between F/R and bifurcations. Given the repetition in values for some F/R ratios, we also calculated the Kendall rank correlation coefficient (τ) to ensure there is no impact from ties in our analyses (Hollander et al., 2014). All correlation coefficients were calculated using the *cor.test()* function in base R. We conducted the same analyses looking at the correlation between F/R and total sinuosity and F/R and channel migration width/channel width. The Pearson, Spearman, and Kendall correlation coefficients all measure the strength of the relationship between two variables (F/R and total sinuosity and F/R and channel migration width/channel width) for parametric (Pearson) or non-parametric (Spearman and Kendall) datasets. We used an alpha (probability of rejecting the null hypothesis when the null hypothesis is true) of 0.05 in all statistical analyses.

4. Results

Results support both our hypotheses that (1) wood-induced bifurcations exist as a continuum of different patterns in anastomosing rivers and (2) the position of a river segment along this continuum correlates with F/R. Our full dataset is included as Supplementary Table 1. We plot F/R with both total sinuosity and channel migration width/channel width as proxies for the types of bifurcations. Our results for both suggest that bifurcation types exist as a continuum based on the ratio of F/R. We report only the Pearson Correlation Coefficients given the agreement between parametric and non-parametric correlation coefficients, but Spearman and Kendall correlation coefficients are included as Supplementary Table 2. Pearson correlation coefficients suggest a positive relationship between F/R and bifurcations ($r = 0.837$ for total sinuosity and $r = 0.829$ for channel migration width/channel width). At higher values of F/R, more channel avulsion is occurring and lateral bifurcations form (Figures 5, 6). At lower values of F/R,

jam bifurcations are transitional or longitudinal but are not lateral (Figures 5, 6). The relationship between F/R and bifurcation type is not linear, but it is progressive.

5. Discussion

Our results suggest that bifurcation types exist as a continuum based on F/R. We observe a relationship between bifurcation type and F/R, where at higher values of F/R, more channel avulsion is occurring and lateral bifurcations with an increasing number of secondary channels and relative lateral extent form. We see the highest F/R and number of lateral bifurcations at the Swan River sites. Not surprisingly, this site has the highest stream power, and we assume highest transport capacity for wood. Visual observations in the field suggest that wood is regularly reworked within the Swan. We observed newly forming anastomosing reaches along the Swan where wood accumulations appear to have been transported and deposited during high flows, causing new bifurcations to form as flow avulsed laterally around logjams. The Swan also has a smaller root depth relative to the coarse layer of sediment, which contributes to more erodible banks relative to other sites. We see the lowest F/R and number of bifurcations along the upper portions of Goat Creek and Lost Creek as well as Hunters Creek. At each of these sites, conifers (>2 m in height) had established on the longitudinal bifurcations and buried pieces of wood were observed along the length of the bifurcation, suggesting the persistence and presence of older logjams. The transition from longitudinal to lateral bifurcations is progressive as F/R increases. This likely reflects a combination of increasing stream power and decreased root depth relative to the coarse layer in the banks, causing less erosional resistance. In other words, a combination of the flow having more erosive power and the banks being less stable as the root depth relative to the total bank height changes drives a transition from longitudinal to lateral bifurcations.

5.1. Significance of wood-induced bifurcations

Understanding the conditions that facilitate different types of wood-induced bifurcations has important implications for the broader physical and biological processes in a river corridor. Wood-induced channel bifurcations support beneficial hydrologic, geomorphic, and ecologic function. In-channel logjams split flow and trap sediment, creating multiple channels and islands that dissipate energy during high flows (Brummer et al., 2006; Wohl, 2011; Collins et al., 2012). The ratio of wood blockage in a channel and F/R can influence the degree to which longitudinal and vertical connectivity is increased and lateral connectivity is decreased. Wood-induced bifurcations promote connectivity in the lateral (Baxter et al., 2005; Kondolf et al., 2006; Wohl, 2013) and vertical (Hester and Doyle, 2008; Sawyer et al., 2011; Marttila et al., 2018; Wilhelmsen et al., 2021) dimensions of a river corridor. Multiple, wood-rich channels that are laterally connected to the floodplain and vertically connected to the hyporheic zone support abundant and diverse habitat and species (Dolloff and Warren, 2003; Herdrich et al., 2018; Venarsky et al., 2018). The connectivity driven by wood-induced bifurcations provides refugia and resilience during disturbances such as flood, drought, and wildfire (Benda et al., 2004). For example, high water table, deep pools, and lateral connectivity provide drought refugia and more stable base flows (Boulton et al., 1998; Bêche et al., 2009; Dixon, 2016; Puttock et al., 2017). Increased lateral connectivity facilitated by logjams and secondary channels helps to attenuate flood peaks and diffuse flood flows across the floodplain (Junk et al., 1989; Poff et al., 1997), making habitats persistent and more resistant to natural and anthropogenic disturbances (Amoros and Bornette, 2002; Henning et al., 2006; Jeffres et al., 2008).

Hydrologic connectivity and interactions with wood are accompanied by hydraulic effects. Wood obstructions can divert and concentrate flow, creating local areas of high velocity and shear stress separated by wood-sheltered areas where velocities and shear stresses are drastically reduced (Gurnell, 2013; Matheson et al., 2017). Wood-induced bifurcations maximize hydraulic heterogeneity through partitioning of flow between branches that widen the range of in-channel depths and velocities (Gordon et al., 1992). Logjams reduce flow velocity and create pools (Beechie and Sibley, 1997; Montgomery and Buffington, 1997; Abbe and Montgomery, 2003) and bifurcations create multiple, marginal zones of slower flow. Both attributes promote bed heterogeneity and maximize morphological features in the channel and on the floodplain (Montgomery et al., 1996; Buffington and Montgomery, 1999), providing high capacity to store sediment and cycle nutrients (Parker et al., 2017). Frequent, small channel adjustments and a high, reliable water table also create optimal settings for germination and growth of aquatic and riparian vegetation (Nadler and Schumm, 1981; Tal and Paola, 2007; Braudrick et al., 2009). Wet woodlands on islands and floodplains supply and retain wood and widespread vegetation proximal to the channel (Fetherston et al., 1995; Gurnell et al., 2001; Montgomery and Abbe, 2006), supporting habitat and increased retention of organic matter and nutrients for other organisms (Bilby, 1981; Flores et al., 2011). Dense, diverse riparian vegetation provides abundant shade which, together with efficient hyporheic exchange, ameliorates water temperatures (Montgomery et al., 1999; Beechie et al., 2005).

5.2. Continuing work

The results summarized here suggest additional questions with respect to wood-induced channel bifurcations. These include potential thresholds of wood blockage, persistence of wood accumulations, and erosive mechanisms. First, is there a threshold size of wood accumulation or wood volume relative to channel dimensions that is necessary to drive bifurcations? Second, how long must wood accumulations persist relative to recurrence of peak flows to create persistent bifurcations? We were not able to directly observe interactions between potentially transient wood accumulations and channel bifurcations. We suspect, based on inference and multi-year field observations of some sites, that one large peak flow is sufficient to form a new bifurcation, even if the peak flow removes the wood accumulation that initiated the process of bifurcation. However, this inference has not been quantitatively tested. Third, what specific erosional

mechanisms create channel bifurcations? Wood accumulations can cause preferential local bank erosion that could develop into a longitudinal bifurcation, for example. Our observations also indicate that diffuse overbank flow across the floodplain can concentrate into secondary channels over multiple seasons of peak flow. We have also observed overbank flow that returns to the channel downstream, creating a floodplain knickpoint at the point of re-entry to the channel during flows below bankfull stage. This knickpoint could presumably erode headward and help to stabilize a secondary channel.

Additional work is also needed across diverse settings to understand whether wood is a key driver of bifurcations in rivers with different hydrologic, wood, and sediment regimes. Our study focuses on snowmelt-dominated rivers with floodplains that are highly erodible (relatively uncohesive upper sediment layers and shallow-rooted conifers) except where willows grow in relatively dense stands. Additional work looking at the effects of flashier peak flow in rainfall-dominated rivers, highly cohesive silts and clays in floodplain alluvium, or different vegetation communities with greater hydraulic roughness and root resistance, would all provide valuable insight into understanding bifurcations across diverse settings.

6. Conclusion

Our results suggest that bifurcation types exist as a positive continuum based on the ratio of F/R. Longitudinal and lateral bifurcations occur at either end of the continuum, with transitional bifurcation types between. At higher values of F/R, more channel avulsion is occurring and lateral bifurcations form across a broader portion of the floodplain. At lower values of F/R, banks are more resistant to erosive forces and wood-induced bifurcations are transitional or longitudinal with a much lower lateral extent. More work considering thresholds of drivers forming new bifurcations across diverse settings will provide further insight into our understanding of the mechanisms behind bifurcations. As the need for resilient and more connected river systems increases in the face of accelerated environmental change, understanding the conditions under which wood accumulations can facilitate different types of bifurcations and the processes involved in these bifurcations is both significant and timely to river corridor science and management.

Data availability statement

The original contributions presented in the study are included in the article/Supplementary material, further inquiries can be directed to the corresponding author.

Author contributions

AM and EW contributed to the conception and design of this study. AM collected field data in MT. EW collected field data in CO. Both authors contributed to the article and approved the submitted version.

Funding

Funding from the Tobacco Root Geological Society and an AGU Horton Research Grant, both awarded to AM, supported field data collection.

Acknowledgments

We thank Mckenna Pressley, Nathan Terault, and Hiromi Uno for assistance in the field, Bob Hall, Diane Whited, and the staff at Flathead Lake Biological Station for support at Montana field sites, and Juli Scamardo for feedback on conceptual figures. This manuscript benefited from comments from MK and DR as reviewers and MS as editor. We acknowledge that that the land this work was conducted on is the traditional and ancestral homelands of the Arapaho, Cheyenne, Ute, and Flathead Nations and recognize, with respect, the Indigenous peoples as original stewards of this land.

Conflict of interest

The authors declare that the research was conducted in the absence of any commercial or financial relationships that could be construed as a potential conflict of interest.

Publisher's note

All claims expressed in this article are solely those of the authors and do not necessarily represent those of their affiliated organizations, or those of the publisher, the editors and the reviewers. Any product that may be evaluated in this article, or claim that may be made by its manufacturer, is not guaranteed or endorsed by the publisher.

Supplementary material

The Supplementary Material for this article can be found online at: https://www.frontiersin.org/articles/10.3389/frwa.2023.1155623/full#supplementary-material

References

Abbe, T. B., and Montgomery, D. R. (2003). Patterns and processes of wood debris accumulation in the queets river basin, Washington. *Geomorphology* 51, 81–107. doi: 10.1016/S0169-555X(02)00326-4

Amoros, C., and Bornette, G. (2002). Connectivity and biocomplexity in waterbodies of riverine floodplains. *Freshwater Biol.* 47, 761–776. doi: 10.1046/j.1365-2427.2002.00905.x

Antos, J., and James, H. (1981). *Successional Development in Abies Grandis (Dougl.) Forbes Forests in the Swan Valley, Western Montana. Northwest Science* Missoula: University of Montana.

Antos, J. A. (1977). *Grand Fir (Abies Grandis (Dougl.) Forbes) Forests of the Swan Valley, Montana*. Missoula: University of Montana.

Baker, V. R. (1978). *Large-Scale Erosional and Depositional Features of the Channeled Scabland. NASA Technical Reports*. Washington, DC: The Channeled Scabland.

Barry, R. G. (1973). A climatological transect on the east slope of the front range, Colorado. *Arctic Alpine Res.* 5, 89–110. doi: 10.2307/1550251

Baxter, C. V., Fausch, K. D., and Saunders, W. C. (2005). Tangled webs: Reciprocal flows of invertebrate prey link streams and riparian zones. *Freshwater Biol.* 50, 201–220. doi: 10.1111/j.1365-2427.2004.01328.x

Bêche, L. A., Connors, P. G., Resh, V., and Merenlender, A. (2009). Resilience of fishes and invertebrates to prolonged drought in two california streams. *Ecography* 32, 778–788. doi: 10.1111/j.1600-0587.2009.05612.x

Beechie, T. J., Liermann, M., Beamer, E. M., and Henderson, R. (2005). A classification of habitat types in a large river and their use by juvenile salmonids. *Trans. Am. Fisheries Soc.* 134, 717–729. doi: 10.1577/T04-062.1

Beechie, T. J., and Sibley, T. H. (1997). Relationships between channel characteristics, woody debris, and fish habitat in northwestern washington streams. *Trans. Am. Fisheries Soc.* 126, 217–29. doi: 10.1577/1548-8659(1997)126<0217:RBCCWD>2.3.CO;2

Benda, L., Poff, L., Miller, D., Dunne, T., Reeves, G., Pess, G., et al. (2004). The network dynamics hypothesis: how channel networks structure riverine habitats. *BioScience* 54, 413–427. doi: 10.1641/0006-3568(2004)0540413:TNDHHC2.0.CO;2

Bilby, R. (1981). Role of organic debris dams in regulating the export of dissolved and particulate matter from a forested watershed. *Ecology* 62, 1234–1243. doi: 10.2307/1937288

Bolla Pittaluga, M., Coco, G., and Kleinhans, M. G. (2015). A unified framework for stability of channel bifurcations in gravel and sand fluvial systems. *Geophys. Res. Lett.* 42, 7521–7536. doi: 10.1002/2015GL065175

Bolla Pittaluga, M., Repetto, R., and Tubino, M. (2003). Channel bifurcation in braided rivers: equilibrium configurations and stability. *Water Res. Res.* 39:112. doi: 10.1029/2001WR001112

Boulton, A. J., Findlay, S., Marmonier, P., Stanley, E. H., and Valett, H. M. (1998). The functional significance of the hyporheic zone in streams and rivers. *Ann. Rev. Ecol. Syst.* 29, 59–81. doi: 10.1146/annurev.ecolsys.29.1.59

Braddock, W. A., and Cole, J. C. (1990). *Geologic Map of Rocky Mountain National Park and Vicinity*. Colorado. IMAP.

Braudrick, C. A., Dietrich, W. E., Leverich, G. T., and Sklar, L. S. (2009). Experimental evidence for the conditions necessary to sustain meandering in coarse-bedded rivers. *Proc. Nat. Acad. Sci.* 106, 16936–16941. doi: 10.1073/pnas.0909417106

Brooks, A. P., Brierley, G. J., and Millar, R. G. (2003). the long-term control of vegetation and woody debris on channel and flood-plain evolution: insights from a paired catchment study in southeastern Australia. *Geomorphology* 51, 7–29. doi: 10.1016/S0169-555X(02)00323-9

Brummer, C. J., Abbe, T. B., Sampson, J. R., and Montgomery, D. R. (2006). Influence of vertical channel change associated with wood accumulations on delineating channel migration zones, washington, USA. *Geomorphology* 80, 295–309. doi: 10.1016/j.geomorph.2006.03.002

Buffington, J. M., and Montgomery, D. R. (1999). Effects of hydraulic roughness on surface textures of gravel-bed rivers. *Water Res. Res.* 35, 3507–3521. doi: 10.1029/1999WR900138

Burchsted, D., Daniels, M., Thorson, R., and Vokoun, J. (2010). The river discontinuum: applying beaver modifications to baseline conditions for restoration of forested headwaters. *BioScience* 60, 908–922. doi: 10.1525/bio.2010.60.11.7

Burge, L. M. (2006). Stability, morphology and surface grain size patterns of channel bifurcation in gravel–cobble bedded anabranching rivers. *Earth Surface Processes Landforms* 31, 1211–1226. doi: 10.1002/esp.1325

Burge, L. M., and Lapointe, M. F. (2005). Understanding the temporal dynamics of the wandering renous river, new brunswick, Canada. *Earth Surface Processes Landforms* 30, 1227–1250. doi: 10.1002/esp.1196

Carling, P., Jansen, J., and Meshkova, L. (2014). Multichannel rivers: their definition and classification. *Earth Surf. Processes Landforms* 39, 26–37. doi: 10.1002/esp.3419

Chang, H. H. (1979). Minimum stream power and river channel patterns. J. *Hydrol.* 41, 303–327. doi: 10.1016/0022-1694(79)90068-4

Cole, J. C., Trexler, J. H., Cashman, P. H., Miller, I. M., Shroba, R. R., Cosca, M. A., et al. (2010). Beyond colorado's front range—a new look at laramide basin subsidence, sedimentation, and deformation in north-central Colorado. *Field Guides* 18, 55–76. doi: 10.1130/2010.0018(03)

Collins, B. D., Montgomery, D. R., Fetherston, K. L., and Abbe, T. B. (2012). The floodplain large-wood cycle hypothesis: a mechanism for the physical and biotic structuring of temperate forested alluvial valleys in the north pacific coastal ecoregion. *Geomorphology*. 139–140, 460–70. doi: 10.1016/j.geomorph.2011.11.011

Curran, J. C., and Hession, W. C. (2013). Vegetative impacts on hydraulics and sediment processes across the fluvial system. *J. Hydrol.* 505, 364–376. doi: 10.1016/j.jhydrol.2013.10.013

Daniels, M. D., and Rhoads, B. L. (2004). Effect of large woody debris configuration on three-dimensional flow structure in two low-energy meander bends at varying stages. *Water Res. Res.* 40:181. doi: 10.1029/2004WR003181

Dixon, S. J. (2016). A dimensionless statistical analysis of logjam form and process. *Ecohydrology* 9, 1117–1129. doi: 10.1002/eco.1710

Dolloff, C. A., and Warren, M. L. (2003). "Fish relationships with large wood in small streams," in *American Fisheries Society Symposium, Vol. 37* (Bethesda, MD), 179–193.

Egozi, R., and Ashmore, P. (2008). Defining and measuring braiding intensity. *Earth Surface Processes Landforms* 33, 2121–2138. doi: 10.1002/esp.1658

Ehlen, J., and Wohl, E. (2002). Joints and landform evolution in bedrock canyons. *Trans. Jap. Geomorphological Union* 23, 237–255.

Fetherston, K. L., Naiman, R. J., and Bilby, R. E. (1995). Large woody debris, physical process, and riparian forest development in montane river networks of the pacific northwest. *Geomorphology* 13, 133–144. doi: 10.1016/0169-555X(95)00033-2

Flores, L., Larrañaga, A., Díez, J., and Elosegi, A. (2011). Experimental wood addition in streams: effects on organic matter storage and breakdown. *Freshwater Biol.* 56, 2156–2167. doi: 10.1111/j.1365-2427.2011.02643.x

Gibling, M. R., Nanson,G. C., and Maroulis, J.C. (1998). Anastomosing river sedimentation in the channel country of central Australia. *Sedimentology* 45, 595–619. doi: 10.1046/j.1365-3091.1998.00163.x

Gordon, N. D., McMahon, T. A., and Finlayson, B. L. (1992). *Stream Hydrology: An Introduction for Ecologists*. Toronto: Wiley.

Gradziński, R., Baryła, J., Doktor, M., Gmur, D., Gradziński, M., Kedzior, A., et al. (2003). Vegetation-controlled modern anastomosing system of the upper narew river (NE Poland) and its sediments. *Sedimentary Geol.* 157, 253–276. doi: 10.1016/S0037-0738(02)00236-1

Güneralp, Í., and Rhoads, B. L. (2011). Influence of floodplain erosional heterogeneity on planform complexity of meandering rivers. *Geophys. Res. Letters* 38, 2–7. doi: 10.1029/2011GL048134

Gurnell, A. M. (1998). The hydrogeomorphological effects of beaver dam-building activity. Progress in physical geography. *Earth Environ.* 22, 167–189. doi: 10.1177/030913339802200202

Gurnell, A. M. (2013). Wood in fluvial systems. *Treatise Geomorphol.* 9, 163–188. doi: 10.1016/B978-0-12-374739-6.00236-0

Gurnell, A. M., and Bertoldi, W. (2020). Extending the conceptual model of river island development to incorporate different tree species and environmental conditions. *River Res. Appl.* 36, 1730–1747. doi: 10.1002/rra.3691

Gurnell, A. M., Petts, G. E., Hannah, D. M., Smith, B. P. G., Edwards, P. J., Kollmann, J., et al. (2001). Riparian vegetation and island formation along the gravel-bed fiume tagliamento, Italy. *Earth Surf. Processes Landforms* 26, 31–62. doi: 10.1002/1096-9837(200101)26:1<31::AID-ESP155>3.0.CO;2-Y

Harwood, K., and Brown, A. G. (1993). Fluvial processes in a forested anastomosing river: flood partitioning and changing flow patterns. *Earth Surface Processes Landforms* 18, 741–748. doi: 10.1002/esp.3290180808

Henning, J. A., and Gresswell, R. A., and Fleming, I. A. (2006). Juvenile salmonid use of freshwater emergent wetlands in the floodplain and its implications for conservation management. *J. Fisheries Manage.* 26, 367–376. doi: 10.1577/M05-057.1

Herdrich, A. T., Winkelman, D. L., Venarsky, M. P., Walters, D. M., and Wohl, E. (2018). The loss of large wood affects Rocky Mountain trout populations. *Ecol. Freshw. Fish* 27, 1023–1036. doi: 10.1111/eff.12412

Hester, E. T., and Doyle, M. W. (2008). In-stream geomorphic structures as drivers of hyporheic exchange. *Water Res. Res.* 44, 5810. doi: 10.1029/2006WR005810

Hofmann, M. H., and Hendrix, M. S. (2010). Depositional processes and the inferred history of ice-margin retreat associated with the deglaciation of the cordilleran ice sheet: the sedimentary record from Flathead Lake, Northwest Montana, USA. *Sedimentary Geol.* 223, 61–74. doi: 10.1016/j.sedgeo.2009.10.004

Hollander, M., Wolfe, D. A., and Chicken, E. (2014). Nonparametric Statistical Methods. New York, NY: Wiley.

Hong, L. B., and Davies, T. R. H. (1979). A study of stream braiding. *GSA Bulletin* 90, 1839–1859. doi: 10.1130/GSAB-P2-90-1839

Jackson, K. J., and Wohl, E. (2015). Instream wood loads in montane forest streams of the colorado front range, USA. *Geomorphology* 234, 161–170. doi: 10.1016/j.geomorph.2015.01.022

Jarrett, R. D. (1990). Paleohydrologic techniques used to define the spatial occurrence of floods. *Geomorphology* 3, 181–195. doi: 10.1016/0169-555X(90)90044-Q

Järvelä, J. (2004). Determination of flow resistance caused by non-submerged woody vegetation. *Int. J. River Basin Manage.* 2, 61–70. doi: 10.1080/15715124.2004.9635222

Jeffres, C. A., Opperman, J. J., and Moyle, P. B. (2008). Ephemeral floodplain habitats provide best growth conditions for juvenile chinook salmon in a california river. *Environ. Biol. Fishes* 83, 449–458. doi: 10.1007/s10641-008-9367-1

Jeffries, R., Darby, S. E., and Sear, D. A. (2003). The influence of vegetation and organic debris on flood-plain sediment dynamics: case study of a low-order stream in the new forest, England. *Geomorphology* 51, 61–80. doi: 10.1016/S0169-555X(02)00325-2

John, S., and Klein, A. (2004). Hydrogeomorphic effects of beaver dams on floodplain morphology: avulsion processes and sediment fluxes in upland valley floors. *Quaternaire* 15219–231. doi: 10.3406/quate.2004.1769

Junk, W., Bayley, P., and Sparks, R. (1989). The flood pulse concept in river-floodplain systems. *Can. Pub. Fish. Aquatic Sci.* 106, 110–127.

King, W. A., and Martini, I. P. (1984). Morphology and recent sediments of the lower anastomosing reaches of the attawapiskat River. *Sedimentary Geology* 37, 295–320. doi: 10.1016/0037-0738(84)90019-8

Klavon, K., Fox, G., Guertault, L., Langendoen, E., Enlow, H., Miller, R., et al. (2017). Evaluating a process-based model for use in streambank stabilization: insights on the bank stability and toe erosion model (BSTEM). *Earth Surface Processes Landforms* 42, 191–213. doi: 10.1002/esp.4073

Kleinhans, M. G., Ferguson, R. I., Lane, S. N., and Hardy, R. J. (2013). Splitting rivers at their seams: bifurcations and avulsion. *Earth Surf. Processes Landforms* 38, 47–61. doi: 10.1002/esp.3268

Knighton, D. A., and Nanson, G. C. (1993). Anastomosis and the continuum of channel pattern. *Earth Surf. Processes Landforms* 18, 613–625. doi: 10.1002/esp.3290180705

Kondolf, G. M., Boulton, A. J., O'Daniel, S., et al. (2006). Process-based ecological river restoration: visualizing three-dimensional connectivity and dynamic vectors to recover lost linkages. *Ecol. Soc.* 11, 5. doi: 10.5751/ES-01747-110205

Larsen, L. G. (2019). Multiscale flow-vegetation-sediment feedbacks in low-gradient landscapes. *Geomorphology* 334, 165–193. doi: 10.1016/j.geomorph.2019.03.009

Laurel, D., and Wohl, E. (2019). The persistence of beaver-induced geomorphic heterogeneity and organic carbon stock in river corridors. *Earth Surf. Processes Landforms* 44, 342–353. doi: 10.1002/esp.4486

Le Lay, Y., Piégay, H., and Rivière-Honegger, A. (2013). Perception of braided river landscapes: implications for public participation and sustainable management. *J. Environ. Management* 119, 1–12. doi: 10.1016/j.jenvman.2013.01.006

Lesica, P. (1996). Using fire history models to estimate proportions of old growth forest in northwest Montana, USA. *Biol. Conserv.* 77, 33–39. doi: 10.1016/0006-3207(95)00130-1

Livers, B., and Wohl, E. (2021). All logjams are not created equal. *J. Geophys. Res.* 126, e2021JF.006076. doi: 10.1029/2021JF006076

Locke, W. W. (1995). Modelling of icecap glaciation of the northern rocky mountains of Montana. *Geomorphology* 14, 123–130. doi: 10.1016/0169-555X(95)00053-5

MacDonald, L. H., and Hoffman, J. A. (1995). Causes of peak flows in northwestern Montana and northeastern Idaho. *Water Resources Bulletin*, 31, 79–95. doi: 10.1111/j.1752-1688.1995.tb03366.x

Makaske, B. (1998). *Anastomosing Rivers: Forms, Processes and Sediments*. Nederlandse Geografische Studies (Netherlands).

Makaske, B. (2001). Anastomosing rivers: a review of their classification, origin and sedimentary products. *Earth Sci. Rev.* 53, 149–196. doi: 10.1016/S0012-8252(00)00038-6

Manga, M., and Kirchner, J. W. (2000). Stress partitioning in streams by large woody debris. *Water Res. Res.* 36, 2373–2379. doi: 10.1029/2000WR900153

Martín-Vide, J. P., Amarilla, M., and Zárate, F. J. (2014). Collapse of the pilcomayo river. *Geomorphology* 205, 155–163. doi: 10.1016/j.geomorph.2012.12.007

Marttila, H., Turunen, J., Aroviita, J., Tammela, S., Luhta, P. L., Muotka, T., et al. (2018). Restoration increases transient storages in boreal headwater streams. *River Res. Appl.* 34, 1278–1285. doi: 10.1002/rra.3364

Matheson, A., Thoms, M., and Reid, M. (2017). Does reintroducing large wood influence the hydraulic landscape of a lowland river system? *Geomorphology* 292, 128–141. doi: 10.1016/j.geomorph.2017.03.035

Montgomery, D. R., and Abbe, T. B. (2006). Influence of logjam-formed hard points on the formation of valley-bottom landforms in an old-growth forest valley, queets River, Washington, USA. *Quaternary Res.* 65, 147–155. doi: 10.1016/j.yqres.2005.10.003

Montgomery, D. R., Abbe, T. B., Buffington, J. M., Peterson, N. P., Schmidt, K. M., Stock, J. D., et al. (1996). Distribution of bedrock and alluvial channels in forested mountain drainage basins. *Nature* 381, 587–589. doi: 10.1038/381587a0

Montgomery, D. R., Beamer, E. M., Pess, G. R., and Quinn, T. P. (1999). Channel type and salmonid spawning distribution and abundance. *Can. J. Fish. Aquatic Sci.* 56, 377–387. doi: 10.1139/f98-181

Montgomery, D. R., and Buffington, J. M. (1997). Channel-reach morphology in mountain drainage basins. *GSA Bulletin* 109, 596–611 doi: 10.1130/0016-7606(1997)109<0596:CRMIMD>2.3.CO;2

Nadler, C. T., and Schumm, S. A. (1981). Metamorphosis of south platte and arkansas rivers, eastern Colorado. *Phys. Geography* 2, 95–115. doi: 10.1080/02723646.1981.10642207

Nanson, G. C., and Croke, J. C. (1992). A genetic classification of floodplains. *Geomorphology* 4, 459–486. doi: 10.1016/0169-555X(92)90039-Q

Nanson, G. C., Rust, B. R., and Taylor, G. (1986). Coexistent Mud braids and anastomosing channels in an arid-zone river: cooper creek, central australia. *Geology* 14, 175–178. doi: 10.1130/0091-7613(1986)14<175:CMBAAC>2.0.CO;2

O'Connor, J. E., Jones, M. A., and Haluska, T. L. (2003). Flood plain and channel dynamics of the quinault and queets rivers, Washington, USA. *Geomorphology* 51, 31–59. doi: 10.1016/S0169-555X(02)00324-0

Parker, C., Henshaw, A. J., Harvey, G. L., and Sayer, C. D. (2017). Reintroduced large wood modifies fine sediment transport and storage in a lowland river channel. *Earth Surf. Processes Landforms* 42, 1693–1703. doi: 10.1002/esp.4123

Parks, S. A., Miller, C., Parisien, M., Holsinger, L. M., Dobrowski, S. Z., Abatzoglou, J., et al. (2015). Wildland fire deficit and surplus in the western United States, 1984–2012. *Ecosphere* 6, 1–13. doi: 10.1890/ES15-00294.1

Piegay, H. (1993). Nature, mass and preferential sites of coarse woody debris deposits in the lower ain valley (Mollon Reach), France. *Regulated Rivers Res. Manage.* 8, 359–372. doi: 10.1002/rrr.3450080406

Poff, L., Allan, J. D., Bain, M. B., Karr, J. R., Prestegaard, K. L., Richter, B. D., et al. (1997). The natural flow regime. *BioScience* 47, 769–784. doi: 10.2307/1313099

Pollen-Bankhead, N., and Simon, A. (2010). Hydrologic and hydraulic effects of riparian root networks on streambank stability: is mechanical root-reinforcement the whole story? *Geomorphology* 116, 353–362. doi: 10.1016/j.geomorph.2009.11.013

Polvi, L. E., and Wohl, E. (2012). The beaver meadow complex revisited – the role of beavers in post-glacial floodplain development. *Earth Surf. Processes Landforms* 37, 332–346. doi: 10.1002/esp.2261

Puttock, A., Graham, H. A., Cunliffe, A. M., Elliott, M., and Brazier, R. E. (2017). Eurasian beaver activity increases water storage, attenuates flow and mitigates diffuse pollution from intensively-managed grasslands. *Sci. Total Environ.* 576, 430–443. doi: 10.1016/j.scitotenv.2016.10.122

R Core Team. (2022). *R: A Language and Environment for Statistical Computing*. Vienna: R Foundation for Statistical Computing.

Rathburn, S. L., Bennett, G. L., Wohl, E. E., Briles, C., McElroy, B., Sutfin, N., et al. (2017). The fate of sediment, wood, and organic carbon eroded during an extreme flood, Colorado Front Range, USA. *Geology* 45, 499–502. doi: 10.1130/G38935.1

Rinaldi, M., and Nardi, L. (2013). Modeling interactions between riverbank hydrology and mass failures. *J. Hydrol. Eng.* 18, 1231–1240. doi: 10.1061/(ASCE)HE.1943-5584.0000716

Rust, B. R. (1981). Sedimentation in an arid-zone anastomosing fluvial system; cooper's creek, central Australia. *J. Sedimentary Res.* 51, 745–755. doi: 10.1306/212F7D97-2B24-11D7-8648000102C1865D

Rust, B. R., Gibling, M. R., and Legun, A. S. (1985). *Coal Deposition in an Anastomosing-Fluvial System: The Pennsylvanian Cumberland Group South of Joggins, Nova Scotia, Canada*. London: John Wiley and Sons, Ltd.

Sawyer, A. H., Bayani Cardenas, M., and Buttles, J. (2011). Hyporheic exchange due to channel-spanning logs. *Water Res. Res.* 47:484. doi: 10.1029/2011WR010484

Schumann, R. R. (1989). Morphology of red creek, wyoming, an arid-region anastomosing channel system. *Earth Surf. Processes Landforms* 14, 277–288. doi: 10.1002/esp.3290140404

Schumm, S. A. (1968). *River Adjustment to Altered Hydrologic Regimen, Murrumbidgee River and Paleochannels*. Australia. U.S. Government Printing Office.

Schumm, S. A. (1985). Patterns of alluvial rivers. *Ann. Rev. Earth Planet. Sci.* 13, 5–27. doi: 10.1146/annurev.ea.13.050185.000253

Schumm, S. A., Erskine, W. D., and Tilleard, J. W. (1996). Morphology, hydrology, and evolution of the anastomosing ovens and king rivers, Victoria, Australia. GSA *Bulletin* 108, 1212–1224. doi: 10.1130/0016-7606(1996)108<1212:MHAEOT>2.3.CO;2

Sibold, J. S., Veblen, T. T., and Gonzalez, M. E. (2006). Spatial and temporal variation in historic fire regimes in subalpine forests across the Colorado Front Range in Rocky Mountain National Park, Colorado, USA. *J. Biogeography* 32, 631–647. doi: 10.1111/j.1365-2699.2005.01404.x

Simon, A., Curini, A., Darby, S. E., and Langendoen, E. J. (2000). Bank and near-bank processes in an incised channel. *Geomorphology* 35, 193–217. doi: 10.1016/S0169-555X(00)00036-2

Simon, A., Pollen-Bankhead, N., and Thomas, R. E. (2011). Development and application of a deterministic bank stability and toe erosion model for stream restoration. *Sci. Approach. Anal. Tools* 194, 453–474. doi: 10.1029/2010GM001006

Smith, D. G. (1973). Aggradation of the alexandra-north saskatchewan river, banff park, Alberta. *Fluvial Geomorphology*. 47, 201–19.

Smith, D. G. (1976). Effect of vegetation on lateral migration of anastomosed channels of a glacier meltwater river. *GSA Bulletin* 87, 857–860. doi: 10.1130/0016-7606(1976)87<857:EOVOLM>2.0.CO;2

Smith, D. G. (1983). *Anastomosed Fluvial Deposits: Modern Examples from Western Canada. Modern and Ancient Fluvial Systems*. London: John Wiley and Sons, Ltd.

Smith, D. G. (1986). Anastomosing river deposits, sedimentation rates and basin subsidence, magdalena river, northwestern Colombia, South America. *Sedimentary Geol.* 46, 177–196. doi: 10.1016/0037-0738(86)90058-8

Smith, D. G., and Smith, N. D. (1980). Sedimentation in anastomosed river systems; examples from alluvial valleys near banff, alberta. *J. Sedimentary Res.* 50, 157–164. doi: 10.1306/212F7991-2B24-11D7-8648000102C1865D

Sutfin, N. A., and Wohl, E. (2019). Elevational differences in hydrogeomorphic disturbance regime influence sediment residence times within mountain river corridors. *Nat. Commun.* 10, 2221. doi: 10.1038/s41467-019-09864-w

Tal, M., and Paola, C. (2007). Dynamic single-thread channels maintained by the interaction of flow and vegetation. *Geology* 35, 347–350. doi: 10.1130/G23260A.1

Triska, F. J. (1984). Role of wood debris in modifying channel geomorphology and riparian areas of a large lowland river under pristine conditions: a historical case study. *SIL Proc.* 22, 1876–1892. doi: 10.1080/03680770.1983.11897589

USDA. (2022). *Natural Resource Conservation Service Web Soil Survey*. Available online at: https://www.nrcs.usda.gov/wps/portal/nrcs/main/soils/survey/ (accessed January, 2023).

Venarsky, M. P., Walters, D. M., Hall, R. O., Livers, B., and Wohl, E. (2018). Shifting stream planform state decreases stream productivity yet increases riparian animal production. *Oecologia* 187, 167–180. doi: 10.1007/s00442-018-4106-6

Wilhelmsen, K., Sawyer, A. H., Marshall, A., McFadden, S., Singha, K., Wohl, E., et al. (2021). Laboratory flume and numerical modeling experiments show log jams and branching channels increase hyporheic exchange. *Water Res. Res.* 57, 030299. doi: 10.1029/2021WR030299

Wohl, E. (2011). Threshold-induced complex behavior of wood in mountain streams. *Geology* 39, 587–590. doi: 10.1130/G32105.1

Wohl, E. (2013). Floodplains and wood. *Earth Sci. Reviews* 123, 194–212. doi: 10.1016/j.earscirev.2013.04.009

Wohl, E. (2017). Connectivity in rivers. *Prog. Phys. Geography* 41, 345–362. doi: 10.1177/0309133317714972

Wohl, E., and Cadol, D. (2011). Neighborhood matters: patterns and controls on wood distribution in old-growth forest streams of the colorado front range, USA. *Geomorphology* 125, 132–146. doi: 10.1016/j.geomorph.2010.09.008

Wohl, E., Lininger, K. B., and Scott, D. N. (2018). River beads as a conceptual framework for building carbon storage and resilience to extreme climate events into river management. *Biogeochemistry* 141, 365–383. doi: 10.1007/s10533-017-0397-7

Wohl, E., Marshall, A. E., Scamardo, J., White, D., and Morrison, R. R. (2022). Biogeomorphic influences on river corridor resilience to wildfire disturbances in a mountain stream of the southern rockies, USA. *Sci. Environ.* 820, 153321. doi: 10.1016/j.scitotenv.2022.153321

Wohl, E., Rathburn, S., Chignell, S., Garrett, K., Laurel, D., Livers, B., et al. (2017). Mapping longitudinal stream connectivity in the north vrain Creek watershed of Colorado. *Geomorphology* 277, 171–181. doi: 10.1016/j.geomorph.2016.05.004

Woo, M., and Waddington, J. M. (1990). Effects of beaver dams on subarctic wetland hydrology. *Arctic* 43, 223–230. doi: 10.14430/arctic1615

frontiers | Frontiers in Water

TYPE Original Research
PUBLISHED 14 September 2023
DOI 10.3389/frwa.2023.1174570

OPEN ACCESS

EDITED BY
Ronald Erwin Pöppl,
University of Vienna, Austria

REVIEWED BY
Jonathan Phillips,
East Carolina University, United States
Anthony Parsons,
The University of Sheffield, United Kingdom

*CORRESPONDENCE
Boris Faybishenko
✉ bafaybishenko@lbl.gov

RECEIVED 26 February 2023
ACCEPTED 07 August 2023
PUBLISHED 14 September 2023

CITATION
Hunt AG, Ghanbarian B and Faybishenko B (2023) A model of temporal and spatial river network evolution with climatic inputs. *Front. Water* 5:1174570. doi: 10.3389/frwa.2023.1174570

A model of temporal and spatial river network evolution with climatic inputs

Allen G. Hunt[1], Behzad Ghanbarian[2] and Boris Faybishenko[3]*

[1]Department of Physics, Wright State University, Dayton, OH, United States, [2]Porous Media Research Lab, Department of Geology, Kansas State University, Manhattan, KS, United States, [3]Lawrence Berkeley Laboratory, Berkeley, CA, United States

Predicting the temporal and spatial evolution of the river network is part of the Earth's critical zone investigations, which has become an important endeavor. However, modeling integration of the river network and critical zone over millions of years is rare. We address the problem of how to predict integrated river length development as a function of time within a framework of addressing the critical zone depth as a function of time. In case of groundwater-river interaction, we find a *non-linear* spatio-temporal scaling relationship between time, t, and total river length L, given by $t \approx L^p$ with power p being near 1.2. The basis of our model is the presumption that groundwater flow paths are relevant to river integration. As river integration may proceed over disconnected basins with irregular relief, the relevant optimal subsurface flow paths are proposed to be defined within a 3D network, with optimal path exponent 1.43. Because the 2D model of the river length has already been shown to relate to a power of the Euclidean distance across a drainage basin with the predicted universal optimal path exponent from percolation theory, $D_{opt} = 1.21$, the optimal groundwater paths should relate to the surface river length with an exponent equaling the ratio $1.43/1.21 = 1.18$. To define a predictive relationship for the river length, we need to use specific length and time scales. We assume that the fundamental specific length scale is a characteristic particle size (which is commonly used to define the pore scale flow network), and the fundamental time scale is the ratio of the particle size to the regional groundwater flow rate. In this paper, we consider cases of predicting spatio-temporal scaling of drainage organization in the southwestern USA–the Amargosa, Mojave, Gila (and its tributaries) and the Rio Grande, and Pecos Rivers. For the Mojave and Gila Rivers, theoretical results for time scales of river integration since ca. 10 Ma are quite predictive, though the predicted time scales exceed observation for the Rio Grande and Pecos.

KEYWORDS

river, network, scaling, fractals, percolation, drainage

1. Introduction

The organization of river drainage systems has an impact on many aspects of geology, geomorphology, and hydrology, including flood magnitude-frequency relations, the water cycle, tectonic response to erosion and its inverse, and so forth. Drainage organization is also key to the type of sediments that rivers deliver to sedimentary basins, since the spatial extent of the drainage basin also controls the sediment transport sources. Important factors limiting the volume of sediments transported are the rate of chemical weathering of bedrock and its conversion to soil (Dixon and Heimsath, 2009; DiBiase and Heimsath, 2012; Egli et al., 2018). DiBiase and Heimsath (2012), and the close relationship between soil erosion

and soil production rates, which are mostly water flux-limited through chemical weathering (e.g., Egli et al., 2018), or, equivalently (Maher, 2010; Stolze et al., 2023), by residence times. Flow rates, of course, depend on specific drainage architecture as well as climatic variables. Thus, predicting the two-dimensional extent of a drainage system together with the rates of weathering of the bedrock and transport of sediments, is the foundation for predicting the total volume and kind of sediments ultimately delivered to sedimentary basins. Indeed, dates for a reorganization of drainage systems are frequently extracted by dating changes in the provenance of deltaic sediments (Matthews et al., 2001; Said et al., 2015; Fielding et al., 2018). Overall, water fluxes, surface and subsurface, can be viewed as primary agents of the evolution of both lateral and vertical dimensions of drainage basins.

Within a river basin, water drains through many smaller watersheds to a large river. Watershed forming factors are: tectonics, climate, vegetation cover, topography, shape, size, soil type, and land use in urban, agriculture, and natural areas (Rhoads, 2020). Beyond the rough descriptions named, characteristics of drainage system organization are quantified in many ways (Horton, 1932, 1945; Schumm, 1956; Strahler, 1964; Scheidegger, 1965; Shreve, 1967). In recognition of the statistical regularities in drainage form and architecture (Kirchner, 1993), a range of principles governing the structural features of river drainages has been proposed (Maritan et al., 1996; Rigon et al., 1996; Pelletier, 1999; Bejan and Errera, 2011). Specific drainage reorganization processes identified include headward erosion through spring sapping (Laity and Malin, 1986; Baker et al., 1990), capture (Young and Spamer, 2001), or basin fill and sill overtopping (Meek, 1989, 1990; Hilgendorf et al., 2020), or combinations of such mechanisms. The basis for such mechanisms lies in combinations of erosion processes; those driven by water can either be mostly chemical or physical in basis, surface or subsurface in location.

Following previous studies (Willgoose et al., 1991; Tucker and Bras, 2000; Gunnell and Harbor, 2010; Willett et al., 2014), we focus on tectonic and climatic drivers of basin (re)organization. Tectonic influences are assumed mainly to be disaggregating (i.e., breaking up), while the convergence of groundwater flow fields (and the flow rate) is assumed to be the ultimate "engineer" of organization. To illustrate the contrasting roles of tectonics and climate, development of surface structures such as mountains and faults can disrupt surface and subsurface flow fields. But subsurface flow fields can reorganize in response to changing regional subsurface gradients in a variety of ways, i.e., chemical dissolution and erosion, which are linked to the surface hydrological processes and organization (Petroff et al., 2013) through surface lowering, thereby influencing surface and subsurface convergence upstream; or through subsurface flow convergence and spring sapping (Laity and Malin, 1986; Baker et al., 1990); or through surface convergence further downgradient, the latter two of which both promote headward erosion. Another particular means by which groundwater flow affects surface erosion processes of a stream is detailed by Xiangjiang and Niemann (2006) below. In our work here, the influence of climate on drainage basin reorganization is expressed predominantly in groundwater flow rates, which are known to be proportional to the difference between precipitation and evapotranspiration (Maxwell et al., 2016).

As Xiangjiang and Niemann (2006) discuss, the river-groundwater interaction occurs primarily in two ways: streams can gain or lose water from inflow or outflow of groundwater through the streambed. In a gaining reach, the water table slopes down toward the stream, but in a losing reach, it slopes away from the stream. Therefore, in arid regions, erosional processes are favored for gaining reaches or streams, and depositional for losing reaches or streams (Grant, 1948). Basin fill is accordingly promoted in losing reaches. Thus, particularly in arid zones, where the surface runoff may be strongly elevation-dependent, both basin fill and sill erosion rates can be enhanced simultaneously, depending on groundwater flow rates. Even in areas where relief is insufficient to generate a climatic signal in groundwater flow rates, we note that in the opposite extreme of river impoundment by dams, failure, and thus reintegration, can occur at least as often by piping as by overtopping (Zhang et al., 2016).

For the above reasons, we model drainage (re)organization as controlled by the assembly of groundwater flow paths into optimal networks. Our present approach, which is scale-independent in concept, is based on a hypothesis quantifying the organization of optimal groundwater flow paths between two vertical planes – a divide and a river – and thus has most in common with Bejan and Errera's (2011) optimization of flow paths between a line and a point. However, our emphasis is on the organization of subsurface flow paths through a three-dimensional optimization. Our description may appear to situate our understanding as allied to headward erosion and capture (as opposed to basin fill and overtopping) as specific reorganization mechanisms, but we would only conclude that purely surface processes dominate integration rates when groundwater fluxes, as expressed in our proposed scaling relationship, do not generate the appropriate time scale for the organization. We, therefore, argue that such a concrete analytical formulation based on groundwater flow speeds may help distinguish when groundwater processes are the limiting process on drainage development and/or reorganization rates, regardless of whether the drainage reorganization is from the bottom up (Young and Spamer, 2001; Dickinson, 2015) or from the top down (Spencer et al., 2001; Repasch et al., 2017).

Our goal is to predict river lengths that can be integrated/achieved over a given time period of evolution which is initialized by tectonic triggers, such as onset of rifting or lateral shifting and mediated by groundwater flow field reorganization. As the surface expression of this organization, namely the river itself, is already known to be compatible with a river sinuosity controlled by the two-dimensional optimal path exponent (Hunt et al., 2021), the groundwater flow architecture, whose organization can extend to kilometer depths, is suggested to relate to the three-dimensional optimal path tortuosity. Our focus on a simple organizational principle does not deny influence of other factors; rather, we suggest a possible means to develop a hierarchy in the importance of influences on drainage basin evolution, on the basis of which it may be possible to more clearly identify anomalies and exceptions to trends. For example, wherever surface and subsurface flow networks do not integrate well, such as in karsts, our understanding may be less helpful.

The data addressed here derive from drainage basin changes between about 100Ma and 10ka; thus, anthropogenic effects such

as agriculture and urbanization are considered negligible. Though the specific pattern of a drainage basin may have an influence on the spatio-temporal scaling of the network, we will neglect the potential impact of this factor at this time. Our initial assumption is that the primary influence of the variability that drainage patterns exert on changes in stream organization can be traced to their influence on subsurface flow paths and rates. It turns out that the dependence of the time for the organization on the fundamental length scale is very weak; therefore, on account of the universality assumed for the flow path tortuosity, it will be necessary only to account for the flow rate(s), when these can be identified.

2. Objectives

In this study, we aim to develop a model to predict a single characteristic of the (re)organization of drainage basins under conditions of climate (change) and tectonic driving forces, namely how overall stream lengths change through the process of stream capture, sapping, or other processes related to groundwater flow. The model developed is then applied to a range of observations to determine when it may, or may not, be accurate. The theoretical framework developed is based on our suggested principles of mostly tectonic triggers and the organization of the response through groundwater flow as influenced by climate. Our framework is generally consistent with previous work (Hunt, 2016a; Hunt et al., 2021), though some uncertainty in explanation is clarified. By comparing with observation, we attempt to diagnose the general means by which the drainage integration has proceeded.

3. Theory

3.1. Background

In this section, we develop the spatio-temporal scaling relationship, relating it to previous research. It has been claimed that the range of Hack's (1957) law exponents relating river length to drainage basin area is 0.57 – 0.6 (Maritan et al., 1996). Because it is known that the Euclidean length across drainage basins is proportional to the drainage basin area to the power of 0.5 (Church and Mark, 1980; Montgomery and Dietrich, 1992). It is logical to relate river sinuosity to optimal 2D percolation, so that the exponent in Hack's law becomes simply half the sinuosity exponent. In percolation theory, sinuosity exponent values range from 1.13 (Ghanbarian et al., 2013) for the simple tortuosity of a river assembled through random connections across a homogeneous substrate to 1.21 for the optimal path exponent (Porto et al., 1997) describing the tortuosity of the connected path of least resistance when the substrate is highly heterogeneous. The above cited relationship between area and Euclidean basin length then leads to a range of predicted Hack's law exponents from 0.565 to 0.605.

Here, we suggest that the optimal path exponent is the correct choice (producing Hack's law exponent 0.605, Rigon et al., 1996) and that the significant variability in conformance of real data to this prediction is possibly a consequence of climatic variability, though Hack's law may overpredict river sinuosity in large drainage basins. Nevertheless, if the interconnected paths for groundwater flow are not more tortuous than the surface paths followed by the streams, then we would predict that the stream assemblage process leads to a linear relationship of the stream length vs. time.

3.2. Model development

The model development is analogs to that used in the development of a model for predictions of the growth of plant roots as a function of time (Hunt, 2016b, 2017). The tortuosity of root growth was hypothesized to be governed by the optimal path exponent of percolation theory. This exponent describes the (fractal) tortuosity of the path through highly disordered 2D or 3D porous media, which produces the minimum total resistance (Porto et al., 1997). This model generates a preferred direction, from smaller orders to larger order, in accord with optimality concepts in energy, which has also been used in drainage basin development treatments (Maritan et al., 1996; Rigon et al., 1996; Bejan and Errera, 2011). Our theoretical development here addresses the organization of optimal flow paths in the subsurface and their effects on drainage reorganization. We suggest that, above a threshold length scale, the surface expression of these optimal flow paths is the drainage network. It is already known that, in Florida, features of stream bifurcation and channel initiation are related to the convergence of groundwater flow paths (Petroff et al., 2013). Furthermore, characteristics of amphitheaters on the Colorado Plateau can be traced to subsurface chemical weathering and erosion from groundwater flow (Laity and Malin, 1986; Baker et al., 1990). These results lend support to our theoretical development. It may still be surprising that the present theoretical development relates large-scale results to pore-scale processes.

We treat the subsurface as a complex network, with heterogeneity on a wide range of scales, from the pore, through the core and facies, and on through structural and landscape to the tectonic scale. At none of these scales do we consider any particular model of the heterogeneity; we simply assume that it exists and is large, adding orders of magnitude potential variability to local flow rates for a given pressure difference. When percolation concepts can be applied to find the dominant flow paths, the range of possible media that allow application of universal percolation results is wide (Hunt et al., 2014).

The second basic assumption is that the dominant surface flow paths are those for which the cumulative resistance is minimized – a quantification of the general concept that water chooses the path of least resistance. This optimization is assumed to be constrained to a thin, roughly horizontal layer; thus, we seek an optimal path in two dimensions (2D). For any Strahler stream order, we make the additional assumption that this path connects two lines; the next higher order stream and any divide. Under such assumptions, the actual length of a river, L from, e.g., a continental divide to its junction with streams of increasing order should be the following function of the (shortest) Euclidean connecting distance, d,

$$L = C_1 d^{1.21} \tag{1}$$

where 1.21 is the percolation theoretical value for the optimal path exponent in 2D (Porto et al., 1997), and C_1 is an unknown

constant. Because d is known to relate to drainage basin area A according to the simple relationship from Euclidean geometry (Montgomery and Dietrich, 1992; proportional to $A^{1/2}$, Church and Mark, 1980), Eq. (1) (Hunt, 2016a) also yields the Hack-type relationship given by

$$L \sim A^{0.605} \tag{2}$$

with an acceptable value of Hack's exponent, sometimes considered to be between 0.57 and 0.6 (Gray, 1961; Maritan et al., 1996; Rigon et al., 1996).

Our fundamental new hypothesis is that the optimal 3D path model provides the tortuosity of the constructed interconnected groundwater flow paths with the lowest cumulative resistance. It is known that the length of such a path, s, connecting two perpendicular planes (the vertical extension of the two lines above) is proportional to the Euclidean separation of the planes, d, to the power D^{opt}, which in 3D is equal to 1.43 (Sheppard et al., 1999). Thus, $s = C_2 d^{1.43}$. The magnitude of the constant, C_2, is not important at this point (see the discussion in the next paragraph). As the stream length, L, is proportional to $d^{1.21}$, this makes $s = C' L^{1.43/1.21} = C' L^{1.18}$, with C' being another constant. In order to make this relationship predictive involving space and time, we need to include in a model fundamental length and time scales. In these choices we are guided by the analogy to the formulation of the scaling relationships for root growth in soil.

A spatio-temporal scaling relationship with similarity to Eq. (1) has been proposed to relate root length RL to root radial extent, RRE, with $RL = K * RRE^{1.21}$ where K is a constant. In that case, the assumption that the root tip extension rate is constant in time leads to the spatio-temporal scaling equation (Hunt, 2017)

$$t = t_0 \left(\frac{x}{x_0} \right)^{1.21} \tag{3}$$

with t_0 and x_0 being fundamental time and length scales required by dimensional analysis. Reorganizing Eq. (3) yields,

$$x = x_0 \left(\frac{t}{t_0} \right)^{1/1.21} \tag{4}$$

Predictions using the non-linear relationships, such as Eqs. (3) and (4), require reference to particular scales, even though they are scale-free, at least over a wide range of spatial and temporal scales. Since the fractal nature of optimal paths in a heterogeneous medium extends from the pore scale to the maximum extent of the critical zone, we chose (Hunt et al., 2021) the typical, or median, particle size to define the fundamental length scale x_0 in Eq. (4). A typical particle size was suggested to be the middle of the silt range, at about 0.00003 m, or 30 μm. Then, in Eq. (4), the ratio x_0/t_0 represents an annual mean vadose zone flow rate. If vadose zone flow is not limited by the hydraulic conductivity of the shallow soil, it is related to the difference between climatic variables – precipitation and evapotranspiration, i.e., it is strongly climate-dependent.

To take into account the vadose zone flow rate, we can rewrite Eq. (4) in the following form (Hunt, 2017):

$$x = x_0 \left(\frac{t}{\frac{x_0}{v_0}} \right)^{1/1.21} \tag{5}$$

Values of v_0 ranged across Earth's climate systems from about 0.025 m/yr (near a minimum for appreciable growth of vascular plants) to about 25 m/yr. One can see that the predictions using Eq. (5) are sensitive to the flow rate, v_0, but nearly insensitive to the fundamental length scale $x_0/(x_0)^{0.83} = x_0^{0.17}$. Thus, an error in the choice of x_0 of a factor of 1000, produces an error in L of a factor near 3.

Using Eq. (5) as an analogy for predicting the spatio-temporal scaling of river networks, retaining the fundamental spatial scale of about 30 microns, but with two distinctions, we can obtain a spatio-temporal scaling equation for the river length, $L = (1/C')s^{1/1.18} = (1/C')\,(t/(x_0/v_0))^{1/1.18}$. One difference from Eq. (5) is in the exponent, which we proposed above should be derived from the quotient 1.43/1.21 = 1.18 (nearly the value, 1.21, for plant growth). The second change is that we employ results for regional groundwater flow rates, v_G, instead of vadose zone mean flow rates, v_0.

We access a result for a typical $v_G = 10\,m\,yr^{-1}$ – $20m\,yr^{-1}$ for groundwater from Blöschl and Sivapalan (1995) with about an order of magnitude variability on either side, which would be something like $1.5m\,yr^{-1}$ to $150m\,yr^{-1}$. According to Bloemendal and Theo (2018) high groundwater flow velocity means $v_G > 25\,m\,yr^{-1}$. And, as the US Geological Survey (2021) puts it "A velocity of 1 foot per day or greater is a high rate of movement for ground water, and ground-water velocities can be as low as 1 foot per year." These latter range corresponds to a range of $0.3\,m\,yr^{-1}$ up $110\,m\,yr^{-1}$. We will take a somewhat narrower (and cleaner) range of $1\,m\,yr^{-1}$ to $100\,m\,yr^{-1}$ to characterize the common spread in these flow rates, a range nearly the same as suggested by Blöschl and Sivapalan (1995). For example, desert regions in both southern California (Kulongoski et al., 2003) and the Sudan (Gossel et al., 2004) have known groundwater flow rates of about $1\,m\,yr^{-1}$. However, in Germany, typically reported values of groundwater flow velocities in the Rhein graben are closer to the upper limit cited by USGS, and can exceed that limit significantly (https://www.umwelt-online.de/regelwerk/cgi-bin/suchausgabe.cgi?pfad=/wasser/ltws/26b.htm&such=RdErl). Nevertheless, when the flow rate for a given system is known, that rate should be utilized, in order to apply Eq. (5) appropriately.

4. Data and sources

Our fundamental assumption is that basin reorganization is triggered by tectonic processes, such as the initiation of faulting due to plate collisions, extensional rifting, or strike-slip transpressional or transtensional strains. The interval is thus measured starting with the trigger event (may also be due to a previous stream capture) and ending with the integration of the drainage. Such length and time scales, while not arbitrary, are also not unambiguous, and considerable uncertainty is present. Frequently, neither the date of the initiation of the drainage basin change nor that of its equilibration is known accurately. For dates that were given in geologic terms, such as early Pleistocene, we used the standard mean of the stated interval. Dates of tectonic triggers are more broadly defined, while discrete steps of drainage integration (or disintegration) due to steam captures are sometimes more narrowly defined. Sometimes river lengths are not reported,

but only annexed drainage basin areas are given. In such cases, Eq. (2), Hack's law (with constant 1.4, when expressed in miles, Rigon et al. (1996), but 2.24, when the constant is expressed in kilometers), could be applied to estimate a river length. Although we applied Hack's original deduced value for C in the two cases where it was necessary, the existence of additional influences on the sinuosity cannot be ruled out. Stream capture occurs by headward erosion of, typically, a second stream at a lower elevation or with greater flow. Such progressions are considered to be bottom up processes. In each type of reorganization, we consider that subsurface flow rates are crucial to the time scale of reorganization.

Because a number of river systems included here were already discussed in Hunt et al. (2021), only those drainages introduced or expanded on here are discussed in what follows.

4.1. Sources

4.1.1. General, at any scale

Two studies of Marshall et al. (2003) and of Mather et al. (2002), cited in Dorsey and Roering (2006), document headward erosion of streams in Costa Rica and Spain, respectively by distances 20 km and 80 km in times of 100 kyr and 320 kyr.

Struth et al. (2020) discussed the reorganization of the 170 km Suarez River basin in Colombia, including its piracy of additional smaller basins along its east side, over a 405 kyr period from its capture by the Magdalena. However, specific distances for the smaller events were not possible to extract. Fan et al. (2018) demonstrated the reorganization of the Daotang basin within 80 kyr of the capture of Yihe River by the Chaiwen, adding 25 km^2 to the Yihe River drainage. Hack's law was used to generate a river length from the basin area.

Goudie (2005) notes that the river systems of Africa are some of the most ancient in the world, dating to the Mesozoic, but that Cenozoic reorganization of several has been important, in particular the Nile, the Niger, and the Limpopo/Zambezi system. The Blue Nile and Niger are discussed in Hunt et al. (2021). For the third system (Limpopo/Zambezi), Said et al. (2015) note that the southern Mozambique basin began filling with sediments much more rapidly about 25 Ma at both the Limpopo and Zambezi River deltas (Matthews et al., 2001; Said et al., 2015), but that superposed on that there was a dramatic shift of sediment volume from the Limpopo to the Zambezi at 5 Ma. This they interpret in terms of an onset of uplift at 25Ma and a capture of the upper Limpopo by the Zambezi at the latter date. The time interval Is 20 Myr, the site of capture is upstream of Victoria Falls, and the length of the Zambezi above there is about 1100 km.

We consider a brief discussion of the drainage reorganization of North America summarized by Wang et al. (2020). According to their Figure 1, drainage of most of the USA was to the north in the early Cretaceous (mean age 122Ma). By the late Paleocene (56Ma) the drainage from roughly the present USA Canada border was to the south, with a kind of paleo-Missouri-Mississippi system extending from Idaho through the middle of the continent, before turning south to the Gulf of Mexico. A model for the length of such a river is the present Missouri-Mississippi, which is 5950 km. By the Eocene (mean age 45Ma) a river drainage had formed parallel to the Rio Grande, which started in southern central present-day Arizona and flowed to the Gulf of Mexico, for which the present Rio Grande length (3016 km) is a reasonable model. Although other estimates could potentially be mined from the map, the relative uncertainty in the time frames for the shorter drainages will be higher, given the diminution of the detail of the recorded inferences.

4.1.2. The (semi-) arid southwestern USA

4.1.2.1. Rio Grande and Pecos

Repasch et al. (2017) describe the development of the Rio Grande in a top-down evolution starting in the San Juan range of southern Colorado at 8Ma. By about 5.7Ma, it had arrived in the lower San Luis Basin of New Mexico, by 5.3 Ma, Albuquerque, by about 4.5 Ma, the Palomas Basin, and by 3.1Ma, the Mesilla Basin near El Paso. The Rio Grande arrived at the Hueco Basin further southeast downstream by 2.06Ma and reached the already existing Pecos River and thus the Gulf of Mexico by 0.8Ma. Information for the Pecos comes from Figure 20 of Repasch et al. (2017) and the statements that at 5.3Ma, the Pecos was divided into two separate segments, one flowing eastward to the Ogallala aquifer and one flowing northwards from the border of Texas. These two had integrated as far south as Texas by 4.5Ma and the Pecos without the Rio Grande was fully integrated to the Gulf of Mexico by about 1.5Ma. An important trigger for the integration of the Pecos may have been the onset of the southwest monsoon at 6Ma.

According to Sanford et al. (2004), groundwater in the middle Rio Grande Basin, in Albuquerque, contains a thin veneer of water with source from the Rio Grande itself overlying groundwater from mountains on both the east and west sides of the Rio Grande rift. The layer immediately below the young water from the river itself has a source in the Jemez mountains, a little over 100 km to the north-northwest and a mean age of 19,000 yr. This value is consistent with a regional flow rate of $\sim$6 m yr^{-1}. That it may be reasonable to use such a value over much of the Rio Grande course is suggested by the review of McMahon et al. (2011), in which it is stated that late Pleistocene groundwater is common in the basins throughout the southwest and Great Plains, but exists further east only in confined aquifers. Any inference that Pleistocene groundwater flow rates may have been greater, as was the case for the Mojave River, was oblique, at best.

4.1.3. Mojave River and other inland southern California drainages

While the Mojave River was already addressed in Hunt et al. (2021), only two relevant data points were extracted there. The initiation of the Mojave River drainage system in California is considered to have occurred (Hillhouse and Cox, 2000) at about 3.8Ma and it became integrated to a length of 200 km by about 25ka. The Mojave River was dammed at Afton for 160 ky during pluvial climates before it finally breached the sill and advanced to the Soda Lake about 40 km downstream (Reheis et al., 2012). Less than 10kyr later, the Mojave River arrived in Dumont Lake, 50 km further, and likely reached Death Valley, nearly 150 km further downstream, but Holocene drying interrupted integration of this drainage system (Enzel et al., 2003). If the Pleistocene pluvial period had continued,

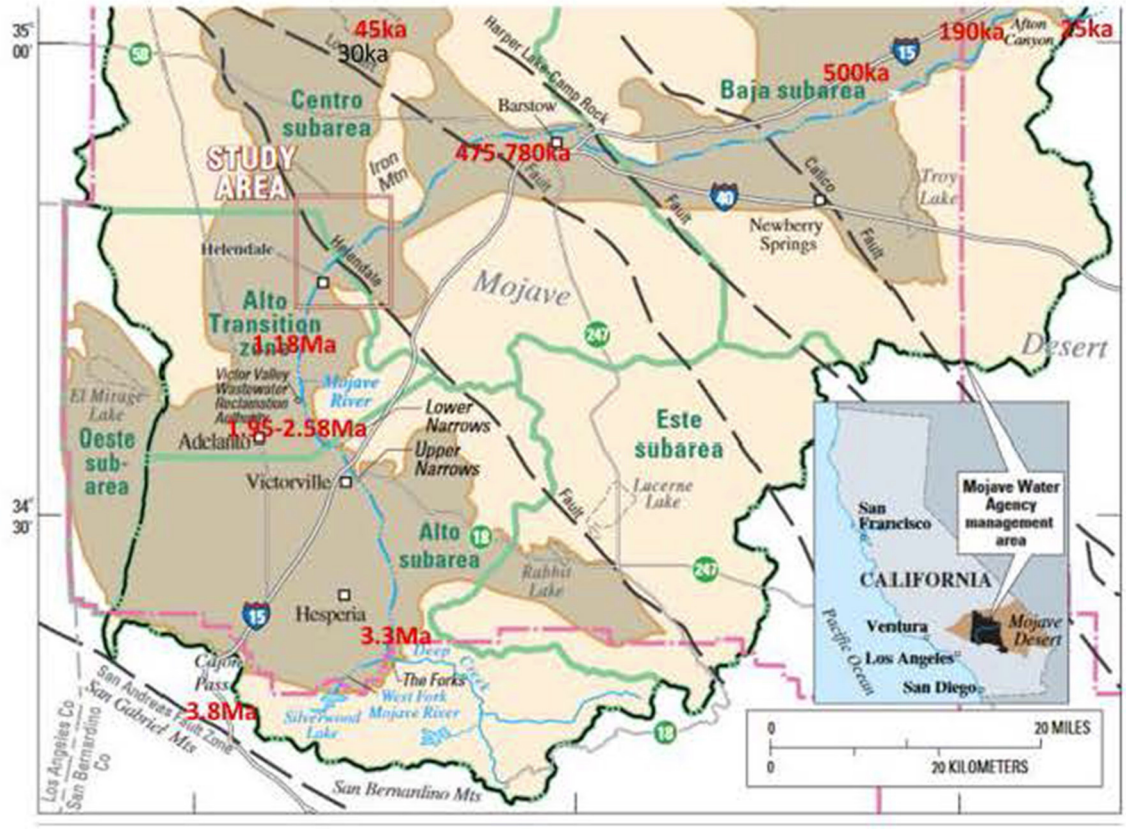

FIGURE 1
After Stamos et al. (2003) with temporal data superimposed from Hillhouse and Cox (2000), Reheis et al. (2012), Enzel et al. (2003), and Garcia et al. (2014). Boundaries of the Mojave River drainage are shown and the drainage area is shaded. Dates carry uncertainties, which are emphasized near Victorville and Barstow. Note that the placement of the date 3.8Ma is approximate, as it is outside the current drainage of the Mojave River (which has since been beheaded by the southeastward flowing Cajon Creek, Hillhouse and Cox, 2000).

its full integration to the distance of Death Valley would have been possible in the future.

The history of the Mojave River in southern California, northeast of the transverse ranges, has been studied by many authors, starting with Hillhouse and Cox (2000). Its known history begins at ~3.8Ma, and is associated with the uplift of the transverse ranges through transpression along the San Andreas fault. From these mountain ranges, the Mojave flows first north and then east to the eastern Mojave Desert. In this region of mostly disconnected, internal drainage systems, the climate is currently arid except in the mountains of the river's source. The Mojave River system currently is given as ~200 km in length, integrating several pluvial lake basins along its length. The specific process of integration cited is primarily basin fill and overtopping (Enzel et al., 2003). Times of the arrival of the Mojave River at various sites are mostly established by dating the bottom of lakebed sequences, or other deposits just below the lakebed sediments. A synthesis of research from various authors (Hillhouse and Cox, 2000; Enzel et al., 2003; Reheis et al., 2012; Garcia et al., 2014) allows us to place the approximate dates of arrival of the Mojave on the map in Figure 1.

Enzel et al. (2003) as well as Reheis et al. (2012) and Garcia et al. (2014) emphasize that the expansion of the Mojave River system to the northeast likely required a much wetter climate than currently, with rainfall much larger than at present. Overall, the evolutionary picture is of significant time periods with the Pacific storm track aimed either at northern California or even southern California (Enzel et al., 2003; Reheis et al., 2012). Kulongoski et al. (2003) give groundwater flow rates along the merged alluvial fans north of the transverse ranges as ca. 1m /yr over the last 20,000 years. However, Maxwell et al. (2016) observe that groundwater flow rates are proportional to the difference of P – ET (P = precipitation, ET evapotranspiration). Given rapidly decreasing flow rates with depth (e.g., Koltzer et al., 2019), higher flow rates are also associated with higher water tables. However, pluvial precipitation in the Mojave Desert has been estimated to have been 1.6 to 4 times higher than at present and temperatures 3 – 8 degrees lower (Harvey et al., 1999). An average of 1.6 and 4 is about 2.8, while the geometric mean is 2.53. The lower temperature likely increased the difference of P – ET further. Thus, groundwater flow rates during such Pleistocene climates with their higher precipitation are likely to have been higher than 1 m/yr by a factor 2–3 or more. Furthermore, Enzel et al. (2003) indicate: "Reducing modern rates of evaporation by 50%, and doubling modern rainfall would result in a full lake almost at the elevation of the Lake Mojave shoreline."

4.1.4. Amargosa River

The Amargosa River rises in southwestern Nevada and flows southward through extreme eastern California before turning west, and then north into Death Valley. It is a mostly ephemeral stream. The Amargosa River in Nevada and California has a history of feeding different lakes in the same (Tecopa) basin multiple times before finally advancing as far as the bottom of Death Valley The discussion here is limited to a quote from the abstract of Reheis et al. (2020). "The High lake reached the highest level achieved in the Tecopa basin, and it may have briefly discharged southward but did not significantly erode its threshold. The High lake was followed by a long hiatus of as much as 300 k.y., during which there is evidence for alluvial, eolian, and groundwater-discharge deposition, but no lakes. We attribute this hiatus, as have others, to blockage of the Amargosa River by an alluvial fan (ca. 20 km) upstream near Eagle Mountain." This discussion leaves us with an estimate for a data point 300k.y., 20 km. It is possible that, as the river system had previously been integrated below the fan, only the length of the segment related to the fan itself should be considered for the length. A better length scale might be 5 km, as the west side of Eagle Mountain is adjacent to the course of the Amargosa for about 5 km.

Over much of its length, the Amargosa River flows through a climate similar to that of the Mojave River drainage; as no additional information was found about groundwater flow rates, it was assumed that the values for the Mojave were probably reasonable first estimates for the Amargosa as well.

4.1.5. San Jacinto Mountains and River

Dorsey and Roering (2006) establish the adjustment of a drainage on the east (desert) side of the San Jacinto Mountains to the uplift. The advantage is in the analogy of its position to that of the Mojave River, on the lee side of the mountains bounding the coastal plain in Southern California, with strong similarity in climate, provenance, and relief. The measure involved is knick point migration, rather than drainage integration *per se*, which could be a disadvantage, as knick point migration incorporates a greater input from surface processes. From the authors, "The total distance of knick point migration is ∼ 30 km as measured along the Clark fault from the pre-SJFZ drainage divide at Borrego Mt. to the area of active stream capture points at the south edge of Burnt Valley. This distance appears to be a minimum because rocks on the NE side of the Clark fault are moving SE toward Borrego Mt. (on the SW side of the fault). An alternate measurement, from the pre-SJFZ divide on the NE side of the Clark fault to the area of modern stream captures at the edge of Burnt Valley, gives an along-fault distance of ∼ 44 km. These values are considered to bracket the total distance of knick point migration."

We use the mean of these two values, 37 km, for the length scale. Assigning a time interval to the process adds uncertainty, in view of its connection with the uplift of the San Jacinto Mountains. The onset of the uplift of the San Jacinto Mountains in southern California is considered to have been triggered by the initiation of offset along the San Jacinto fault. This has been a challenge on account of the necessity to apportion offsets among many approximately parallel faults over the relatively recent geologic time scale of about 2.5 million years. While disagreement in the timing of the onset has persisted, with some inferring a 2.5 Ma onset (based on a smaller rate of relative motion) more recently the geophysical data have been more uniformly understood to imply ca. 1Ma, or perhaps a few hundred thousand years earlier (Langenheim et al., 2004; Janecke et al., 2010).

A second inference, with greater uncertainty, is available from the coastal side of the San Jacinto Mountains. The San Jacinto River flows through two lake basins to merge with the Santa Ana River 68 km downstream from its source. However, its flow is only rarely sufficient to fill either basin, the San Jacinto (Wang et al., 1995) or Lake Elsinore (3 times since 1900 and 20 times since 1769, Kirby et al., 2007), and reach the Santa Ana River and, thereby, the ocean. This combination suggests a relatively recent integration of the San Jacinto River through its length (68 km). Note that the climate on the coastal side of these mountain ranges is significantly wetter than on the desert side, though the San Jacinto Mountains overall are drier than the San Bernardino and San Gabriel ranges, where the headwaters of the Mojave River are located. Additionally, due to the rainshadow effect from the Santa Ana Mountains (reaching 1620 m), the San Jacinto basin is the driest inland valley in southern California.

4.1.6. Gila River and tributaries

The Gila River system represents the longest integrated drainage system within the state of Arizona, excluding the through flowing Colorado River. Its chief moisture source and permanent stream tributaries originate in the mountains of the Mogollon Rim extending northwest to southeast from Arizona to New Mexico. These streams include the Verde River, Tonto Creek, and the Salt River.

Larson et al. (2020) state that, "A ca. 2.5 Ma age for the initiation of top-down integration of the Verde River from the upper Verde Valley into what are now downstream basins is consistent with the presence of a 3.3 Ma volcanic tephra…" "The basins depicted here were formerly endorheic, but integrated within the last ∼2.2–2.8 Ma. The integration of these basins resulted in the modern through-flowing drainage networks of the (320 km) Salt, (272 km) Verde, and Gila Rivers of central Arizona." The same time frame was implicitly extended to the Salt River. However, the integration of the Gila River itself has been a much longer process, commencing between 15Ma and 12Ma (13.5Ma mean) near the lower Colorado River and continuing to the present, where headward erosion is still occurring and, in discrete steps, lengthening the drainage into disconnected basins nearer the continental divide (Dickinson, 2015). Its length is currently 1044km.

In the text, Dickinson (2015) describes initiation of the incision of Quiburis Basin at 5.75Ma, the Safford Basin at 3.5Ma, and the Duncan Basin at 2Ma, in the process of headward erosion of the Gila River. He also states that headward erosion of the Santa Cruz River was finished by 2Ma. These dates correspond fairly closely to dates given on his maps in his Figures 6 and 7, which yield two data points on the Santa Cruz, two on the San Simon, and five on the San Pedro River. Two important dates are, however, missing. These are the date associated with the bifurcation at the confluence of the San Pedro and Gila Rivers, as well as the corresponding date

for a bifurcation near the confluence of the Santa Cruz and Gila Rivers. In neither case is it certain that the date is the same for the further evolution of both mainstem river and its tributary; however, it would be unjustified to assume two different dates. The date for the former bifurcation was estimated by extrapolation down the San Pedro from the last known date to find 7.5Ma, and the second by extrapolation down the Gila from the confluence with the San Pedro to find about 9.5Ma. The remaining dates are read off Dickinson's Figures 6 and 7. Upstream distances from the most recent dates given are also required. The distance from the site roughly midway between Duncan and Redrock to the Gila source was estimated at 300km.

For spring water emerging near the Mogollon Rim in the Verde River catchment, Beisner et al. (2018) find that the oldest ages were 4000-6000 years and those paths were traced to the southern slopes of the San Francisco peaks and the Flagstaff area, about 50 km to the north. This yields a flow rate of about 10 m/yr, but the aquifer is a fractured limestone, and the precipitation at the source is nearly the largest in the state. The same recharge area, located about 80 km from Grand Canyon Village, and somewhat further from Cataract Canyon, was determined to be a source for ancient (> 10,000 yr old) groundwater emerging from springs below the South Rim of the Grand Canyon (Solder et al., 2020). This ancient water mixed in various proportions, up to 100%, with local groundwater. This suggests a regional groundwater flow rate of <8 m/yr.

Tucson groundwater has a wide range of ages. Remaining groundwater in the vicinity of Tucson has been getting older as pumping has drawn down the water levels (Kalin, 1994). Experiments from 1965 revealed ages <2000 yr; by 1989, however, the maximum age had increased to over 6000 yr. In both cases, the greatest ages were found along the axis of the valley. The middle of the measured aquifer lies about 10 km from the recharge sources in the Tucson Mountains to the southwest and about 15 km from the Catalina and Rincon Mountains to the Northeast. Pertinent flow rates thus range from about 2 m yr^{-1} to about 10 m yr^{-1}. Contours in Figure 77 of Kalin (1994) reveal flow rates near the center of the valley at of about 8 m yr^{-1}. The relatively large flow rate under Tucson is consistent with its proximity to the Catalina Mountains, with maximum annual precipitation near the summit of nearly 90 cm (Whittaker and Niering, 1975).

Results are also available for groundwater flow rates in the middle San Pedro basin. According to Hopkins et al. (2014), "Groundwater in the lower basin fill aquifer (semi-confined) was recharged at high elevations in the fractured bedrock and has been extensively modified by water-rock reactions (increasing F and Sr, decreasing ^{14}C) over long timescales (up to 35,000 years B.P.)." As these mountains are 15 km to 20 km from the San Pedro River (Cordova et al., 2015), this generates an estimate of the flow rate as ≥0.5m/yr. In the lower San Pedro river basin, further north, groundwater ages (Robertson, 1992) are closer to 8kyr B.P. to 15kyr B.P., but the mountain ridges are closer, too, at typical distances of 10 km to 15 km from the valley bottom. Thus, in this area, flow rates of about 1 m/yr are common, a value identical to what was measured in the upper Mojave watershed.

The wide range of flow rates is not completely unexpected in view of the range of P-ET values found across Arizona from south to north (Sanford et al., 2004) as well as the known proportionality of groundwater flow rates to P – ET (Maxwell et al., 2016). The region around Flagstaff, according to Sanford et al. (2004) has a net surplus of precipitation compared with ET of about 18cm/yr (63 cm/yr – 45 cm/yr), while the surplus in the San Pedro and Santa Cruz valleys is approximately 3 cm/yr (38 cm/yr−35 cm/yr). The value of the ratio of these two fluxes, 18/3 = 6, is highly uncertain because of the similarity of the terms 38 and – 35 the denominator. However, the finding of Maxwell et al. (2016), that groundwater flow rates are proportional to the difference of P and ET, would indicate that flow rates in southern Arizona should be a factor 6 smaller than in the vicinity of Flagstaff. The inferences from climate are in general accord with the data accessed, and imply a tendency for regional groundwater flow rates to decrease significantly from north to south across the Gila River catchment.

Finally, we mention a literature survey of groundwater ages in 34 alluvial basins in the Basin-and-Range Province and the Transition Zone of Arizona (Eastoe and Towne, 2018). Late Pleistocene water is known in 6 basins below the Mogollon Rim, from Golden Valley in the northwest through Wikieup, Wickenburg, and Phoenix, to Tucson, as well as in 3 basins along the next lineament northeast, Tonto, Safford, and Duncan. Safford and Duncan indeed lie along the Gila River. A Pleistocene age > 10ka, suggests broadly similar regional flow rates all along the dropped down margins of Arizona's topographic high at the Mogollon Rim.

4.2. Climatic summary

For purposes of comparison of world river basins, for which no detailed groundwater flow rates were found, climatic conditions for each drainage basin were assessed as humid, neutral, or dry (arid). Those river drainages integrated under wet or dry conditions are summarized in Table 1; unlisted river systems were considered neutral. Past conditions may not be equivalent to today. Specifically, although the Zambezi River drainage today is mostly rather humid, its past conditions are considered arid: "Some researchers extrapolate low denudation rates across the entire Cenozoic on the basis of the prevailing aridity of the climate and the lack of substantial uplift throughout that period…" (Said et al., 2015). While not all researchers agreed on effects of relatively low relief, there was no disagreement with the classification of the Zambezi basin paleoclimate as arid. While the Rio Grande of today is located in a mostly arid climatic regime, the paleodrainage referenced in Wang et al. (2020) was integrated under much wetter conditions than today.

Areas classified as neither "humid" nor" dry" include four rivers on the west side of India, the Blue Nile, rivers that drain the north side of the Tibetan Plateau (the Yellow River), a river in Italy and one of the river systems from Spain. The Almanzora River, however, assigned to "dry," is located in what is currently the most arid region of Spain, its southeast. In some of these "neutral" river drainages, the headwaters are in humid climates, while the lower reaches are in arid climates. This particular combination is difficult to classify, though for southwestern USA rivers, our choice tended to the "dry" classification.

TABLE 1 General climatic conditions within river drainages.

Humid	Dry
Aare	Colorado
Rhine	Morocco
Suarez	Almanzora
Amazon	Verde
Yangtze	Salt
Dadu	Amargosa
Katonga	Mojave
Meuse	Gila
Cahabon	San Pedro
Mississippi	Santa Cruz
Niger	San Simon
Orinoco	San Jacinto
Costa Rica	Zambezi
Rio Grande[a]	Rio Grande[b]
Gunnison	

[a]Paleo Rio Grande analog (before 40Ma). [b]Modern Rio Grande (after 8Ma).

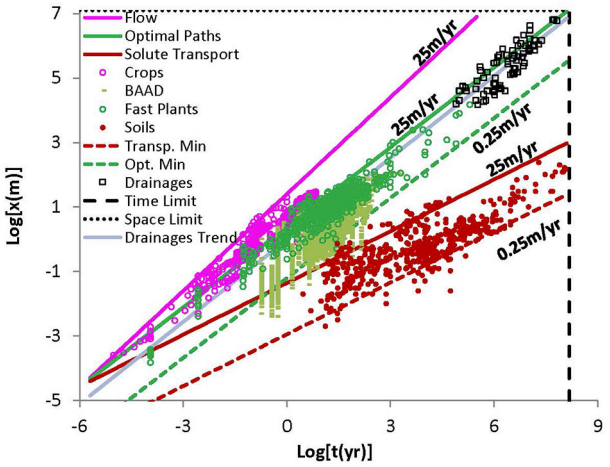

FIGURE 2
Plotted bilogarithmically are results for plant height or root radial extent (RRE) as a function of time for "fast plants," (relatively rapidly growing tree species, such as Sequoias and Eucalypts), "BAAD," (Biometric and Allometric Database), crop heights (without water or nutrient limitations), and soil depths, as well as predictions of equations analogous to Eq. (5), but with the exponent 1/1.87 appropriate to solute transport (soil predictions), 1 (appropriate for crop height predictions), or 1/1.21 (optimal paths or "biological transport"), appropriate for vegetation. The upper and lower bounds of 25 m/yr and 0.25 m/yr are reasonable for unsaturated zone flow, relevant for transpiration or infiltration, though the lower bound could be extended somewhat. Note that the scaling exponent for vegetation growth (1/1.21) is very similar to the power-law extracted from the data for drainage system development (1/1.18). Drainage basin data are consistent with a range of flow rates between 1 m/yr and 100 m/yr, as designated typical by the USGS. The designations "time limit" and "space limit" correspond to the period of a Wilson tectonic cycle and the linear extent of a supercontinent; thus, drainages have at most a time of about one Wilson cycle to develop, and can achieve a length that is, at most, about 1 supercontinent extent.

5. Results

5.1. Comparison across processes and across climates

In Figure 2, we include our new results for scaling of river lengths with time with existing plots of soil depth and root radial extent (RRE) as functions of time (Hunt, 2017). This figure clearly reveals a relationship between the scaling of river drainages and root systems. However, flow rates governing river lengths appear to be larger than for vegetation, in accord with the afore-mentioned comparisons of regional groundwater flow rates with vadose zone flow rates.

In Figure 3, we focus on the upper right-hand corner of Figure 2, in order to improve clarity and distinguish better between potential influences from climate and tectonics. Thus, we apply specifically the range of regional subsurface flow rates given by the USGS (1 m/yr to 100 m/yr) to generate minimum and maximum predictions for river length together with a linear spatio-temporal scaling relationship from tectonics. We also include a qualitative designation of climatic conditions. Thus, drainage basins were assessed as humid, neutral, or wet. Specific classifications are given in Table 1; unlisted river systems were considered neutral. Further investigations into paleoclimates may be warranted.

Areas classified as neither "humid" nor "dry" include four rivers on the west side of India, the Blue Nile, rivers that drain the north side of the Tibetan Plateau (the Yellow River), a river in Italy and one of the river systems from Spain. The Almanzora River, assigned to "arid," is located in what is currently the most arid region of Spain, its southeast. In some of these "neutral" river drainages, the headwaters are in humid climates, while the lower reaches in arid climates. This particular combination is difficult to classify, though for southwestern USA rivers, our choice tended to the "arid" classification. An additional complication is that changes in past climate, which were not considered, may render some of our classifications inaccurate.

Figure 3 suggests some potentially fundamental conclusions regarding river drainages. Arid drainages are found above, but mostly near, the tectonic rate, almost never below it. These arid drainages include the Gila River, its tributaries and the south-eastern California river drainages. Consider, e.g., that the Santa Cruz River does not really reach the Gila River (e.g., Dickinson, 2015). Moreover, a critical scarcity of water exists in the San Pedro drainage somewhat further east, while the Mojave River only reaches the end of its current drainage when rainfall in southern California is especially heavy, and even the Gila River rarely flows all the way to the Colorado River. These results are not purely due to an effect of the arid climate, as water impoundment for human use also plays an important role in current surface water depletion. At the time scales investigated, the rate of drainage integration for these rivers, measured as a spatial velocity, barely exceeds typical extensional tectonic velocities. Thus, the rate of integration is close to the rate at which basins can be pulled apart. In an even drier climate, subsurface flow rates would presumably

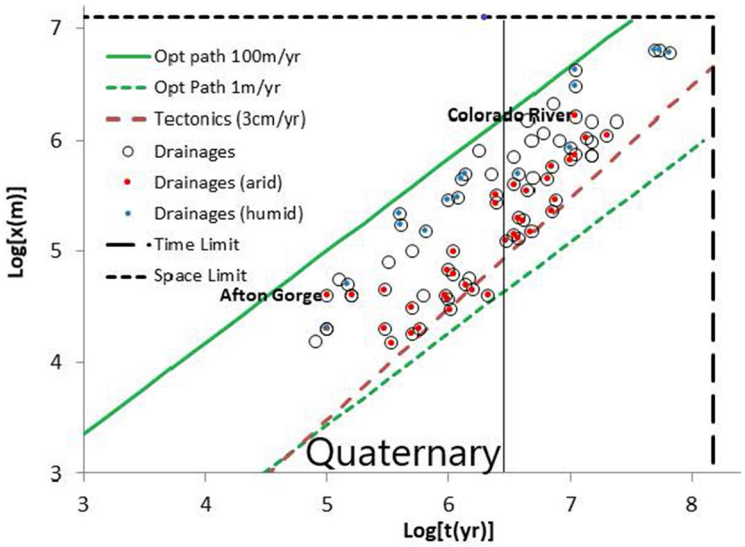

FIGURE 3
The upper right corner of Figure 2, with crops, vegetation and soil depth removed, but with limiting regional groundwater velocities taken from the US Geological Survey (2021). We distinguished between more arid and more humid climatic conditions in the corresponding river drainages according to the designations from Table 1. We also include a typical continental-scale tectonic rate of about 3 cm yr-1 and the designations "Time Limit" and "Space Limit." The time limit of about 150 Ma represents the interval since the break-up of the supercontinent Pangaea, while the space limit of about 12,000 km represents the linear dimension of the land mass of Pangaea. An approximate median groundwater flow rate of about 20 m yr', a rapid tectonic rate of about 6 cm yr-1, and the regression line from the observed draines would all meet very nearly at the intersection of "time limit" and "space limit."

be too small to accomplish the integration and the river drainages would disaggregate (become discontinuous). This argument does not incorporate the tendency for surface processes, such as wind transport of sand, or gravity-based elevation diffusion, to fill in channels. Consequently, it is not surprising that the Gila River, particularly its southern tributaries, as well as the Mojave and Amargosa Rivers from California, represent the slowest rates of basin integration that we found. At yet longer time scales in, e.g., the Sahara Desert, even river drainages that were once organized, disaggregate (McCauley et al., 1986; Ghoneim et al., 2005), particularly with the existing low flow rates (Gossel et al., 2004).

Second, we point out that several drainage basins located largely within regions of arid climate, the Pecos River, the Colorado River, and the Rio Grande (as well as, in particular, the Afton Gorge segment of the Mojave River), became integrated more rapidly than other drainages with similar aridity, and more rapidly than some in much more humid climates. This anomaly may be partly due to the locations of their sources in areas of significantly larger values of P – ET (the Rocky Mountains and the southern California transverse ranges). These factors may also contribute to a greater role of lake spillover in the process of drainage reorganization, which has been invoked in each case (Meek, 1989, 1990; Spencer et al., 2001; Crow et al., 2021). In these drainages, the oldest dates marking the position of the rivers are, indeed, found furthest upstream. However, this observation need not exclude alternate mechanisms of drainage integration in the same drainage basin predominantly due to subsurface flow. We expect that uncertainty may sometimes be resolved by considering the actual rates of drainage integration.

5.2. Mojave River and related southern and eastern California drainages

Because we have located more detailed data for both flow rates and drainage integration in the cases of the Mojave and Gila River drainages, we consider the two of them in greater detail. In Figure 4 we plot the lengths of the Mojave River sections that were integrated over particular time scales against those times. We use Eq. (5) for prediction and choose a value for the pore-scale flow rate of 2.5 m/yr, generally compatible with P – ET greater than current observations by at least a factor 2.5, as the known groundwater speeds are close to 1 m/yr. The predicted result, except for three data points, is in excellent agreement with observation. The two large discrepancies represent the time for the Mojave River to reach Lake Manix from the vicinity of Barstow, and the time required for the Mojave River to overtop the sill at Lake Afton and arrive downstream at Soda and Silver Lakes. As pointed out by several authors (Meek, 1989, 1990; Reheis et al., 2012), particularly the latter event is considered to have a completely different mechanism than what can be explained through groundwater flow. The overall development of the Mojave over the 3.8Myr time span is also somewhat faster than predicted, largely on account of the two counterexamples identified. This suggests a potential application of Eq. (5) for diagnosis of chief modes of drainage basin development. However, a potential confounding role of uncertainties in dating should also be considered, because a much earlier arrival of the Mojave River in the Barstow area than the mean of the range of the dates given is also possible, shifting the discrepancy between our prediction and observation upstream to the section between Victorville and Barstow.

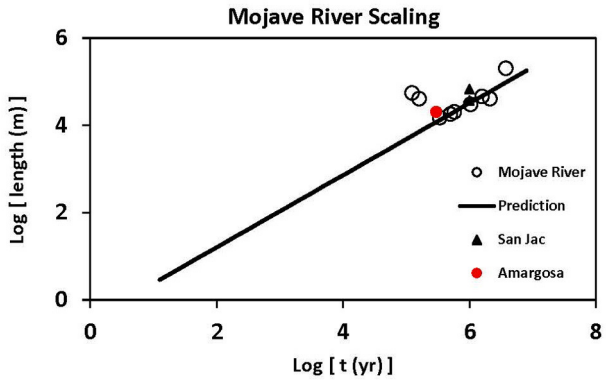

FIGURE 4
Mojave Desert River scaling of length vs. time. These California rivers are shown: The Mojave and the Amargosa. San Jac (with two data points) stands for two separate rivers flowing off the San Jacinto Mountains: a river flowing down the east side of the southern San Jacinto mountains toward Anza-Borrego Desert State Park and the San Jacinto River, on the west side of the San Jacinto Mountains. The first three examples are all in similar climates on the desert side of the southern California mountains. The fourth is in a somewhat wetter climate on the west side of the San Jacinto Mountains, but the desert side of the Santa Ana Mountains. In the case of the three Mojave River points that are well above the predicted power-law, we interpret the drainage integration below Barstow as having been driven primarily by surface processes with higher fundamental rates.

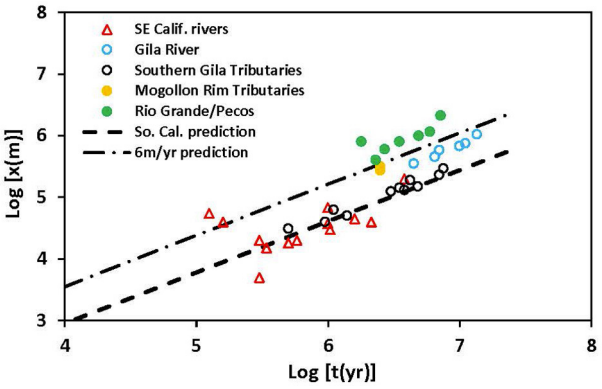

FIGURE 5
Gila and left and right (south and north) side drainage organization according to time scales. Note that the south side tributaries follow very nearly the same trend as the results of the Mojave River system. The north side tributaries and the Gila River itself are consistent with a scaling function that has the same exponent, but a somewhat larger flow rate, nearly 6 m yr-1, instead of 2.5 m yr-1. The Rio Grande and Pecos Rivers, however, are significantly above the 6 m yr-1 prediction.

Note that the time scale for the upstream knickpoint migration on the desert side of the San Jacinto Mountains is also predicted nearly exactly from Eq. (5), although both the Amargosa evolution and the San Jacinto River development are both somewhat underestimated. The underestimation of the Amargosa River length may come from applying Eq. (5) to a prediction of the entire distance to Tecopa Lake from the alluvial fans at Eagle Mountain, instead of merely across the fan. The San Jacinto River drainage basin, on the coastal side of the California peninsular ranges, receives at least double the rainfall that is measured on the desert side and for the Mojave River drainage, which means that using the groundwater flow rates for the Mojave basin would be expected to lead to an underestimation by a factor on the order of 2.

Note that it is actually well-known that the rate of, e.g., upstream knickpoint migration, slows over time (Mather et al., 2002), though previously it has mostly been assumed that other phenomena, associated with surface erosion, are responsible.

5.3. Gila River and associated drainages; Rio Grande and Pecos

Figure 5 shows the scaling of drainage basin evolution in the desert southwest of the USA. The results appear in accord with the scaling law predicted by Eq. (5). Further, the fundamental flow rates that appear in the equation (2.5 m yr^{-1} for southern California and 6 m yr^{-1} for the Gila and its northern tributaries), which define time scales in terms of the basic network size and the flow rate, are reasonably in accord with a gradient in such flow rates from $>$ 0.5 m/yr on the southern margins of the Gila Basin to 10 m/yr on the northern margins. As wetter climates in the Mojave during the Pleistocene were cited above to justify employing a subsurface flow rate of 2.5 m/yr, instead of the more recently observed 1 m/yr, it is important that there is also evidence for the existence of lakes in the enclosed basins of south-eastern Arizona over similar time frames (30,000ky B.P to 10,000ky B.P.) (Waters, 1989), in particular Lake Cochise in the Wilcox basin. Thus, application of a larger flow rate than is currently observed may be appropriate there as well. The Rio Grande, however, for which evidence cited above exists, that a 6 m yr^{-1} regional groundwater flow rate may be appropriate, lies well above the prediction. Any one or combination of the following three factors may play a role: (1) the orientation of the rift is more favorable to drainage basin expansion than in the Basin and Range province, where the principle relief lies athwart the drainages, (2) surface hydrologic processes had a greater relative importance, and (3) groundwater flow rates were higher at relevant times in the past.

We note that two of the data points for the Mojave River, which account for the advance of the Mojave from Barstow to Lake Manix, and from Afton Lake to Soda Lake, are well above the remaining points. These can, as already suggested, be associated with a different process of drainage reorganization, sill overtopping, promoted by Meek (1989, 1990) and supported by Reheis et al. (2012) and Hilgendorf et al. (2020). When we address the two northern tributaries of the Gila, the Salt and the Verde, however, their positions on the graph do not indicate a significant departure from the prediction by Eq. (5). Although they are slightly higher than the points for the mainstem Gila River, the present data do not allow for a definite distinction between overtopping and headward erosion, particularly since groundwater flow rates tend to increase toward the north. Dickinson (2015) and Skotnicki et al. (2021) raised questions regarding mechanisms of these processes, which may be more readily and certainly resolved, if: (1) the present theoretical framework is accurate enough, (2) paleodata to infer groundwater flow rates that are sufficiently precise can be obtained,

or (3) more simply, though not necessarily conclusively, if geologic dating methods reveal progressions in age.

6. Conclusions

We propose a solution of a fundamental problem in geology and geomorphology, the spatio-temporal scaling of river basin organization, based on principles tested within the disciplines of soil physics, hydrology, and percolation theory. We seek a solution based on a physical definition of a principle of scale-independency of hydrological processes, in particular, the tendency of water to "seek" paths of least resistance, in order to apply results from the modern theory of percolation across scales (Hunt et al., 2014). In order to predict river length as a function of time subsequent to tectonic or other events triggering drainage basin reorganization, we use a spatio-temporal scaling relationship for transport time scales of mass transported along fractal paths of least resistance, the so-called optimal paths defined in percolation theory. The specific spatio-temporal scaling relationship used for drainage basins is suggested on the assumption of the analogy to the vegetation growth model, but based on using (a) regional groundwater flow rates to establish the relationship between fundamental length and time scales, and (b) the exponent given as the ratio of the 3D optimal path exponent for integration of groundwater flow paths to the 2D exponent that describes the surface expression of river drainage. The proposed relationship is consistent with Hack's law. Our range of predicted river lengths as a function of time, based on a summary of the range of subsurface groundwater flow rates available from the US Geological Survey, captures the observed variability fairly precisely, on time scales from about 10 ka to 100 Ma. In this comparison, drainages in humid climates (re)organized themselves as much as ten times more rapidly than in arid climates.

Using specific Pleistocene, rather than modern, estimates for regional groundwater flow rates, we generate accurate estimates of the temporal scaling of stream lengths for the Amargosa River, the Gila River main stem as well as its tributaries, and most of the Mojave River. However, we underestimate length segments in the Mojave River below Barstow, particularly in the Afton gorge area, as well as the entire Rio Grande and the Pecos River. For the Rio Grande and Pecos Rivers, it is likely that higher Pleistocene regional groundwater flow rates contribute to the discrepancies arising from our use of current flow rates. But probably the more favorable orientation of the geologic lineaments parallel to the evolving stream plays a part as well. In the case of the Mojave River below Barstow, however, the contrast between our prediction and field results seems to require a greater role of surface hydrological processes than our model incorporates. Our model also underpredicts the length of the Colorado River, even though groundwater flow has been recognized as an important contribution to downstream extension of the Colorado River below Lake Mead (Crossey et al., 2015).

We find that the quantitative treatment developed here may also help explain questions posed in the literature. For example, for time scales in the tens of millions of years and length scales beyond a thousand kilometers, river drainage integration may be restricted to groundwater flow rates that generate integration velocities larger than tectonic rates, as Figure 3 reveals an almost complete lack of drainage basin integration in the most arid climates at time scales beyond about 1 Myr. The implied increasing restriction on climates for which drainage basins can be integrated beyond a time scale of 1 Myr is also in agreement with Roberts' (2019) assertion of an increase in the universality of drainage basin features at time scales beyond about 1Ma "At large spatial ($\geq$10 km) and temporal ($\geq$1 Ma) scales drainage networks appear to have a synchronized response to uplift and erosional processes," though the reorganization of major river basins need not occur gradually.

We note that confirmation of the relevance of fundamental, local-scale, groundwater flow rates to drainage basin evolution does not appear to restrict the validity of the predictions to either headward erosion or silting up basins and spilling over, though, certainly, not all individual locations are accurately treated with the method introduced here.

Because the distinction between surface and subsurface processes is different in submarine and subsurface environments, we suggest that establishment of the importance of such groundwater flow rates in fixing time scales for the development of connected subaerial drainages may also help distinguish subaerial and submarine channel development (Dobbs et al., 2019) in the geologic record.

Data availability statement

The raw data supporting the conclusions of this article will be made available by the authors, without undue reservation.

Author contributions

Concept development and text writing: AH. Text writing: BG and BF. All authors contributed to the article and approved the submitted version.

Funding

AH is grateful for special publication funds from Wright State University. BF work was partially supported by the SFA Watershed Project funded by the U.S. DOE Office of Sciences.

Conflict of interest

The authors declare that the research was conducted in the absence of any commercial or financial relationships that could be construed as a potential conflict of interest.

Publisher's note

References

Baker, V. R., Kochel, R. C., Laity, J. E., and Howard, A. E. (1990). Spring sapping and valley network development. *GSA Special Paper* 252, 235. doi: 10.1130/SPE252-p235

Beisner, K. R., Gardner, W. P., and Hunt, A. G. (2018). Geochemical characterization and modeling of regional groundwater contributing to the Verde River, Arizona between Mormon Pocket and the USGS Clarkdale gage. *J. Hydrol.* 564, 99–114. doi: 10.1016/j.jhydrol.2018.06.078

Bejan, A., and Errera, M. (2011). Deterministic tree networks for fluid flow: geometry for minimal flow resistance between a volume and one point. *Fractals* 5, 685–695. doi: 10.1142/S0218348X97000553

Bloemendal, M., and Theo, O. (2018). ATES systems in aquifers with high ambient groundwater flow velocity. *Geothermics* 75: 81–92.

Blöschl, G., and Sivapalan, M. (1995). Scale issues in hydrological modelling: a review. *Hydrol. Proc.* 9, 251–290. doi: 10.1002/hyp.3360090305

Church, M., and Mark, D. M. (1980). On size and scale in geomorphology. *Prog. Phys. Geograph.* 4, 302. doi: 10.1177/030913338000400302

Cordova, J. T., Dickinson, J. E., Beisner, K. R., Hopkins, C. B., Kennedy, J. R., Pool, D. R. (2015). *Hydrology of the Middle San Pedro Watershed, Southeastern Arizona, US Geological Survey, Scientific Investigations Report 2013–5040. Prepared in Cooperation With the Arizona Department of Water Resources*. Menlo Park, CA: U.S. Department of the Interior U.S. Geological Survey U.S. Department of the Interior.

Crossey, L. C., Karlstrom, K. E., Dorsey, R., Pearce, J., Wan, E., Beard, L. S., et al. (2015). Importance of groundwater in propagating downward integration of the 6–5 Ma Colorado River system: Geochemistry of springs, travertines, and lacustrine carbonates of the Grand Canyon region over the past 12 Ma. *Geosphere* 11, 660–682. doi: 10.1130/GES01073.1

Crow, R. S., Schwing, J., Karlsrom, K. E., Heizler, M., Pearthree, P. A., House, P. K., et al. (2021). Redefining the age of the lower Colorado River, southwestern United States. *Geology* 49, 635–640. doi: 10.1130/GEOL.S.13530698.v1

DiBiase, R. A., and Heimsath, A. M. (2012). Hillslope response to tectonic forcing in threshold landscapes. *Earth Surf. Proc. Landf.* 289, 134–144. doi: 10.1002/esp.3205

Dickinson, W. R. (2015). Integration of the Gila River drainage system through the Basin and Range province of southern Arizona and southwestern New Mexico. *Geomorphology* 236, 1–24. doi: 10.1016/j.geomorph.2015.02.004

Dixon, J. L., and Heimsath, A. M. (2009). The critical role of climate and saprolite weathering in landscape evolution. *Earth Surf. Proc. Landf.* 34, 1507–1521. doi: 10.1002/esp.1836

Dobbs, S. C., McHargue, T., Malkowski, M. A., Gooley, J. T., Jaikla, C., White, C. J., et al. (2019). Are submarine and subaerial drainages morphologically distinct? *Geology* 47, 1093–1097. doi: 10.1130/G46329.1

Dorsey, R. J., and Roering, J. J. (2006). Quaternary landscape evolution in the San Jacinto fault zone, Peninsular Ranges of Southern California: transient response to strike-slip fault initiation. *Geomorphology* 73, 0169-555X. doi: 10.1016/j.geomorph.2005.06.013

Eastoe, C., and Towne, D. (2018). Regional zonation of groundwater recharge mechanisms in alluvial basins in Arizona: interpretation of isotope mapping. *J. Geochem. Expl.* 194, 134–145. doi: 10.1016/j.gexplo.2018.07.013

Egli, M., Hunt, A. G., Dahms, D., Raab, G., Derungs, C., Raimondi, S., et al. (2018). Prediction of soil formation as a function of age using the percolation theory approach. *Front. Environ. Sci.* 28, 108. doi: 10.3389/fenvs.2018.00108

Enzel, Y., Wells, S. G., and Lancaster, N. (2003). Late Pleistocene lakes along the Mojave River, southeast California. *Geol. Soc. Am. Special Papers* 368, 61–77. doi: 10.1130/0-8137-2368-X.61

Fan, N., Chu, Z., Jiang, L., Hassan, M. A., Lamb, M. P., Liu, X., et al. (2018). Abrupt drainage reorganization following a Pleistocene river capture. *Nat. Commun.* 9, 3756. doi: 10.1038/s41467-018-06238-6

Fielding, L., Najman, Y., Millar, I., Butterworth, P., Garzanti, E., Vezzoli, G., et al. (2018). The initiation and evolution of the river Nile. *Earth Planet. Sci. Lett.* 489, 166–178. doi: 10.1016/j.epsl.2018.02.031

Garcia, A. L., Knott, J. R., Mahan, S. A., and Bright, J. (2014). Geochronology and paleoenvironment of pluvial Harper Lake, Mojave Desert, California, USA. *Quaternary Res.* 81, 305–317. doi: 10.1016/j.yqres.2013.10.008

Ghanbarian, B., Hunt, A. G., Ewing, R. P., and Sahimi, M. (2013). Tortuosity in porous media: a critical review. *Soil Sci. Soc. Am.* 77, 1461–1477. doi: 10.2136/sssaj2012.0435

Ghoneim, E., Benedotti, M., and El-Baz, F. (2005). An integrated remote sensing and GIS analysis of the Kufrah paleoriver, eastern Sahara. *Geomorphology* 140, 242–257. doi: 10.1016/j.geomorph.2011.10.025

Gossel, W., Ebraheem, A. M., and Wycisk, P. (2004). A very large scale GIS-based groundwater flow model for the Nubian sandstone aquifer in Eastern Sahara (Egypt, northern Sudan and eastern Libya). *Hydrogeol. J.* 12, 698–713. doi: 10.1007/s10040-004-0379-4

Goudie, A. S. (2005). The drainage of Africa since the Cretaceous. *Geomorphology* 67, 437–456. doi: 10.1016/j.geomorph.2004.11.008

Grant, U. S. (1948). Influence of the water table on beach aggradation and degradation. *J. Marine Res.* 7, 655–660.

Gray, D. M. (1961). Interrelationships of watershed characteristics. *J. Geophys. Res.* 66, 1215–1223. doi: 10.1029/JZ066i004p01215

Gunnell, Y., and Harbor, D. J. (2010). Butte detachment: how pre-rift geological structure and drainage integration drive escarpment evolution at rifted continental margins. *Earth Surf. Proc. Landforms* 35, 1373–1385. doi: 10.1002/esp.1973

Hack, J. T. (1957). *Studies of Longitudinal Profiles in Virginia and Maryland*. Washington DC: USGS Professional Papers.

Harvey, A. M., Wigand, P. E., and Wells, S. G. (1999). Response of alluvial fan systems to the late Pleistocene to Holocene climatic transition: contrasts between the margins of pluvial Lakes Lahontan and Mojave, Nevada and California, USA. *Catena* 36, 255–281. doi: 10.1016/S0341-8162(99)00049-1

Hilgendorf, Z., Wells, G., Larson, P. H., Millett, J., and Kohout, M. (2020). From basins to rivers: Understanding the revitalization and significance of top-down drainage integration mechanisms in drainage basin evolution. *Geomorphology* 352, 107020. doi: 10.1016/j.geomorph.2019.107020

Hillhouse, J. W., and Cox, B. F. (2000). *Pliocene and Pleistocene Evolution of the Mojave River, and Associated Tectonic Development of the Transverse Ranges and Mojave Desert, Based on Borehole Stratigraphy Studies*. Victorville, CA: US Department of the Interior, US Geological.

Hopkins, C. B., McIntosh, J. C., Eastoe, C., Dickinson, J. E., and Meixner, T. (2014). Evaluation of the importance of clay confining units on groundwater flow in alluvial basins using solute and isotope tracers: the case of Middle San Pedro Basin in southeastern Arizona (USA). *Hydrogeol. J.* 22, 829–849. doi: 10.1007/s10040-013-1090-0

Horton, R. E. (1932). Drainage basin characteristics. *Trans. Am. Geophys. Union* 13, 350–361. doi: 10.1029/TR013i001p00350

Horton, R. E. (1945). Erosional development of streams and their drainage basins; hydrophysical approach to quantitative morphology. *Geol. Soc. Am. Bull.* 56, 275–370. doi: 10.1130/0016-7606(1945)56[275:EDOSAT]2.0.CO;2

Hunt, A., Faybishenko, B., and Ghanbarian, B. (2021). Non-linear hydrologic organization. *Nonlin. Proc. Geophys.* 28, 599–614. doi: 10.5194/npg-28-599-2021

Hunt, A. G. (2016a). Possible explanation of the values of Hack's drainage basin, river length scaling exponent. *Non-Lin. Proc. Geophys.* 23, 91–93. doi: 10.5194/npg-23-91-2016

Hunt, A. G. (2016b). Spatio-temporal scaling of vegetation growth and soil formation from percolation theory. *Vadose Zone J.* 15, 1–15. doi: 10.2136/vzj2015.01.0013

Hunt, A. G. (2017). Spatiotemporal scaling of vegetation growth and soil formation: explicit predictions. *Vadose Zone J.* 16, 1–12. doi: 10.2136/vzj2016.06.0055

Hunt, A. G., Ewing, R. P., and Ghanbarian, B. (2014). *Percolation Theory for Flow in Porous Media, Lecture Notes in Physics*. Berlin: Springer.

Janecke, S. U., Dorsey, R. J., Forand, D., Steely, A. N., Kirby, S. M., Lutz, A. T., et al. (2010). High geologic slip rates since early pleistocene initition of the San Jacinto and San Felipe fault zones in the San Andreas fault system: Southern California, USA. *The Geol. Soc. Am. Spec. Paper* 25, 4752010. doi: 10.1130/2010.2475

Kalin, R. M. (1994). *The Hydrogeochemical Evolution of the Groundwater of the Tucson Basin With Application to 3-Dimensional Groundwater Flow Modelling*. Arizona: University of Arizona.

Kirby, M., Lund, S., Anderson, M., and Bird, B. (2007). Insolation forcing of Holocene climate change in Southern California: a sediment study from Lake Elsinore. *J. Paleolimnol.* 38, 395–417. doi: 10.1007/s10933-006-9085-7

Kirchner, J. W. (1993). Statistical inevitability in Horton's laws and the apparent randomness of stream channel networks. *Geology* 21, 591–594. doi: 10.1130/0091-7613(1993)021<0591:SIOHSL>2.3.CO;2

Koltzer, N., Scheck-Wenderoth, M., Cacace, M., Frick, M., and Bott, J. (2019). Regional hydraulic model of the Upper Rhine Graben. *Adv. Geosci.* 49, 197–206. doi: 10.5194/adgeo-49-197-2019

Kulongoski, J. T., Hilton, D. R., and Izbicki, J. A. (2003). Helium isotope studies in the Mojave Desert, California: implications for groundwater chronology and regional seismicity. *Chem. Geol.* 202, 95–113. doi: 10.1016/j.chemgeo.2003.07.002

Laity, J. E., and Malin, M. (1986). Sapping processes and the development of theater headed valley networks on the Colorado Plateau. *GSA Bulletin* 96, 203–217. doi: 10.1130/0016-7606(1985)96<203:SPATDO>2.0.CO;2

Langenheim, V. E., Jachens, R. C., Morton, D. M., Kistler, R. W., and Matti, J. C. (2004). Geophysical and isotopic mapping of preexisting crustal structures that

influenced the location and development of the San Jacinto fault zone. *GSA Buletin* 116, 1143–1157. doi: 10.1130/B25277.1

Larson, P. H., Dorn, R. I., Skotnicki, J., Seong, Y. B., Jeong, A., Deponty, J., et al. (2020). Impact of drainage integration on basin geomorphology and landform evolution: A case study along the Salt and Verde rivers, Sonoran Desert, USA. *Geomorphology* 371 107439 doi: 10.1016/j.geomorph.2020.107439

Maher, K. (2010). The dependence of chemical weathering rates on fluid residence time. *Earth Planet. Sci. Lett.* 294, 101–110. doi: 10.1016/j.epsl.2010.03.010

Maritan, A., Rinaldo, A., Rigon, R., Giacometti, A., and Rodriguez-Iturbe, I. (1996). Scaling laws for river networks. *Phys. Rev. E* 53, 1510–1515. doi: 10.1103/PhysRevE.53.1510

Marshall, J. S., Idleman, B. D., Gardner, T. W., and Fisher, D. M. (2003). Landscape evolution within a retreating volcanic arc Costa Rica. *Central Am. Geol.* 31, 419–4222. doi: 10.1130/0091-7613(2003)031<0419:LEWARV>2.0.CO;2

Mather, A. E., Stokes, M., and Griffiths, J. S. (2002). Quaternary landscape evolution: a framework for understanding contemporary erosion. *Spain Land Deg. Dev.* 13, 89–109. doi: 10.1002/ldr.484

Matthews, A., Lawrence, S. R., Mamad, A. V., and Fortes, C. (2001). Mozambique basin may have bright future under new geological interpretation. *Oil Gas. J.* 2, 70–76.

Maxwell, R., Condon, L. E., Kollet, S. J., Maher, K., Haggerty, R., Forrester, M. M., et al. (2016). The imprint of climate and geology on the residence times of groundwater. *Geophys. Res. Lett.* 43, 701–708. doi: 10.1002/2015GL066916

McCauley, J. F., Breed, C. S., Schaber, G. G., McHugh, W. P., Bahayissawi, C. V., Haynes, V., et al. (1986). Paleodrainages of the Eastern Sahara, the radar rivers revisited, (SIR-A / B Implicatins for a Mid-Tertiary rans-African drainage system). *IEEE Trans. Geosci. Remote Sensing. 24, 678*. doi: 10.1109/TGRS.1986.289678

McMahon, P. B., Plummer, L. N., Böhlke, J. K., Shapiro, S. D., and Hinkle, S. R. (2011). A comparison of recharge rates in aquifers of the United States based on groundwater-age data. *Hydrogeol. J.* 19, 779–800. doi: 10.1007/s10040-011-0722-5

Meek, N. (1989). Geomorphologic and hydrologic implications of the rapid incision of afton canyon, mojave desert. *Geology* 12, 7–10. doi: 10.1130/0091-7613(1989)017<0007:GAHIOT>2.3.CO;2

Meek, N. (1990). *Late Quaternary geochronology and geomorphology of the Manix Basin, San Bernardino County, California* [Ph.D. thesis] Los Angeles, CA: University of California.

Montgomery, D. R., and Dietrich, W. E. (1992). Channel initiation and the problem of landscape scale. *Science* 255, 826–830. doi: 10.1126/science.255.5046.826

Pelletier, J. D. (1999). Self-organization and scaling relationships of evolving river networks. *J. Geophys. Res.* 104, 7359–7375. doi: 10.1029/1998JB900110

Petroff, A. P., Devauchelle, O., Seybold, H., and Rothman, D. H. (2013). Bifurcation dynamics of natural drainage networks. *Philos. Trans. Royal Soc.* 371, 365. doi: 10.1098/rsta.2012.0365

Porto, M., Havlin, S., Schwarzer, S., and Bunde, A. (1997). Optimal path in strong disorder and shortest path in invasion percolation with trapping. *Phys. Rev. Lett.* 79, 4060–4062. doi: 10.1103/PhysRevLett.79.4060

Reheis, M. C., Bright, J., Lund, S. P., and Miller, D. M. (2012). A half-million year record of paleoclimate from the Lake Manix core, Mojave Desert, California. *Palaeogeograph. Palaeoclim. Palaeoecol.* 366, 11–37. doi: 10.1016/j.palaeo.2012.09.002

Reheis, M. C., Caskey, J., Bright, J., Paces, J. B., Mahan, S., Wan, E., et al. (2020). Pleistocene lakes and paleohydrologic environments of the Tecopa basin, California: constraints on the drainage integration of the Amargosa River. *GSA Bulletin* 132, 1537–1565. doi: 10.1130/B35282.1

Repasch, M., Karlstrom, K., Heizler, M., and Pecha, M. (2017). Birth and evolution of the Rio Grande fluvial system in the past 8Ma: progressive downward integration and the influence of tectonics, volcanism, and climate. *Earth Sci. Rev.* 168, 113–164. doi: 10.1016/j.earscirev.2017.03.003

Rhoads, B. (2020). *The Dynamics of Drainage Basins and Stream Networks. River Dynamics: Geomorphology to Support Management*. Cambridge: Cambridge University Press, 15–46.

Rigon, R., Rinaldo, A., Rodriguez-Iturbe, I., Bras, R. L., and Ijjasz-Vasquez, E. (1996). Optimal channel networks: a framework for the study of river basin morphology. *Water Resources Res.* 29, 1635–1646. doi: 10.1029/92WR02985

Roberts, G. (2019). Scales of similarity and disparity between drainage networks. *Geophys. Rese. Lett.* 46, 3781–3790. doi: 10.1029/2019GL082446

Robertson, F. N. (1992). Radiocarbon dating of a confined aquifer in southeast Arizona. *Radiocarbon* 34, 664–676. doi: 10.1017/S0033822200063955

Said, A., Moder, C., Clark, S., and Ghorba, B. (2015). Creatceous-Cenozoic sedimentary budgets of the southern Mozambique Basin: Implications for uplift history of the South African Plateau. *J. African Earth Sci.* 109, 1–10. doi: 10.1016/j.jafrearsci.2015.05.007

Sanford, W. E., Plummer, L. N., McAda, D. P., Bexfield, L. M., and Anderholm, S. K. (2004). Hydrochemical tracers in the middle Rio Grande Basin, USA:2. Calibration of a groundwater-flow model. *Hydrogeol. J.* 12, 389–407. doi: 10.1007/s10040-004-0326-4

Scheidegger, A. E. (1965). The algebra of stream order numbers. *US Geol. Survey Prof. Paper* 52, 187–189.

Schumm, S. A. (1956). Evaluation of drainage system and slopes in badlands at Perth Amboy, New Jersey. *Geol. Soc. Am. Bull* 67, 597–646. doi: 10.1130/0016-7606(1956)67[597:EODSAS]2.0.CO;2

Sheppard, A. P., Knackstedt, M. A., Pinczewski, W. V., and Sahimi, M. (1999). Invasion percolation: new algorithms and universality classes. *J. Phys.* 32, L521. doi: 10.1088/0305-4470/32/49/101

Shreve, R. L. (1967). Infinite topologically random channel networks. *The J. Geol.* 75, 178–186. doi: 10.1086/627245

Skotnicki, S. J., Seong, Y. B., Dorn, R. I., Larson, P. H., DePonty, J., Jeong, A., et al. (2021). Drainage integration of the Salt and Verde rivers in a Basin and Range extensioal landscape, central Arizona, USA. *Geomorphology* 374, 107512. doi: 10.1016/j.geomorph.2020.107512

Solder, J. E., Beisner, K. R., and Anderson, J., and Bills, D. J., (2020). Rethinking groundwater flow on the South Rim of the Grand Canyon, USA: characterizing recharge sources and flow paths with environmental tracers. *Hydrogeol. J.* 28, 1593–1613. doi: 10.1007/s10040-020-02193-z

Spencer, J. E., Pearthree, P. A., Young, R. A., and Spamer, E. E. (2001). Headward erosion versus closed-basin spillover as alternative causes of Neogene capture of the ancestral Colorado River by the Gulf of California. *Colorado River* 12, 215–219.

Stamos, C. L., Cox, B. F., Izbicki, J. A., and Mendez, G. O. (2003). *Geologic Setting, Geohydrology and Ground-Water Quality near the Helendale Fault in the Mojave River Basin, San Bernardino County, California, Prepared in cooperation with the Mojave Water Agency, Sacramento, Water-Resources Investigations Report 03-40697208-24.* Washington, DC: U.S. Department of the interior, U.S. Geological Survey.

Stolze, L., Arora, B., Dwivedi, D., Steefel, C., Li, Z., Carrero, S., et al. (2023). Aerobic respiration controls on shale weathering. *Geochimica et Cosmochimica Acta* 340, 172–188. doi: 10.1016/j.gca.2022.11.002

Strahler, A. N. (1964). "Geology. Part II. Quantitative geomorphology of drainage basins and channel networks," in *Handbook of Applied Hydrology*, ed V.T. Chow (McGraw-Hill: Wiley), 4–76.

Struth, L., Giachetta, E., Willett, S. D., and Owen, L. A., and Teson, E., (2020). Quaternary drainage network reorganization in the Colombian eastern cordillera plateau. *Easrth Surf. Process. Landforms* 45, 1789–1804. doi: 10.1002/esp.4846

Tucker, G. E., and Bras, R. L. (2000). A stochastic approach to modeling the role of rainfall variability in drainage basin evolution. *Water Resources Res.* 36, 1953–1964. doi: 10.1029/2000WR900065

US Geological Survey. (2021). *General Facts and Concepts About Ground Water*. Available online at: https://pubs.usgs.gov/circ/circ1186/html/gen_facts.html (accessed April 3, 2021).

Wang, C., Mortazavi, B., Liang, W. K., Sun, N. Z., and Yeh, W. W. -G. (1995). Model development for conjunctive use study of the San Jacinto Basin California, Paper No. 93148 of the water resources bulletin. *J. Am. Water Res. Assoc*. 31, 227–241. doi: 10.1111/j.1752-1688.1995.tb03376.x

Wang, H., Gurnis, M., and Skogseid, J. (2020). Continent-wide drainage reorganization in North America driven by mantle flow. *Earth Planet. Sci. Letters* 530 115910. doi: 10.1016/j.epsl.2019.115910

Waters, M. R. (1989). Late Quaternary lacustrine history and palaeoclimatic significance of pluvial Lake Cochise, southeastern Arizona. *Quat. Res.* 32, 1–11. doi: 10.1016/0033-5894(89)90027-6

Whittaker, R. H., and Niering, W. A. (1975). Vegetation of the Santa Catalina Mountains Arizona, V. Biomass, production, and diversity along the elevation gradient. *Ecology* 56, 71–90. doi: 10.2307/1936291

Willett, S. D., McCoy, S. W., Perron, J. T., Goren, L., and Chen, C.-Y. (2014). Dynamic reorganization of river basins. *Science* 343, 1248765. doi: 10.1126/science.1248765

Willgoose, G., Bras, R. L., and Rodriguez-Iturbe, I. (1991). Results from a new model of river basin evolution. *Earth Surf. Proc. Landforms* 16, 237–254. doi: 10.1002/esp.3290160305

Xiangjiang, H., and Niemann, J. D. (2006). Modelling the potential impacts of groundwater hydrology on long-term drainage basin evolution. *Earth Surf. Proc. Landforms* 31, 1802–1823. doi: 10.1002/esp.1369

Young, R. A., and Spamer, E. E. (2001). *The Colorado River: Origin and Evolution*. Grand Canyon, AZ: Grand Canyon Association Monograph.

Zhang, L., Peng, M., Chang, D., and Xu, Y. (2016). *Dam Failure Mechanisms and Risk Assessment*. Pondicherry: John Wiley and Sons.

frontiers | Frontiers in Water

TYPE Original Research
PUBLISHED 15 September 2023
DOI 10.3389/frwa.2023.1227167

OPEN ACCESS

EDITED BY
Ronald Erwin Pöppl,
University of Vienna, Austria

REVIEWED BY
Andrés Iroumé,
Universidad Austral de Chile, Chile
Jens Turowski,
GFZ German Research Centre for Geosciences, Germany

*CORRESPONDENCE
Caleb B. Fogel
✉ caleb.fogel@colorado.edu

RECEIVED 22 May 2023
ACCEPTED 11 August 2023
PUBLISHED 15 September 2023

CITATION
Fogel CB and Lininger KB (2023) Geomorphic complexity influences coarse particulate organic matter transport and storage in headwater streams. *Front. Water* 5:1227167. doi: 10.3389/frwa.2023.1227167

Geomorphic complexity influences coarse particulate organic matter transport and storage in headwater streams

Caleb B. Fogel* and Katherine B. Lininger

Department of Geography, University of Colorado Boulder, Boulder, CO, United States

Coarse particulate organic matter (CPOM; organic matter 1–100 mm in diameter, excluding small wood) stored in streams provides an important energy source for aquatic ecosystems, and CPOM transport provides downstream energy subsidies and is a pathway for watershed carbon export. However, we lack understanding of the magnitude of and processes influencing CPOM storage and transport in headwater streams. We assessed how geomorphic complexity and hydrologic regime influence CPOM transport and storage in the Colorado Front Range, USA. We compared CPOM transport during snowmelt in a stream reach with high retentive feature (e.g., wood, cobbles, and other features) frequency to a reach with low retentive feature frequency, assessing how within-a-reach geomorphic context influences CPOM transport. We also compared CPOM transport in reaches with differing valley geometry (two confined reaches versus a wide, multi-thread river bead) to assess the influence of geomorphic variations occurring over larger spatial extents. Additionally, we compared CPOM storage in accumulations in reaches (n = 14) with flowing water or dry conditions in late summer and investigated how small pieces of organic matter [e.g., woody CPOM and small wood (>1 m in length and 0.05–1 m in diameter or 0.5–1 m in length and >0.1 m in diameter)] influence CPOM storage. We found that within-a-reach retentive feature frequency did not influence CPOM transport. However, valley geometry influenced CPOM transport, with a higher CPOM transport rate (median: 1.53 g min^{-1}) downstream of a confined stream reach and a lower CPOM transport rate (median: 0.13 g min^{-1}) downstream of a low gradient, multi-thread river bead. Additionally, we found that particulate organic carbon (POC) export (0.063 Mg C) in the form of CPOM was substantially lower than dissolved organic carbon (DOC) export (12.3 Mg C) in one of these headwater streams during the 2022 water year. Dry reaches stored a higher volume of CPOM (mean = 29.18 m^3 ha^{-1}) compared to reaches with flowing water (15.75 m^3 ha^{-1}), and woody CPOM pieces trapped 37% of CPOM accumulations. Our results demonstrate that the influence of geomorphic context on CPOM transport depends on the scale and type of geomorphic complexity, POC may be lower than DOC export in some headwater streams, and small woody organic material is important for trapping CPOM small streams.

KEYWORDS

coarse particulate organic matter, fluvial geomorphology, headwater streams, CPOM, particulate organic carbon, organic matter transport, organic matter storage, river beads

1. Introduction

Coarse particulate organic matter (CPOM) is an important component of stream ecosystems (Fisher and Likens, 1973; Vannote et al., 1980) and watershed carbon cycling (Turowski et al., 2016). The composition and origin of CPOM varies, with CPOM particles ranging from autochthonous algal and plant fragments to allochthonous woody material (e.g., very small wood pieces, twigs), leaves, fruits, and coniferous needles and cones (Bunte et al., 2016; Iroumé et al., 2020; Gaillard et al., 2021; Marshall et al., 2021). Here, we define CPOM as organic matter 1–100 mm in diameter that does not meet the criteria of small wood, as defined by Galia et al. (2018). Freshwater ecosystems in headwater streams are highly dependent on stored CPOM as a food and energy source (Fisher and Likens, 1973; Bilby and Likens, 1980; Vannote et al., 1980). In many headwater streams, the majority of CPOM is terrestrial in origin; therefore, CPOM represents an important subsidy of organic matter and carbon to aquatic systems (Wallace et al., 1995; Turowski et al., 2016). The nature of this subsidy depends in part upon the mobility of CPOM particles within the stream network. Riverine CPOM transport provides a major pathway for watershed carbon export (Turowski et al., 2016) and downstream organic matter export (Vannote et al., 1980). However, we lack understanding of the magnitude of and processes influencing CPOM export in headwater streams, particularly across differing hydrologic regimes (e.g., intermittent or ephemeral systems compared to perennial streams) (Bunte et al., 2016; Turowski et al., 2016; Shumilova et al., 2019). In addition, the role of geomorphic complexity, including variations in valley geometry and the frequency of instream retentive features (e.g., wood), in mediating CPOM transport has only rarely been studied [see Jochner et al. (2015), Marshall et al. (2021)]. Here, we investigate how geomorphic and hydrologic setting influence CPOM transport and storage in headwater streams.

The magnitude and frequency of high flow events can determine the likelihood that stored CPOM will be mobilized (Small et al., 2008), but how geomorphic complexity modifies CPOM transport rates during high flow events is unclear. The vast majority of CPOM transport occurs during periods of high flow, particularly on the rising limb of higher flows such as peak snowmelt discharge (Bunte et al., 2016; Gaillard et al., 2021; Marshall et al., 2021). Features associated with CPOM retention (e.g., channel-spanning logjams) may in some cases limit local CPOM transport (Jochner et al., 2015), but among the few studies that exist, some have found that the opposite is true, and that logjams do not influence local CPOM transport (Marshall et al., 2021). In addition, the influence of broader-scale geomorphic context (e.g., valley bottom geometry) on CPOM transport has not yet been investigated. Features that create geomorphic complexity and heterogeneity, such as logjams, are often associated with retention and longitudinal discontinuity (i.e., the reduced downstream transport of water, sediment, and organic matter at the reach scale) (Sear et al., 2010; Wohl and Beckman, 2014; Poeppl et al., 2020). Additionally, river beads, defined as wide, low-gradient sections of rivers (Stanford et al., 1996; Wohl et al., 2018) can attenuate dissolved organic carbon (DOC) transport rates compared to steep, narrow reaches (Wegener et al., 2017), and beads can be sites of enhanced storage of large wood (Wohl and Cadol, 2011; Sutfin et al., 2021) and reduced longitudinal connectivity (Wohl and Beckman, 2014; Wohl et al., 2019a). To our knowledge, no studies have evaluated the effect of river beads on particulate organic carbon (POC) or CPOM transport rates, although a study in the Salmon River, Idaho did find that CPOM travel distance was limited in river beads compared to confined reaches (Bellmore and Baxter, 2014). Further investigation of how geomorphic variation both within a reach (i.e., the frequency of wood, coarse grains, and pools within the stream channel), and between reaches (i.e., river beads versus confined, narrow valley bottoms) influences CPOM transport would be beneficial to understanding longitudinal and lateral CPOM connectivity and disconnectivity across scales.

CPOM storage can increase with increased frequency of features such as large wood (>1 min length and >0.1 min diameter) and small wood (>1 min length and 0.05–1 min diameter or 0.5–1 min length and >0.1 min diameter, defined in Galia et al., 2018), coarse sediment, and low-velocity depositional zones (e.g., backwaters and pools) (Benfield et al., 2000; Lepori et al., 2005; Small et al., 2008; Jochner et al., 2015; Pfeiffer and Wohl, 2018; Bovill et al., 2020). Large and small wood pieces can effectively trap CPOM, and the size of wood pieces can influence the likelihood of long-term retention of CPOM accumulations (Small et al., 2008). However, large wood has historically received much more attention than any other wood size category. Although small wood pieces may be important to CPOM storage (Small et al., 2008), the role of smaller woody material such as woody CPOM pieces (< the dimensions of small wood and > 0.2 min length) in trapping and storing other CPOM particles has not been explored.

Understanding CPOM dynamics is also important for constraining watershed carbon budgets (Turowski et al., 2016). Freshwater systems influence carbon cycling through their ability to transport, export, and store a substantial quantity of terrestrially derived carbon such as CPOM (Vannote et al., 1980; Gomez et al., 2003; Cole et al., 2007; Hilton et al., 2011; Keith et al., 2014). Carbon within freshwater systems can be returned to the atmosphere as CO_2 through outgassing or respiration, sequestered in sediments, or transported to oceans (Cole et al., 2007; Wohl et al., 2017; Battin et al., 2023). Estimates indicate that the global export of DOC to the oceans is greater than that of POC (Battin et al., 2008; Wohl et al., 2017), however, POC export may be of greater relative importance in small mountainous streams (Hilton et al., 2008; Turowski et al., 2016; Bright et al., 2020). Several studies have shown that CPOM and large wood can contribute significantly to POC and total organic carbon (OC) export. For example, Seo et al. (2008) found that large wood can account for as much as 36.8% of POC export, and Turowski et al. (2016) found that POC in the form of CPOM and large wood could account for ~36–80% of the total decadal organic carbon (OC) export in some watersheds. Still, data quantifying POC export, and the relative importance of POC versus DOC, in small mountainous rivers, are limited (Goñi et al., 2013; Turowski et al., 2016).

Understanding CPOM processes in small headwater and intermittent or ephemeral streams will be of increasing importance, as climate models project an increase in the number of intermittent streams in headwater regions worldwide (Larned et al., 2010).

Small headwater streams comprise a large percentage of the total channel length of river networks (Wohl, 2017; Fritz et al., 2019), and the cumulative effects of small stream processes can exert a substantial influence on overall watershed processes (Vannote et al., 1980). CPOM storage in perennial streams is often spatially concentrated and driven by obstacles that trap and retain CPOM (Benfield et al., 2000; Small et al., 2008; Jochner et al., 2015; Pfeiffer and Wohl, 2018; Bovill et al., 2020). In contrast, although CPOM storage in ephemeral or intermittent streams is likely still driven by retentive features, limited transport capacity during periods of minimal to no flow can result in additional CPOM storage in more spatially extensive mats (Wohl and Scamardo, 2022). Limited streamflow in ephemeral or intermittent streams can also increase the residence time of CPOM stored within stream channels (Fritz et al., 2019; Wohl and Scamardo, 2022), and in turn, impact processes reliant on CPOM transport and storage (e.g., carbon export and ecosystem energy levels).

In this study, we quantify CPOM transport in stream reaches with differing geomorphic complexity to increase our understanding of how geomorphic conditions influence CPOM transport. We also assess CPOM storage in reaches that become dry and reaches with flowing water. We address three primary questions related to CPOM transport and storage in small headwater streams. First, what is the relative magnitude of POC export compared to DOC export in headwater streams (Q1)? Second, how do geomorphic characteristics (i.e., within-a-reach retentive feature frequency and valley context) impact CPOM transport rates (Figure 1) (Q2)? We hypothesize that reaches with high within-a-reach retentive feature frequency (e.g., a high abundance of wood within the stream) will have greater CPOM transport rates at the upstream end compared to the downstream end due to within-reach trapping during transport (Figure 1B), and that reaches with lower densities of retentive features will have more longitudinally homogenous CPOM transport rates (Figure 1A) (H2a). Additionally, we hypothesize that CPOM transport rates downstream of wide valley bottom reaches with abundant lateral connectivity (i.e., river beads) will be lower than CPOM transport rates downstream of more confined reaches (H2b) (Figure 1C), assessing the influence of longitudinal variation in valley geometry across a larger spatial extent on CPOM transport. Finally, what factors (e.g., presence and frequency of retentive features, stream flow conditions, and other geomorphic and forest stand characteristics) influence CPOM storage (Q3)? We expect that reaches with higher retentive feature frequency will have higher CPOM storage (H3a). Additionally, we expect that wood, especially small wood and woody CPOM, will store more CPOM than any other type of retentive feature (H3b). Given the importance of both CPOM transport and storage to ecosystem functioning and carbon storage and export, understanding CPOM transport and storage within streams allows for more effective management of aquatic ecosystem functioning and better constraints on watershed carbon budgets. In addition, studies of CPOM under varying hydrological conditions, including intermittent streams, will inform scientists and watershed managers on how CPOM dynamics in small headwater streams may evolve in a changing climate.

2. Methods

2.1. Study area

We conducted our study in Gordon Gulch and Como Creek, two headwater streams within the Boulder Creek Watershed on the eastern slope of the Colorado Front Range Mountains, USA (Figure 2). Particular attention has been paid to critical zone processes in both watersheds in recent years [e.g., Anderson et al. (2011, 2014, 2021), Hinckley et al. (2014), Dethier et al. (2022)]; however, studies of CPOM dynamics at these sites have not been conducted.

Gordon Gulch (Figure 2B) drains ~2.6 km^2 within the montane elevational zone (~1,707–2,896 m) and ranges 2,440–2,730 min elevation. Winter (December-March) snow cover is intermittent, with higher quantities of persistent snow residing on north-facing slopes (Anderson et al., 2014). Peak snowmelt and discharge both typically occur between April and June, and peak rainfall occurs throughout the spring (March-June) and summer (June-September) (Anderson et al., 2014; Anderson and Ragar, 2021; Barnard et al., 2023). Streamflow is perennial throughout much of the basin, however, portions of Gordon Gulch are characterized by intermittent flow during summer. Vegetation in Gordon Gulch is comprised of a mixed pine forest with dense cover of lodgepole pines (*Pinus contorta*) on the north-facing slopes and an open ponderosa pine (*Pinus ponderosa*) canopy on the south-facing slopes (Adams et al., 2014; Anderson et al., 2014). Broadleaf deciduous tree species such as aspen (*Populus tremuloides*), alder (*Alnus spp.*), and willow (*Salix spp.*) also grow near the stream channel.

Como Creek (Figure 2C) spans the subalpine (~2,743–3,353 m) and alpine (> ~3353 m) elevational zones, ranging from ~3,000 to nearly 4,000 min elevation, and drains ~4.9 km^2. Persistent snow cover is present from October to June, and peak streamflow driven by snowmelt occurs in late spring to early summer (May-June) [National Ecological Observatory Network (NEON), 2022]. Streamflow declines sharply in the late summer and remains low throughout the winter. Forests within the Como Creek watershed are dominated by mixed conifers including lodgepole and limber pines (*Pinus flexilis*), subalpine fir (*Abies lasiocarpa*) and Engelmann spruce (*Picea engelmannii*), although broadleaf deciduous species such as aspen are also present.

2.2. Field data collection

We identified 14 study reaches at Gordon Gulch: two in which we measured CPOM transport and storage, and 12 in which we measured CPOM storage only. We selected the two CPOM transport and storage study reaches based on their proximity to the lower stream gage at Gordon Gulch (Figure 2B), as well as the number of wood pieces or accumulations and pools documented in each reach during an initial survey. The high retentive feature (Hi-ret) reach (65 m length) had a higher frequency of retentive features than the low retentive feature (Lo-ret) reach (23 m length) (Figure 2B), allowing us to test the hypothesis that within-a-reach retentive feature density would

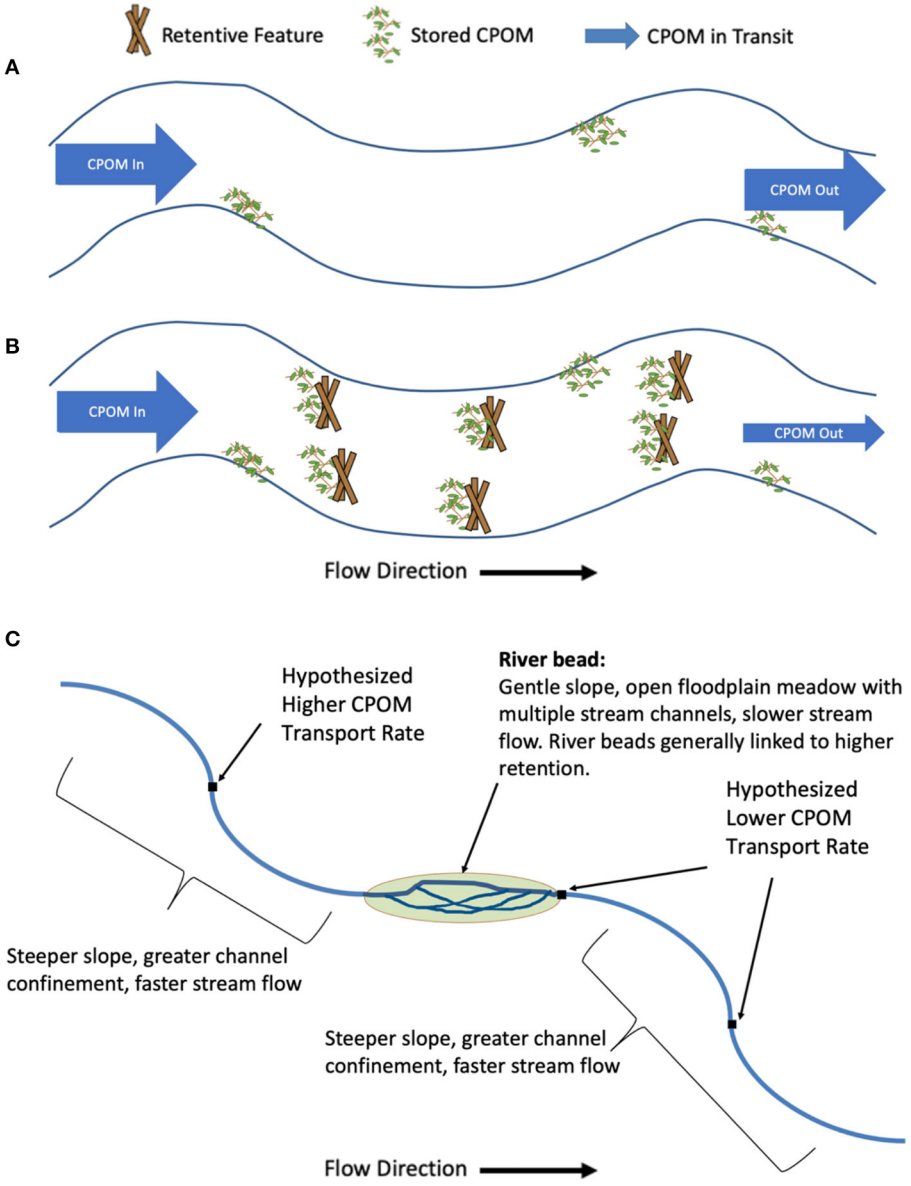

FIGURE 1
Conceptual model of H2a in reaches with **(A)** low and **(B)** high retentive feature frequency, indicating expected lower CPOM transport rate at the downstream end of **(A)** due to within reach trapping. CPOM arrow size shows predicted CPOM transport rate relative magnitude. **(C)** Conceptual model of H2b, indicated expected reduction in CPOM transport rate due to between reach differences in valley geometry (e.g., the presence of a river bead).

influence CPOM transport. We randomly selected the 12 additional reaches for storage measurement only (GG1-GG12) (Figure 2B) after stratifying potential reaches by stream slope (low slope/high slope), channel type (single-/multi-threaded), and late summer flow conditions (flowing water versus dry) through a combination of geospatial analysis of a digital elevation model and field investigations. Given that we only sampled one field season, we categorized flow conditions as either dry or flowing water because we did not continuously monitor flow conditions over multiple years to determine whether reaches were consistently perennial or intermittent over longer time periods. The stratified random sampling approach ensured that a mix of different slope, channel type, and streamflow categories were included.

At Como Creek, we identified three reaches in which we measured CPOM transport; we did not measure CPOM storage at Como Creek. We selected the three reaches based on their proximity to a river bead ~150 m long (Figure 2C). These reaches were located 190 m downstream (CC1; 27 m length), immediately downstream (CC2; 21 m length), and 90 m upstream (CC3; 38 m length) of the river bead (Figure 2C), allowing us to test the hypothesis that valley geometry influences CPOM transport. There are no tributary additions of discharge between the study reaches on Como Creek and the Como Creek discharge gage just upstream of CC3 (Figure 2C).

We surveyed geomorphic and forest stand characteristics along transects perpendicular to the stream at each study reach. We

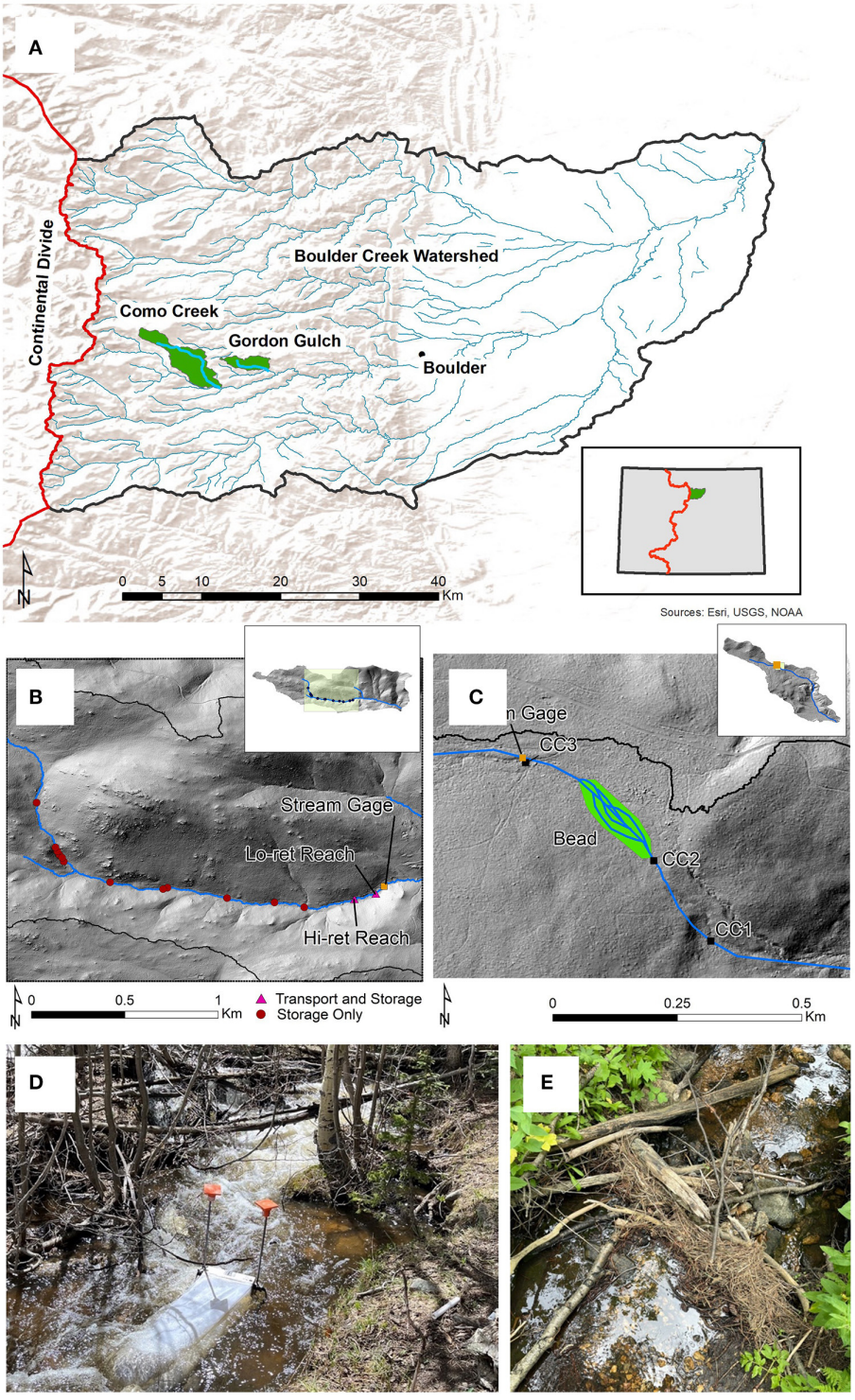

FIGURE 2
(A) Boulder Creek Watershed, Colorado, USA. Study watersheds highlighted in green. Inset in **(A)** shows the location of Boulder Creek Watershed (green) within the state of Colorado (gray). **(B)** Gordon Gulch study reaches. Hi-ret reach is a reach with a high frequency of instream retentive features, and Lo-ret is a reach with a lower frequency of instream retentive features. **(C)** Como Creek study reaches and river bead. Inset maps in **(B)** and **(C)** show locations of study reaches within each watershed. Green rectangles show the extent of sampling locations within each watershed. In **(B)**, reaches where both CPOM transport and storage were measured are indicated with triangles, and reaches where only storage was measured are indicated with circles. **(D)** CPOM transport sampling at CC1. **(E)** CPOM storage in an accumulation in Gordon Gulch.

measured bankfull and valley bottom width (m) and stream slope (%) using a laser rangefinder (TruPulse 360), canopy density (%) using a densiometer, basal area (m ha^{-1}) using a Panama angle gage, and median (D50) and 84th percentile (D84) grain size (mm) through Wolman pebble counts (Wolman, 1954). The number of transects (3 to 5) varied by reach depending on reach length.

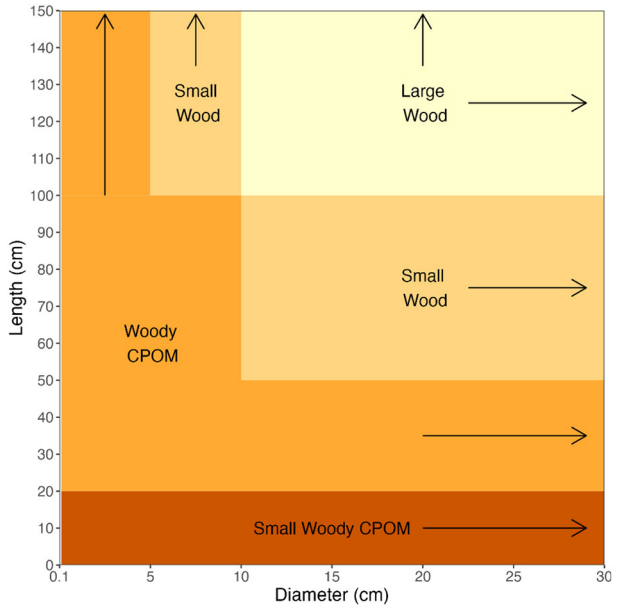

FIGURE 3
Diagram of woody organic material size classes used, including large wood (>1 min length and > 0.1 min diameter), small wood (>1 min length and 0.05-0.1 min diameter or 0.5-1 min length and > 0.1 min diameter), woody CPOM (< the dimensions of small wood and > 0.2 min length); and small woody CPOM (<0.2 min length).

Reach lengths differed so that the geomorphic context did not vary significantly within a reach (e.g., slope was relatively consistent and reaches did not contain both single and multi-threaded channels). In multithreaded reaches, we averaged measurements of bankfull width across the multiple threads. Additionally, we measured retentive feature frequency (number of retentive features per m) in Gordon Gulch. Retentive features included wood pieces and accumulations, woody CPOM pieces, coarse grains protruding above the water's surface, live vegetation, pools, stream banks and bars, and low velocity zones. We surveyed woody organic material within each study reach, and categorized pieces as large wood (>1 min length and > 0.1 min diameter) (Ruiz-Villanueva et al., 2016; Wohl et al., 2019b); small wood (>1 min length and 0.05–0.1 min diameter or 0.5–1 min length and > 0.1 min diameter, from Galia et al. (2018); woody CPOM (< the dimensions of small wood and > 0.2 min length); and small woody CPOM (twigs) (<0.2 min length) (Figure 3). We used existing classifications for large and small wood to align with previous studies, and added two new categories, woody CPOM and small woody CPOM, to assess the influence of smaller woody material on CPOM dynamics. We measured the dimensions (length, diameter) of all large, small, and woody CPOM pieces, but did not measure the dimensions of small woody CPOM.

We measured CPOM transport at the Gordon Gulch Lo-ret and Hi-ret reaches and the Como Creek reaches using modified bedload samplers [see Bunte et al. (2007, 2016), Turowski et al. (2013, 2016), Iroumé et al. (2020)] consisting of a 1 mm diameter mesh net, with an opening ~30 × 20 cm, held in place by a metal box (Bunte et al., 2007) (Figure 2D). Although previous studies have used larger mesh (3.4–6 mm diameter) to avoid CPOM clogging the mesh (Bunte et al., 2016; Turowski et al., 2016), we chose to use a 1 mm diameter mesh because CPOM particles transported in our study reaches were often smaller than 3.4 mm and would have been missed by a larger diameter mesh. On the rare occasions when we anticipated CPOM transport could be high enough to clog the netting, we used a shorter sampling period to avoid clogging. We did not notice a ballooning of the net from water flowing through the mesh during our sampling (Bunte et al., 2015), and thus the small diameter mesh size likely did not bias our measured sampling rates. We deployed the bedload samplers on the streambed for periods ranging from ~15 mins to one hour depending on streamflow. Although previous studies have deployed multiple bedload traps at once per reach (Bunte et al., 2016), we deployed a single trap at each reach during each sampling period due to the smaller wetted widths of the stream channels. We placed each bedload trap in the thalweg of the stream; therefore, our estimates of CPOM transport rates that take into account the entire width of the stream (see section 2.3) may represent a maximum CPOM transport rate for each stream. We intentionally placed traps in a straight portion of each reach that was absent of immediately adjacent retentive features (e.g., wood, pools, etc.) to limit bias introduced by differences in trap placement across sites. We separated CPOM from any inorganic sediment collected in the traps in the field; inorganic sediment was minimal. We used stream discharge measurements collected immediately downstream of the Lo-ret reach at Gordon Gulch (Figure 2B) (Barnard et al., 2023) and upstream of CC3 at Como Creek (Figure 2C) [National Ecological Observatory Network (NEON), 2022] to relate stream flow to CPOM transport rate. We did not sample CPOM transport rate overnight in either stream because after assessing discharge trends at each site, we found relatively little 24-h variability in flow. In addition, other studies have found that the diurnal cycle does not significantly impact CPOM transport (Marshall et al., 2021).

To assess how reach-level variations in retentive feature frequency influenced CPOM transport, we measured CPOM transport at the upstream and downstream ends of the Gordon Gulch Hi-ret and Lo-ret reaches. We proceeded from downstream to upstream when sampling CPOM transport so as not to impact downstream transport measurements. We measured CPOM transport at Gordon Gulch 1–2 times per week between late April and mid-July. After mid-July, stream flow was low, and we visually observed little to no CPOM transport. Although late summer CPOM transport may have been elevated during potential higher flow periods during summer storms, we did not survey CPOM transport during and following summer storms at Gordon Gulch. However, analysis of the measured discharge during storms confirmed that snowmelt was the highest discharge for the 2022 water year (defined as October 1 through September 30) that we sampled.

To assess how variations in valley bottom geometry (i.e., a river bead) influenced CPOM transport, we collected CPOM at the downstream end of each reach at Como Creek ~1–2 times per week between mid-May and mid-July 2022. We sampled CC1 first, and proceeded upstream to avoid impacting CPOM transport sampling downstream of a given sampling location. During high flows, we stacked two bedload samplers to sample the entire water column.

To investigate the controls on CPOM storage, we estimated CPOM storage within the bankfull channel of all 14 study reaches at Gordon Gulch under low-flow conditions following peak flow (early August). We measured the surface area (m^2) and thickness (m) of each CPOM accumulation, and used visual porosity estimates (%) (Livers et al., 2020) to calculate the CPOM volume of each accumulation, taking into account pore spaces present in most CPOM accumulations. We took samples of a known volume at approximately every tenth accumulation, which we used to estimate the bulk density of CPOM accumulations. We then burned seven samples at 550°C for 8 h to estimate ash free dry mass (AFDM) of CPOM samples, calculated the AFDM per volume for each sample, and converted CPOM volume to CPOM mass using the mean of the AFDM samples. Because the AFDM of samples did not vary significantly by CPOM composition, we applied a mean conversion of all samples to determine AFDM in g m^{-2}. We report results in CPOM volume per ha, but use the AFDM conversion to compare to other studies of CPOM storage. For each accumulation, we noted the mechanisms responsible for retaining the accumulation and the primary composition of the CPOM stored (i.e., leaves, needles, cones, etc.). Retention mechanisms, or features which may induce CPOM storage over time (Bovill et al., 2020), were categorized as wood (large and small), woody CPOM, small woody CPOM (see Figure 3), coarse sediment, pools, live vegetation, and other, a category that included CPOM trapped by areas of low velocity or flow or stream banks. We used the CPOM storage measurements to assess the influence of reach-scale retentive feature frequency and wood and woody CPOM frequency on CPOM storage.

2.3. Data and laboratory analysis

To provide context for the hydrologic conditions during the 2022 water year, we compared streamflow magnitude during the 2022 water year to previous years using 10 years of discharge data from Gordon Gulch (2012–2019 and 2021–2022) (Anderson and Ragar, 2021; Barnard et al., 2023), and 6 years of discharge data from Como Creek (2017–2022) [National Ecological Observatory Network (NEON), 2022]. Discharge data were available at 10 min intervals from a gage just downstream of the Lo-ret reach at Gordon Gulch (Barnard et al., 2023), and at 1 min intervals from a gage just upstream of CC3 at Como Creek [National Ecological Observatory Network (NEON), 2022]. We filled two data gaps in the 2022 Como Creek discharge dataset using stage-discharge relationships and water surface elevation datasets from two locations at Como Creek prior to our analysis (See Supplementary material S1). To determine the mass of CPOM transported during each sampling interval, we then dried the CPOM samples collected in the field at 105°C for 24 h and measured the dry mass. We used the following equation from Bunte et al. (2007), which accounts for the fact that the bedload samplers do not cover the entire stream channel, to calculate the CPOM transport rate for a given sampling period:

$$CPOM_{transport} = \frac{w_c}{w_s} * \frac{m}{t} \quad (1)$$

where m is the CPOM dry mass from a given sampling period, w_c is the stream channel width, w_s is the width of the bedload sampler, and t is the sampling duration.

We developed rating curves for CPOM transport in relation to discharge at each reach by fitting a linear regression in log-transformed space, regressing log-transformed CPOM transport rate (g min^{-1}) against log-transformed discharge data at the time of sampling at each reach. The relationship was then explained by a power function. Given the relatively short reach lengths at Gordon Gulch, we developed reach-level rating curves for Hi-ret (65 m) ~ and Lo-ret (23 m) by including the upstream and downstream CPOM transport measurements for Hi-ret to create the Hi-ret rating curve, and the upstream and downstream transport measurements for Lo-ret to create the Lo-ret rating curve. We estimated the annual CPOM yield (kg yr^{-1}) at each site for the 2022 water year using the rating curve developed for each site. We then applied the same rating curve to discharge data from previous years to estimate CPOM yield over multiple years ($n = 10$ at Gordon Gulch; $n = 6$ at Como Creek). To assess the relative contributions of POC and DOC to total carbon export in headwater streams, we compared DOC concentration data collected at Como Creek [National Ecological Observatory Network (NEON), 2023] with our CPOM export results from CC3. DOC data were collected near the upstream end of CC3. We converted CPOM mass export to OC mass export using a conversion factor of 50% (Intergovernmental Panel on Climate Change, 2006; Turowski et al., 2016), assuming that approximately half the mass of CPOM is OC.

We compared CPOM transport rates at the upstream and downstream ends of both transport reaches at Gordon Gulch to determine whether within-a-reach geomorphic context influences CPOM transport rate, and tested for statistical significance of differences between upstream and downstream transport rates using paired Wilcoxon rank sum tests. Additionally, we compared CPOM transport rates across study reaches at Como Creek to determine whether valley context influences CPOM transport rate.

We performed statistical analyses in R (R Core Team, 2022) to identify relationships between CPOM load (m^3 ha^{-1}) and frequency (# m^{-1}) and reach-level geomorphic and forest stand characteristics. First, we performed Wilcoxon rank sum tests to assess differences in CPOM load and frequency between reaches classified as dry versus flowing in late summer, and single versus multi-thread. We also performed multiple linear regression analyses, using a model selection approach, to assess controls on CPOM load and frequency, using numeric geomorphic and forest stand characteristics as potential predictor variables. To begin, we assessed correlations between response and potential predictor variables and multicollinearity of potential predictor variables using the Kendall's tau and removed any strongly correlated variables ($\tau > 0.8$) from our multiple linear regression analysis. Additionally, we performed Variance Inflation Factor (VIF) tests in R, sequentially removing the variable with the highest VIF value until all values were less than 10 (Craney and Surles, 2002; Thompson et al., 2017). Following correlation and VIF tests, potential predictor variables for the CPOM load model included stream slope (%), basal area (m^2 ha^{-1}), canopy density (%), bankfull width (m), pool area (m^2), wood load (including large and small wood; m^3 per ha), and retentive feature frequency (#

per m). Retentive feature frequency includes the number per meter of large and small wood, woody CPOM, small woody CPOM, coarse sediment, and pools. Potential predictor variables for the CPOM frequency model included slope, basal area, canopy density, bankfull width, pool frequency (# per meter), number of wood pieces or jams (including large and small wood; # per m), wood load, and retentive feature frequency. We then conducted all-subsets regression with potential predictor variables using the dredge function from the MuMIn package in R (Bartoń, 2022). We considered all models within a two-unit range of the lowest AICc (Akaike Information Criterion corrected for small sample sizes) (Wagenmakers and Farrell, 2004), and chose a top model for each response variable as the model with the lowest AICc with the fewest number of predictor variables. We also ranked the importance of model predictor variables by summing the Akaike weights (Wagenmakers and Farrell, 2004). We checked the residuals of all models for homoscedasticity and normality to ensure the models met model assumptions. We compared p values to a significance level of $\alpha = 0.05$ and report p values less than $\alpha = 0.10$ to assess weaker patterns and trends in the data.

3. Results

3.1. Geomorphic and forest stand characteristics of study reaches

Retentive feature frequency at Gordon Gulch study reaches ranged from 1.80 features per min GG8 to 4.29 features per min GG11 (Table 1). The frequency of wood pieces or accumulations ranged from 0.26 per min GG7 to 1.54 in GG9. Retentive feature frequencies between the Hi-ret and Lo-ret site differed by 0.12 features per m (1.91 in Lo-ret, 2.03 in Hi-ret), whereas the frequency of wood pieces or accumulations differed by 0.55 pieces per m between the two reaches (0.35 in Lo-ret, 0.89 in Hi-ret). Small wood, woody CPOM, and small woody CPOM were more common than large wood across all study reaches at both Gordon Gulch and Como Creek. Stream slope, bankfull width, and channel type varied across the three study reaches at Como Creek (Table 1). CC1 and CC3 contained slightly wider, single channels, whereas CC2 was multi-threaded with multiple narrow channels and a lower slope. At CC2, lateral connectivity between the stream channel and floodplain was apparent, as areas of the floodplain were saturated, in contrast to CC1 and CC3.

3.2. CPOM transport during snowmelt: transport rate-discharge rating curve and annual CPOM yield

Peak discharge for the 2022 water year at Gordon Gulch was 31.90 liters per second (l s^{-1}) and occurred on May 31. The highest peak annual flow over the 10-year discharge record at Gordon Gulch was 117.021 s^{-1} on May 8, 2021, whereas the lowest peak annual flow was 19.071 s^{-1} on April 25, 2018, and the mean peak annual flow was 42.821 s^{-1}. The Gordon Gulch discharge record excludes an extreme rainfall event that occurred across the Colorado Front Range in September 2013 (Gochis et al., 2015), causing significant flooding. Although discharge during the September 2013 flood exceeded the 117.021 s^{-1} recorded in 2021, the gage at Gordon Gulch was lost during the flood; therefore, discharge data are unavailable for this period (Anderson and Ragar, 2021). Peak annual discharge at Gordon Gulch occurred during snowmelt rather summer convective storms in water year 2022 and for every water year on record except for 2012 and 2013.

Peak discharge for the 2022 water year at Como Creek was 405.141 s^{-1} and occurred on June 12. The highest peak annual flow during the 6 years of discharge sampling at Como Creek was 1792.711 s^{-1} on June 10, 2017, whereas the lowest peak annual flow was 357.261 s^{-1} on June 18, 2018. The mean peak annual flow over the 6-year period of discharge sampling was 743.421 s^{-1}. Peak annual discharge in water year 2022 and for each water year on record occurred during snowmelt.

CPOM transport rate (g min^{-1}) was highest on the rising limb at all sampling locations, and both CPOM transport rate and stream discharge were considerably higher at Como Creek than at Gordon Gulch during our study (Figure 4). Exceptionally high CPOM transport occurred at Como Creek CC3 on June 6, 2022, prior to peak flow (Figure 4E). Hysteresis of CPOM transport rate (higher on the rising limb compared to the same discharge on the falling limb) was evident at Lo-ret, CC1, and CC3 (Figure 5), and less evident at Hi-ret and CC2 (See Supplementary material S2), but the relatively low CPOM transport rate at Hi-ret may have resulted in an inability to detect hysteresis.

We found statistically significant power law rating curves between CPOM transport rate and stream discharge on both the rising and falling limbs in the Lo-ret, Hi-ret and CC3 reaches (Figure 6). Given the relatively short lengths of the Hi-ret and Lo-ret reaches, and the small difference in transport rate between the upstream and downstream ends of the two reaches (see section 3.3 below), we included CPOM transport rate data points from both the upstream and downstream sampling locations within each reach to develop reach-level rating curves for Gordon Gulch (Figures 6A, B). We were unable to develop statistically significant rating curves between CPOM transport rate and discharge at several of the four Gordon Gulch sampling locations (See Supplementary material S2) and at both CC1 and CC2, the two sites located downstream of the river bead at Como Creek (See Supplementary material S2).

We used the rating curves shown in Figure 6 and discharge data for both Gordon Gulch and Como Creek to calculate the annual CPOM yield (kg ha^{-1} yr^{-1}) at Lo-ret, Hi-ret, and CC3 (Figure 6D). The annual CPOM yield for the 2022 water year was 2.07×10^{-2} at Lo-ret, and 5.69×10^{-3} kg ha^{-1} yr^{-1} at Hi-ret. The mean annual yield at Lo-ret calculated using 10 years of discharge data and our CPOM-discharge rating curve was 13.00 kg ha^{-1} yr^{-1} (median = 0.013 kg ha^{-1} yr^{-1}). In Hi-ret, the mean annual yield over that same 10-year time period was 0.29 kg ha^{-1} yr^{-1} (median = 0.004 kg ha^{-1} yr^{-1}). The annual CPOM yield

TABLE 1 Geomorphic and forest stand characteristics of study reaches.

Reach	Bankfull width (m)	Canopy density (%)	Basal area (m^2 ha^{-1})	Slope (%)	D50 (mm)	D84 (mm)	Retentive feature frequency (# m^{-1})	Wood frequency (# m^{-1})
Lo-ret	1.41	60.48	15.06	4.78	29.00	92.00	1.91	0.35
Hi-ret	1.00	84.01	16.95	5.38	31.50	100.00	2.03	0.89
GG1	1.92	62.21	7.53	4.93	18.50	59.48	2.11	0.90
GG2	1.11	81.54	25.11	5.97	28.00	86.00	2.14	1.24
GG3	1.51	92.55	32.64	7.51	49.00	160.48	3.99	1.50
GG4	0.90	82.75	17.57	4.85	21.00	79.12	2.38	0.58
GG5	1.15	90.73	30.13	10.31	0.10	26.00	3.45	1.13
GG6	0.88	79.98	20.71	9.16	2.00	65.80	2.49	0.55
GG7	0.94	81.97	12.55	15.82	48.00	182.24	2.65	0.26
GG8	0.82	86.31	15.06	17.56	43.50	254.84	1.80	0.88
GG9	0.92	59.01	12.55	30.77	41.50	279.16	3.85	1.54
GG10	1.00	58.01	9.41	31.73	27.00	160.00	2.72	0.70
GG11	0.90	78.88	13.18	18.05	44.00	125.40	4.29	0.68
GG12	0.80	76.86	22.60	16.67	66.00	151.16	3.16	0.75
CC1	1.99	87.21	19.58	15.07	116.00	260.00	NA	NA
CC2	2.63	78.20	19.37	6.13	64.00	168.08	NA	NA
CC3	2.46	93.97	30.13	9.66	104.00	260.00	NA	NA

for the 2022 water year at CC3 was 0.15 kg ha^{-1} yr^{-1}. The mean annual yield calculated using 6 years of discharge data and our CPOM-discharge rating curve for Como Creek was 2.04 kg ha^{-1} yr^{-1} (median = 1.43 kg ha^{-1} yr^{-1}) (Figure 6D). For Como Creek, DOC export over the 2022 water year at CC3 was 12.3 Mg C, whereas POC export from CPOM over the same time period was 0.063 Mg C.

3.3. Geomorphic controls on CPOM transport

CPOM transport rate at Gordon Gulch was generally slightly higher in Lo-ret compared to Hi-ret during the summer 2022 sampling period (Figure 4). Mean CPOM transport rate over the entire summer was highest at the upstream end of Lo-ret (0.12 g min^{-1}), followed by the downstream end of Lo-ret (0.05 g min^{-1}), the downstream end of Hi-ret (0.02 g min^{-1}), and finally, the upstream end of Hi-ret (0.02 g min^{-1}). However, there was no significant difference between upstream and downstream sampling locations for either Hi-ret (p = 0.22) or Lo-ret (p = 0.76) when comparing measurements taken on the same sampling date (Figure 7). Como Creek CPOM transport rate was highest at CC3 and lowest at CC2 on the vast majority of our sampling dates (Figures 4E, F). Differences in CPOM transport rate between sampling locations at Como Creek were most apparent at higher flows between June 6 and June 21 (Figures 4E, F). During this time, CPOM transport rates at CC3, the most upstream site, were 14.5–694.8 times that of CC2 (just downstream of the bead), and 4.2–86.5 times that of CC1 (furthest downstream).

3.4. Controls on CPOM storage at Gordon Gulch

CPOM load was higher in dry (n = 5) reaches compared to those with flowing water (n = 9) (p= 0.08; Figure 8B), but there was no difference in CPOM accumulation frequency when comparing dry and flowing water reaches (p = 0.52; Figure 8D). Similarly, there was no difference between multi-thread and single thread reaches in CPOM load (p = 0.17; Figure 8A) or frequency (p = 0.37; Figure 8C), although the sample size for multi-thread reaches was extremely small (n = 3). Converting volume per area of CPOM accumulations to mass per area, reach-level AFDM at Gordon Gulch ranged from 2.40 to 9.23 g m^{-2}, with a mean of 5.55 g m^{-2}.

The selected models of CPOM load (volume per area) and CPOM frequency (number of accumulations per m), chosen as the models with the lowest AICc value and fewest predictor variables, are shown in Table 2. The model of CPOM load included bankfull width as the only predictor variable (Figure 9A, Table 2), whereas the model of CPOM accumulation frequency included retentive feature frequency as the only predictor variable (Figure 9B, Table 2). Additional models with AICc within two units of the lowest AICc value are presented in Supplementary material S3 and Table 2 also shows the three variables with the highest relative ranked importance across all models using the sum of the Akaike weights, indicating that

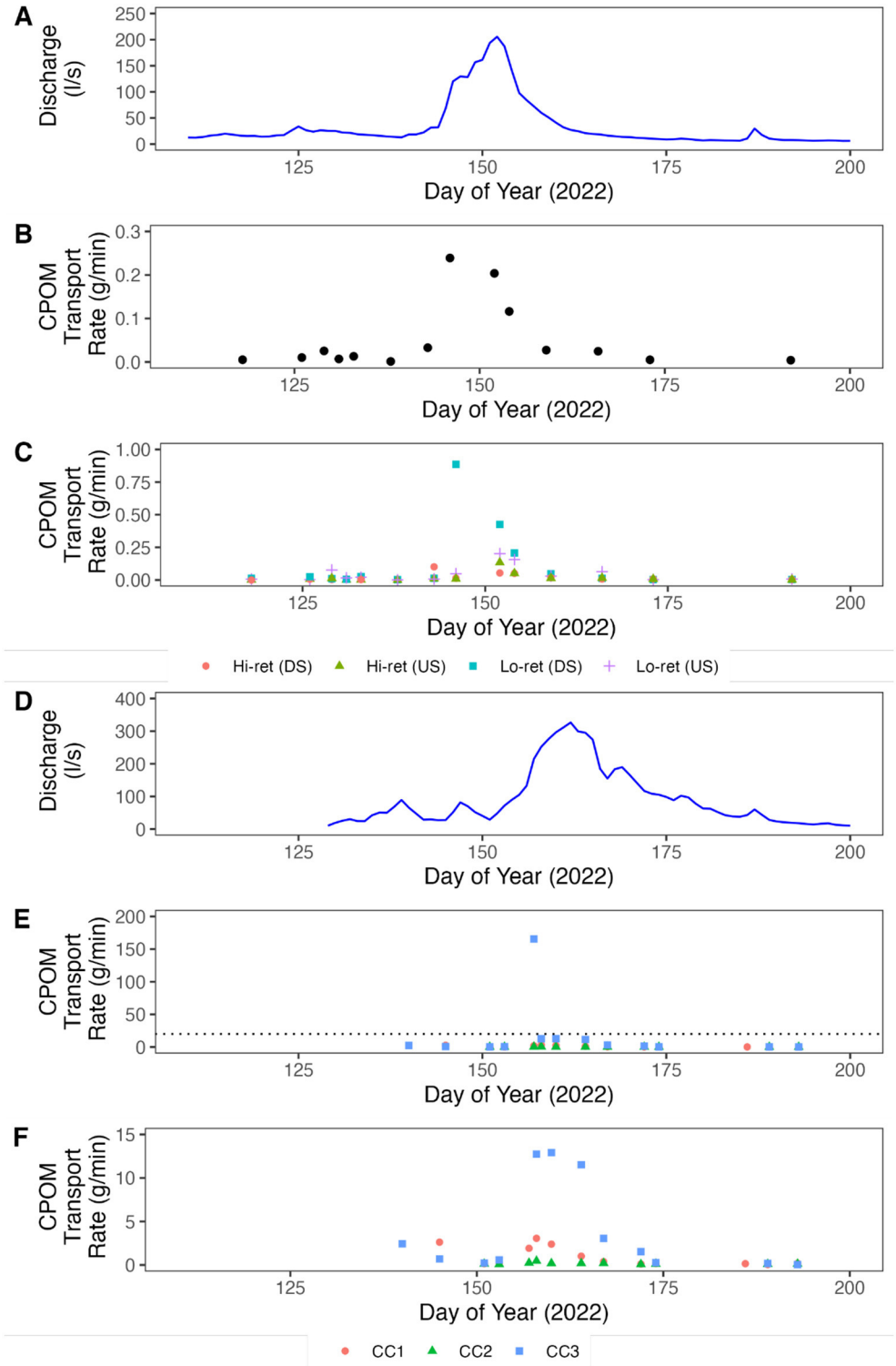

FIGURE 4
CPOM transport under varying flow conditions. **(A)** Mean daily discharge at Gordon Gulch. **(B)** CPOM transport rates for Gordon Gulch. Points represent the mean transport rate across all four locations (upstream and downstream for Lo-ret and Hi-ret) for a given day. **(C)** CPOM transport rates for Gordon Gulch showing measurements at individual sampling locations. **(D)** Mean daily discharge at Como Creek. **(E)** CPOM transport rates for Como Creek. Dotted line indicates y-axis limit for subsequent plot **(F)**. **(F)** CPOM transport rates for Como Creek with the high measurement at CC3 on day 157 removed to highlight lower magnitude trends during peak flow period.

bankfull width is an important variable for CPOM load and that retentive feature frequency is an important variable for CPOM frequency. We found a significant positive correlation between CPOM accumulation frequency and retentive feature frequency ($\tau = 0.80$, $p < 0.001$) (Figure 9B), but no other variables were significantly correlated with either CPOM

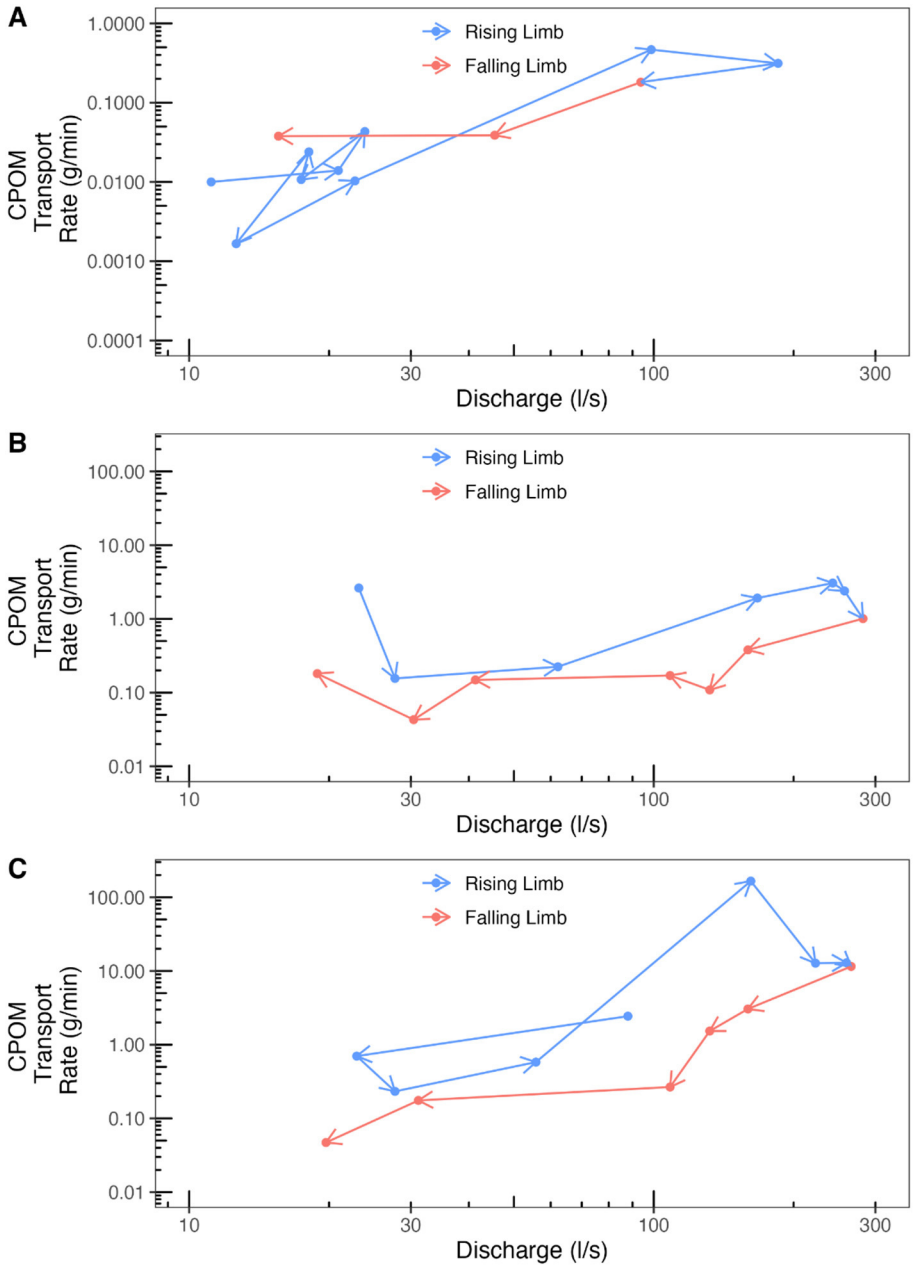

FIGURE 5
CPOM transport rate-discharge relationship through time, demonstrating hysteresis, at **(A)** Lo-ret reach, **(B)** CC1, and **(C)** CC3. Arrows show the forward progression of time. Axes are on a log scale. Note different y-axis scales for Gordon Gulch and Como Creek study reaches.

load or CPOM accumulation frequency (Figures 9C–F). Additional correlations between all variables are provided in Supplementary material S4.

Woody CPOM pieces stored a higher proportion of the total number of CPOM accumulations than any other retention mechanism at Gordon Gulch (Figure 10A). Woody CPOM pieces also stored the highest proportion of the total volume of CPOM across the surveyed reaches of Gordon Gulch (Figure 10B), followed by live vegetation. Woody CPOM key pieces responsible for trapping and storing CPOM accumulations were excluded from estimates of CPOM load in the proportion analysis shown in Figure 10A so as to avoid double counting woody CPOM as both a retention mechanism and stored CPOM.

4. Discussion

4.1. CPOM transport rate-discharge relationships, multi-year CPOM yield, and POC export

Our results indicate discharge is a primary control on CPOM transport rate, since there were significant positive relationships

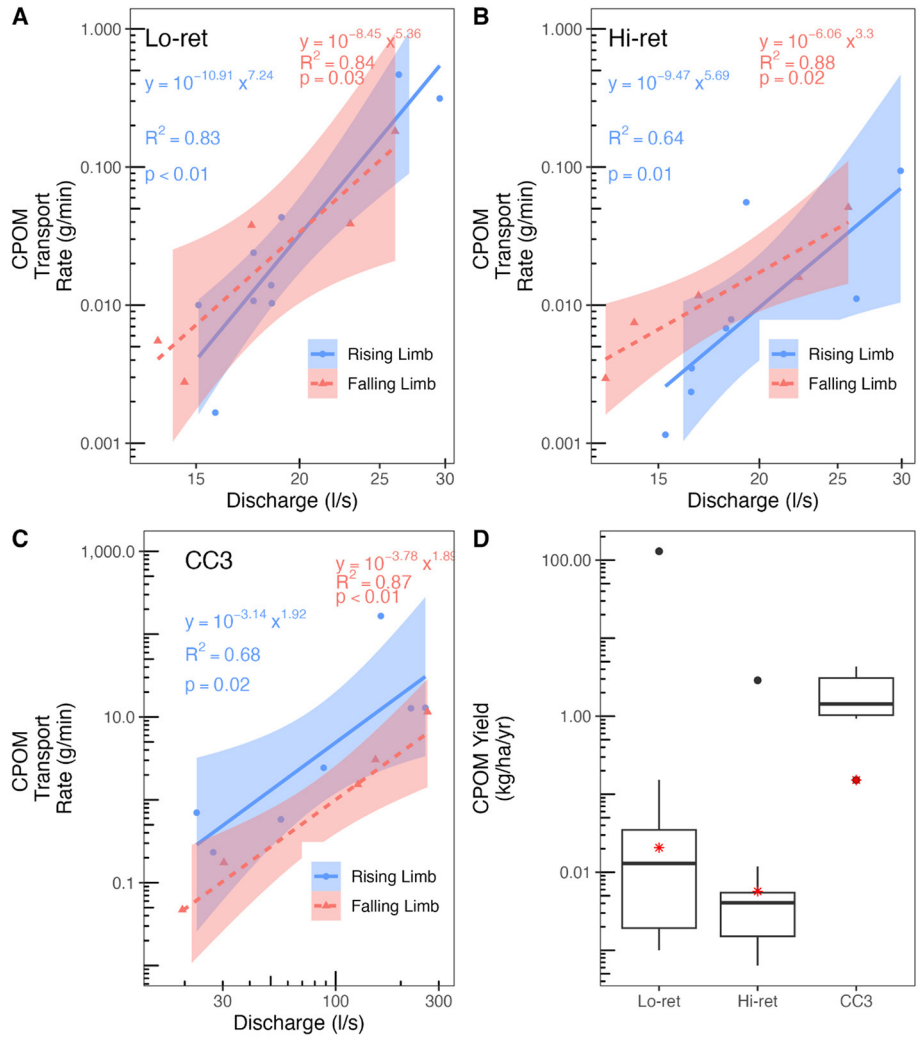

FIGURE 6
Power law rating curves for CPOM transport vs discharge at **(A)** Lo-ret (exponent $\beta = 7.24 \pm 1.25$ on rising limb; $\beta = 5.36 \pm 1.37$ on falling limb) ($\pm$ standard error), **(B)** Hi-ret ($\beta = 5.69 \pm 1.63$ on rising limb; $\beta = 3.30 \pm 0.70$ on falling limb), and **(C)** CC3 ($\beta = 1.92 \pm 0.59$ on rising limb; $\beta = 1.89 \pm 0.36$ on falling limb). Axes are on a log scale. Shaded area in panels A, B, and C shows 95% confidence interval. **(D)** Range in annual CPOM yield over 10-year period in Gordon Gulch (Lo-ret, Hi-ret), and 6-year period in Como Creek (CC3). Red stars represent CPOM yields during the 2022 water year, the solid line within the box represents the median value, the top and bottom of the box represent the upper and lower quartiles respectively, and the whiskers show the 10th and 90th percentiles. The y-axis is on a log scale.

between CPOM transport rate and stream discharge at our study sites (Figure 6). Similar relationships have been observed previously in the Rocky Mountains (Bunte et al., 2016; Marshall et al., 2021), Swiss Alps (Turowski et al., 2013, 2016), and Chilean Coastal Mountain Range (Iroumé et al., 2020). We also observed clear clockwise hysteresis in CPOM transport rate at Como Creek, and weaker clockwise hysteresis at Gordon Gulch (Figure 5), indicating that flows of similar magnitude were associated with higher CPOM transport rates on the rising limb than the falling limb (Figure 4). Clockwise hysteresis has been observed in several other streams in the Rocky Mountains (Bunte et al., 2016; Marshall et al., 2021). Hysteresis may be evidence that the stream is CPOM transport limited prior to peak flow and supply limited following peak flow, as has been hypothesized for other Rocky Mountain streams (Bunte et al., 2016). This assumes that high quantities of CPOM are stored in the stream channel and mobilized on the rising limb of snowmelt discharge. On the falling limb, much of the potentially mobile CPOM likely has already been mobilized, leading to reduced CPOM transport rates, unless stocks of CPOM are replenished by litterfall or from upstream sources (e.g., mobilized CPOM from logjam or other retentive feature failure). Previous studies have shown that considerable quantities of CPOM are deposited into river channels during fall when riparian vegetation sheds leaves and needles (Minshall et al., 1992; Wallace et al., 1995; Benfield et al., 2000), and we also observed this at our field sites, although we did not quantify fall (September-December) CPOM loads. CPOM deposited in the fall is likely not subjected to mobilizing streamflow until the following spring or summer in our snowmelt-dominated study sites. When snowmelt is high enough to increase discharge, CPOM is mobilized on the rising limb of the snowmelt peak (Figure 5), indicating a seasonal pattern of CPOM transport rates. However, this seasonal pattern is likely

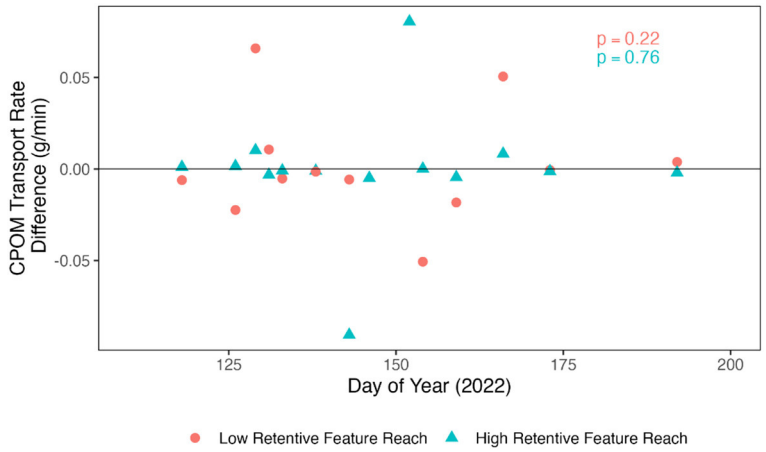

FIGURE 7
Difference in CPOM transport rate at the upstream versus downstream end of each reach at Gordon Gulch (Lo-ret and Hi-ret) on each sampling date. P-values were calculated using the paired Wilcoxon rank sum test to determine whether upstream transport rate was significantly different than downstream transport rate (paired by sampling date) at each reach.

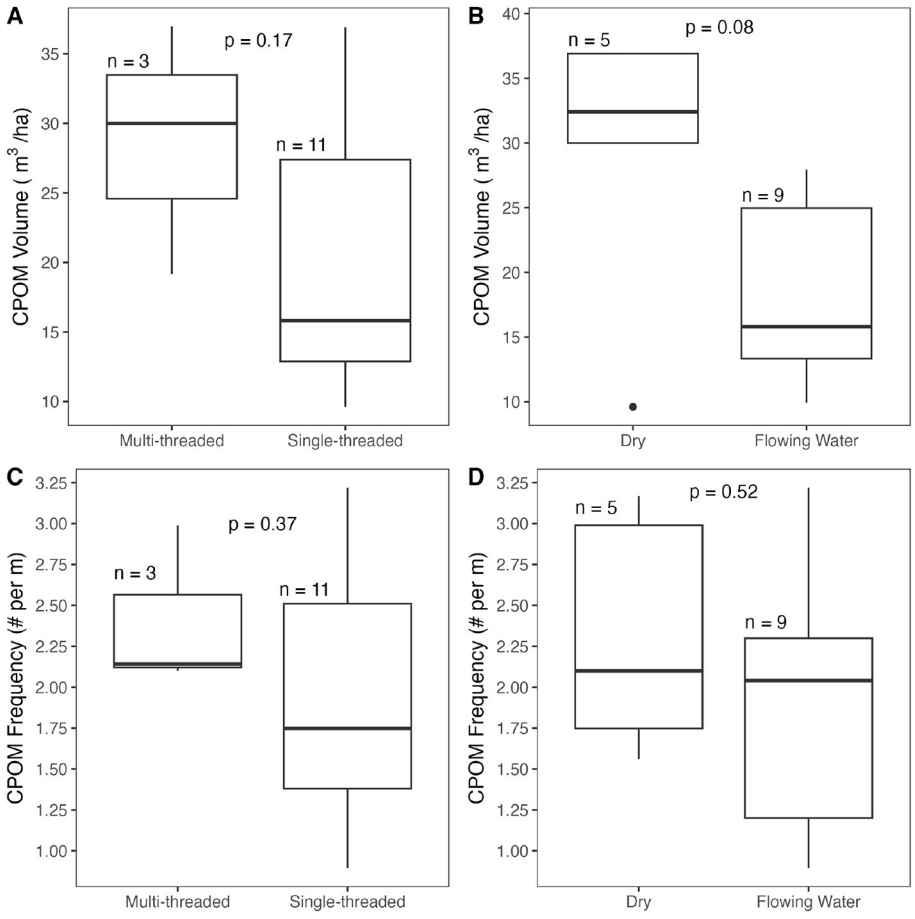

FIGURE 8
Plots of CPOM load and frequency at Gordon Gulch, including **(A)** CPOM volume per hectare in single- and multi-threaded reaches, **(B)** CPOM volume per hectare in dry reaches and reaches with flowing water, **(C)** CPOM accumulations per meter in single- and multi-threaded reaches, and **(D)** CPOM accumulations per meter in dry reaches and reaches with flowing water. The solid line within the box represents the median value, the top and bottom of the box represent the upper and lower quartiles respectively, and the whiskers show the 10th and 90th percentiles.

TABLE 2 Top model for CPOM load and frequency, chosen as the model with the lowest AICc and fewest predictor variables.

Response variable	Predictor variables [*p* value]	β	(R^2) and [*p* value] of model	Importance
CPOM load (m^3 ha^{-1})	Bankfull width [0.04]	−17.05	(0.30) [0.04]	Bankfull Width: 57% Wood volume: 35% Slope: 24%
CPOM frequency (# m^{-1})	Retentive feature frequency [<0.01]	0.86	(0.86) [<0.01]	Retentive feature frequency: 100% Wood volume: 44% Basal area: 25%

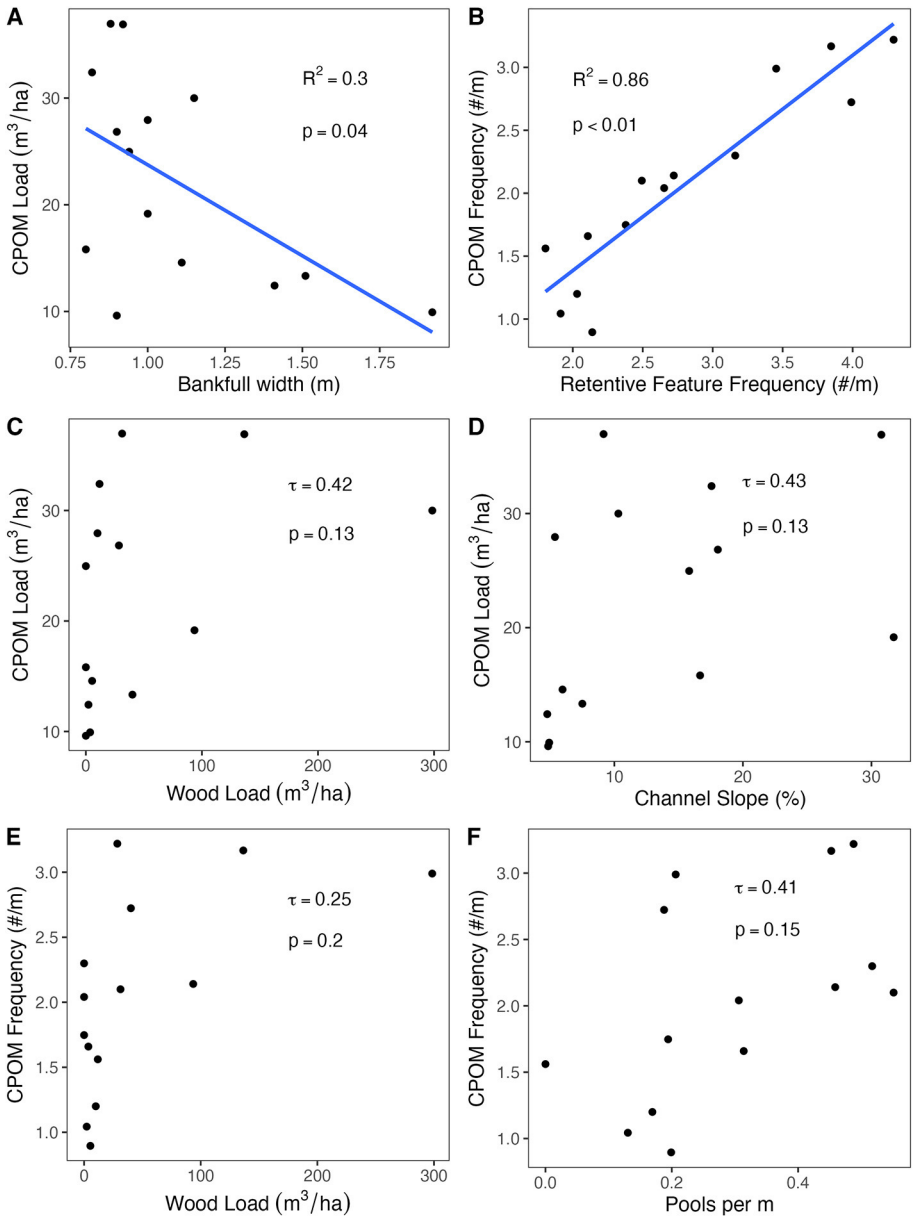

FIGURE 9
Scatter plots of **(A)** CPOM load versus bankfull width with linear regression line included (see Table 2), **(B)** CPOM frequency versus retentive feature frequency with linear regression line included (see Table 2), **(C)** CPOM load versus wood load, **(D)** CPOM load versus stream slope, **(E)** CPOM frequency versus wood load, **(F)** CPOM frequency versus pool frequency.

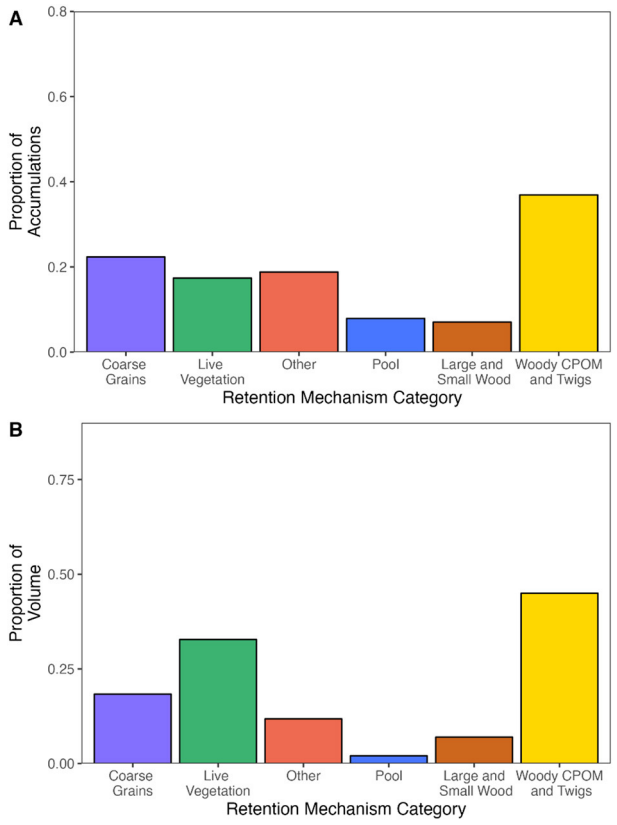

FIGURE 10
(A) Proportion of the number of CPOM accumulations stored by each retention mechanism class. **(B)** Proportion of CPOM volume (m^3) stored by each retention mechanism class. Size classes include large wood: >1m in length by >0.1 m in diameter; small wood: >1 m in length by 0.05–0.1 m in diameter or 0.5–1 m in length by >0.1 m in diameter; woody CPOM: smaller than small wood category and > 0.2 m in length; small woody CPOM (twigs): <0.2 m length. Note that accumulations may be stored by more than one category, and therefore, total proportions may be greater than 1. Key woody CPOM pieces responsible for storing CPOM accumulations were removed from estimates of CPOM load in Figure 10 so as to avoid double counting woody CPOM pieces as contributing to both retention and total volume.

quite different in other regions; for example, in rainfall-dominated deciduous forests, large spikes in CPOM transport have been observed following leaf abscission in the fall and winter (Wallace et al., 1995).

Because there is a strong seasonal pattern of CPOM transport rates, expected reductions in mountain snowpack and snowmelt streamflow magnitude due to climate change (Mote et al., 2018; Musselman et al., 2021; Hale et al., 2022) may modify the relationship between discharge and CPOM transport rates. Climate change impacts may reduce the CPOM transport capacity of many small headwater streams in snowmelt dominated systems or modify the timing of significant CPOM export from snowmelt peaks to peaks driven by summer convective storms. For example, increased precipitation in the form of rain following leaf abscission could shift the timing of CPOM transport toward the fall and winter, shifting previously snowmelt dominated systems toward patterns observed in deciduous, rainfall-dominated watersheds (Wallace et al., 1995).

Peak CPOM transport rates preceded peak discharge at both Gordon Gulch and Como Creek (Figure 4), suggesting that a critical discharge threshold for CPOM transport may exist, above which the majority of CPOM stored in a stream is mobilized. The threshold for CPOM mobility likely depends on the retentiveness of features storing CPOM (i.e., the ability of a feature to store CPOM for longer periods of time), and the mobility of CPOM particles has been shown to vary due to composition and size of stored CPOM particles (Webster et al., 1994; Wallace et al., 1995). Future research into critical discharge thresholds (or critical shear stresses) for a range of CPOM particles under a range of retentive feature types could help identify this threshold for a wider range of rivers with different geomorphic settings.

When comparing CPOM yields at Como Creek and Gordon Gulch to CPOM yields at other sites from previous studies, there is not a clear pattern in CPOM yield between climate regions (Table 3). Annual CPOM yields for the 2022 water year at our study sites, calculated using our CPOM transport rate-discharge rating curves, were lower than those estimated elsewhere in previous studies (Table 3) (Bilby and Likens, 1980; Bunte et al., 2016; Turowski et al., 2016; Iroumé et al., 2020). Although the 2022 water year CPOM yield was lower than published estimates from other studies, the multi-year average CPOM transport rates for our study reaches were similar to previous studies, with the exception of lower average yield calculated for the Hi-ret reach (Table 3). The one study in which CPOM yield is much greater than our study sites is the Erlenbach Torrent in Switzerland (Turowski et al., 2016). Although the contribution of large wood to CPOM yield in the Erlenbach was negligible, their definition of CPOM varied from ours in that it included what we consider small wood in our study, but the high CPOM yield in the Erlenbach indicates there are likely substantial variations in CPOM yield between watersheds (Table 3). It is important to note that our multi-year average CPOM yield was based on a single year of CPOM transport rate sampling and then applying a rating curve from one year to multiple years highlighting the need for continued, multi-year sampling of CPOM transport at Gordon Gulch, Como Creek, and other locations. Additionally, given the low background levels of CPOM transport at Gordon Gulch, small increases in CPOM transport rate—for example the addition of a single intact leaf or stick fragment falling into the stream—would have resulted in significant spikes in CPOM, adding further uncertainty to our CPOM transport rate-discharge rating curves. Rating curves produced through least squares regression can also contain biases which can significantly affect annual and multi-year yields. In their study, Ferguson (1986) found that rating curves using log-log scales can underestimate river sediment, solute, and pollutant loads by as much 50%. Published estimates of CPOM yield in wetter climates with higher mean annual precipitation, and thus likely more aboveground biomass and potential CPOM inputs to stream, do not appear to have consistently higher CPOM yields compared to drier climates. We also note that published studies of CPOM yield use differing sampling durations, ranging from several minutes to several days (Turowski et al., 2013; Bunte et al., 2016; Iroumé et al., 2020). The lack of patterns across climate regions highlights the need for additional data and standardization of CPOM sampling procedures across studies including sampling

TABLE 3 Comparison of annual CPOM yield with results from previous studies.

Stream	Drainage area (km^2)	Mean annual precipitation (mm)	Mean annual temperature (°C)	Annual study year CPOM yield (kg ha^{-1} yr^{-1})	Multi-year average annual CPOM yield (kg ha^{-1} yr^{-1})	Annual CPOM yield range (kg ha^{-1} yr^{-1})
Gordon Gulch Lo-ret Reach (Colorado, USA)	3.6	500–520[a,b]	5–6.1[a,b]	0.02	13.00 (10 years)[c]	0.001–129.79[d]
Gordon Gulch Hi-ret Reach (Colorado, USA)	3.6	500–520[a,b]	5–6.1[a,b]	0.01	0.29 (10 years)[e]	0.0006–2.88[f]
Como Creek (Colorado, USA)	4.9	1,020[b]	1[b]	0.15	2.03 (6 years)	0.015–4.32
Vuelta de Zorra (Los Ríos, Chile) Iroumé et al. (2020)	5.85	>2,400	12.2	0.8–6.8	6.8 (10 years)	0.68–6.98
Little Granite Creek (Wyoming, USA) Bunte et al. (2016)	13.09	300	1[g]	2.75	8.63 (10 years)[h]	NA
East St Louis Creek (Colorado, USA) Bunte et al. (2016)	8.03	750	0.6[i]	3.99	12.70 (10 years)[h]	NA
Erlenbach Torrent (Canton of Schwyz, Switzerland) Turowski et al. (2016)	0.70	2,290[h]	4.5[j]	NA	246 (10 years)[k]	NA
Hubbard Brook Watershed 5 (New Hampshire, USA) Bilby and Likens (1980)	< 0.77	1,400	4.1–6.4 [l]	2.4–11.2	7.17 (12 years)	2.4–11.2
Hubbard Brook Watershed 6 (New Hampshire, USA) Bilby and Likens (1980)	<0.77	1,400	4.1–6.4[l]	1.0–6.7	3.11 (12 years)	1.0–6.7

[a] Anderson et al. (2021).
[b] Swetnam et al. (2017).
[c] Mean CPOM yield with exceptionally high 2021 water year included. Mean CPOM yield with 2021 water year excluded was 0.03 kg ha^{-1} yr^{-1}.
[d] Range in CPOM yield with exceptionally high 2021 water year included. Range in CPOM yield with 2021 water year excluded was 0.001–0.15 kg ha^{-1} yr^{-1}.
[e] Mean CPOM yield with exceptionally high 2021 water year included. Mean CPOM yield with 2021 water year excluded was 0.004 kg ha^{-1} yr^{-1}.
[f] Range in CPOM yield with exceptionaly high 2021 water year included. Range in CPOM yield with 2021 water year excluded was 0.0006–0.01 kg ha^{-1} yr^{-1}.
[g] Ryan et al. (2011).
[h] Calculated as geometric mean of measured CPOM yield during study and their 10-fold values (Bunte et al., 2016).
[i] Jochner et al. (2015).
[j] Rhoades et al. (2017).
[k] Decadal average includes large wood pieces, which were not measured as part of CPOM transport rates in our study.
[l] Bailey et al. (2003).

equipment, timing, and duration, to constrain CPOM transport drivers and processes, and may point to CPOM transport as a stochastic process.

Our comparison of DOC versus POC export demonstrated that DOC export from CC3 (12.3 Mg C) during the 2022 water year was substantially higher than our estimate of POC export in the form of CPOM (0.063 Mg C). In comparison to other studies, DOC export at CC3 was nearly 1.5 times the estimated DOC export of the Erlenbach Torrent, Switzerland (7.9 Mg C) (Turowski et al., 2016). CPOM and large wood accounted for a substantial percentage (~80%) of the total carbon export in the Erlenbach Torrent (Turowski et al., 2016). However, we did not measure large wood transport in our OC export estimate, and given the flow magnitudes observed in our study basins and stream size, we do not expect significant large wood transport. Furthermore, our study was conducted during a relatively low water year. Given that CPOM transport is associated with flow magnitude (Figures 4, 6), CPOM transport may constitute a greater proportion of total carbon export at our study sites during higher flow years. In addition, measurement during a higher flow year may result in different rating curves compared to the rating curves developed for the 2022 water year. Additional studies under different flow conditions would help improve our understanding of how CPOM transport rates influence total OC export from small headwater streams.

4.2. The impact of geomorphic characteristics on CPOM transport rates

Our results from Gordon Gulch did not support our hypothesis that within-a-reach retentive feature frequency would significantly impact local CPOM transport (H2a). We expected that high retentive feature frequency in Hi-ret would reduce longitudinal connectivity of CPOM, resulting in lower CPOM transport rates at the downstream end of Hi-ret. However, there was no significant difference between CPOM transport rates at the upstream and

downstream ends of either Hi-ret or Lo-ret (Figures 4, 7). This suggests that retentive feature frequency within a reach may not significantly impact downstream CPOM transport. It also suggests that our study reaches may be close to a steady state in terms of CPOM transport, where the amount of CPOM entering the reach is relatively equal to the amount of CPOM leaving the reach, despite the difference in retentive feature frequency between Lo-ret and Hi-ret. In another study in the Colorado Rocky Mountains, Marshall et al. (2021) found that CPOM transport was not impacted by an upstream channel-spanning log jam (i.e., accumulation) compared to a site without a log jam just upstream, demonstrating that a single retentive instream feature likely does not modify localized CPOM transport rates. Our study design differed in that our Hi-ret site contained many retentive features rather than a single feature, but our results also indicate that within-a-reach retention does not have a measurable impact on CPOM transport rates. However, it is possible that factors such as the low peak streamflow magnitude during the year of our study may have limited our ability to test hypothesis H2a. CPOM stored behind some retentive features, such as stable log jams, may require flows of exceptional magnitude (e.g., 20-year recurrence interval) to become mobilized (Jochner et al., 2015). Peak annual discharge for the 2022 water year was lower than that of five out of the past 10 years for which there are discharge data at Gordon Gulch, and thus it is possible that we missed certain CPOM transport trends that would have been exaggerated under higher-magnitude flows such as during the 2021 water year, the 2013 flood (Gochis et al., 2015), or in a year with multiple high flows (e.g., snowmelt with additional peaks due to late summer convective storms). Additionally, although we assessed the impact of retentive features on CPOM transport rates over a distance of 65m in our Hi-ret reach, and 23 min our Lo-ret reach, it is possible that the lengths of our two study reaches did not fully capture trends in CPOM transport through highly retentive streams over greater distances.

Although we did not find evidence that within-a-reach retentive features impact CPOM transport rates in Gordon Gulch, our results from Como Creek suggest that differences in valley bottom geometry (i.e., river beads versus narrow, confined reaches) are associated with differences in CPOM transport rates. At Como Creek, our results supported our hypothesis that retentive reaches such as river beads would result in lower downstream CPOM transport compared to locations downstream of more confined reaches (i.e., CC3) (H2b). CPOM transport was highest at CC3, the reach upstream of the river bead, and lowest at CC2, the reach just downstream of the river bead (Figures 4E, F), suggesting that CPOM is retained in wide, multithreaded, gradually sloping valley bottoms. Because CC1, the furthest downstream reach, also had reduced CPOM transport relative to the reach above the river bead, the impact of the river bead on CPOM transport rates likely extends downstream. Our results support previous studies that have identified river beads as regions of high organic matter retentiveness, for example in the form of large wood (Wohl et al., 2018; Sutfin et al., 2021). River beads store a disproportionate amount of organic carbon relative to the total stream length they cover in many watersheds (Sutfin et al., 2016, 2021; Wohl et al., 2018). Floodplain deposition of CPOM in tandem with reduced transport capacity of CPOM in beads relative to steeper, more confined reaches may reduce CPOM transport rates at river bead outlets and in reaches downstream of—but in close proximity to—river beads, explaining the lower rates of CPOM transport at our two downstream study reaches (CC1 and CC2). Given the scarcity of prior research into the impacts of valley bottom geometry on CPOM transport, further research is necessary to assess the scales at which geomorphic complexity influences CPOM transport.

4.3. Controls on patterns in CPOM storage

The results of our correlation analyses and regression model selection indicate that retentive feature frequency was strongly correlated and associated with CPOM accumulation frequency but was not significantly correlated with CPOM load (Figure 9B, Table 2; Supplementary materials S3, S4), partially supporting our hypothesis that high retentive feature frequency would be associated with higher CPOM storage (H3a). Although CPOM accumulation frequency increased with increased retentive feature frequency, not all CPOM accumulations trapped by retentive features were large, which may explain why retentive feature frequency does not appear to exert a strong influence on CPOM load. Bankfull width was strongly associated with CPOM load, with narrow stream channels associated with increased CPOM load (Figure 9A, Table 2). CPOM storage measurements occurred in early August under low flow conditions, after peak snowmelt flows, indicating that under low flow conditions during which transport capacity is reduced, narrower channels may have a higher capacity for CPOM retention or trapping. This may be due to an increased probability of CPOM particles interacting with the channel boundary and associated retentive features in narrower channels compared to wider channels.

Among the six retention mechanisms for CPOM accumulations that we assessed, woody CPOM trapped the greatest amount of CPOM in terms of both load and frequency (Figure 10). Large and small wood have been found to be highly effective retentive features for CPOM (Small et al., 2008; Jochner et al., 2015), however the role of woody CPOM and small woody CPOM in initiating the storage of additional CPOM in rivers has not been previously assessed. Furthermore, neither wood load nor wood frequency was included in the top model produced through our regression analysis, although wood was one of the retentive features included in retentive feature frequency. Thus, wood is just one of the retentive features associated with CPOM retention, and other factors also exert a strong control (e.g., woody CPOM, bankfull width). Hydrologic regime also appears to impact CPOM storage, with dry reaches associated with higher CPOM loads (Figure 8B). Few previous studies have measured CPOM storage under different hydrologic regimes, however, one other study found that intermittent streams were associated with widespread CPOM mats and longer residence time of CPOM (Wohl and Scamardo, 2022), suggesting that hydrologic regime (i.e., intermittent vs. perennial reaches) may influence the mode and residence time of CPOM storage. At our sites, it is likely that there was decreased mobilization and increased deposition of CPOM in the dry reaches. These results add to our limited understanding of CPOM storage in streams with intermittent flow regimes, which

may be more prevalent in small headwater streams in the future (Larned et al., 2010).

We found that woody CPOM and small woody CPOM were responsible for storing significant proportions of CPOM volume and of accumulations (Figure 10), supporting our hypothesis H3b, but other retention mechanisms were also effective. This result is significant, because although several previous studies have identified the importance of small wood in rivers (Figure 10) (Small et al., 2008; Galia et al., 2018; Wohl et al., 2019a), and the importance of wood in storing CPOM (Small et al., 2008; Jochner et al., 2015; Pfeiffer and Wohl, 2018), we are unaware of any studies that have examined potential feedback loops under which woody CPOM pieces can have an amplifying effect on subsequent CPOM storage in rivers. Our finding that woody CPOM and small woody CPOM key pieces stored the overwhelming majority of CPOM is likely due to the relatively small drainage area (and channel width) and low discharge of our basin. However, it highlights that future studies in headwater streams should use smaller woody size classes to investigate the role of wood in influencing CPOM dynamics. In addition, our results point to the need to understand how the relative influence of different size classes of wood scale with channel geometry metrics and drainage area.

4.4. Comparison of CPOM storage between regions

Comparisons of CPOM storage in Gordon Gulch to published estimates in different climate regimes demonstrate that CPOM storage is generally lower in semi-arid climates than in more temperate environments (Smock et al., 1989; Minshall et al., 1992; Benfield et al., 2000; Gorecki et al., 2006; Flores et al., 2011; Galia et al., 2022), likely due in part to increased primary productivity in wetter environments. Previous studies have used several different metrics to report CPOM storage, making broad comparisons across numerous studies difficult. However, post peak flow CPOM loads in semi-arid Gordon Gulch (9.61–36.96 m^3 ha^{-1}, mean = 22.20 m^3 ha^{-1}) were higher than those of the Krathis (mean = 5.44 m^3 ha^{-1} in lower Krathis; mean = 15.65 m^3 ha^{-1} in upper Krathis) and Kerinitis (mean = 4.85 m^3 ha^{-1}), two semi-arid, intermittent mountainous streams in Greece (Galia et al., 2022). Gordon Gulch CPOM storage was lower than in the temperate Kangaroo River, NSW, Australia (range of 17.1 to 46.6 m^3 ha^{-1} depending on river style (confined, alluvial, partially-confined), mean = 41.8 m^3 ha^{-1}) (Gorecki et al., 2006). At our sites in Gordon Gulch, post peak flow CPOM AFDM storage (range: 2.40 to 9.23 g m^{-2}; mean = 5.55 g m^{-2}) was somewhat lower than some other published studies. For example, in the semiarid Lower Salmon River, Idaho, USA coarse benthic organic matter AFDM ranged from 2.2 to 49.6 g m^{-2} (mean = 18.03 g m^{-2}), although the Salmon River is a much larger system than Gordon Gulch (Minshall et al., 1992). In Ball Creek and Coweeta Creek in North Carolina, USA, estimated coarse benthic organic matter AFDM was greater than 100 g m^{-2} at two study locations and greater than ~250 g m^{-2} in two other study locations (Benfield et al., 2000), indicating that CPOM storage is likely higher is the wetter, warmer southeastern USA. CPOM AFDM was significantly higher in Buzzards Branch (3356 g m^{-2}) and Colliers Creek (922 g m^{-2}) two headwater streams in Virginia (Smock et al., 1989), another regions with higher precipitation than our semi-arid study sites. An additional study conducted in four streams in the Basque Country, Spain, found that CPOM storage ranged from 9.3 to 631.9 g m^{-2}, and the CPOM storage was even higher after additional wood was intentionally placed in the stream (Flores et al., 2011). The potential influence of climate on CPOM storage is in contrast to comparisons of CPOM yield across climate regimes, which showed no clear trends between climate regime and CPOM yield (Table 3).

5. Conclusion

CPOM storage provides an important food source for benthic organisms, and CPOM export from headwater streams is a mechanism for energy transfer within watersheds and influences watershed OC cycling. However, there are few studies on the influence of geomorphic complexity on CPOM transport, and CPOM storage in streams with differing hydrologic regimes has only rarely been explored. We found that CPOM transport was related to discharge at both study sites, with CPOM transport rates higher on the rising limb of snowmelt discharge and decreasing through to the falling limb. We interpreted these findings as indicative of a transport limited environment on the rising limb, and a supply limited environment on the falling limb. POC export in the form of CPOM was much lower than DOC export at one of the study locations. Although we did not find a significant relationship between within-a-reach retentive feature frequency and CPOM transport, we did find that variations in valley bottom geometry influence CPOM transport, highlighting the importance of river beads in influencing longitudinal connectivity and mediating transport through the river network. Retentive feature frequency and bankfull width were the most important variables influencing CPOM frequency and CPOM load, respectively. Woody CPOM was the most effective retentive feature in storing additional CPOM in Gordon Gulch. This finding is important because it suggests that future studies should assess the role of woody material from a range of sizes including woody CPOM, especially in small headwater streams such as Gordon Gulch. Our results indicate that the processes driving CPOM transport and storage are complex and include geomorphic context and hydrology. Direct (e.g., dam construction water diversions, wood removal, logging) and indirect (e.g., changes to precipitation patterns and snowpack conditions) alterations to streams that modify peak flow magnitude frequency, valley bottom geometry and lateral connectivity, and instream wood and woody CPOM load could substantially impact CPOM transport and storage in headwater streams. Therefore, it is important to consider these potential impacts on CPOM transport and storage when managing headwater streams. However, more research is needed to fully understand the processes driving CPOM transport and storage in small headwater streams.

Data availability statement

The datasets presented in this study can be found in online repositories. The names of the repository/repositories and accession number(s) can be found below: https://www.hydroshare.org/resource/10f42e54d6144fd6a76ff726739bdf57/.

Author contributions

All authors listed have made a substantial, direct, and intellectual contribution to the work and approved it for publication.

Funding

Funding for this work was provided by the National Science Foundation Award # 2012669 Collaborative Research: Network Cluster: Quantifying controls and feedbacks of dynamic storage on critical zone processes in western montane watersheds. Additional funding and support were provided by the University of Colorado Department of Geography.

Acknowledgments

We thank Dr. Holly Barnard and Dr. Eve-Lyn Hinckley for their thorough review and feedback which have greatly improved this study. Aidan Fletcher provided incredible support throughout the entire summer field season, and for this we owe him our deepest gratitude. We would also like to thank Dr. Kristin Bunte who loaned us sampling equipment and provided insight into CPOM transport measurement techniques. The CU Boulder Laboratory for Interdisciplinary Statistical Analysis provided assistance with statistical methods used in this project.

Conflict of interest

The authors declare that the research was conducted in the absence of any commercial or financial relationships that could be construed as a potential conflict of interest.

Publisher's note

All claims expressed in this article are solely those of the authors and do not necessarily represent those of their affiliated organizations, or those of the publisher, the editors and the reviewers. Any product that may be evaluated in this article, or claim that may be made by its manufacturer, is not guaranteed or endorsed by the publisher.

Supplementary material

The Supplementary Material for this article can be found online at: https://www.frontiersin.org/articles/10.3389/frwa.2023.1227167/full#supplementary-material

References

Adams, H. R., Barnard, H. R., and Loomis, A. K. (2014). Topography alters tree growth–climate relationships in a semi-arid forested catchment. *Ecosphere* 5, art148. doi: 10.1890/ES14-00296.1

Anderson, S. P., Anderson, R. S., Hinckley, E.-L. S., Kelly, P., and Blum, A. (2011). Exploring weathering and regolith transport controls on Critical Zone development with models and natural experiments. *Appl. Geochemistr.* 26, S3–S5. doi: 10.1016/j.apgeochem.2011.03.014

Anderson, S. P., Hinckley, E.-L., Kelly, P., and Langston, A. (2014). Variation in critical zone processes and architecture across slope aspects. *Procedia Earth Planetar. Sci.* 10, 28–33. doi: 10.1016/j.proeps.2014.08.006

Anderson, S. P., Kelly, P. J., Hoffman, N., Barnhart, K., Befus, K., and Ouimet, W. (2021). "Is this steady state? weathering and critical zone architecture in gordon gulch, colorado front range," in *Hydrogeology, Chemical Weathering, and Soil Formation* (American Geophysical Union (AGU)), 231–252.

Anderson, S. P., and Ragar, D. (2021). *BCCZO—Streamflow/Discharge—(GGL_SW_0_Dis)—Gordon Gulch: Lower—(2011-2019), HydroShare*. Available online at: https://www.hydroshare.org/resource/c2384bd1743a4276a88a5110b1964ce0/

Bailey, A. S., Hornbeck, J. W., Campbell, J. L., and Eagar, C. (2003). *Hydrometeorological database for Hubbard Brook Experimental Forest: 1955-2000* (NE-GTR-305; p. NE-GTR-305). U.S. Department of Agriculture, Forest Service, Northeastern Research Station.

Barnard, H. R., Hornslein, N., Schiff, M., and Parrish, E. (2023). *DWCZ—CO—Gordon Gulch, 1 and 2—Streamflow/Discharge/Conductivity—(DWCZ-GG1-GG2_SW_0)—(2020-ongoing), HydroShare*. Available online at: https://www.hydroshare.org/resource/6a2503c69a0d4cd28cd5bfad7cd5b079/ (accessed May 15, 2023).

Bartoń, K. (2022). *MuMIn: Multi-Model Inference* (1.47.1) [Computer software]. Available online at: https://CRAN.R-project.org/package=MuMIn

Battin, T. J., Kaplan, L. A., Findlay, S., Hopkinson, C. S., Marti, E., Packman, A. I., et al. (2008). Biophysical controls on organic carbon fluxes in fluvial networks. *Nat. Geosci.* 1, 2. doi: 10.1038/ngeo101

Battin, T. J., Lauerwald, R., Bernhardt, E. S., Bertuzzo, E., Gener, L. G., Hall, R. O., et al. (2023). River ecosystem metabolism and carbon biogeochemistry in a changing world. *Nature* 613, 7944. doi: 10.1038/s41586-022-05500-8

Bellmore, J. R., and Baxter, C. V. (2014). Effects of geomorphic process domains on river ecosystems: a comparison of floodplain and confined valley segments. *River Res. Applicat.* 30, 617–630. doi: 10.1002/rra.2672

Benfield, E. F., Webster, J. R., Hutchens, J. J., Tank, J. L., and Turner, P. A. (2000). Organic matter dynamics along a stream-order and elevational gradient in a southern Appalachian stream. *SIL Proceed.* 27, 1341–1345. doi: 10.1080/03680770.1998.11901454

Bilby, R. E., and Likens, G. E. (1980). Importance of organic debris dams in the structure and function of stream ecosystems. *Ecology* 61, 1107–1113. doi: 10.2307/1936830

Bovill, W. D., Downes, B. J., and Lake, P. S. (2020). A novel method reveals how channel retentiveness and stocks of detritus (CPOM) vary among streams differing in bed roughness. *Freshwater Biol.* 65, 1313–1324. doi: 10.1111/fwb.13496

Bright, C. E., Mager, S. M., and Horton, S. L. (2020). Catchment-scale influences on riverine organic matter in southern New Zealand. *Geomorphology* 353, 107010. doi: 10.1016/j.geomorph.2019.107010

Bunte, K., Swingle, K., Abt, S., and Cenderelli, D. (2015). *Effects of Bedload Sampler Netting Properties on Hydraulic and Sampling Efficiency*.

Bunte, K., Swingle, K. W., and Abt, S. R. (2007). *Guidelines for using bedload traps in coarse-bedded mountain streams: Construction, installation, operation, and sample processing (Gen. Tech. Rep. RMRS-GTR-191; p. 91)*. U.S. Department of Agriculture, FOrest Service.

Bunte, K., Swingle, K. W., Turowski, J. M., Abt, S. R., and Cenderelli, D. A. (2016). Measurements of coarse particulate organic matter transport in steep mountain streams and estimates of decadal CPOM exports. *J. Hydrol.* 539, 162–176. doi: 10.1016/j.jhydrol.2016.05.022

Cole, J. J., Prairie, Y. T., Caraco, N. F., McDowell, W. H., Tranvik, L. J., Striegl, R. G., et al. (2007). Plumbing the global carbon cycle: integrating inland waters into the terrestrial carbon budget. *Ecosystems* 10, 172–185. doi: 10.1007/s10021-006-9013-8

Craney, T. A., and Surles, J. G. (2002). Model-dependent variance inflation factor cutoff values. *Qual. Eng.* 14, 391–403. doi: 10.1081/QEN-120001878

Dethier, D. P., Williams, N., and Fields, J. F. (2022). Snowmelt-driven seasonal infiltration and flow in the upper critical zone, niwot ridge (Colorado), USA. *Water* 14, 15. doi: 10.3390/w14152317

Ferguson, R. I. (1986). River loads underestimated by rating curves | semantic scholar. *Water Resour. Res.* 22, 74–76. doi: 10.1029/WR022i001p00074

Fisher, S. G., and Likens, G. E. (1973). Energy flow in bear brook, new hampshire: an integrative approach to stream ecosystem metabolism. *Ecologic. Monograph.* 43, 421–439. doi: 10.2307/1942301

Flores, L., Larrañaga, A., Díez, J., and Elosegi, A. (2011). Experimental wood addition in streams: effects on organic matter storage and breakdown. *Freshwater Biol.* 56, 2156–2167. doi: 10.1111/j.1365-2427.2011.02643.x

Fritz, K. M., Pond, G. J., Johnson, B. R., and Barton, C. D. (2019). Coarse particulate organic matter dynamics in ephemeral tributaries of a central appalachian stream network. *Ecosphere* 10, e02654. doi: 10.1002/ecs2.2654

Gaillard, J., Chanudet, V., Cunillera, G., and Dambrine, E. (2021). Coarse and fine particulate organic matter transport by a fourth-order mountain stream to lake bourget (France). *Water* 13, 19. doi: 10.3390/w13192783

Galia, T., Ruiz-Villanueva, V., Tichavsk,ý, R., Šilhán, K., Horáček, M., and Stoffel, M. (2018). Characteristics and abundance of large and small instream wood in a Carpathian mixed-forest headwater basin. *Forest Ecol. Manage.* 424, 468–482. doi: 10.1016/j.foreco.2018.05.031

Galia, T., Škarpich, V., and Vala, O. (2022). Trees and shrubs as components of the storage of coarse particulate organic matter and instream wood in Mediterranean intermittent streams. *Ecohydrol. Hydrobiol.* 8, 3. doi: 10.1016/j.ecohyd.2022.08.003

Gochis, D., Schumacher, R., Friedrich, K., Doesken, N., Kelsch, M., Sun, J., et al. (2015). The Great Colorado flood of september 2013. *Bull. Am. Meteorologic. Soc.* 96, 1461–1487. doi: 10.1175/BAMS-D-13-00241.1

Gomez, B., Trustrum, N. A., Hicks, D. M., Rogers, K. M., Page, M. J., and Tate, K. R. (2003). Production, storage, and output of particulate organic carbon: Waipaoa River basin, New Zealand. *Water Resour. Res.* 39, 6. doi: 10.1029/2002WR001619

Goñi, M. A., Hatten, J. A., Wheatcroft, R. A., and Borgeld, J. C. (2013). Particulate organic matter export by two contrasting small mountainous rivers from the Pacific Northwest, U.S.A. *J. Geophysic. Res. Biogeosci.* 118, 112–134. doi: 10.1002/jgrg.20024

Gorecki, V. I., Fryirs, K. A., and Brierley, G. J. (2006). The relationship between geomorphic river structure and coarse particulate organic matter (CPOM) storage along the Kangaroo River, New South Wales, Australia. *Austral. Geograph.* 37, 285–311. doi: 10.1080/00049180600954757

Hale, K. E., Wlostowski, A. N., Badger, A. M., Musselman, K. N., Livneh, B., and Molotch, N. P. (2022). Modeling streamflow sensitivity to climate warming and surface water inputs in a montane catchment. *J. Hydrol. Reg. Stud.* 39, 100976. doi: 10.1016/j.ejrh.2021.100976

Hilton, R. G., Galy, A., and Hovius, N. (2008). Riverine particulate organic carbon from an active mountain belt: importance of landslides. *Global Biogeochem. Cycles* 22, 05. doi: 10.1029/2006GB002905

Hilton, R. G., Galy, A., Hovius, N., Horng, M.-J., and Chen, H. (2011). Efficient transport of fossil organic carbon to the ocean by steep mountain rivers: an orogenic carbon sequestration mechanism. *Geology* 39, 71–74. doi: 10.1130/G31352.1

Hinckley, E.-L. S., Ebel, B. A., Barnes, R. T., Anderson, R. S., Williams, M. W., and Anderson, S. P. (2014). Aspect control of water movement on hillslopes near the rain–snow transition of the Colorado Front Range. *Hydrologic. Process.* 28, 74–85. doi: 10.1002/hyp.9549

Intergovernmental Panel on Climate Change (2006). *2006 IPCC Guidelines for National Greenhouse Gas Inventories, Volume 4: Agriculture, Forestry and Other Land Use*. Available online at: https://www.ipcc-nggip.iges.or.jp/public/2006gl/vol4.html (accessed May 15, 2023).

Iroumé, A., Ruiz-Villanueva, V., and Salas-Coliboro, S. (2020). Fluvial transport of coarse particulate organic matter in a coastal mountain stream of a rainy-temperate evergreen broadleaf forest in southern Chile. *Earth Surface Process. Landforms* 45, 3216–3230. doi: 10.1002/esp.4961

Jochner, M., Turowski, J. M., Badoux, A., Stoffel, M., and Rickli, C. (2015). The role of log jams and exceptional flood events in mobilizing coarse particulate organic matter in a steep headwater stream. *Earth Surface Dynam.* 3, 311–320. doi: 10.5194/esurf-3-311-2015

Keith, M. K., Sobieszczyk, S., Goldman, J. H., and Rounds, S. A. (2014). Investigating organic matter in Fanno Creek, Oregon, Part 2 of 3: sources, sinks, and transport of organic matter with fine sediment. *J. Hydrol.* 519, 3010–3027. doi: 10.1016/j.jhydrol.2014.07.027

Larned, S. T., Datry, T., Arscott, D. B., and Tockner, K. (2010). Emerging concepts in temporary-river ecology. *Freshwater Biol.* 55, 717–738. doi: 10.1111/j.1365-2427.2009.02322.x

Lepori, F., Palm, D., and Malmqvist, B. (2005). Effects of stream restoration on ecosystem functioning: detritus retentiveness and decomposition. *J. Appl. Ecol.* 42, 228–238. doi: 10.1111/j.1365-2664.2004.00965.x

Livers, B., Lininger, K. B., Kramer, N., and Sendrowski, A. (2020). Porosity problems: comparing and reviewing methods for estimating porosity and volume of wood jams in the field. *Earth Surface Process. Landforms* 45, 3336–3353. doi: 10.1002/esp.4969

Marshall, A., Iskin, E., and Wohl, E. (2021). Seasonal and diurnal fluctuations of coarse particulate organic matter transport in a snowmelt-dominated stream. *River Res. Applicat.* 37, 815–825. doi: 10.1002/rra.3802

Minshall, G. W., Petersen, R. C., Bott, T. L., Cushing, C. E., Cummins, K. W., Vannote, R. L., et al. (1992). Stream ecosystem dynamics of the Salmon River, Idaho: an 8th-order system. *J. North Am. Benthologic. Soc.* 11, 111–137. doi: 10.2307/1467380

Mote, P. W., Li, S., Lettenmaier, D. P., Xiao, M., and Engel, R. (2018). Dramatic declines in snowpack in the western US. *Npj Clim. Atmospheric Sci.* 1, 1. doi: 10.1038/s41612-018-0012-1

Musselman, K. N., Addor, N., Vano, J. A., and Molotch, N. P. (2021). Winter melt trends portend widespread declines in snow water resources. *Nat. Clim. Change* 11, 5. doi: 10.1038/s41558-021-01014-9

National Ecological Observatory Network (NEON) (2022). *NEON (National Ecological Observatory Network). Discharge field collection, RELEASE-2022 (DP1.20048.001) (RELEASE-2022, p. 35.4 MB) [Csv]*.

National Ecological Observatory Network (NEON) (2023). *Chemical properties of surface water (DP1.20093.001): RELEASE-2023 (RELEASE-2023, p. 90.7 MB) [Csv]. National Ecological Observatory Network (NEON)*.

Pfeiffer, A., and Wohl, E. (2018). Where does wood most effectively enhance storage? network-scale distribution of sediment and organic matter stored by instream wood. *Geophysic. Res. Lett.* 45, 194–200. doi: 10.1002/2017GL076057

Poeppl, R. E., Fryirs, K. A., Tunnicliffe, J., and Brierley, G. J. (2020). Managing sediment (dis)connectivity in fluvial systems. *Sci. Total Environ.* 736, 139627. doi: 10.1016/j.scitotenv.2020.139627

R Core Team (2022). *R: A Language and Environment for Statistical Computing* [Computer software]. R Foundation for Statistical Computing, Vienna, Austria. Available online at: https://www.R-project.org/

Rhoades, C. C., Hubbard, R. M., and Elder, K. (2017). A decade of streamwater nitrogen and forest dynamics after a mountain pine beetle outbreak at the fraser experimental forest, Colorado. *Ecosystems* 20, 380–392. doi: 10.1007/s10021-016-0027-6

Ruiz-Villanueva, V., Piégay, H., Gurnell, A. M., Marston, R. A., and Stoffel, M. (2016). Recent advances quantifying the large wood dynamics in river basins: new methods and remaining challenges. *Rev. Geophys.* 54, 611–652. doi: 10.1002/2015RG000514

Ryan, S. E., Dwire, K. A., and Dixon, M. K. (2011). Impacts of wildfire on runoff and sediment loads at Little Granite Creek, western Wyoming. *Geomorphology* 129, 113–130. doi: 10.1016/j.geomorph.2011.01.017

Sear, D. A., Millington, C. E., Kitts, D. R., and Jeffries, R. (2010). Logjam controls on channel:floodplain interactions in wooded catchments and their role in the formation of multi-channel patterns. *Geomorphology* 116, 305–319. doi: 10.1016/j.geomorph.2009.11.022

Seo, J. I., Nakamura, F., Nakano, D., Ichiyanagi, H., and Chun, K. W. (2008). Factors controlling the fluvial export of large woody debris, and its contribution to organic carbon budgets at watershed scales. *Water Resour. Res.* 44, 53. doi: 10.1029/2007WR006453

Shumilova, O., Tockner, K., Gurnell, A. M., Langhans, S. D., Righetti, M., Lucía, A., et al. (2019). Floating matter: A neglected component of the ecological integrity of rivers. *Aquatic Sci.* 81, 25. doi: 10.1007/s00027-019-0619-2

Small, M. J., Doyle, M. W., Fuller, R. L., and Manners, R. B. (2008). Hydrologic versus geomorphic limitation on CPOM storage in stream ecosystems. *Freshwater Biol.* 53, 1618–1631. doi: 10.1111/j.1365-2427.2008.01999.x

Smock, L. A., Metzler, G. M., and Gladden, J. E. (1989). Role of debris dams in the structure and functioning of low-gradient headwater streams. *Ecology* 70, 764–775. doi: 10.2307/1940226

Stanford, J. A., Ward, J. V., Liss, W. J., Frissell, C. A., Williams, R. N., Lichatowich, J. A., et al. (1996). A general protocol for restoration of regulated rivers. *Regul. Riv. Res. Manage.* 12, 391–413.

Sutfin, N. A., Wohl, E., Fegel, T., Day, N., and Lynch, L. (2021). Logjams and channel morphology influence sediment storage, transformation of organic matter, and carbon storage within mountain stream Corridors. *Water Resour. Res.* 57, e2020WR028046. doi: 10.1029/2020WR028046

Sutfin, N. A., Wohl, E. E., and Dwire, K. A. (2016). Banking carbon: a review of organic carbon storage and physical factors influencing retention in floodplains and riparian ecosystems. *Earth Surfac. Process. Landforms* 41, 38–60. doi: 10.1002/esp.3857

Swetnam, T. L., Brooks, P. D., Barnard, H. R., Harpold, A. A., and Gallo, E. L. (2017). Topographically driven differences in energy and water constrain climatic control on forest carbon sequestration. *Ecosphere* 8, e01797. doi: 10.1002/ecs2.1797

Thompson, C. G., Kim, R. S., Aloe, A. M., and Becker, B. J. (2017). Extracting the variance inflation factor and other multicollinearity diagnostics from typical regression results. *Basic Appl. Soc. Psychol.* 39, 81–90. doi: 10.1080/01973533.2016.1277529

Turowski, J., Badoux, A., Bunte, K., Rickli, C., Federspiel, N., and Jochner, M. (2013). The mass distribution of coarse particulate organic matter exported from an Alpine headwater stream. *Earth Surface Dynam.* 1, 1–11. doi: 10.5194/esurf-1-1-2013

Turowski, J., Hilton, R. G., and Sparkes, R. (2016). Decadal carbon discharge by a mountain stream is dominated by coarse organic matter. *Geology* 44, 27–30. doi: 10.1130/G37192.1

Vannote, R. L., Minshall, G. W., Cummins, K. W., Sedell, J. R., and Cushing, C. E. (1980). The river continuum concept. *Canad. J. Fisher. Aquatic Sci.* 37, 130–137. doi: 10.1139/f80-017

Wagenmakers, E.-J., and Farrell, S. (2004). AIC model selection using Akaike weights. *Psychonom. Bull. Rev.* 11, 192–196. doi: 10.3758/BF03206482

Wallace, J. B., Whiles, M. R., Eggert, S., Cuffney, T. F., Lugthart, G. J., and Chung, K. (1995). Long-term dynamics of coarse particulate organic matter in three appalachian mountain streams. *J. North Am. Benthologic. Soc.* 14, 217–232. doi: 10.2307/1467775

Webster, J. R., Covich, A. P., Tank, J. L., and Crockett, T. V. (1994). Retention of coarse organic particles in streams in the southern appalachian mountains. *J. North Am. Benthologic. Soc.* 13, 140–150. doi: 10.2307/1467233

Wegener, P., Covino, T., and Wohl, E. (2017). Beaver-mediated lateral hydrologic connectivity, fluvial carbon and nutrient flux, and aquatic ecosystem metabolism. *Water Resour. Res.* 53, 4606–4623. doi: 10.1002/2016WR019790

Wohl, E. (2017). The significance of small streams. *Front. Earth Sci.* 11, 447–456. doi: 10.1007/s11707-017-0647-y

Wohl, E., and Beckman, N. D. (2014). Leaky rivers: Implications of the loss of longitudinal fluvial disconnectivity in headwater streams. *Geomorphology* 205, 27–35. doi: 10.1016/j.geomorph.2011.10.022

Wohl, E., Brierley, G., Cadol, D., Coulthard, T. J., Covino, T., Fryirs, K. A., et al. (2019a). Connectivity as an emergent property of geomorphic systems. *Earth Surface Process. Landforms* 44, 4–26. doi: 10.1002/esp.4434

Wohl, E., and Cadol, D. (2011). Neighborhood matters: patterns and controls on wood distribution in old-growth forest streams of the Colorado Front Range, USA. *Geomorphology* 125, 132–146. doi: 10.1016/j.geomorph.2010.09.008

Wohl, E., Hall, J.r., R. O., Lininger, K. B., Sutfin, N. A., and Walters, D. M. (2017). Carbon dynamics of river corridors and the effects of human alterations. *Ecologic. Monographs* 87, 379–409. doi: 10.1002/ecm.1261

Wohl, E., Kramer, N., Ruiz-Villanueva, V., Scott, D. N., Comiti, F., Gurnell, A. M., et al. (2019b). The natural wood regime in rivers. *BioScience* 69, 259–273. doi: 10.1093/biosci/biz013

Wohl, E., Lininger, K. B., and Scott, D. N. (2018). River beads as a conceptual framework for building carbon storage and resilience to extreme climate events into river management. *Biogeochemistry* 141, 365–383. doi: 10.1007/s10533-017-0397-7

Wohl, E., and Scamardo, J. (2022). Patterns of organic matter accumulation in dryland river corridors of the southwestern United States. *Sci. Total Environ.* 833, 155136. doi: 10.1016/j.scitotenv.2022.155136

Wolman, M. G. (1954). A method of sampling coarse river-bed material," in *Eos, Transactions American Geophysical Union, Vol. 35*, 951–956. doi: 10.1029/TR035i006p00951

frontiers | Frontiers in Water

TYPE Hypothesis and Theory
PUBLISHED 23 November 2023
DOI 10.3389/frwa.2023.1241622

OPEN ACCESS

EDITED BY
Ronald Erwin Pöppl,
University of Vienna, Austria

REVIEWED BY
Andrew Stumpf,
University of Illinois at Urbana-Champaign, United States
John Pitlick,
University of Colorado Boulder, United States

*CORRESPONDENCE
Se Jong Cho
✉ scho@usgs.gov

RECEIVED 16 June 2023
ACCEPTED 20 October 2023
PUBLISHED 23 November 2023

CITATION
Cho SJ, Karwan DL, Skalak K, Pizzuto J and Huffman ME (2023) Sediment sources and connectivity linked to hydrologic pathways and geomorphic processes: a conceptual model to specify sediment sources and pathways through space and time.
Front. Water 5:1241622.
doi: 10.3389/frwa.2023.1241622

Sediment sources and connectivity linked to hydrologic pathways and geomorphic processes: a conceptual model to specify sediment sources and pathways through space and time

Se Jong Cho[1]*, Diana L. Karwan[2], Katherine Skalak[3], James Pizzuto[4] and Max E. Huffman[4]

[1]U.S. Geological Survey, Water Resources Mission Area, Baltimore, MD, United States, [2]Department of Forest Resources, University of Minnesota, St Paul, MN, United States, [3]U.S. Geological Survey, Water Resources Mission Area, Reston, VA, United States, [4]Department of Earth Sciences, University of Delaware, Newark, DE, United States

Sediment connectivity is a conceptualization for the transfer and storage of sediment among different geomorphic compartments across upland landscapes and channel networks. Sediment connectivity and dysconnectivity are linked to the water cycle and hydrologic systems with the associated multiscale interactions with climate, soil, topography, ecology, and landuse/landcover under natural variability and human intervention. We review current sediment connectivity and modeling approaches evaluating and quantifying water and sediment transfer in catchment systems. Many studies highlight the interaction between sediment and water in defining landscape connectivity, but many efforts to quantify and/or simulate sediment connectivity rely on the topographic/structural controls on sediment erosion and delivery. More recent modeling efforts integrate functional and structural connectivity to capture hydrologic properties influencing sediment delivery. Though the recent modeling development is encouraging, a comprehensive sediment connectivity framework, which integrates geomorphic and hydrologic processes across spatiotemporal scales, has not yet been accomplished. Such an effort requires understanding the hydrologic and geomorphic processes that control sediment source, storage, and transport at different spatiotemporal scales and across various geophysical conditions. We propose a path for developing this new understanding through an integrated hydrologic and sediment connectivity conceptual model that broadly categorizes dominant processes and patterns relevant to understanding sediment flux dynamics. The conceptual model describes hydrologic–sediment connectivity regimes through spatial-temporal feedback between hydrologic processes and geomorphic drivers. We propose that in combining hydrologic and sediment connectivity into a single conceptual model, patterns emerge such that catchments will exist in a single characteristic behavior at a particular instance, which would shift with space and time, and with landscape disturbances. Using the conceptual model as a "thinking" tool, we extract case studies from a multidisciplinary literature review—from hydrology, geomorphology, biogeochemistry, and watershed modeling to remote-sensing technology—that correspond to each of the dominant hydrologic–sediment connectivity regimes. Sediment and water interactions in real-world examples through various observational and modeling techniques illustrate the advancements in the spatial

and temporal scales of landscape connectivity observations and simulations. The conceptual model and case studies provide a foundation for advancing the understanding and predictive capability of watershed sediment processes at multiple spatiotemporal scales. Plain language summary: Soil erosion and movement across the landscape are closely linked to rain events and flow pathways. Landscape connectivity is a way to consider how soil erosion from different parts of the landscape is connected to the streams. We explore where soil erosion occurs and how eroded soil moves across the landscape through the interaction with rainfall and drainage. The comprehensive understanding of sediment connectivity and its dependence on rainfall characteristics and watershed hydrology may help to inform the effective distribution of conservation funds and management actions to address water pollution from excess sediment.

KEYWORDS

sediment, hydrological (dis)connectivity, hydrological (water) cycle, sediment delivery, sediment connectivity, sediment–surface runoff, connectivity, sediment–water interface

1 Introduction

The understanding of changing sediment and water dynamics over different spatial and temporal scales, under a range of environmental conditions, is critical for developing monitoring and modeling approaches to quantify and predict sediment delivery, as well as, for developing effective water quality management strategies. The concept of sediment connectivity gained increasing interest in the earth science community to consider the continuum and interplay of landscape features and processes in catchment sediment cascades (Wainwright et al., 2011; Fryirs, 2013; Bracken et al., 2015; Wohl et al., 2017). Sediment connectivity involves the processes and controls involved in the transfer of sediment from a source to a sink via the interplay of structural components (terrain/morphology) and process/functional components (flow of energy/transport vectors and materials) of the landscape (Wainwright et al., 2011; Bracken et al., 2015). Information about hydrologic processes, associated with functional components of connectivity, and landscape sediment sources and sinks, associated with structural components of connectivity, at multiple spatial and temporal scales over various environmental settings, can provide an important "toolkit" for unpacking dominant sediment sourcing and primary transport scenarios (Karwan et al., 2018). Additionally, understanding connectivity will inform water quality mitigation efforts through effective allocation of landscape management strategies that consider both "direct effects" associated with surface runoff, erosion, and transport of overland sediment sources (e.g., silt fencing) and "indirect effects" associated with subsurface flow and corresponding activation of sediment sources or deposits of in- and near-channel environments (e.g., stream restoration) (McEachran et al., 2021).

In this study, the conceptualization and application of sediment connectivity are reviewed in terms of how they frame the continuum of sediment sources, stores, and routes of transport operating under different hydrologic conditions. The sediment connectivity research in recent decades indicates that to move toward a better understanding of sediment transport processes, a conceptualization that accounts for both sediment and hydrologic connectivity is needed to specify provenance, pathway, and storage along sediment cascades (e.g., Wainwright et al., 2011; Bracken et al., 2015; Keesstra et al., 2018). In the second part of the study, we propose a hydrologic and sediment connectivity conceptual model to broadly categorize dominant sediment and hydrologic processes and patterns relevant to understanding and predicting sediment flux dynamics. Conceptual models provide a tool for integrating information and a space for understanding complex environmental systems (Fortuin et al., 2011). Thus, using the hydrologic and sediment connectivity conceptual model as a "thinking" tool, we extract case studies from a multidisciplinary literature review—from hydrology, geomorphology, biogeochemistry, and watershed modeling to remote-sensing technology—to examine sediment and water interactions in real-world examples using various observational and modeling techniques.

The hydrologic and sediment connectivity conceptual model can guide a strategy for collecting environmental data, given the anticipated dominant sediment sources and hydrologic pathways derived from observable environmental characteristics. Numerical simulation of landscape connectivity with strategically acquired data can help to effectively diagnose and forecast sediment source, transport, and storage across spatial and temporal scales. We discuss future research steps to illustrate a broad application of the conceptual model before concluding.

2 Review of the concepts of connectivity

In this section, we review the connectivity concept from its foundation in geomorphology and hydrology to contemporary applications of structural and functional components of connectivity in both conceptual and numerical models. The aim of the review was to (i) provide an overview of how the conceptualization of sediment and hydrologic processes and their interactions has evolved over the years and (ii) identify gaps in the development of a systematic harmonization of hydrologic and geomorphic connectivity.

We approach the second aim by organizing spatial and temporal dimensions of sediment delivery into a single coherent framework.

The variable source area (VSA) or partial area concept of runoff production posits that the portion of a watershed contributing storm runoff can expand or contract during a rain event, depending on rainfall duration, return flow, and soil and topographic characteristics (Hewlett and Hibbert, 1963; Dunne and Black, 1970). The River Continuum Concept (RCC) considers the longitudinal structure and variation along a river system (Vannote et al., 1980), while the Process Domain Concept (PDC) considers the spatial and temporal variability in geomorphic influences and their links across process domains (e.g., hillslopes, hollows, channels, and floodplains) (Montgomery, 1999). Together, these foundational concepts form a useful framework for linking geomorphic structures and dynamics with environmental forcing or landscape disturbances to understand sediment detachment and transport processes. Since the introduction of these foundational concepts on spatial and temporal variability in the operation of sediment cascades, the *landscape connectivity concept* has been adopted from graph theory and ecological applications (Bunn et al., 2000) as a way to describe and quantify structural (e.g., topographic information capturing landscape paths, slope lengths, and buffers) and functional (hydrologic properties capturing runoff and stream routing) influences on the fluxes of water and sediment at different spatial and temporal scales (Wainwright et al., 2011; Bracken et al., 2015; Keesstra et al., 2018). For example, Fryirs (2013) developed a framework using spatial linkages operating in a catchment to assess different types of "(dis)connectivity": longitudinal, lateral, and vertical linkages of the sediment cascade that dictate the strength of coupling between catchment compartments and sediment conveyance across the watershed. Such a conceptual framing can help to systematically recognize various processes, their variabilities, and interactions involved in the sourcing, movement, and storage of sediment across the basin system to the outlet.

In addition to the conceptual framing of connectivity, there have been various efforts to quantify the structural controls on sediment delivery by defining *indices* of *connectivity* (IC) as a function of landscape terrain, in the advent of increasingly high-resolution digital terrain models, such as those derived from aerial LiDAR (Borselli et al., 2008). For example, Cavalli et al. (2013) implemented IC computation in two small catchments in the Italian Alps to assess the degree of linkages between upland sediment sources to downstream drainage lines as functions of drainage area, slope, and surface path length. However, the formulation of IC does not explicitly express the functional component of connectivity [i.e., interaction between geomorphology and hydrology (Keesstra et al., 2018)]. To include the functional component, a modified formulation of IC was proposed (*hydrosedimentological connectivity index* or HCI), where precipitation-derived variables (rainfall intensity, runoff generation, and antecedent soil moisture) are represented to estimate the space–time variation of water and sediment connectivity in a catchment (Zanandrea et al., 2021). Both IC and HCI only consider runoff-generated sheet erosion on upland surface omitting contributions from near-/in-channel sources (e.g., streambank erosion) on sediment yield. Near-/in-channel sources can be significant contributors to sediment yield in many watersheds (see examples in Section 3.2 and Table 2), with substantial economic and environmental importance for stakeholders who must select effective soil conservation actions (Cho et al., 2019). To address this management concern, Cho et al. (2018, 2022) developed a watershed-scale stochastic sediment delivery model that explicitly represents both upland *and* near/in-channel sources with topography-driven sediment connectivity formulations.

More recent modeling efforts have incorporated both structural and functional components of sediment connectivity by coupling topographic information with hydrologic simulation models (i.e., SWAT to estimate watershed hydrology and channel dynamics) (Mahoney et al., 2018). In Mahoney et al. (2020a,b) modeling application, sediment connectivity is quantified as spatially explicit intersecting probabilities for sediment supply, detachment, transport, and buffers to sediment loading as functions of watershed hydrology and geomorphic conditions, including runoff depth, soil conditions, excess shear stress, topography, and river discharge. Many current geomorphometric and hydrosedimentological aspects of connectivity, and their application in watershed modeling, focus on topographic underpinnings to quantify sediment connectivity from upland sources to the stream network in overland flow-dominated systems. Hence, they omit the role of surface–subsurface connectivity in upland-channel coupling, as well as near/in-channel processes involving erosion, transport, and deposition along stream corridors within channel networks before reaching a gage location or sediment sink. A Lagrangian transport model based on dynamic connectivity framework addresses some of the limitations concerning the processes within stream networks (Czuba and Foufoula-Georgiou, 2015). This network-based river routing model with specific attributes of sediment source area incorporates network topology, channel characteristics, and transport-process dynamics within streams to simulate the transport of mixed-sized sediment (Czuba, 2018). Refer to Table 1 for further details regarding recent studies of sediment connectivity.

Our review of connectivity literature suggests it has long been recognized that the spatial and temporal variabilities in geomorphic influences are linked with distinct hydrologic processes and landscape features (Vannote et al., 1980; Montgomery, 1999; Fryirs, 2013). It also indicates that a systematic harmonization of hydrologic and geomorphic connectivity is needed to explain sediment dynamics in different environmental systems over appropriate time scales and disturbances (Wainwright et al., 2011; Bracken et al., 2015; Keesstra et al., 2018). Strategies and applications of numerical simulation emerged to quantify the topographic influences on sediment delivery, focusing on the structural component of sediment connectivity (e.g., Borselli et al., 2008; Cavalli et al., 2013; Cislaghi and Bischetti, 2019). Later numerical simulation efforts integrated surface hydrodynamics to structural components of sediment connectivity (e.g., Mahoney et al., 2018, 2020a,b; Zanandrea et al., 2021). This selective review of landscape sediment connectivity research undertaken in the last several decades reveals that representation of the interactions between hydrologic and sediment processes remains piecemeal and

TABLE 1 Review of landscape sediment connectivity concept and modeling.

References	Connectivity formulation	Hydrologic processes and sediment connectivity interaction/formulation	Spatial and temporal variabilities
Montgomery (1999)	*Process Domain Concept (PDC)*: Spatial and temporal variabilities in geomorphic influences are linked, in which systematic, landscape-scale patterns to disturbances exert distinct influences on geomorphic, hydrologic, and ecologic processes. Basic set of process domains includes hillslopes, hollows, channels, and floodplains. Though the landscape connectivity concept has yet to be introduced to the field of geomorphology, PDC lays the foundation for thinking about different components of the landscape and various influences on sediment delivery and storage.	According to PDC, topographic convergences that focus on surface and subsurface flows, which elevate soil moisture and colluvial saturation, could lead to erosion and landslides. *River Continuum Concept (RCC)* (Vannote et al., 1980) considers routing processes in channels (i.e., "longitudinal linkages" defined by Fryirs, 2013).	Systematic, landscape patterns influence spatial and temporal variability in geomorphic processes. Spatial hierarchy for geologic and topographic control is used to define the dominant geomorphic process domain. i.e., Lithologies define finer-scale area with similar topography and geology and within which similar suites of geomorphic processes occur. At the highest level of this hierarchy, tectonic setting defines the long-term uplift rates and boundary conditions that drive physiographic evolution. Next level of hierarchy is geomorphic provinces given climate, geology, and topography control on geomorphic processes. Within the geomorphic province, different lithologies are identified by local control on the structure.
Wainwright et al. (2011)	Structural and functional connectivities are distinguished in different environmental components. *Groundwater and surface-water connectivity:* Reach-scale subsurface flowpaths influence hyporheic flowpaths, benthic ecosystem, stream and groundwater hydrochemistry, and biogeochemical processes. Spatial variability of flow interactions and solute exchange in groundwater and surface-water connectivity is influenced by geomorphic and hydrogeologic constraints. *Surface and subsurface connectivity in the slope-channel coupling:* interactions between precipitation, soil moisture, infiltration, runoff, runon, stream stage, ephemeral streams, and springs affect landscape processes, including erosion, sedimentation, and sediment transport and storage. *Surface connectivity in land degradation:* Ecological and hydrologic responses to landscape disturbance influence landscape connectivity.	"Holistic approach to connectivity," based on the integration of a range of structural, functional, and systems approaches, examines water and sediment fluxes and different behaviors across different structural settings of the case studies. In groundwater and surface-water connectivity, continuous variations in lithology and structure control the landscape-scale flow fields (i.e., structural connectivity). And there are feedbacks between hydrologic flow and sediment transport, as well as ecological forcings (i.e., functional connectivity). The timing and duration of storms, as well as direct antecedent conditions, affect runoff, infiltration, erosion, and sediment transport.	The conceptualization accounts for temporal and spatial dynamics to understand different structural and functional connectivity and their feedback.
Fryirs (2013)	Structural and functional connectivities are distinguished into three forms of linkages. *Lateral linkages:* Hillslope-channel network interaction in a wider landscape. *Longitudinal linkages:* Upstream-downstream and tributary-trunk interactions in channel network. *Vertical linkages:* Surface–subsurface interaction of water and sediment.	Connectivity is defined as "water-mediated transfer of sediment" across the catchment sediment cascade, and the defined linkages consider the interaction of water and sediment.	Sediment cascade and variability over large spatial areas or temporal scales are influenced by the types and strength of different linkages.
Bracken et al. (2015)	Hydrological processes and sediment connectivity are considered to understand (1) the spatial and temporal feedbacks between structural and process components of landscape connectivity; (2) mechanisms of sediment detachment and transport; and (3) frequency-magnitude distribution of sediment detachment, transport, and storage processes.	Sediment and water interactions are central to this conceptual framing of landscape connectivity. Sediment transfer from a source to a sink in a catchment, and movement of sediment between different zones within the catchment (i.e., over hillslopes, between hillslope and channels, and within channels) are considered as sediment behavior in *fully linked* to *fully unlinked* hydrologic processes.	The challenge to scale up small-magnitude processes to produce landscape form motivated the formulation of the conceptual framework to understand the processes involved in sediment transfer across multiple scales through the feedback between hydrologic and sediment connectivity.

(Continued)

TABLE 1 (Continued)

References	Connectivity formulation	Hydrologic processes and sediment connectivity interaction/formulation	Spatial and temporal variabilities
Borselli et al. (2008)	$IC = log_{10}\left(\frac{D_{up}}{D_{dn}}\right) = f\left(d_i, S_i, \overline{S}, A\right)$ *Where* $D_{dn} = \sum_i \frac{d_i}{W_i S_i}$ $D_{up} = \overline{W}\overline{S}\sqrt{A}$ *IC= index of connectivity [-]* d_i *= length of the* ith *cell along downslope path [m]* W_i *=weight of the* ith *cell [-]* S_i *= slope gradient of the* ith *cell [m/m]* $\overline{W}$ *= average weighing factor of the upslope contributing area [-]* $\overline{S}$ *= average slope gradient of the upslope contributing area [-]* A *= upslope contributing area*	"Hydrological connectivity" is defined as the internal linkages between runoff and sediment sources in the upper parts of catchments and the corresponding sinks. The GIS approach is developed to quantify the structural connectivity in the downslope component based on topographic configuration (slope gradient and flow length). Upslope component of the connectivity is a function of the drainage area and slope gradient. Thus, the connectivity formulation captures landscape connectivity by surface runoff, which is controlled by topographic and drainage configurations on the upland. The rainfall characteristics (intensity, duration, and magnitude) and watershed hydrology are not explicitly captured in the formulation, but runoff generation and soil erosion are implicitly captured through use of USLE, RUSLE, or SCS-CN with IC to compute sediment yield.	The connectivity maps generated by this GIS approach are constant over time and do not vary with rainfall characteristics and the watershed's hydrological response. The method can be applied to any spatial scale to map hillslope connectivity to the channel network, but the in-channel source erosion and connectivity to the downstream point are not considered in this formulation.
Cavalli et al. (2013)	Modification to Borselli et al. (2008) formulation with a new weighting factor that considers the surface characteristics that influence runoff and sediment fluxes: $W = 1 - \left(\frac{RI}{RI_{MAX}}\right)$ $RI = \sqrt{\sum_{i=1}^{n^2} \frac{(x_i - x_m)^2}{n^2}}$ *where* W *= weighting factor* RI *= roughness index* n^2 *= number of the processing cells within nxn cells moving window* x_i *= value of one specific cell of the residual topography* x_m *= mean of the* n^2 *cells values*	The new weighting factor implicitly considers hydrologic influence on sediment delivery. Roughness index as standard deviations of residual topography values to consider the terrain influence on runoff. But similar to Borselli et al. (2008) method, there is no explicit consideration of rainfall characteristics and watershed hydrology to quantify infiltration, runoff, erosion, and sediment transport.	see above
Czuba and Foufoula-Georgiou (2015)	$d_{k,l}(t) = \lvert \mathbf{X}_{Pk}(t) - \mathbf{X}_{Pl}(t) \rvert_{\substack{Along \\ network}}$, $M_j(t) = \sum_{\substack{parcels\ P_k,\ P_l \\ in\ cluster\ j \\ at\ time\ t}} m,\ s.t. d_{k,l}(t) \leq d^*$, $L_j(t) = \sum_{\substack{parcels\ P_k,\ P_l \\ in\ cluster\ j \\ at\ time\ t}} d_{k,l}(t),\ s.t. d_{k,l}(t) \leq d^*$ $CPI_i = \int_{\substack{over\ all \\ times\ t}} M_j^i(t)\ dt$	Sediment connectivity is considered along the river network based on network topology (i.e., links, junctions, and outlet) and hydraulic and geomorphic attributes (i.e., length, geometry, drainage area, slope, and stream flow). Sediment mass contribution (m) is injected as parcel (P_k) in the basin at an initial time (t_0) and their trajectories ($\mathbf{X}(t)$) are followed over space and time ($m(\mathbf{X_i}, t_i)$). Travel time of sediment parcels (t_i) is computed by decomposing volumetric transport rate given hydraulic geometry, flow length, upstream drainage area, grain attributes, and streamflow velocity.	"Dynamic Connectivity" refers to how the connectivity of fluxes changes in time. The formulation rests on the link between Eulerian and Lagrangian transport formalism to establish the relation between the space–time trajectories of sediment connectivity along the river network. A set of consecutively connected river links over time is defined as "cluster." Cluster persistence index (CPI) is a measure of dynamic connectivity used to identify hotspots of fluvial geomorphic change and to evaluate driving mechanism of this change.

(Continued)

TABLE 1 (Continued)

References	Connectivity formulation	Hydrologic processes and sediment connectivity interaction/formulation	Spatial and temporal variabilities
	Where $d_{k,l}(t)$ = *distance between adjacent parcel* P_k *and* P_l $\mathbf{X}(t)$ = *parcel* (P_k) *trajectory at time t* $M_j(t)$ = *total mass at cluster j at time t as the sum of all parcel mass (m) of inter-parcel distances* $(d_{k,l})$ *less than threshold distance* (d^*) $L_j(t)$ = *total upstream and immediate downstream length at time t along the network as the sum of inter-parcel distances* $(d_{k,l})$ *less than threshold distance* (d^*) CPI_i = *cluster persistent index as the cumulative effects of all clusters j on every link i from time* $t = 0$ *until all parcels have left the system*		
Mahoney et al. (2018, 2020a,b)	$$P(C) = P(S) \cap P(G) \cap P(T) \cap \{1 - P(B)\}$$ where $P(C)$ = *Probability of spatial connectivity* $P(S)$ = *Probability of transportable sediment supply* $P(G)$ = *Probability of sediment detachment and entrainment in flow* $P(T)$ = *Probability of transport of sediment* $P(B)$ = *Probability of a buffer/disconnectivity*	Discretized *P(C)* for each space–time unit incorporates both structural and functional components of landscape connectivity. *P(G)* considers hydrologic detachment of sediment and *P(T)* hydrologic transport of sediment. *P(G)* is a binary probability (i.e., 1 if soil is detached; 0 otherwise) as a function of excess shear stress given runoff and soil conditions. *P(T)* is a binary probability (i.e., 1 if hydrologic transport happens; 0 otherwise) as a function of gradient slope and critical slope for transport, which is a function of upstream drainage area, CN, and rock fragment cover of the soil.	The probabilistic landscape connectivity is a function of watershed's surface hydrology with computation of runoff generation via CN method through the application of SWAT model. Thus, the landscape connectivity varies with different hydrological events. This method routes sediment from upland sources to stream network, and in-stream sediment transport is computed using SWAT algorithm. Longitudinal connectivity, or how in-channel sediment sources are connected to the downstream point, is not comprehensively considered in the model.
Keesstra et al. (2018)	Landscape connectivity and feedback between phases and fluxes are outlined. *External Drivers:* Tectonic, climate, fire regime, and human intervention in the landscape (e.g., landuse/landcover, and water management) drive connectivity conditions. *System Phase:* Defines the structural connectivity at particular moments in time, depending on the system's geology, soil structure, hydrology, geomorphology, ecology, and human interventions. It influences structural connectivity and self-organizing patterns. *System Fluxes:* Describes the transfer of water and sediment within a system. It influences functional connectivity and landscape patterns. *Equilibrium:* Responds to changes in connectivity conditions.	Interacting phases and fluxes are conceptually represented as co-evolution of system state, such that structures emerge in response to fluxes within the system and the patterns of fluxes are influenced by the structure. Observational approaches to quantify water and sediment fluxes at various spatiotemporal scales are proposed.	Multiple spatial and temporal scales of the conceptual model application are considered.
Cislaghi and Bischetti (2019)	$$HSCI = P\left[FS < 1 \cap L > d_{\min}\right] = P\left[L > d_{\min} \mid FS < 1\right] \cdot P[FS < 1]$$ where *HSCI = Hillslope-Stream Connectivity Index* *FS = Factor of Safety (i.e., P[FS<1] indicates soil erosion or landslide)* $P\left[L > d_{\min} \mid FS < 1\right]$ = *Probability of total travel distance to reach channel*	Factor of Safety is calculated as a ratio between resisting forces (basal resistance force, shear resistance, tensile root reinforcement acting on the upslope side minus force acting on the upslope wedge) and driving forces (downslope component of the block weight). This formulation extends beyond topographic factors influencing landscape connectivity and includes the soil physics, 3D slope stability and geometry, and vegetation factor.	The method can be applied to any spatial scales, but in-channel source connectivity to the downstream point is not considered in this formulation.

(Continued)

TABLE 1 (Continued)

References	Connectivity formulation	Hydrologic processes and sediment connectivity interaction/formulation	Spatial and temporal variabilities
Zanandrea et al. (2021)	$IHC = \log_{10}\left(\frac{\overline{RS}Ips\sum Q_{runoff}}{\sum_i \frac{d_i}{RS_iS_i}}\right)$ *where* *RS = Relative Smoothness calculated using the local Manning Coefficient [-]* *Ips = precipitation index for sediment [-]* Q_{runoff} *= surface runoff calculated using the SCS Runoff Curve Number (CN) method [L]* d_i *= length of the* ith *cell along downslope path [L]* S_i *= slope gradient of the* ith *cell [L/L]*	*Hydrosedimentological Connectivity Index* (IHC) concerns both runoff generation with antecedent condition and structural features of the landscape. It builds on Borselli et al. (2008) formulation of *Connectivity Index* (IC) to include precipitation and surface runoff characteristics as functional component of the formulation.	IHC is mapped event-by-event cases for any spatial scales to map hillslope connectivity to channel network, but the in-channel source connectivity to the downstream point is not considered in this formulation.
McEachran et al. (2021)	Direct Effects are associated with overland flow, erosion, and sediment transport, where topography, drainage area, soil, landcover, and rainfall characteristics influence the extent of sediment connectivity. Indirect Effects are caused by altered long-term hydrologic behavior of the watershed, such as increased infiltration and baseflow recharge and heightened peak streamflow, and the consequent erosion of near- and in-channel sources.	Sediment and water interactions are built into the direct/indirect effect framework. Hydrologic connectivity on hillslope and in-channel is considered along with sediment connectivity from both hillslope and in-channel sources, as well as the feedback between the structural and functional components.	The framework makes it explicit that the hydrologic and sediment connectivity are not coincident in both space and time. Direct effects are observed at the hillslope scale in the timespan of single storm or season (i.e., temporally localized effect). With increasing variable source area and disturbance extent, direct effects can dominate sediment yield drivers. Indirect events are at the watershed-scale changes in hydrologic flowpaths and distribution, and generally larger in spatial scale than the direct effects.

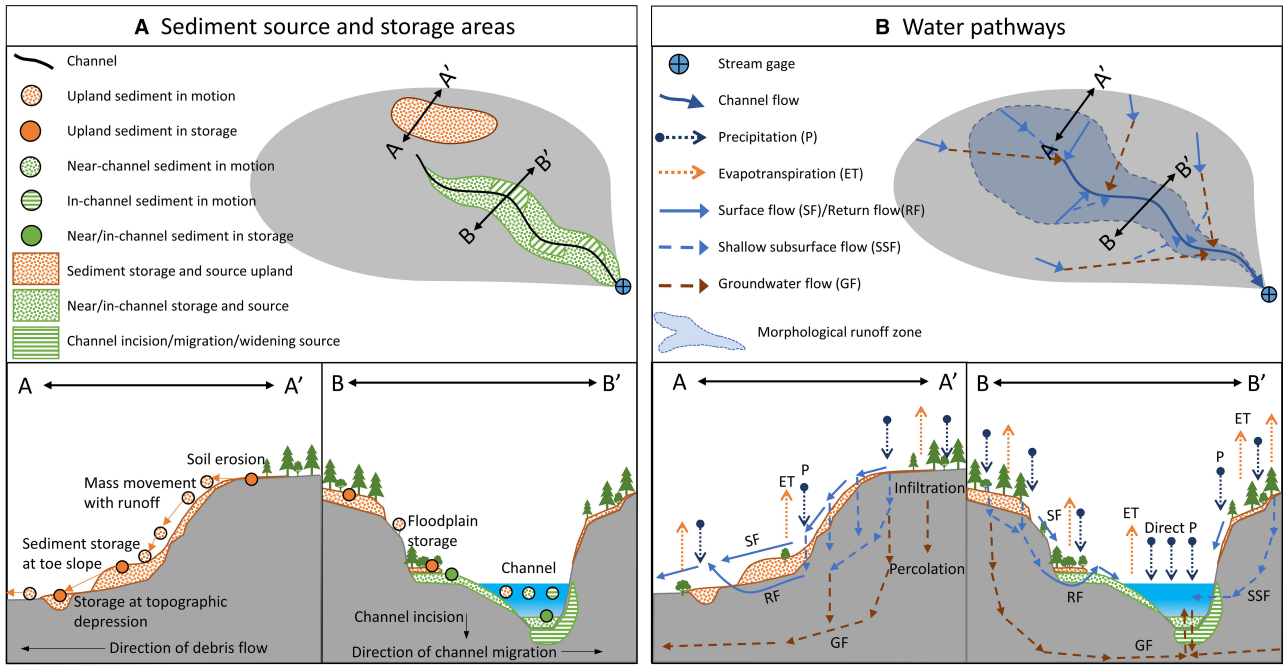

FIGURE 1
Illustration and definition of **(A)** sediment sources and storage areas on hillslope (erosion and mass movement) and near/in-channel (floodplains, streambank, bed, and bars) and **(B)** surface and subsurface hydrologic pathways on hillslope to channels (runoff, infiltration, return flow, percolation, and groundwater flow). The morphological runoff zone indicates the areas of direct surface flow and sediment contributions to the stream.

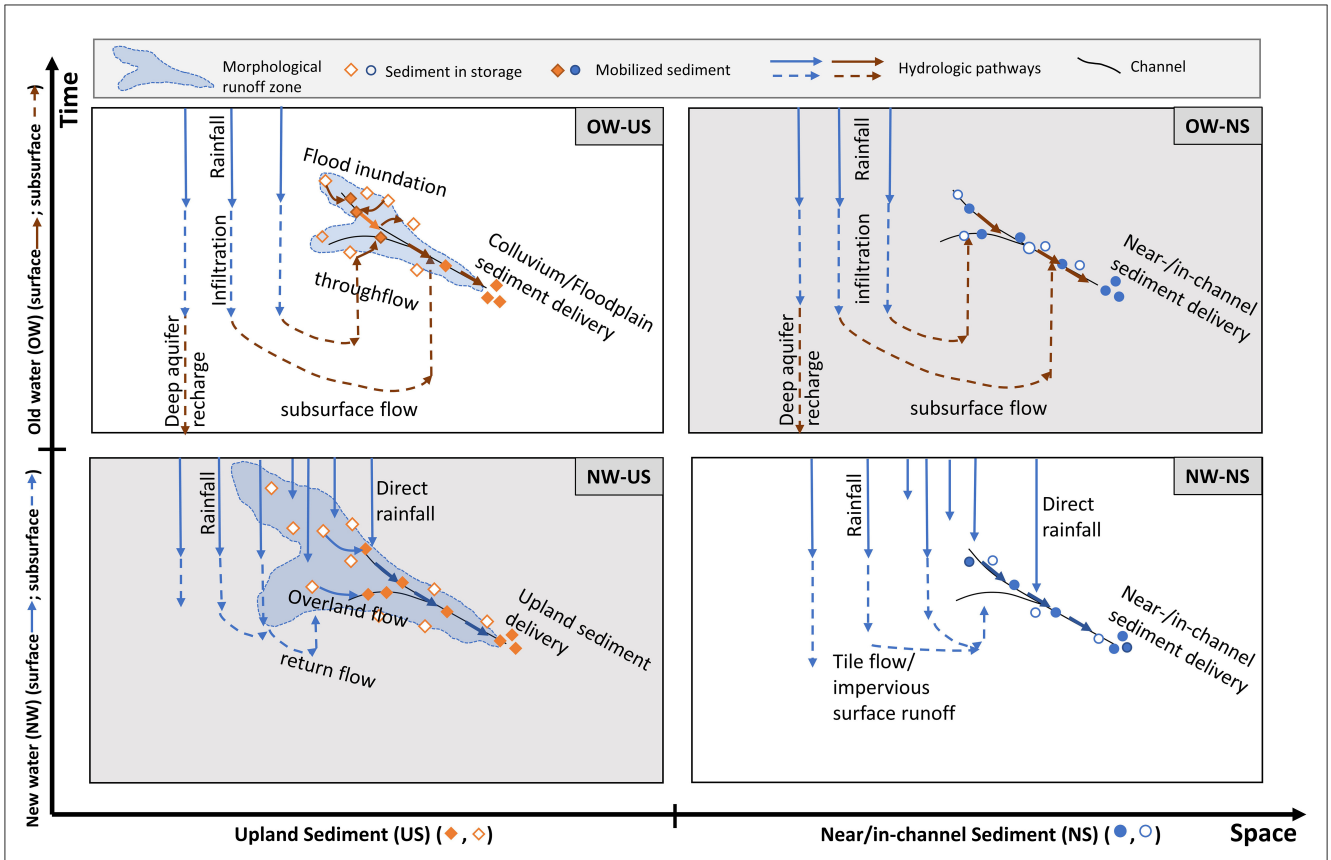

FIGURE 2
Conceptual model of sediment and hydrologic connectivity: OW-US, Old Water-Upland Sources; OW-NS, Old Water-Near/in-channel Sources; NW-US, New Water-Upland Sources; NW-NS, New Water-Near/in-channel Sources.

subjective and depends on specific environmental circumstances (i.e., study site location, catchment characteristics, and methods of inference) (Bracken et al., 2015).

To measure and predict water quality at gage-relevant spatial scales (HUC 8 watershed scales, for example), a model is needed that includes elements for provenance, pathways, and storage along sediment cascades and addresses the response to different hydrologic forcings and landscape disturbances (McEachran et al., 2021). Quantification of sediment sources and delivery for a given landscape would require an effective synthesis of a range of conceptual approaches with monitoring and modeling techniques that integrate hydrologic processes and structural components of sediment connectivity. Spatial variability in geomorphic processes that influence temporal patterns of connectivity may be mapped by identifying sediment sources along with hydrologic pathways. A conceptual model in the following section can help to develop time- and space-variant connectivity scenarios and can guide data collection and model development needed to quantitatively evaluate them.

3 Sediment-hydrologic connectivity

3.1 Conceptual model

While it is impossible to cover all spatial and temporal combinations of sources and transport processes, we put forth an integrated hydrologic and sediment connectivity conceptual model to broadly categorize dominant sediment and hydrologic processes and patterns relevant to understanding and predicting sediment flux dynamics. We consider two major hydrologic pathway s (surface vs. subsurface) and two major sediment sources (upland vs. near/in-channel) of an idealized watershed (Figure 1). Various combinations of hydrologic pathways and sediment sources are associated with different spatial distribution and timing of source erosion, storage, and loading. Figure 1A illustrates sediment source and storage areas in the upland (hillslope and toe slope) and near/in-channel (floodplain and channel). Active sediment sources include areas of stored mass (e.g., fallow field, colluvium at the bottom of hillslope, wetland and other areas of depression, deposits on floodplains, channel beds, and bars) in interaction with watershed hydrology and/or geomorphic drivers. Active sources may change over time, such as throughout a storm hydrograph (e.g., land surface erosion via rainfall impact to streambank erosion from peak flows), or over engineering timeframes with management implementations (e.g., grassed waterways and stream restorations) and up to geomorphic time scales (i.e., landscape evolution and stream morphology). As a result, event water composition and pathways can influence dominant sediment sourcing and routing and appropriate management strategies (McEachran et al., 2021). Therefore, adopted from the idea of *variable source area* (VSA) (Dunne and Black, 1970), we define the *morphological runoff zone* (MRZ) to indicate those areas in the watershed where runoff generation results in sediment delivery

from upland sources to the river network. Figure 1B illustrates various hydrologic pathways and contributions to streamflow. Through the empirical implications of isotopic compositional differences, streamflow may be separated into event water (often called "new water" indicated with blue arrows in Figure 1B) and pre-event water ("old water" indicated with brown arrows) using the distinct chemical (e.g., isotopic) signals in soil water and groundwater (Klaus and McDonnell, 2013). New water is primarily derived from an ongoing precipitation event (e.g., surface runoff, snowmelt, and direct precipitation). Old water consists primarily of water that is stored in the catchment prior to the stream flow generating precipitation event and delivered primarily through subsurface pathways (e.g., soil water and ground water) (Shanley et al., 2002).

Hydrologic processes through different pat hways and timing have different effects on structural connectivity as they have access to different sediment sources, storage areas, and transit pathways. For sediment sources in upland areas (A—A' of Figure 1A), the extent of overland flow and the availability of upland sources influences sediment connectivity to the channel network, including slope-channel (e.g., rain splash and sheet erosion) and channel floodplain (e.g., return flow flushing and flood inundation) relations (Wainwright et al., 2011; Fryirs, 2013). The strength and patterns of the connectivity are likely controlled by hillslope hydrology and relationships between precipitation characteristics, antecedent conditions, surface flow, subsurface flow, and ground water (A—A' of Figure 1B). Materials derived upslope and their proximity to the channel network may also be relevant (Wainwright et al., 2011). For sediment sources near/in-channels (B—B' of Figure 1A), the extent of upstream-downstream connectivity reflects the ability of the channel to erode and transfer sediments downstream, which may be assessed in terms of surface and subsurface flow contributions and their timing, stream power, transport regime, and network structure, given the base level or bed profile of the channel (B—B' of Figure 1B) (Fryirs, 2013; Bracken et al., 2015).

Various upland-channel-outlet linkages within a watershed are organized into four dominant sediment and hydrologic connectivity regimes in a conceptual model (Figure 2). The partition on the x-axis broadly categorizes structural characteristics of connectivity, linked to the landscape geomorphology and *spatial dimensions* of sediment sources. The partition on the y-axis characterizes the functional aspects, linked to the hydrological properties and *time-scale variation* in sediment connectivity. The conceptual model organizes these different categorizations of dominant sediment and hydrologic processes and patterns to navigate various spatial dimensions and time scales of connectivity. Each sediment and hydrologic connectivity regime illustrates distinct interactions between water and sediment, and they are named based on the primary hydrologic sources relative to the event scale (Old Water vs. New Water) and sediment source areas (Upland vs. Near/in-channel Sources).

We propose that in combining hydrologic and sediment connectivity into a single conceptual model, patterns will emerge such that catchments (i.e., small hydrologic units with identifiable dominant processes) will exist in a single characteristic behavior at a particular instance. Furthermore, the conceptual model can describe shifts in dominant processes with different spatial (e.g., reach scale vs. watershed scale of greater hydrologic units) and temporal scales (e.g., seasonally with individual storm events vs. annual trends), as well as with landscape disturbances (e.g., wildfire, landslide, and landuse/landcover change). In other words, the conceptual model can be used to describe the dominant connectivity regime at a particular space and time and its response to landscape disturbance and/or natural variability. As such, the conceptual model can provide guidance to management actions that will need to uniquely address the hydrology and/or sediment connectivity dominant in each watershed given different conservation objectives and timeframes (e.g., control mean daily sediment loading at a gage location and determine effective Best Management Practices). For example, timber harvest or agriculture (or landcover changes more broadly) can result in increased surface runoff and increased upland sediment connectivity affecting local, reach-scale water quality. At the same time, shifts in hydrologic processes due to tree removal or tile drainage (e.g., alterations to evapotranspiration, infiltration, and runoff) may account for the increases in subsurface and surface flows to the stream such that the changes to downstream water quality are not predicated upon overland sediment delivery to the stream but is attributed to in-stream processes (e.g., stream bank erosion, channel meander, incision, and widening) over longer time scales (Foufoula-Georgiou et al., 2015; McEachran et al., 2021). In such cases, management of downstream water quality degradation does not only rely on management actions on uplands to trap sediment but also on controlling watershed hydrology and in-stream erosion processes (McEachran et al., 2021).

3.2 Sediment-hydrologic connectivity scenarios

Recent advancements in landscape observational techniques involving geochemical tracers, remote sensing, increasing availability and frequency of hydrologic monitoring data, and the integration of various data analytic methods (e.g., isotopic hydrograph separation, stormflow concentration–discharge, and hysteretic behavior analysis) and watershed modeling have broadened the spatial and temporal scales of geomorphic observations and understanding of sediment connectivity. Through the descriptions of the anticipated dominant hydrologic and geomorphic regimes using the conceptual model (Figure 2), we examine sediment and hydrologic interactions in real-world examples (Table 2 organizes the following examples by study location, study method, main geomorphic and hydrologic processes, and space/time scales of evaluation):

- **Connectivity Scenario: Old Water-Upland Sediment (OW-US)**
  The OW-US regime indicates that the primary hydrologic drivers consist of pre-event water from subsurface storage and pathways, and the dominant sediment sources consist of upland mass wasting processes and colluvial deposits at the bases of slopes. For example, in headwater streams in

TABLE 2 Sediment-hydrologic connectivity scenarios and case studies.

Sediment-hydrologic connectivity scenario	Case study	Study location	Study method	Main geomorphic and hydrologic processes	Space/time scales
Old Water- Upland Sediment (OW-US)	(Montgomery et al., 2002)	Study catchments in the Mettman Ridge of Oregon Coast Range in Oregon (US) consist of steep, highly dissected soil-mantled hillslopes with steep channels typical of the Pacific Northwest Coast Range. -Drainage area: 0.86 km^2 (CB1 catchment), 3.27 km^2 (CB2 catchment) -Land Use/Land Cover: Forested with young Douglas fir -Annual Rainfall: 1,500 mm -Lithology/soil: Fractured and weathered bedrock with increasingly thick soil toward hollows (1.4–2 m) with local variability	Experimental study compares two steep valleys to (1) document colluvium accumulation from landslide, (2) measure shallow bedrock flow in both storm runoff and base flow generation, and (3) observe the influence on debris-flow initiation in the colluvium-mantled sites. -Instrumentations: Bedrock and soil piezometers, automated piezometer nest, automated rain gauge along hillslope, and weirs at the bottom of hillslope in nested catchments -Experiments 1–2: February 1992 observations from experiments and natural storms -Experiments 3: May–June 1992 observations -Runoff measurement at the weir: December 1989–February 1992	Landslides are major geomorphic process and channels begin at landslide scars. Hydrologic interaction between colluvial soil and fractured bedrock influences runoff generation mechanism. Lateral saturated drainage through spatially heterogenous near-surface fractured bedrock system determines locations of debris-flow initiation.	-Event dynamics: Interplay between flow in the colluvial soil and underlying fractured bedrock was observed during intense storms in winter months. During lower intensity storm events in Spring months, nearly all runoff passes through the bedrock before emerging from the soil. Soil and bedrock conductivity distribution implies that the colluvial soil is highly conductive in general, depending on the gradients and bedrock/colluvium contact. -Seasonal variation: though consistent event-driven response was documented in the fractured bedrock, which varied depending on antecedent soil moisture and available bedrock storage, near-surface bedrock response showed seasonal dynamics, implying slow vertical unsaturated flow and lateral drainage of the near-surface bedrock.
	(Kukulak et al., 2022)	Central Western Carpathians and adjacent part of the Outer Western Carpathian, at the foothills of the Tatra Mountains (EU), where landslide sites intersect with Czarny Dunajec River and its tributaries in Wielki Rogoznik. -Drainage Area: 134 km^2 (Czarny Dunajec); 125 km^2 (Wielki Rogoznik) -Land Use/Land Cover: Dense forestation mixed with deforestation and agricultural conversion in low-mountain area -Annual Rainfall: 900–1,100 mm with seasonal variation and freeze-thaw cycle. -Lithology/soil: A tectonic basin with Neogene freshwater mudstones, claystones, and sandstones and overlying Quaternary alluvial sediments of the Podhale Flysch series	Geomorphic mapping: detailed soil profiles of the undercut landslide fronts, which are differently positioned in relation to rivers and rates/volumes of colluvium removal were measured using terrestrial LiDAR. Frequency of mapping: 6 times after spring thawing episodes (2013–2019) and 12 times after major water-level rises (2 times in 2013, 2015, and 2017; 6 times in 2019) Daily recording of water levels in 2013–2019 at river gauging stations.	A rotational landslide originated in 1980 and great displacements occurred episodically in 1997 and 2001, but the front of colluvium continue to descend to the river and being undercut by lateral erosion. Particularly with water level rising, erosion in the front of colluvium occurred, which was immediately replaced by new supplies of colluvium from the reactivated landslide. Transverse/diagonal landslide was triggered by undercutting of a concave bank of a migrating river bend over its whole length since 1934. Groundwater infiltration into mudstone from the overlying gravel contributed to the basal detachment of the landslide, and during high stage of river, erosion occurred in the massive cohesive mudstones and in the displaced and rotated colluvium.	Erosion and removal of colluvium and its mudstone foundation occurred episodically during high flow events with abundant rainfall or sudden thaw in 2014 (4–6 days) and again in 2017 when the water level reached similar values. Smaller sediment connectivity to colluvium in the landslide front occurred during the observation period of normal flow conditions with landslide saturation and small to normal water level oscillations. Many factors contributed to the timing and spatial extent of erosion and supply of colluvium, including intensity of precipitation, rate of water infiltration, lithology and mechanical properties of colluvium, landslide tongue mobility, shape and size of the river channel, and temporal dynamics of river discharge.

(Continued)

10.3389/frwa.2023.1241622

TABLE 2 (Continued)

Sediment-hydrologic connectivity scenario	Case study	Study location	Study method	Main geomorphic and hydrologic processes	Space/time scales
	(Rose et al., 2018)	White Clay Creek in the Delaware drainage basin (US) located within the Piedmont physiographic province. -Drainage Area: 7.25 km^2 -Land Use/Land Cover: Agriculture (pasture and row crop) with hardwood forest cover in riparian areas -Annual Rainfall: 860–1,320 mm -Lithology: Micaceous schist and gneiss to quartzite bedrock overlain by deep, unglaciated soils.	Samples of suspended particulate material (SPM) were collected during 15 storms from 2011 to 2012, including Hurricane Irene in August 2011 with 167 mm of rainfall over 30 h and Tropical Storm Lee 8 days later adding 171 mm of rain fall in 48 h. Hurricane Sandy occurred in October 2012 with 137 mm of rainfall over 66 h. -SPM collection: particulate organic carbon (POC) and nitrogen (PON) contents, stable isotopic composition, grain size, Brunauer-Emmett-Teller (BET) mineral surface area, and major elements. -Source material collection: same suite of physical and chemical analyses as SPM in landscape surface and subsurface materials, as well as from near/in-channel (streambank, gulley wall, and riparian trails).	Comparison of source materials with SPM samples collected during seasonal and hurricanes/tropical storms indicates different contributions of source materials. During high flows, landscape source areas throughout the watershed were the primary contributor through hydrologic connectivity and physical transport on land surface (see **NW-US** scenario). During low flows, groundwater flowpaths shifted throughout the hydrograph and the particulate material fingerprinting indicates resuspension and delivery of upland sediment in temporary storage within the stream.	Event sediment sourcing and dynamics were closely related to the magnitude and intensity of storm events in this small catchment system. Also, the sourcing of primary sediment depended on characteristics of previous storms and dominant flow paths. Thus, the understanding of the sediment dynamics over long periods relied on the individual events and their sequence.
New Water-Upland Sediment (NW-US)	(Alessio et al., 2021; Morell et al., 2021)	Burned hillslopes generated debris flow in six catchments above Montecito, California (US) -Drainage Area: 19.5 km^2 -Land Use/Land Cover: forest burned to ashy cover -Annual Rainfall: 460 mm -Lithology/soil: Juncal shale, Matilija Sandstone, Cozy Dell Shale, and Coldwater Sandstone. Loam with sand, silt, clay, silt loams	Field observation and soil samples were collected from rill channels and rill networks on both shale and sandstone units several weeks after a rainstorm. Structure from Motion (SfM) photogrammetry and LiDAR DEM were used for spatial analyses. Rill networks were mapped and measured using SfM-derived DEM using TopoToolbox. Interrill erosion estimates were made using regression equations for the solids-concentration in the runoff as a function of rainfall intensity and plot gradient. Catchment-wide soil evacuation volumes were estimated using the relationship that combine the effects of width, depth, and spacing of rill and interrill erosion to the average lowering of the hillslope surface. Runoff modeling was conducted given the infiltration capacity of the soil during the rainstorm (Philip infiltration equation), burn intensity and severity, and soil texture (Manning roughness coefficient). Topsoil stability and slurry discharge were estimated.	In post-fire conditions, the largest contribution of sediment was colluvium during rill formation and debris-flow deposit accumulation in streams activated by a brief, intense rainstorm. The extent, pattern, and volumes of post-fire hillslope erosion depended on rainfall, runoff, and landscape characteristics. Different lithological and topographic features affected the extent and dimensions of rills and volumes of slurry mixing of water and sediment.	The occurrence of wildfire altered the hydrologic and sediment connectivity for a long period afterwards.

(Continued)

10.3389/frwa.2023.1241622

TABLE 2 (Continued)

Sediment-hydrologic connectivity scenario	Case study	Study location	Study method	Main geomorphic and hydrologic processes	Space/time scales
	(Blake et al., 2009)	A first order tributary of Blue Gum Creek in the Nattain National Park, New South Wales (AU) -Drainage area: 0.9 km^2 -Land Use/Land Cover: Native eucalypt woodland/forest conservation zone, which was burnt extensively in 1968, 1994, and 2001/2002 -Annual Rainfall: 840 mm -Lithology/soil: Hawkesbury Sandstone. Sandy loams and loamy sands.	Fallout radionuclides ($^{210}Pb_{xs}$, ^{7}Be, ^{137}Cs) tracers and sediment budget approaches were used to compare constituent landscape units.	Upland sources (ridgetops and steep valley sideslopes) made up the dominant part of the sediment budget given post-fire erosion susceptibility in hillslope according to a sediment budget analysis using fallout radionuclide (FRN) tracers in a post-fire catchment.	Compared to Morell et al. (2021) and Alessio et al. (2021) providing insights into post-fire hydrologic and sediment connectivity with a multi-watershed-scale study, this study, localized at first order stream, showed consistent runoff and sediment response to rainfall events.
	(Bartley et al., 2007)	Weany Creek is a subcatchment of the Burdekin Catchment in North Queensland (AU) -Drainage area: 13.5 km^2 -Land Use/Land Cover: Cattle grazing land with grass and canopy vegetation -Annual rainfall: 584 mm -Lithology/soil: granodiorite bedrock	Erosion measurement methods (erosion pins, flumes, and cross-section survey) were applied to estimate hillslope erosion, gully erosion and deposition, bank erosion, channel bed erosion and storage, and fine sediment export at the catchment outlet.	The sediment budget compiled for this arid and grazed small catchment during drought conditions indicates high sediment connectivity between hillslopes and the channel network particularly at headcut locations and gullies, where they make up the largest proportion of the sediment budget	In a semiarid environment, runoff is activated from summer convective storms, snowmelt runoff, and rainfall on snowpack. Overland flow generation is critical in soil erosion and delivery, and its patterns are influenced by infiltration. Thus, sediment connectivity is event-based, and the removal of sediment sourced from upland by overland flow depend on the spatial organization of the lithology, topography, surface roughness.
New Water-Near/in-channel Sediment (NW-NS)	(Gellis et al., 2020)	Dead Run urban watershed in Baltimore, Maryland (US): All natural stream channels were buried during urbanization in this Mid-Atlantic urban stream. -Drainage area: outlet of buried channel network (0.369 km^2) nested in the Dead Run watershed (1.63 km^2) -Land Use/Land Cover: About one-half of the area is impervious (roads, rooftops, and parking lots) and the other half is non-impervious and open space (lawns, parks, and green space) -Annual Rainfall: 1,500 mm -Lithology/soil: Mount Washington Amphibolite subunit of the Baltimore Complex of the Piedmont Physiographic province.	Rainfall, stormwater runoff, pavement sediment, soil, streambank material, and fluvial sediment were collected during three period between 2017 and 2018 seasons. Geochemical fingerprinting using radiogenic and elemental tracers (^{7}Be, $^{210}Pb_{ex}$, and ^{137}Cs) in the rain, runoff, pavement sediment, and soil (surficial soil and eroding streambanks) samples was conducted. Fluvial sediment and bed material samples were collected at gage locations after rainfall.	All surface runoff was routed through buried channel network via numerous storm drains to open channels. Rainfall-runoff entrained a relatively small amount of sediment from impervious surfaces. Runoff from impervious surfaces and storm drain network resulted in high peak flows in open channels, leading to channel widening, streambank erosion, and channel incision (57% of the budget) as verified by the numerical tagging of ^{7}Be and $^{210}Pb_{ex}$ activities. Pavement sediment contributed only 4% at the Dead Run watershed outlet demonstrating the relatively small contribution from upland connectivity.	The analysis evaluates event-scale urban hydrology and sediment connectivity of various sources, ranging from topsoil, pavement soil to streambank. The nested study design allowed evaluation of sediment connectivity at different spatial scales.

(Continued)

10.3389/frwa.2023.1241622

TABLE 2 (Continued)

Sediment-hydrologic connectivity scenario	Case study	Study location	Study method	Main geomorphic and hydrologic processes	Space/time scales
	(Cashman et al., 2018)	Difficult Run urban/suburban watershed, Virginia is one of the most urbanized and densely populated areas in US -Drainage area: 14.2 km^2 -Land Use/Land Cover: High intensity development, low-density residential, and forested and open land -Annual Rainfall: 1,100 mm -Lithology/soil: Gneiss and schist bedrock. Channels exhibit mill dam legacy sediment stratification	Sediment sampling from spring 2010 and summer 2011 at source locations (streambanks, forest soil, and road dust). Suspended sediment target and bed samples were collected at USGS gage location across 18 storm events (50 samples) from 2008 to 2012. Fingerprinting analysis was conducted using SEDiment Source Assessment Tool (SEDSAT). Sediment delivery ratio was calculated by taking the source-specific fraction of the suspended sediment load and dividing by source-specific erosion inputs.	With impervious surfaces across the watershed, streams exhibited flashy hydrograph through rapid draining of urban areas and increased volume of storm runoff delivered to the channel over short time frame, resulting in greater peak flows and energy. Streambank materials were in storage in bed and contributed to suspended sediment loads. Bank-derived sediment was remobilized from in-channel storage and made up the greatest proportion of the sediment budget (85%).	Compared to Gellis et al. (2020), this study covering a larger urban/suburban drainage area with mixed land use showed similar observation of streambank erosion and resuspension of fine sediment in bed storage in response to flashy hydrograph. The study site is affected by the historical agricultural land use and post-colonial sediment accumulations (i.e., legacy sediment) in valley bottoms, which affect the contemporary sediment budget, indicating the importance of long-term land use changes on both hydrological and sediment connectivity.
	(Dalzell and Mulla, 2018)	Seven Mile Creek, located in south-central Minnesota (US) -Drainage area: 90 km^2 -Land Use/Land Cover: Corn and Soybean agriculture -Annual Rainfall: 833 mm -Lithology/soil Poorly drained glacial geology with subsurface drainage tiles and ditches on flat terrain (<1%)	Precipitation, flow, and water quality data were collected at three locations (two at the drainage of flat upland and one at the watershed outlet) from 2002 to 2008. Sediment loads were generated with the FLUX model. Soil and Water Assessment Tool (SWAT) model was set up to operate at daily time-step and relies on both process-based and empirically based approaches to simulate agricultural management practices. The extent of tile drainage was mapped using aerial photograph analysis	~96% of the cultivated land is in tile drainage. Under the current watershed condition, ~76% of sediment loading originated from non-field sources, including streambanks and ravines with increased water yield and streamflow. And the modeling results demonstrate that a relatively minor shift in cropping system to include more perennial vegetation, or conservation practices to effectively store more water on the landscape, showed potential to reduce significant sediment export by changing the water budget of the landscape, illustrating the important coupling between sediment sources and watershed hydrology.	Watershed-scale hydrologic and sediment simulation model was used to aggregate the local effects of tile drainage on watershed hydrology and in-channel processes. The model was run at daily time step to simulate these processes from 2002 to 2008 to demonstrate long-term water and sediment impact of changing agricultural practices.

(Continued)

10.3389/frwa.2023.1241622

TABLE 2 (Continued)

Sediment-hydrologic connectivity scenario	Case study	Study location	Study method	Main geomorphic and hydrologic processes	Space/time scales
Old Water - Near/in-channel Sediment (OW-NS)	(Lloyd et al., 2016)	Comparative study of Hampshire Avon catchments in UK (here we focus on groundwater-dominated chalk catchment, Wylye). -Drainage Area: 50.22 km^2 -Land Use/Land Cover: Agriculture mixed with semi-natural woodland, pasture, and arable land -Annual Rainfall: 860-970 mm -Lithology/soil: chalk geology	15-min interval stage height, stream velocity, and turbidity measures. A 30-min interval nitrate-N (UV optical sensor) and total phosphorus (wet chemistry analyzer) data. A storm was defined as any hydrological response to rainfall which resulted in a rising and falling limb with discharge increase of 20% of baseflow. In 60 storms for turbidity were observed. Antecedent precipitation indices (API) and hysteresis indices (HI) were calculated for all the storms defined.	Wylye is primarily groundwater driven with slow-changing baseflow component of the hydrograph with flashy responses during storm events from overland contribution. Short-term discharge dynamic affected the hysteretic direction and strength, and the antecedent conditions influenced the hysteretic behavior indicating importance of hydrologic residence time on sediment sourcing and mobilization. Strong clockwise hysteresis occurred during larger storm events, indicating near- and in-channel sources or resuspension of fine-grained sediment stored in channel bed might dominate sediment loading in the river system.	Relative change in discharge influenced the hysteretic behavior more significantly than the absolute magnitude of the storm.
	(Rose and Karwan, 2021)	Plum Creek in northeastern Wisconsin, US -Drainage Area: 54.3 km^2 -Land Use/Land Cover: Mixed use agriculture (cultivated crops, grassland/pasture, developed areas, forest, and wetlands) -Annual Rainfall: 830 mm -Lithology/soil: silt loams, silty clays, and clay loams	Stream water for total suspended sediment (TSS) and soluble reactive phosphorus (SRP) were collected during five events at nested upper agricultural tributary and during eight events at the watershed outlet. Antecedent precipitation in the week prior to each event was quantified. Quantitative metrics: (1) linear best-fit slope of log(C)-log(Q) relationship to discern "enrichment" "dilution" or "chemostatic" patterns; (2) the ratio of the coefficient of variation of concentration and discharge (CV_C/CV_Q) to differentiate chemostatic and non-linear chemodynamic patterns; (3) HI to characterize hydrologic and biogeochemical dynamics using visual inspection; Flushing Index (FI) to examine dilution or enrichment on the rising limb; linear regression to evaluate the relationships between precipitation and event characteristics and TSS/SRP responses.	In the upstream portion of the watershed primarily in agricultural land use, strong anti-clockwise hysteresis was observed associated with streambank failure in the falling limb as the storm water receded. At the downstream portion, characterized by steep slope channels and high streambank erosion, clockwise hysteresis was dominant, indicating mobilization of sediment stored in stream or near-channel.	Non-linear chemodynamic TSS response may have reflected occurrences of mass streambank failure during non-peak flow periods. A longer recovery period between events increased the pool of sediment available for transport during subsequent events. Main source of sediment (upland vs. near-channel) depended on watershed wetness (i.e., API) from previous events. Thus, **OW-NS** can readily shift to a different sediment-hydrologic connectivity regime (e.g., N—US), event by event. Thus, the understanding of the sediment dynamics over long periods relies on individual events and their sequence.

(Continued)

10.3389/frwa.2023.1241622

TABLE 2 (Continued)

Sediment-hydrologic connectivity scenario	Case study	Study location	Study method	Main geomorphic and hydrologic processes	Space/time scales
	(Belmont et al., 2011)	The incised downstream portion of the Le Sueur River Basin in southcentral Minnesota, US -Drainage Area: 2,880 km^2 -Land Use/Land Cover: row crop agriculture with tile drainage -Annual Rainfall: 833 mm -Lithology/soil: a series of stacked fine-grained tills, deposited over several glacial cycles, interbedded with glaciofluvial sands and gravels.	Sediment budgets constrained through analyses of high-resolution LiDAR topography data and dating of strath terraces. Geochemical fingerprinting using naturally occurring radiogenic tracers measured in suspended sediment samples at multiple gages and Lake Pepin sediment cores.	Increased river discharge in the watershed–from landscape modification with agricultural tile drainage coupled with changing rainfall patterns–has accelerated erosion of streambanks and bluffs, amplifying natural incisional process initiated by baselevel drop that occurred at the beginning of Holocene. Near/in-channel sources (streambank, bluff erosion, channel) became the greatest contributor of the sediment budget (80%) of the watershed.	Long-term changes in the main sediment sources determined using multiple lines of evidence highlight the complexity of large watershed as well as changes in climate and land use that alter both watershed hydrology and sediment supply.
	(Day et al., 2013a,b)	Le Sueur River Basin (see Belmont et al., 2011)	Aerial photographs from 1938 and 1971 were digitized and georeferenced then compared against 2005 photographs. LiDAR topographic data is used to map bluffs, and their retreat rates extrapolated using historic aerial photographs. Terrestrial laser scanning data were collected annually from 2007–2010 at 15 sites to produce high-resolution data on 482 surveyed bluffs.	Bluffs as tall as 65 m line ~80 km of the incised channel in downstream portion of the Le Sueur River Basin and are the largest sediment source (46–54% of the total sediment load). Sapping from groundwater and freeze-thaw processes, along with toe erosion through fluvial abrasion and shear, weaken and erode till material on bluffs. Additionally, given the analysis of stable water isotopes in agricultural landscape in Minnesota (Zhang et al., 2022) and the watershed configuration, river discharge in the incised channel in the downstream portion of the Le Sueur River Basin consist of water that traveled through tiles, ditches, and subsurface pathways from the flat terrain in the upper portion of the watershed over many months.	Long-term changes in channel morphology using historical photographs at watershed-scale and short-term high-resolution study at specific bluff locations were used to quantify the impact of watershed hydrology on near-channel contribution. Synthesis of these various observational methods provided robust estimates of erosion over varying time scales, and the effects of anthropogenic changes to landcover and hydrology.

10.3389/frwa.2023.1241622

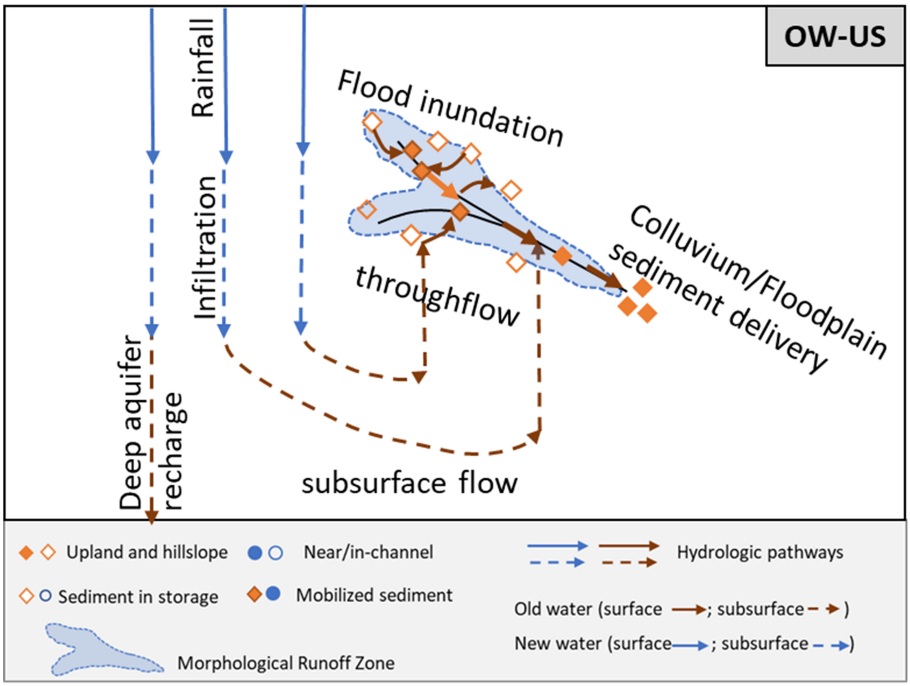

FIGURE 3
Old Water (OW)-Upland Sediment (US) scenario conceptual model.

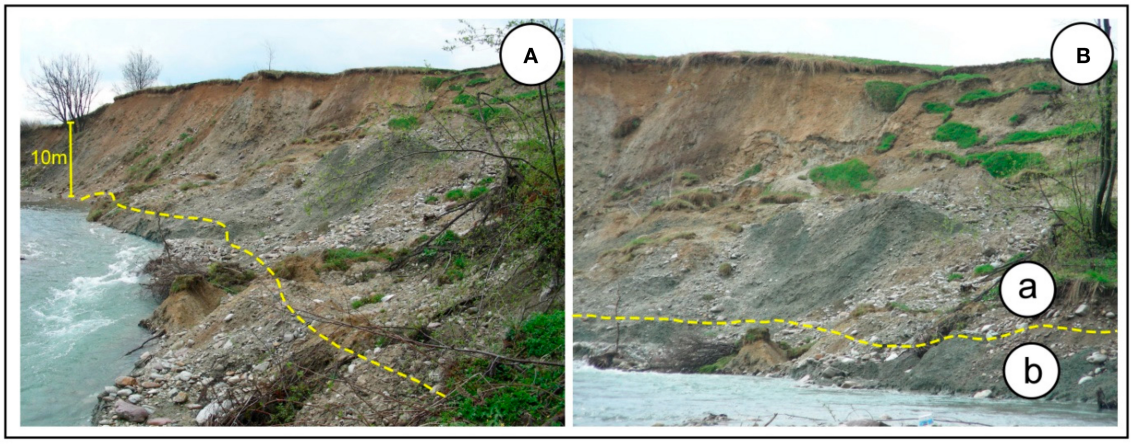

FIGURE 4
Field photographs **(A, B)** in Figure 8 from Kukulak et al. (2022) show landslide colluvium along the River Channels of Podhale (Polish Highlands of Western Carpathians) in southern Poland. The dashed lines mark the colluvium deposit from the landslide above the undisturbed bedrock base.

mountainous regions dominated by steep confined valleys with little to no flood accommodation areas, landslides and debris flows are important sources of sediment (Ward, 1997). Additionally, if the landscape exhibits high infiltration rates and limited overland flow, streams are mainly charged through groundwater discharge [i.e., Old Water (OW)]. In such a system, stream stages are maintained by baseflow, and connectivity is established with Upland Sediment (US) through flushing temporarily stored colluvium in the valley bottom or through slope failure following rainfall events (e.g., infiltration and drainage, resulting in increased pore pressure, and landsliding). At the same time, the stream sediment delivery capacity is increased for a prolonged period after rainfall events through continued subsurface recharge (Figure 3).

The OW-US scenario may be observed in both colluvial headwater channels and floodplain channels, depending on a site's topographic, geologic, and climatic characteristics. For example, Montgomery et al. (2002) document the accumulation of colluvium from landslides and the

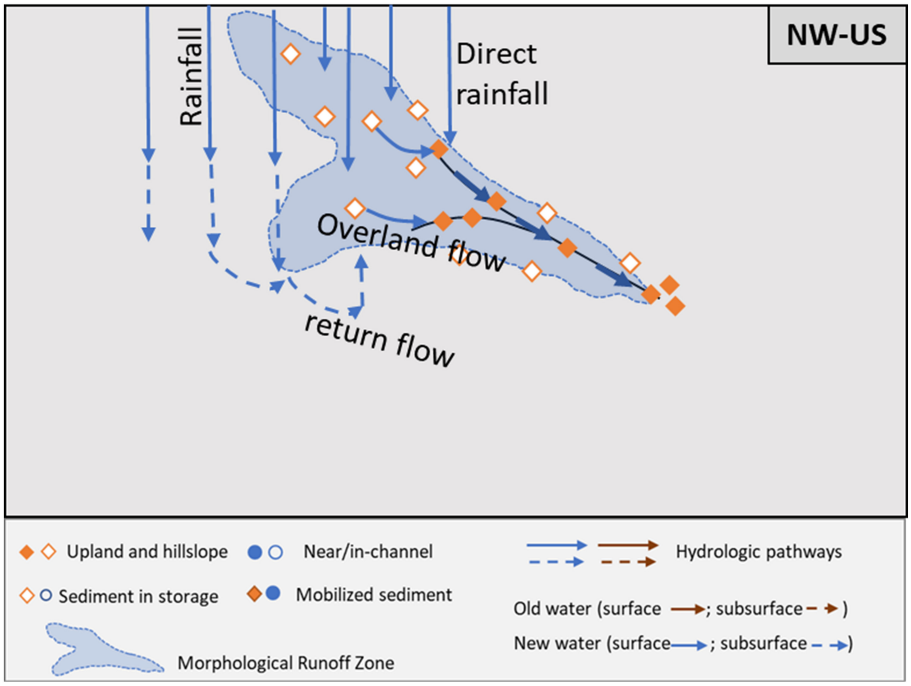

FIGURE 5
New Water (NW)-Upland Sediment (US) scenario conceptual model.

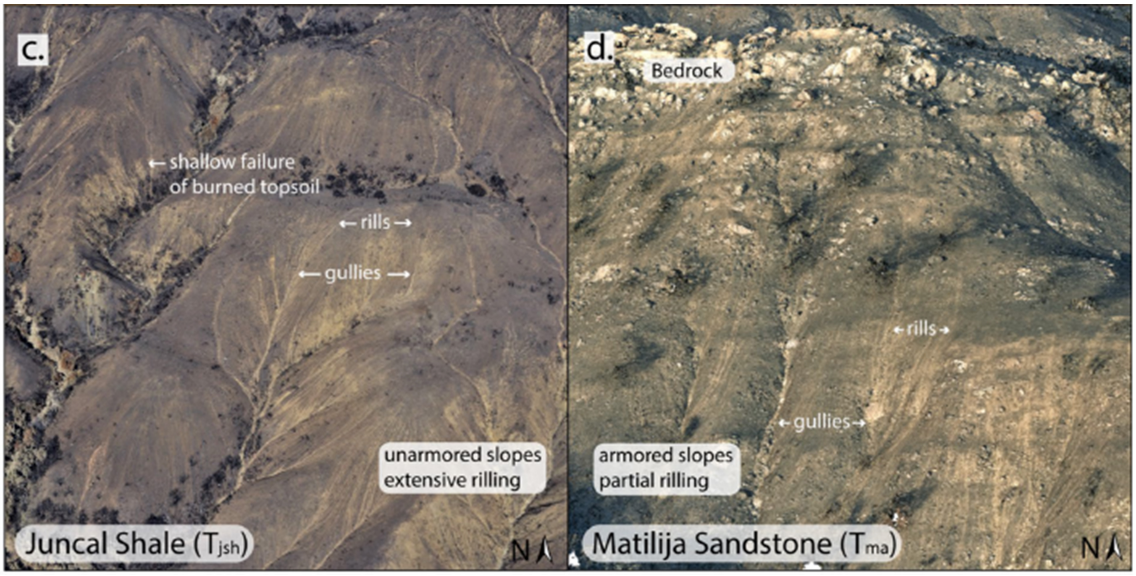

FIGURE 6
Field photographs c and d in Figure 4 from Alessio et al. (2021) show the field condition in extensive rilling on Juncal shale (c) vs. partial rilling on the Matilija sandstone through aerial image taken about a month after the rainstorms that generated rills (d). In Juncal shale aerial imagery, dark-colored patches represent the upper 4–5 cm of burnt soil, and lighter streaks are rills and gullies. In Matiligia sandstone, armored slopes with bedrock outcrop disrupted rill network development.

importance of shallow bedrock flow in both storm runoff and base flow generation, from which the influence on debris-flow initiation was observed in the colluvium-mantled sites. Similarly, Kukulak et al. (2022) report hydrological factors affecting the rate and patterns of fluvial erosion of landslide colluvium at its contact with river flows along river channels of Podhale in southern Poland. In this study site, groundwater seepage through the landslide tongue toward the channel instigated creep and steep scarp formation within the colluvium exposed at the channel banks. The colluvium

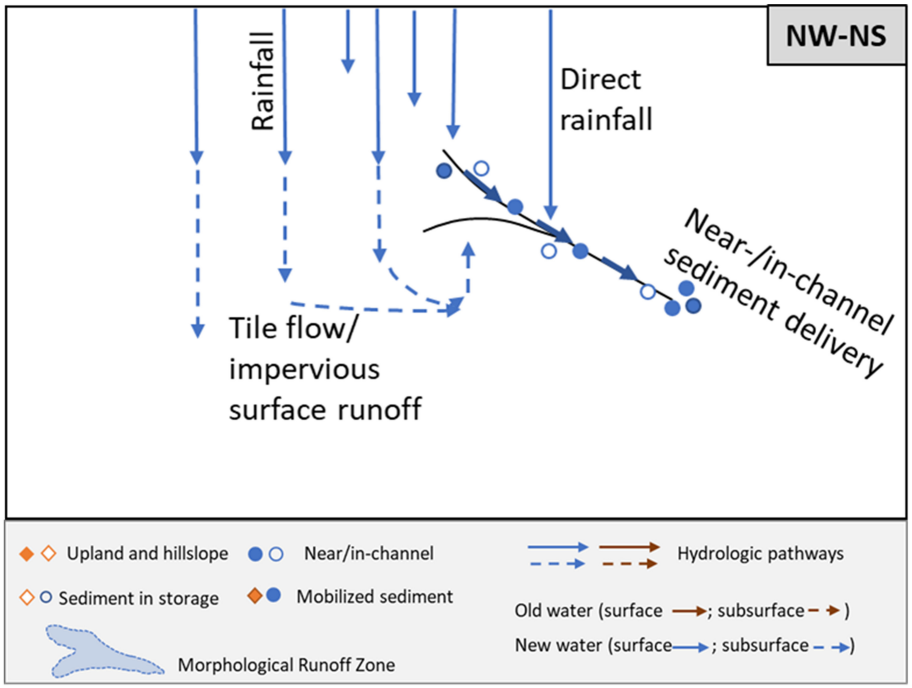

FIGURE 7
New Water (NW)-Near/in-channel Sediment (NS) scenario conceptual model.

deposited from landslide events (in Figure 4, dashed lines mark the colluvial deposit from the landslide above the undisturbed bedrock) was accessed during high flows as the enduring high river stages over many days forced rises of phreatic level in colluvium adjacent to the channel and lowered its friction resistance to failure. On the falling limb, the river water continued to erode the colluvial layer as the pore water drained during a rapid fall of the flood wave when the river is mainly recharged through baseflow. Rise in the groundwater level through infiltration within landslides after a rainfall event also led to the reactivation of slope failure and increased the supply of colluvium to the channels (Kukulak et al., 2022).

In another exampl e from a small stream in the Mid-Atlantic USA, Rose et al. (2018) observed the combination of OW and US loading during an extreme climate event (ECE). During Hurricane Sandy (137 mm of rainfall from 23 to 30 October 2012), spatially variable groundwater inputs to the stream throughout the hydrograph were observed (Sawyer et al., 2014), and fingerprinting of particulate material indicated resuspension and delivery of US in temporary storage within the stream. However, during a previous ECE (Hurricane Irene with 167 mm rainfall over 30 h on 27–28 August 2011), upland source areas throughout the watershed were the primary contributor through precipitation runoff and physical transport on the land surface (see **NW-US** scenario). This study illustrates that event sediment sourcing and dynamics are closely related to the magnitude and intensity of storm events. In addition, the sourcing of primary sediment depends on characteristics of previous storms and their impact on the extent and rates of erosion in both upland and near-/in-channel. Thus, the understanding of the sediment dynamics over long periods relies on individual events and their sequence.

- **Connectivity Scenario: New Water-Upland Sediment (NW-US)**

  The NW-US regime indicates that primary hydrologic drivers consist of event water from precipitation runoff on surface pathways, and the dominant sediment sources consist of upland mass wasting and colluvium stored at the bases of slopes. For example, in a landscape dominated by overland flow with little infiltration, storm flow consists of New Water (NW). Given limited infiltration where rainfall contributes mostly to runoff generation, the MRZ is where overland flow-activated upland sources are greatest in extent, which contrasts with the OW-US scenario. Particularly with the limited availability of near-channel sources (e.g., bedrock, vegetative buffers, gabion walls, and/or other erosion control measures), the main sediment source would consist of US (Figure 5).

  The NW-US scenario may be observed in a semiarid environment, where runoff is activated from summer convective storms, snowmelt runoff, and rainfall on snowpacks, which can initiate incision of montane arroyos and gullies (Gellis, 1998). Overland flow generation is critical in soil erosion and delivery, and its patterns are influenced by infiltration (Kirkby and Chorley, 1967; Dunne and Leopold, 1978). Numerical simulation models of hydrological connectivity conducted in semi-arid environments demonstrate that three factors are important in determining the form of discharge hydrographs: topography (slope length, gradient, flow paths, and convergence),

lithology (infiltration rates), and vegetation (roughness) at the hillslope-channel connection (Reaney et al., 2014). Thus, detachment and transport of sediment from uplands by overland flow depend on the spatial organization of lithology, topography, and surface roughness (Blackburn, 1975; Reaney et al., 2014). For example, a sediment budget compiled for an arid and grazed small catchment during drought conditions indicates high sediment connectivity between hillslopes and the channel network particularly at headcut locations and gullies (Bartley et al., 2007). At the same time, vegetation in the stream promotes the process of sedimentation and increases the resistance to erosion in dryland river channels (Sandercock et al., 2007). In these conditions, the main sediment contribution is the erosion of upland sources from runoff generation where streams act as a net sediment sink.

Landscape disturbance, such as wildfire, can alter watershed hydrology, leading to the NW-US regime. Saturation overland flow develops in the topographic convergence of valley axes (Dunne and Black, 1970) and in areas of soil water repellency, a common post-fire condition (MacDonald and Huffman, 2004). In such conditions, overland flow and soil erosion processes are enhanced, as observed in an *in situ* study coupled with rainfall simulation modeling in a fire-prone bluegum eucalyptus (*Eucalyptus globulus*) plantation in Portugal (Leighton-Boyce et al., 2007). In another study using LiDAR differencing and field observation to map volumes and sources of sediment mobilization from mountain canyons by large post-wildfire debris flows in Montecito, California, it is shown that the largest contribution of sediment was bouldery colluvium and debris-flow accumulation activated by a brief, intense rainstorm (Morell et al., 2021). The extent, pattern, and volumes of post-fire hillslope erosion depended on rainfall, runoff, landscape characteristics, and burn severity. In the same study site in Montecito, the distribution of rills and cross-sectional geometries was mapped on burned hillslopes in the source catchments to demonstrate that different lithological and topographic features affect the extent and dimensions of rills and volumes of slurry mixing of water and sediment (Alessio et al., 2021). Figure 6 illustrates post-rainstorm rill erosion on burned hillslopes of different bedrock compositions from Alessio et al. (2021). Though in-stream erosion can contribute to the overall sediment loading during post-fire storm events, upland sources (ridgetops and steep valley sideslopes) made up the dominant part of the sediment budget given post-fire erosion susceptibility in hillslopes according to a sediment budget analysis using fallout radionuclide (FRN) tracers by Blake et al. (2009). In fact, post-fire conditions can shift dominant sediment sources from gully and riverbank erosion to topsoil derived from hillslope surface erosion. With fire occurrences, transport-limited conditions can be created in channel conduits, where in-channel and floodplains are more likely to store sediment, particularly with high interannual hydrologic variability (Wilkinson et al., 2009).

Additionally, anthropogenic lands cape disturbances, such as urbanization and intensive agriculture, particularly without effective soil conservation in upland areas, can accelerate erosion of topsoil, creating NW-US scenarios. Wolman (1967) presented the process of urbanization of the landscape, particularly from the period of construction, linked to large pulses of sediment yield. Agriculture can also accelerate upland and hillslope erosion, compared to native vegetation and long-term geologic erosion (Montgomery, 2007). Prior to the widespread adoption of agricultural soil erosion control measures (e.g., conservation tillage, grassed waterways, and buffers), upland sources have contributed dominantly to sediment budgets (Trimble, 1985). For example, a sediment fingerprinting study in the Upper Mississippi River Basin demonstrates a pulse of soil erosion from agricultural fields during the mid-20th century, followed by a subsequent shift back toward near-channel sources (i.e., see **NW-NS** scenario) in the recent decades after widespread agricultural soil erosion control measures were adopted in the region (Belmont et al., 2011).

FIGURE 8
Channel enlargement (location of tree roots indicate original location of channel bank) caused by urban runoff in an urban stream in Baltimore, Maryland [Photo Source: Allen Gellis (USGS) as appear in Figure 2B of Gellis et al. (2020)].

- **Connectivity Scenario: New Water-Near/in-Channel Sediment (NW-NS)**

  The NW-NS regime indicates that primary hydrologic drivers consist of event water from precipitation runoff on surface pathways, and the dominant sediment sources consist of near/in-channel erosional processes. For instance, in a landscape system with small infiltration rates, overland precipitation runoff, and drainage management (e.g., ditches, tiles, and other artificial drainage) control the rapid overland movement of water. Subsequently, streams are flooded with large quantities of NW increasing the erosivity and delivery capacity of the channel during the rainfall event. With the limited availability of overland sediment sources (e.g., impervious surface, vegetative cover, and/or erosion control measures), the primary sediment sources consist of Near-channel Sediment (NS) (Figure 7).

  Anthropogenic landscape disturbance, such as urbanization or intensive agriculture, can alter watershed hydrology and

FIGURE 9
Agricultural artificial subsurface tiles draining to a ditch system (photo source: University of Minnesota Extension; https://extension.umn.edu/agricultural-drainage/how-agricultural-drainage-works).

impact dominant sediment sources, leading to a NW-NS scenario. In a study that examines the effects of urbanization on hydrology, it is shown that impervious surfaces and stormwater drainage systems increase and drive runoff (i.e., NW) and amplify the overall peak flood discharge and duration (Paul and Meyer, 2001), which is followed by channel erosion and channel widening or enlargement (i.e., NS), while the sediment production from urbanized landscapes is minimal (Chin, 2006). In a Mid-Atlantic urban stream in Maryland, runoff from impervious surfaces and storm drain network have resulted in high peak flows in open channels, leading to channel widening, streambank erosion, and channel incision (Figure 8) as verified by the numerical tagging of ^{7}Be and $^{210}Pb_{ex}$ activities (Gellis et al., 2020). Similarly, studies using sediment sampling, elemental tracers, and radionuclide analysis in urban watersheds in Maryland and Virginia show that streambank contributed the greatest quantity of fine sediment (Devereux et al., 2010; Cashman et al., 2018) to the Chesapeake Bay.

Additionally, agricultural tile drainage (Figure 9), particularly at shallow depths or with narrow spacing, is often considered to carry a characteristic concentration–discharge signature of surface runoff (Radcliffe et al., 2015; Smith et al., 2015, 2019). Tile drainage networks and ditch systems have artificially extended the drainage of many watersheds with low permeability on the flat terrain of the headwaters of the Mississippi River Basin (Kelley and Nater, 2000). A modeling study with stream monitoring data from various locations across south-central Minnesota, in which ~96% of the cultivated land is in tile drainage, evaluates the impacts of altered hydrology on sediment sources (Dalzell and Mulla, 2018). Under current watershed conditions, ~76% of sediment loading originates from non-field sources, including streambanks and ravines because of increased water yield and streamflow. The modeling results of alternate landscape management demonstrate that a relatively minor shift in cropping systems to include more perennial vegetation, or conservation practices to effectively store more water on the landscape, showed the potential to reduce significant sediment export by changing the water budget of the landscape, illustrating the important coupling between sediment sources and watershed hydrology (Dalzell and Mulla, 2018).

- **Connectivity Scenario: Old Water-Near/in-Channel Sediment (OW-NS)**

  The OW-NS regime indicates that the primary hydrologic drivers consist of pre-event water from subsurface storage, and the dominant sediment sources consist of near/in-channel erosional processes. For instance, in a landscape dominated by steep confined valleys with little to no flood accommodation areas, where stream flow is mainly charged through subsurface flow (OW), the erosivity and delivery capacity of the river are heightened with increased stream flow for a prolonged period following a rain event. In such a system the major sediment contribution consists of near/in-channel sediment sources (NS) through incision, widening, and lateral channel migration of meander (Figure 10).

  In a comparative study of hydrogeological control on hysteresis, Lloyd et al. (2016) demonstrate that in a groundwater-dominated mixed-landuse watershed, slow-changing baseflow with relatively attenuated but flashy responses is observed during storm events. Short-term discharge dynamics affected the hysteretic direction and strength, and the antecedent conditions influenced the hysteretic behavior, indicating the importance of hydrologic residence time on sediment sources and mobilization (Lloyd et al., 2016). Stron g clockwise hysteresis occurred during larger storm events, indicating that flushing of readily erodible near- and in-channel sources might dominate sediment loading in the river system. Alternately, Rose and Karwan (2021) infer major sediment sources from concentration–discharge relationships and chemodynamics of Plum Creek in northeastern Wisconsin: Strong anti-clockwise hysteresis is associated with streambank failure observable in the incised channels, which can mobilize large amounts of suspended materials to the stream, as the storm water recedes under baseflow conditions (i.e., Old Water/Near-channel Sediment). These examples demonstrate that the main sources of sediment (upland vs. near-channel) depend on watershed wetness (i.e., antecedent precipitation indices) from previous events. Thus, OW-NS can readily shift to a different regime event by event. The understanding of the sediment dynamics over long periods relies on individual events and their sequence.

  In another example, a comprehensive sediment budget was developed using multiple lines of evidence, ranging from field surveys, stream gaging, and sediment fingerprinting to remote-sensing analysis in the Le Sueur River Basin of south-central Minnesota, which is undergoing a transient incisional process following the initial carving of the landscape ~13,000 years ago that created the baselevel drop of up to 65 m from the surrounding drainage basins to the Minnesota River Valley (Gran et al., 2013). As a result, bluffs as tall as 65 m comprise 1,280 km of channel in the knick zone of the watershed–a high-gradient reaches that have adjusted to the new baselevel (Figure 11). Sapping from groundwater

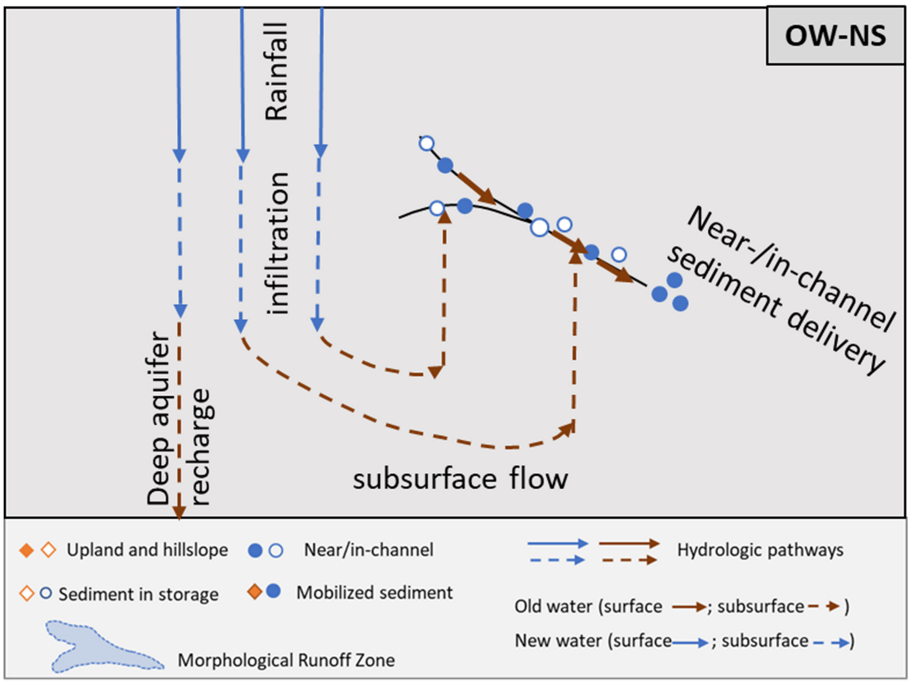

FIGURE 10
Old Water (OW)-Near/in-channel Sediment (NS) scenario conceptual model.

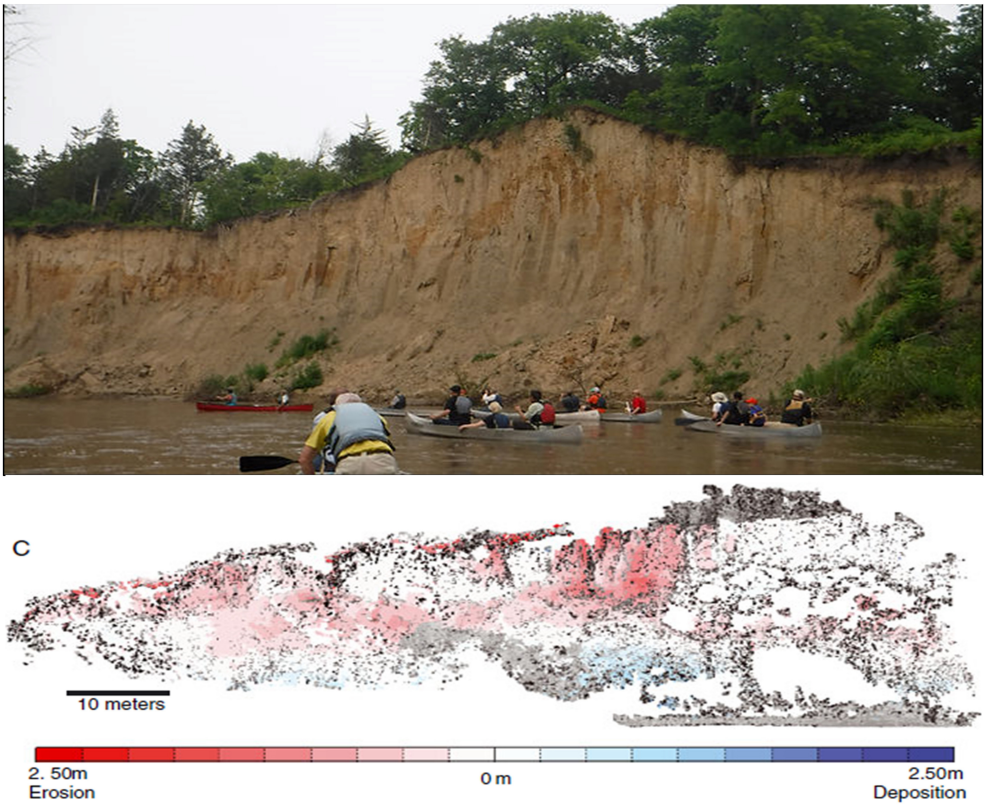

FIGURE 11
Field photograph from Mankato State University Water Resource Center **(top)** shows a typical bluff face along the Le Sueur River with kayakers as a scale. Image C in Figure 7 from Day et al. (2013a) **(bottom)** shows a normally consolidated till bluff where erosion at the top face of the bluff and deposition at the toe are mapped between 2007 and 2008 with terrestrial laser scanning (TLS).

and freeze-thaw processes, along with toe erosion through fluvial abrasion and shear, have weakened and eroded till material on bluffs of the Le Sueur River (i.e., NS) (Day et al., 2013b). Evaluation of the sediment supply in the watershed, derived from geochemical fingerprinting and a suite of geomorphic change detection techniques, indicates that although agricultural soil erosion remains large, the dominant sediment source has shifted from agricultural field erosion to accelerated erosion and over steepening of stream banks and bluffs, driven by increased river discharge (Belmont et al., 2011). In a regional analysis of stable water isotopes, deuterium, and oxygen-18 data from agricultural landscapes of western South Dakota to eastern Minnesota show that precipitation took an average of 9 months to move through different pathways (Zhang et al., 2022). Given the watershed configuration that progressively narrows toward the outlet, along with the independent assessment of water residence time in the region, the water discharge in the incised section of the Le Sueur River likely consists of water that traveled through tiles, ditches, and subsurface pathways from the flat upper portion of the watershed over many months (i.e., OW).

4 Next steps: applying the sediment-hydrologic connectivity conceptual model

The conceptual model and case studies using various observational and modeling techniques can provide guidance for collecting and assembling environmental data. For instance, through the synthesis of existing datasets and monitoring sites with new, coordinated sampling, we can investigate how hydrologic and sediment connectivity affect sediment mobilization at different spatiotemporal scales as illustrated in the selected case studies. In addition, an understanding of how dominant processes shift with different environmental forcing and/or landscape disturbances may be derived from strategic data assemblage using the conceptual model (e.g., various observational and modeling approaches to characterize post-fire sediment delivery described in the NW-US scenarios). Specifically, the collection of distinct isotopic signals in stream water samples collected for various storm events across the watershed can help to characterize dominant flow pathways and residence times at different spatial scales from reaches to basin outlets. Remote-sensing analysis coupled with stream gaging and chemical tracers collected and aggregated over different spatial and temporal scales can provide critical guidance on dominant sediment sources and how they shift with storm size and with changing temporal and spatial scales. For more discussion on environmental measurement techniques for system fluxes (e.g., water discharge and sediment delivery) vs. system phases (e.g., geology, soil, ecology, and geomorphology) to design effective measurement schemes and models at different scales, refer to Keesstra et al. (2018) and the various observational approaches highlighted in the case studies of the previous section.

Numerical simulation of landscape connectivity combined with strategic data collection can help to effectively evaluate and forecast sediment delivery, transport, and storage across spatial and temporal scales and to predict how connectivity shifts with different environmental forcing and landscape disturbances. The conceptual model will be particularly useful when compiling relevant data to characterize water and sediment connectivity using data-driven analyses such as machine-learning (ML) applications. For example, ML models have been developed to predict sediment transport from a wide range of publicly available environmental features by training them with physically collected water and sediment samples (Lund et al., 2022). The more efficient assemblage of available geospatial data could help model interpretation and prediction accuracy. It has been noted that dataset biases occur in ML applications when the training data are not fully representative of the landscape characteristics and planned uses, and the results can be contaminated with the desired outcome and user biases (Zhong et al., 2021). The conceptual model proposed here can be used to check the implicit biases toward desired outcomes by considering the broad spectrum of sediment and hydrologic processes.

5 Conclusion

The understanding of changing sediment and water dynamics over different spatial and temporal scales, under a range of environmental conditions, is critical for developing monitoring and modeling approaches to quantify and predict sediment loading, as well as, for developing effective water quality management strategies. The conceptualization and application of sediment connectivity are reviewed in terms of how they frame the continuum of sediment sources, stores, and routes of transport operating under different hydrologic conditions. The landscape connectivity research in recent decades indicates that both sediment connectivity and hydrologic processes affect provenance, pathways, and storages along the sediment cascade and influence their timing and magnitude. We propose an integrated hydrologic and sediment connectivity conceptual model to broadly categorize dominant sediment and hydrologic processes and patterns relevant to understanding and predicting sediment flux dynamics. Using the conceptual model as a "thinking" tool, we extract case studies from a multidisciplinary literature review—from hydrology, geomorphology, biogeochemistry, and watershed modeling to remote-sensing technology—that correspond to each of the dominant hydrologic–sediment connectivity regimes to examine sediment and water interactions in real-world examples using various observational and modeling techniques. The conceptual model and case studies provide an important foundation for advancing the understanding and predictive capability of watershed sediment processes at multiple spatiotemporal scales and various environmental conditions.

Author contributions

SJC, DLK, KS, JP, and MEH contributed to conception and design of the study. SJC organized and reviewed the literature and wrote the first draft of the manuscript. SJC and DLK wrote sections of the manuscript. All authors contributed to manuscript revision, read, and approved the submitted version.

Funding

This study was funded by the U.S. Geological Survey's Mendenhall Postdoctoral Fellowship (SJC). DLK received funding from the USGS Water Resources Research Act Program. Foundational work was done under NSF EAR 1424147 by DLK, KS, and JP.

Acknowledgments

The authors like to thank the support of the USGS peers, Trevor F. Partridge and Michelle P. Katoski and two reviewers who helped them improve the manuscript. The authors are also grateful to those who provided and permitted the use of illustrative images and photographs: Paul Alessio of University of California, Santa Barbara; JoAnne Makela of University of Minnesota Extension; Brent Dalzell of USDA Agricultural Research Service; Kimberly Musser of Water Resources Center, Minnesota State University, Mankato; and Jozef Kukulak et al., and Day et al., whose full citations can be found in the References. Any use of trade, firm, or product names is for descriptive purposes only and does not imply endorsement by the U.S. Government.

Conflict of interest

The authors declare that the research was conducted in the absence of any commercial or financial relationships that could be construed as a potential conflict of interest.

Publisher's note

All claims expressed in this article are solely those of the authors and do not necessarily represent those of their affiliated organizations, or those of the publisher, the editors and the reviewers. Any product that may be evaluated in this article, or claim that may be made by its manufacturer, is not guaranteed or endorsed by the publisher.

References

Alessio, P., Dunne, T., and Morell, K. (2021). Post-wildfire generation of debris-flow slurry by rill erosion on colluvial hillslopes. *J. Geophys. Res.* 126, e2021JF006108. doi: 10.1029/2021JF006108

Bartley, R., Hawdon, A., Post, D. A., and Roth, C. H. (2007). A sediment budget for a grazed semi-arid catchment in the Burdekin basin, Australia. *Geomorphology* 87, 302–321. doi: 10.1016/j.geomorph.2006.10.001

Belmont, P., Gran, K. B., Schottler, S. P., Wilcock, P. R., Day, S. S., Jennings, C., et al. (2011). Large shift in source of fine sediment in the Upper Mississippi River. *Environ. Sci. Technol.* 45, 8804–8810. doi: 10.1021/es2019109

Blackburn, W. H. (1975). Factors influencing infiltration and sediment production of semiarid Rangelands in Nevada. *Water Resources Research* 11, 929–937. doi: 10.1029/WR011i006p00929

Blake, W. H., Wallbrink, P. J., Wilkinson, S. N., Humphreys, G. S., Doerr, S. H., Shakesby, R. A., et al. (2009). Deriving hillslope sediment budgets in wildfire-affected forests using fallout radionuclide tracers. *Geomorphology* 104, 105–116. doi: 10.1016/j.geomorph.2008.08.004

Borselli, L., Cassi, P., and Torri, D. (2008). Prolegomena to sediment and flow connectivity in the landscape: a GIS and field numerical assessment. *Catena* 75, 268–277. doi: 10.1016/j.catena.2008.07.006

Bracken, L. J., Turnbull, L., Wainwright, J., and Bogaart, P. (2015). Sediment connectivity: a framework for understanding sediment transfer at multiple scales. *Earth Surface Proc. Landf.* 40, 177–188. doi: 10.1002/esp.3635

Bunn, A. G., Urban, D. L., and Keitt, T. H. (2000). Landscape connectivity: a conservation application of graph theory. *J. Environ. Manag.* 59, 265–278. doi: 10.1006/jema.2000.0373

Cashman, M. J., Gellis, A., Sanisaca, L. G., Noe, G. B., Cogliandro, V., and Baker, A. (2018). Bank-derived material dominates fluvial sediment in a suburban Chesapeake Bay watershed. *River Res. Applic.* 34, 1032–1044. doi: 10.1002/rra.3325

Cavalli, M., Trevisani, S., Comiti, F., and Marchi, L. (2013). Geomorphometric assessment of spatial sediment connectivity in small Alpine catchments. *Geomorphology* 188, 31–41. doi: 10.1016/j.geomorph.2012.05.007

Chin, A. (2006). Urban transformation of river landscapes in a global context. *Geomorphology* 79, 460–487. doi: 10.1016/j.geomorph.2006.06.033

Cho, S. J., Wilcock, P., and Gran, K. (2022). Implementing landscape connectivity with topographic filtering model: a simulation of suspended sediment delivery in an agricultural watershed. *Sci. Total Environ.* 836, 155701. doi: 10.1016/j.scitotenv.2022.155701

Cho, S. J., Wilcock, P., and Hobbs, B. (2018). Topographic filtering simulation model for sediment source apportionment. *Geomorphology* 309, 1–19. doi: 10.1016/j.geomorph.2018.02.014

Cho, S. J., Wilcock, P. R., Belmont, P., Gran, K. B., and Hobbs, B. F. (2019). Simulation model for collaborative decision making on sediment source reduction in an intensively managed watershed. *Water Resour. Res.* 55, 1544–1564. doi: 10.1029/2018WR024324

Cislaghi, A., and Bischetti, G. B. (2019). Source areas, connectivity, and delivery rate of sediments in mountainous-forested hillslopes: a probabilistic approach. *Sci. Total Environ.* 652, 1168–1186. doi: 10.1016/j.scitotenv.2018.10.318

Czuba, J. A. (2018). A lagrangian framework for exploring complexities of mixed-size sediment transport in gravel-bedded river networks. *Geomorphology* 321, 146–152. doi: 10.1016/j.geomorph.2018.08.031

Czuba, J. A., and Foufoula-Georgiou, E. (2015). Dynamic connectivity in a fluvial network for identifying hotspots of geomorphic change. *Water Resour. Res.* 51, 1401–1421. doi: 10.1002/2014WR016139

Dalzell, B. J., and Mulla, D. J. (2018). Perennial vegetation impacts on stream discharge and channel sources of sediment in the minnesota river basin. *J. Soil Water Conserv.* 73, 120–132. doi: 10.2489/jswc.73.2.120

Day, S. S., Gran, K. B., Belmont, P., and Wawrzyniec, T. (2013a). Measuring bluff erosion part 1: terrestrial laser scanning methods for change detection. *Earth Surface Proc. Landforms* 38, 1055–1067. doi: 10.1002/esp.3353

Day, S. S., Gran, K. B., Belmont, P., and Wawrzyniec, T. (2013b). Measuring bluff erosion part 2: pairing aerial photographs and terrestrial laser scanning to create a watershed scale sediment budget. *Earth Surface Proc. Landforms* 38, 1068–1082. doi: 10.1002/esp.3359

Devereux, O. H., Prestegaard, K. L., Needelman, B. A., and Gellis, A. C. (2010). Suspended-sediment sources in an urban watershed, Northeast Branch Anacostia River, Maryland. *Hydrol. Proc.* 24, 1391–1403. doi: 10.1002/hyp.7604

Dunne, T., and Black, R. D. (1970). Partial area contributions to storm runoff in a small new England watershed. *Water Resour. Res.* 6, 1296–1311. doi: 10.1029/WR006i005p01296

Dunne, T., and Leopold, L. B. (1978). *Water in Environmental Planning*. New York: W.H. Freeman and Co.

Fortuin, K. P., Van Koppen, C. S. A., and Leemans, R. (2011). The value of conceptual models in coping with complexity and interdisciplinarity in environmental sciences education. *BioScience* 61, 802–814. doi: 10.1525/bio.2011.61.10.10

Foufoula-Georgiou, E., Takbiri, Z., Czuba, J. A., and Schwenk, J. (2015). The change of nature and the nature of change in agricultural landscapes: hydrologic regime shifts modulate ecological transitions. *Water Resour. Res.* 51, 6649–6671. doi: 10.1002/2015WR017637

Fryirs, K. (2013). (Dis)Connectivity in catchment sediment cascades: a fresh look at the sediment delivery problem. *Earth Surface Proc. Landforms* 38, 30–46. doi: 10.1002/esp.3242

Gellis, A. C. (1998). *Characterization and Evaluation of Channel and Hillslope Erosion on the Zuni Indian Reservation, New Mexico, 1992-95*. U.S. Department of the Interior, U.S. Geological Survey.

Gellis, A. C., Fuller, C. C., Van Metre, P. C., Mahler, B. J., Welty, C., Miller, A. J., et al. (2020). Pavement alters delivery of sediment and fallout radionuclides to urban streams. *J. Hydrol.* 588, 124855. doi: 10.1016/j.jhydrol.2020.124855

Gran, K. B., Finnegan, N., Johnson, A. L., Belmont, P., Wittkop, C., and Rittenour, T. (2013). Landscape evolution, valley excavation, and terrace development following abrupt postglacial base-level fall. *Bulletin* 125, 1851–1864. doi: 10.1130/B30772.1

Hewlett, J. D., and Hibbert, A. R. (1963). Moisture and energy conditions within a sloping soil mass during drainage. *J. Geophys. Res.* 68, 1081–1087. doi: 10.1029/JZ068i004p01081

Karwan, D. L., Pizzuto, J. E., Aalto, R., Marquard, J., Harpold, A., Skalak, K., et al. (2018). Direct channel precipitation and storm characteristics influence short-term fallout radionuclide assessment of sediment source. *Water Resour. Res.* 54, 4579–4594. doi: 10.1029/2017WR021684

Keesstra, S., Nunes, J. P., Saco, P., Parsons, T., Poeppl, R., Masselink, R., et al. (2018). The way forward: Can connectivity be useful to design better measuring and modelling schemes for water and sediment dynamics? *Sci. Total Environ.* 644, 1557–1572. doi: 10.1016/j.scitotenv.2018.06.342

Kelley, D. W., and Nater, E. A. (2000). Historical sediment flux from three watersheds into Lake Pepin, Minnesota, USA. *J. Environ. Quality* 29, 561–568. doi: 10.2134/jeq2000.00472425002900020025x

Kirkby, M. J., and Chorley, R. J. (1967). Throughflow, overland flow and erosion. *Int. Assoc. Sci. Hydrol. Bull.* 12, 5–21. doi: 10.1080/02626666709493533

Klaus, J., and McDonnell, J. J. (2013). Hydrograph separation using stable isotopes: review and evaluation. *J. Hydrol.* 505, 47–64. doi: 10.1016/j.jhydrol.2013.09.006

Kukulak, J., Augustowski, K., and Olszak, J. (2022). Factors affecting the rates and modes of landslide colluvium removal in river channels of Podhale (Western Carpathians). *Water* 14, 3577. doi: 10.3390/w14213577

Leighton-Boyce, G., Doerr, S. H., Shakesby, R. A., and Walsh, R. P. D. (2007). Quantifying the impact of soil water repellency on overland flow generation and erosion: a new approach using rainfall simulation and wetting agent on in situ soil. *Hydrol. Proc.* 21, 2337–2345. doi: 10.1002/hyp.6744

Lloyd, C. E., Freer, J. E., Johnes, P. J., and Collins, A. L. (2016). Using hysteresis analysis of high-resolution water quality monitoring data, including uncertainty, to infer controls on nutrient and sediment transfer in catchments. *Sci. Total Environ.* 543, 388–404. doi: 10.1016/j.scitotenv.2015.11.028

Lund, J. W., Groten, J. T., Karwan, D. L., and Babcock, C. (2022). Using machine learning to improve predictions and provide insight into fluvial sediment transport. *Hydrol. Proc.* 36, e14648. doi: 10.1002/hyp.14648

MacDonald, L. H., and Huffman, E. L. (2004). Post-fire soil water repellency. *Soil Sci. Soc. Am. J.* 68, 1729–1734. doi: 10.2136/sssaj2004.1729

Mahoney, D. T., Fox, J., Al-Aamery, N., and Clare, E. (2020a). Integrating connectivity theory within watershed modelling part i: model formulation and investigating the timing of sediment connectivity. *Sci. Total Environ.* 740, 140385. doi: 10.1016/j.scitotenv.2020.140385

Mahoney, D. T., Fox, J., Al-Aamery, N., and Clare, E. (2020b). Integrating connectivity theory within watershed modelling part II: Application and evaluating structural and functional connectivity. *Sci. Total Environ.* 740, 140386. doi: 10.1016/j.scitotenv.2020.140386

Mahoney, D. T., Fox, J. F., and Al Aamery, N. (2018). Watershed erosion modeling using the probability of sediment connectivity in a gently rolling system. *J. Hydrol.* 561, 862–883. doi: 10.1016/j.jhydrol.2018.04.034

McEachran, Z. P., Karwan, D. L., and Slesak, R. A. (2021). Direct and indirect effects of forest harvesting on sediment yield in forested watersheds of the United States. *JAWRA* 57, 1–31. doi: 10.1111/1752-1688.12895

Montgomery, D. R. (1999). Process domains and the river continuum. *JAWRA J.* 35, 397–410. doi: 10.1111/j.1752-1688.1999.tb03598.x

Montgomery, D. R. (2007). Soil erosion and agricultural sustainability. *Proc. Natl. Acad. Sci.* 104, 13268–13272. doi: 10.1073/pnas.0611508104

Montgomery, D. R., Dietrich, W. E., and Heffner, J. T. (2002). Piezometric response in shallow bedrock at CB1: Implications for runoff generation and landsliding. *Water Resour. Res.* 38, 10–11. doi: 10.1029/2002WR001429

Morell, K. D., Alessio, P., Dunne, T., and Keller, E. (2021). Sediment recruitment and redistribution in mountain channel networks by post-wildfire debris flows. *Geophys. Res. Lett.* 48, 24. doi: 10.1029/2021GL095549

Paul, M. J., and Meyer, J. L. (2001). Streams in the urban landscape. *Ann. Rev. Ecol. System.* 32, 333–365. doi: 10.1146/annurev.ecolsys.32.081501.114040

Radcliffe, D. E., Reid, D. K., Blombäck, K., Bolster, C. H., Collick, A. S., Easton, Z. M., et al. (2015). Applicability of models to predict phosphorus losses in drained fields: a review. *J. Environ. Quality* 44, 614–628. doi: 10.2134/jeq2014.05.0220

Reaney, S. M., Bracken, L. J., and Kirkby, M. J. (2014). The importance of surface controls on overland flow connectivity in semi-arid environments: results from a numerical experimental approach. *Hydrol. Proc.* 28, 2116–2128. doi: 10.1002/hyp.9769

Rose, L. A., and Karwan, D. L. (2021). Stormflow concentration–discharge dynamics of suspended sediment and dissolved phosphorus in an agricultural watershed. *Hydrol. Proc.* 35, e14455. doi: 10.1002/hyp.14455

Rose, L. A., Karwan, D. L., and Aufdenkampe, A. K. (2018). Sediment fingerprinting suggests differential suspended particulate matter formation and transport processes across hydrologic regimes. *J. Geophys. Res.* 123, 1213–1229. doi: 10.1002/2017JG004210

Sandercock, P. J., Hooke, J. M., and Mant, J. M. (2007). Vegetation in dryland river channels and its interaction with fluvial processes. *Progr. Phys. Geogr.* 31, 107–129. doi: 10.1177/0309133307076106

Sawyer, A. H., Kaplan, L. A., Lazareva, O., and Michael, H. A. (2014). Hydrologic dynamics and geochemical responses within a floodplain aquifer and hyporheic zone during hurricane sandy. *Water Resour. Res.* 50, 4877–4892. doi: 10.1002/2013WR015101

Shanley, J. B., Kendall, C., Smith, T. E., Wolock, D. M., and McDonnell, J. J. (2002). Controls on old and new water contributions to stream flow at some nested catchments in Vermont, USA. *Hydrol. Proc.* 16, 589–609. doi: 10.1002/hyp.312

Smith, D. R., King, K. W., Johnson, L., Francesconi, W., Richards, P., Baker, D., et al. (2015). Surface runoff and tile drainage transport of phosphorus in the midwestern United States. *J. Environ. Quality* 44, 495–502. doi: 10.2134/jeq2014.04.0176

Smith, D. R., Macrae, M. L., Kleinman, P. J. A., Jarvie, H. P., King, K. W., and Bryant, R. B. (2019). The latitudes, attitudes, and platitudes of watershed phosphorus management in North America. *J. Environ. Quality* 48, 1176–1190. doi: 10.2134/jeq2019.03.0136

Trimble, S. W. (1985). Perspectives on the history of soil erosion control in the eastern United States. *Agric. Hist.* 59, 162.

Vannote, R. L., Minshall, G. M., Cummins, K. W., Sedell, J. R., and Cushing, C. E. (1980). The river continuum concept. *Canad. J. Fisher. Aquat. Sci.* 37, 130–137. doi: 10.1139/f80-017

Wainwright, J., Turnbull, L., Ibrahim, T. G., Lexartza-Artza, I., Thornton, S. F., and Brazier, R. E. (2011). Linking environmental regimes, space and time: Interpretations of structural and functional connectivity. *Geomorphology* 126, 387–404. doi: 10.1016/j.geomorph.2010.07.027

Ward, J. V. (1997). An expansive perspective of riverine landscapes: pattern and process across scales. *GAIA Ecol. Perspect. Sci. Soc.* 6, 52–60. doi: 10.14512/gaia.6.1.6

Wilkinson, S. N., Wallbrink, P. J., Hancock, G. J., Blake, W. H., Shakesby, R. A., and Doerr, S. H. (2009). Fallout radionuclide tracers identify a switch in sediment sources and transport-limited sediment yield following wildfire in a eucalypt forest. *Geomorphology* 110, 140–151. doi: 10.1016/j.geomorph.2009.04.001

Wohl, E., Magilligan, F. J., and Rathburn, S. L. (2017). Introduction to the special issue: connectivity in geomorphology. *Geomorphology* 277, 1–5. doi: 10.1016/j.geomorph.2016.11.005

Wolman, M. G. (1967). A cycle of sedimentation and erosion in urban river channels. *Geografiska Annaler* 49, 385–395. doi: 10.1080/04353676.1967.11879766

Zanandrea, F., Michel, G. P., Kobiyama, M., Censi, G., and Abatti, B. H. (2021). Spatial-temporal assessment of water and sediment connectivity through a modified connectivity index in a subtropical mountainous catchment. *Catena* 204, 105380. doi: 10.1016/j.catena.2021.105380

Zhang, L., Magner, J., and Strock, J. (2022). Exploring a climate gradient of Midwestern USA agricultural landscape runoff using deuterium (δD) and oxygen-18 (δ18O). *Water* 14, 1629. doi: 10.3390/w14101629

Zhong, S., Zhang, K., Bagheri, M., Burken, J. G., Gu, A., Li, B., et al. (2021). Machine learning: new ideas and tools in environmental science and engineering. *Environ. Sci. Technol.* 55, 12741–12754. doi: 10.1021/acs.est.1c01339

frontiers | Frontiers in Water

TYPE Original Research
PUBLISHED 06 December 2023
DOI 10.3389/frwa.2023.1254225

OPEN ACCESS

EDITED BY
Dipankar Dwivedi,
Berkeley Lab (DOE), United States

REVIEWED BY
Christina Tague,
University of California, Santa Barbara, United States
Jinwoo Im,
Berkeley Lab (DOE), United States

*CORRESPONDENCE
Bisesh Joshi
✉ bjoshi@udel.edu

RECEIVED 06 July 2023
ACCEPTED 16 November 2023
PUBLISHED 06 December 2023

CITATION
Joshi B, Bacmeister E, Peck E, Peipoch M, Kan J and Inamdar S (2023) Sediment-Nitrogen (N) connectivity: suspended sediments in streams as N exporters and reactors for denitrification and assimilatory N uptake during storms. *Front. Water* 5:1254225. doi: 10.3389/frwa.2023.1254225

Sediment-Nitrogen (N) connectivity: suspended sediments in streams as N exporters and reactors for denitrification and assimilatory N uptake during storms

Bisesh Joshi[1]*, Eva Bacmeister[2], Erin Peck[2], Marc Peipoch[3], Jinjun Kan[3] and Shreeram Inamdar[2]

[1]Water Science and Policy Graduate Program, University of Delaware, Newark, DE, United States, [2]Department of Plant & Soil Sciences, University of Delaware, Newark, DE, United States, [3]Stroud Water Research Center, Avondale, PA, United States

Nitrogen (N) pollution in riverine ecosystems has substantial environmental, economic, and policy consequences. Various riverine N removal processes include permanent dissimilatory sinks such as denitrification (U_{den}) and temporary assimilatory sink such as microbial N uptake (U_{assim}). Both processes have been extensively evaluated in benthic sediments but only sparsely in the water column, particularly for storm flows producing high suspended sediment (SS) concentrations. Stormflows also increase the sediment bound N (Sed-N) export, and in turn, the overall N exports from watersheds. The balance between N removal by U_{den} and U_{assim} vs. Sed-N export has not been studied and is a key knowledge gap. We assessed the magnitude of U_{den} and U_{assim} against stormflow Sed-N exports for multiple storm events of varying magnitude and across two drainage areas (750 ha and 15,330 ha) in a mixed landuse mid-Atlantic US watershed. We asked: How do the U_{den} and U_{assim} sinks compare with Sed-N exports and how do these N fluxes vary across the drainage areas for sampled storms on the rising and falling limbs of the discharge hydrograph? Mean U_{den} and U_{assim} as % of the Sed-N exports ranged between 0.1–40% and 0.6–22%, respectively. Storm event U_{assim} fluxes were generally slightly lower than the corresponding U_{den} fluxes. Similarly, comparable but slightly higher U_{den} fluxes were observed for the second order vs. the fourth order stream, while U_{assim} fluxes were slightly higher in the fourth-order stream. Both of these N sinks were higher on the falling vs. rising limbs of the hydrograph. This suggests that while the N sinks are not trivial, sediment bound N exports during large stormflows will likely overshadow any gains in N removal by SS associated denitrification. Understanding these N source-sink dynamics for storm events is critical for accurate watershed nutrient modeling and for better pollution mitigation strategies for downstream aquatic ecosystems. These results are especially important within the context of climate change as extreme hydrological events including storms are becoming more and more frequent.

KEYWORDS

denitrification, assimilatory, uptake, stormflow, riverine, nitrogen, sediment, export

Introduction

Excessive amounts of nitrogen (N) from agriculture, wastewater facilities, and chemical industries are discharged into rivers and streams resulting in N pollution in approximately 42% of US rivers and streams (Rashleigh et al., 2013; Xia et al., 2018). Excessive nitrogen in riverine ecosystems can cause many environmental problems, including eutrophication, enhanced nitrous oxide production, and hypoxia (Galloway et al., 2004; Fowler et al., 2013) with economic consequences related to purifying contaminated drinking water, treating health issues, and restoring impaired ecosystems (Xia et al., 2018; Katz, 2020). These effects of N pollution can also reach estuaries and coastal ecosystems and cause the collapse of fish and shellfish industries creating major economic and societal problems (Randall, 2004; USEPA, 2023). These challenges underscore the need for a better understanding of riverine nitrogen processes, particularly nitrogen sinks, and removal processes throughout river networks, that may help manage and mitigate nitrogen pollution in our waterways.

Denitrification is a key microbial process of N removal in riverine ecosystems that converts reactive nitrate N into inert nitrogen gas thus mitigating N pollution (Giles et al., 2012; Xia et al., 2018; Xin et al., 2019). While denitrification is a more permanent sink, N can also be temporarily retained via microbial assimilatory uptake in the water column (Reisinger et al., 2015, 2016; Wang et al., 2022). Mulholland et al. (2008) suggested that stream denitrification is more related to ecosystem respiration where nitrate in water is released as gaseous form of nitrogen in atmosphere. Similarly, total stream N uptake was related to ecosystem primary production as the process is primarily driven by photosynthesis and biotic uptake (Mulholland et al., 2008). Arango et al. (2008) reported assimilatory uptake rates higher than denitrification and nitrification rates in small streams with varying land use. Denitrification typically occurs under reducing conditions (low oxygen availability) and is affected by various factors including temperature, nitrate-N, and dissolved organic carbon (Canfield et al., 2010; Xia et al., 2018). In comparison, assimilatory uptake is affected by water temperature, algal biomass, and light availability (Rode et al., 2016).

Compared to denitrification, fewer studies have quantified the contribution of assimilatory uptake to N removal at the watershed scale. In river ecosystems, denitrification has typically been observed to be highest in reducing sediments within stream/river hyporheic and riparian zones (Lowrance et al., 1997; Merill and Tonjes, 2014; Xia et al., 2018). These interfaces are rich in organic carbon and other electron donors—energy sources required for the microbial denitrification processes (Revsbech et al., 2005; Xia et al., 2013; Kim et al., 2016). Previously, it was believed that rivers were less efficient than small streams in terms of N removal. This was because a much smaller percentage of the N originating in headwater streams reached coastal zones while the vast majority of N inputs to large rivers were delivered to the ocean (Alexander et al., 2007, 2008). However, rivers are equally efficient as small streams at removing N when considering that N entering small streams is not necessarily removed in them but throughout the entire river network (Seitzinger et al., 2002). This in turn suggests a rather constant removal per stream order (Hall et al., 2013), where stream order characterizes the size of the streams (Scheidegger, 1965). All of this work, however, is fundamentally based on the removal of N per area of a streambed during conditons in which water-column N demand is expected to be minimal due to low concentrations of suspended particles.

Recently, however, high-concentration plumes of suspended sediment in rivers have been identified as important reactive surfaces that may also enhance denitrification rates and thus nitrogen removal from the water column (Jia et al., 2016; Xia et al., 2017a,b, 2018; Wang et al., 2022). Denitrification rates were found to increase with an increase in the concentration of suspended sediment (Liu et al., 2013), sediment surface area and total organic content (Jia et al., 2016; Wang et al., 2022). High bacterial diversity, abundance, and metabolic rates occur with an increase in suspended sediment concentrations as microbes tend to attach to sediment's surface (Xia et al., 2013). Microbial processes such as ammonification (Xia et al., 2013) and nitrification (Xia et al., 2009) were also reported to be enhanced by increasing suspended sediment concentrations. Furthermore, Xia et al. (2017b) found that 1,000 mg/l of suspended sediment concentration enhanced riverine N loss via coupled nitrification-denitrification by 25–120% for Yangtze and Yellow Rivers. Wang et al. (2022) reported high denitrification rates in high order streams (third to eighth orders in China) and attributed this to an increase in suspended sediment surface area as well as larger water columns (due to deeper water depths). Wang et al. (2022) also observed that water column denitrification rates were positively correlated with dissolved inorganic N, temperature, suspended sediment concentrations, and total organic carbon. In comparison, Reisinger et al. (2015) noted that water column nutrient uptake rates (i.e., nitrate, ammonium, and soluble reactive phosphorous in first through fifth order streams) may not be significantly affected by stream size. Later, Reisinger et al. (2016) also found that N loss via denitrification can be similar or higher in rivers compared to smaller headwater streams.

Sediment-bound (particulate) N loads can be high, especially during large storms, and can exceed the dissolved loads by orders of magnitude (Meybeck, 1982; Dhillon and Inamdar, 2013, 2014). While nutrient mobilization and export by suspended sediments during stormflows are well recognized (Royer et al., 2006; Edwards and Withers, 2008; Inamdar et al., 2015; Jiang et al., 2020), the influence of high sediment loads on N removal is poorly understood. How the increased exports of N compare with the increased potential for denitrification or assimilatory N uptake in storm sediment plumes remains unknown. How assimilatory N uptake and denitrification fluxes vary across different stream orders and how the size and seasonal timing of storm events affect these fluxes is also unknown. In addition, hydrologic pathways and sediment and nutrient sources, concentrations, and composition can vary on the rising and falling limbs of the storm hydrograph (Buttle, 1994; McGlynn and McDonnell, 2003; Inamdar et al., 2013; Klaus and Mcdonnell, 2013; Johnson et al., 2018) and can alter the rates of denitrification and assimilatory N uptake and need to be investigated. Studies have also shown that microbial communities that affect N processing could also differ across and within storms (rising and falling limbs; Kan, 2018).

Here we examine some of these key questions at the watershed scale by estimating assimilatory N uptake and denitrification fluxes for individual storms at two watershed drainage locations. Specifically, we ask: What is the proportion of assimilatory N uptake (hereafter referred to as U_{assim}) and denitrification (U_{den}) loss to suspended-sediment bound nitrogen load (Sed-N) and how do they vary across drainage areas, storm sizes, and the rising and falling limbs of the storm hydrograph? We hypothesize that while U_{assim} and U_{den} amounts will increase with storm size, the mass exports of Sed-N will be higher and will outpace the U_{assim} and U_{den} amounts. Addressing these questions is important for developing more accurate and reliable mass estimates of N removal at the drainage network or watershed scales and including these processes in watershed models for N transport and fate.

Methodology

Study area and site description

This study was conducted at two drainage locations on the White Clay Creek, Pennsylvania USA (Figure 1). The upstream site was adjacent to the USGS gage station near London Grove (U.S. Geological Survey #01478100; Coordinates: 39.858 N, 75.783 W). Similarly, the downstream location is next to the USGS gage station #01478245 at Strikersville (Coordinates: 39.747 N, 75.770 W). At the upstream site, White Clay Creek is a second order stream with a drainage area of 750 ha of which 22% is cultivated crops, 43% pasture, 17% forested lands, and 7% is open space developed area (StreamStats/US Geological Survey, 2023). At the downstream location, the creek drains a fourth order watershed with a drainage area of 15,330 ha consisting of 15% cultivated crops, 26% pasture, 24% forested lands, and 30% developed area (StreamStats/US Geological Survey, 2023). Both drainage areas are located within the Piedmont region and have soil types of Glenilg channery silt loam, Worsham silt loam, Wehadkee silt loam, Guthrie silt loam, with Kaolinite clay (Sweeney, 1993), and are underlain mostly by weathered crystalline rocks, shales, schist, gneiss marbles (Pennsylvania Geological Survey, 2017). The potential anthropogenic sources of nitrogen in the watersheds include synthetic fertilizers and manures from agricultural fields and urban areas. The average values for daily discharge are 0.156 (min: 0.066, max: 0.245) m^3/s for upstream site and 3.228 (min: 0.651, max: 21.209) m^3/s for downstream site (USGS Water Data for the Nation, 2023a,b). The average suspended sediment concentration obtained from our sampling combined with USGS sampled data are 256.4 (min:1.5, max: 1,220) mg/l for the upstream and 1,499.8 (min: 1.6, max: 14,476.8) mg/l the downstream sites.

Data collection and analysis

We collected data on stream water chemistry and N process rates (U_{assim} and U_{den}) from selected storms at two drainage locations between September 2020 and December 2021. A total of 33 stream water samples were analyzed for water chemistry and N process rates across the two study sites (20 samples for one April and four September-October events at the downstream site, and 13 samples were used for three September-October events at the upstream site). We used a combination of passive sampling and grab sampling methods to collect stream water on the rising and falling limb of storm events. We built passive samplers following Diehl's design for a modified siphon sampler tower (Diehl, 2008) to collect water on the rising limb. Each sampler tower was built to contain three vertically stacked 1-L HDPE sample bottles inside half of a PVC pipe. Flexible vinyl intake and air tubing were installed through the bottle caps to create a siphon allowing water and SS to flow into the sample bottles once the water level reached the intake tube. We installed metal T-posts to hold the passive samplers near the streambank at each site, which remained at the same location for the duration of the study period. Before storm events, we deployed three passive sampler towers equaling nine total sample bottles at each site with intake tubing facing the stream channel at the same height so that three replicate samples would be collected at a given stage height. At the time of passive sampler deployment at each site, stage height and the distance from the water level to each intake tube were also recorded. This made it possible to calculate the stage height when each sample bottle was filled and determine the sample collection time and discharge values using USGS gage data from each site. On the falling limb of the storm, we removed the passive samplers from the T-posts and collected three replicate grab samples from the water column at each site using a 1-L HDPE bottle attached to a swing sampler (e.g., Nasco 3.65 m Swing Sampler). All samples were then transported to lab facilities in a chilled cooler.

To process samples for collecting water chemistry data, we pooled replicate samples at each stage height from the rising limb and falling limb. We collected subsamples for dissolved organic carbon (DOC) and nitrate-N (NO_3-N) and vacuum-filtered the subsamples through 0.45-μm and 0.7-μm borosilicate fiber filters, respectively. Subsamples for DOC were then analyzed using an Aurora 1,030 W TOC Analyzer (Oceanographic Int., College Station, Texas, United States) and chemical oxidation (Menzel and Vaccaro, 1964). Analysis of NO_3^--N was performed via discrete colorimetric analysis using an AQ300 discrete analyzer (SEAL Analytical, Wisconsin, United States) following standard procedures (APHA, 2017). We collected an additional subsample of each pooled sample and vacuum-filtered this through a pre-weighed 0.7-μm borosilicate fiber filter, repeating this step to generate two filters per pooled sample. One set of filter samples we oven-dried at 60°C for 72 hours, weighed on a Sartorius (Goettingen, Germany) MC1 analytical balance, combusted at 500°C for 5 to 6 h (Steinman et al., 2006), and reweighed for calculation of dry mass and ash-free dry mass (e.g., OM). We repeated only the first two drying and weighing steps for the second set of filters and then collected a one-cm subsample from each filter which we weighed and packaged in an aluminum tin capsule. For these subsamples, organic C and N content on SS (as a percentage of dry mass) was determined via combustion using an Elemental Analyzer (University of Maryland, Center for Environmental Science).

We measured ambient denitrification and assimilatory uptake rates for stream water using microcosm experiments. We took three 250-ml aliquots from each pooled sample, generating three replicates per stage height. We poured each aliquot into a microcosm chamber (Kimble 250 ml wide-mouth media bottle)

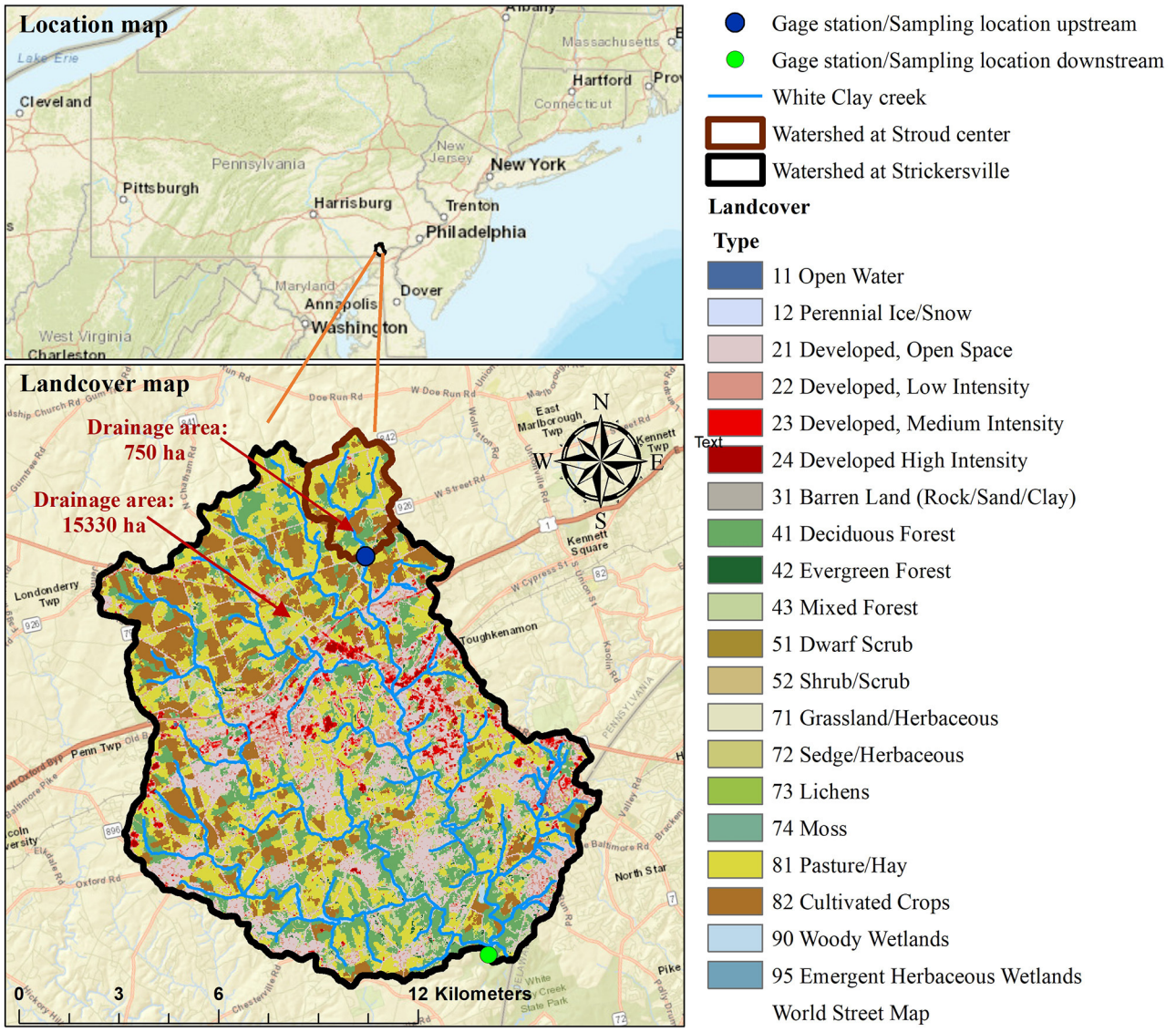

FIGURE 1
Location of the White Clay Creek watershed in the mid-Atlantic USA, and the drainage area and landcover map for the two sampled sites within the White Clay Creek watershed. The drainage area for the upstream site is 750 ha (second order stream) while the drainage area for the downstream site is 15,330 ha (fourth order stream).

and then enriched all chambers with 1 ml of a 796 mg/l solution of $Na^{15}NO_3$. We placed a magnetic stir bar in each chamber, and closed chambers with a screw cap in which septa had been installed. We placed all chambers on a magnetic stir plate and then evacuated (3 min) and flushed with He gas (one min) by inserting tubing with syringe needles attached into the septa of each microcosm chamber (Dodds et al., 2017). The evacuating and flushing cycle was repeated three times before incubation began. We then moved all microcosms to magnetic stir plates inside an incubator set to 25°C. We set stir plates to 360 rpm to ensure particles remained in suspension during the incubation period (Jia et al., 2016). Then, we incubated the microcosms for a period of 24 h in the dark. We collected gas samples at 4 and 24 h after the start of incubation using a gas-tight syringe (Hamilton 25 ml Model 1025TLL) to sample 12 ml of gas from each chamber into 12 ml pre-evacuated Exetainers (Labco Ltd., High Wycombe, United Kingdom). Each gas sample was analyzed for $\delta^{15}N$ of N_2 and N_2O via continuous flow isotope ratio mass spectrometry (IRMS, ThermoScientific Delta V Plus) at the University of California-Davis Stable Isotope Facility. Denitrification rates on SS were measured from a production rate of $^{29}N_2$ and $^{30}N_2$ following Nielsen (1992). Similarly, assimilatory uptake rates were determined by measuring the increase in the ^{15}N to ^{14}N ratio of suspended organic matter at the end of incubation and the tracer 15N: 14N ratio in the microcosm NO_3- following Mulholland et al. (2000). Further details of these denitrification and assimilatory uptake calculations are described in Bacmeister et al. (2022).

We obtained additional information on manual and high frequency (15-min) discharge (Q), Turbidity (Td), and SS concentrations from the USGS stations at the selected drainage

locations for the study time period of September 2020 to December 2021 (USGS Water Data for the Nation, 2023a,b). We used this information to develop regression models and compute event mass fluxes for water, SS, and N described below. Additionally, we obtained seven-day average antecedent temperatures of water prior to sampled events at both upstream and downstream sites from the USGS (USGS Water Data for the Nation, 2023a,b) at respective USGS gage stations, and the closest precipitation and 7-day antecedent rainfall data was obtained from "Ag farm weather station" at Newark (National Weather Service, 2023a).

Regression models for estimation of storm-event suspended sediment

We combined our manually sampled SS data with USGS discharge, turbidity, and SS concentrations to increase sample size and develop stronger regression models. The combined data set included 106 data points for the downstream site (67 on falling limb, 39 on rising limb) and 31 data for the upstream site (25 on falling limb, six on rising limb). We separated rising and falling limbs by the discharge peak, and the end of a storm was identified as the time point when recession discharge was within 10% of the starting storm event discharge (Inamdar et al., 2015). The start of the storm was identified as the point where streamflow discharge exceeded by 10% following the start of rainfall (Inamdar et al., 2015). Separate regression models were developed using a Python programming language for each site and for rising and falling limbs. Rising limb and falling limb datasets were standardized using the natural logarithmic function for developing and testing different statistical models to predict SS concentrations with better r-squared values (R^2). We applied simple regression models that are preferable for a relatively small dataset (Trevor et al., 2008; Montgomery et al., 2012). Equations (1)–(4) represent the regression models developed for rising and falling limbs of upstream and downstream sites respectively.

$$Log\,(SS_{rv}) = 0.537709^{*}\,Log\,(Q) + 0.747813^{*}\,Log\,(Td) - 0.422535;\ R^2 = 0.79 \quad (1)$$

$$Log\,(SS_{fv}) = 0.660033^{*}\,Log\,(Q) + 0.693710^{*}\,Log\,(Td) - 0.747623;\ R^2 = 0.74 \quad (2)$$

$$Log\,(SS_{rd}) = 0.859130^{*}\,Log\,(Q) + 0.103909^{*}\,Log\,(Td) + 0.706358;\ R^2 = 0.86 \quad (3)$$

$$Log\,(SS_{fd}) = 0.994430^{*}\,Log\,(Td) + 0.446886;\ R^2 = 0.65 \quad (4)$$

Where *SS* is suspended sediment concentration (mg/l), *Q* is discharge (cfs), and *Td* is turbidity (FNU). Subscripts *rv, fv, rd, and fd* represent rising limbs and falling limbs for the downstream and upstream sites, respectively.

Events selection and their hydrologic parameter assessment

Three summer/fall storms (Sep-Oct) were available for the upstream site and five storms were sampled at the downstream site across a broader season (Apr-Oct, Table 1). Hydro-meteorological parameters were determined to characterize the events (Table 1). Seven-day average antecedent temperature was determined by determining the average of the daily mean water temperature at the USGS gage stations, and 7-day cumulative antecedent precipitation and event day precipitation were obtained by summing the precipitation data for these time periods. Similarly, we computed the percentage exceedance of peak discharge of storm events based on 2 years of the daily maximum flows (Acharya and Joshi, 2020) at the study sites from 2021 through 2022. Storm discharge for each site was normalized to the drainage area to allow for comparative analysis between the two study sites.

Flux computation and analysis of U_{assim} and U_{den}

Fluxes for SS were computed by multiplying the flow-weighted average modeled concentration for SS on the rising and falling limbs with the discharge amounts for these periods. The total event SS flux was the sum of the SS fluxes for the rising and falling limbs. We scaled up the U_{assim} and U_{den} rates measured in the microcosm experiments to the watershed-level (g/ha) by multiplying microcosm-level rates (g N/kg of sediment/hr) by the duration (hr) and SS flux (kg/ha) of each period (rising and falling limbs) and storm event. Similarly, fluxes for sediment-bound N and C (Sed-N, and Sed-C) were computed in g/ha by multiplying the weighted average %N and %C with the corresponding sediment loads. Other fluxes such as NO_3-N and DOC were calculated based on their weighted average concentration (obtained from grab and passive sampling) and volume of stormflow on rising and falling limbs. The N uptake computed from both study sites were then compared and analyzed against each other, and other similar studies.

Results

Selected storms and their hydrologic variables across the two drainage sites

Three storm events, E3 (Sep 1), E4 (Sep 23), and E5 (Oct 29) (Table 1), were sampled at both upstream and downstream sites including E3 which is associated with tropical storm Ida (National Weather Service, 2023b). Among the three storms analyzed for the upstream site, storm E4 contributed the smallest runoff (4.1 mm) with a peak discharge of 2.6 m^3/s while tropical storm Ida produced a storm runoff of 29.6 mm with a peak discharge of 11 m^3/s. The exceedance levels for peak discharges for these events ranged between 1.48–0.28%. For the downstream site, storm runoff, and peak discharge were lowest for E2 (2.5 mm and 22.7 m^3/s) and highest for Ida (E3: 40 mm and 203 m^3/s). For both sites, antecedent 7-days average stream water temperatures for the Sep-Oct events

10.3389/frwa.2023.1254225

TABLE 1 Hydrologic, sediment, nutrient parameters, and N process rates for sampled storm events at the downstream and upstream study sites on White Clay Creek.

Site	Downstream (15,330 ha)					Upstream (750 ha)		
Events	E1	E2	E3	E4	E5	E3	E4	E5
Date	Apr 10, 2021	Aug 19, 2021	Sep 1, 2021	Sep 23, 2021	Oct 29, 2021	Sep 1, 2021	Sep 23, 2021	Oct 29, 2021
7-day average antecedent temperature (°C)	13.8	25.4	24.5	21.6	14.9	21.1	19.3	14.5
7-day cumulative antecedent precipitation (mm)	0.0	82.8	23.4	0.8	40.1	23.4	0.8	40.1
Event precipitation (mm)	12.2	2.8	113.5	48.5	49.0	113.5	48.5	49.0
Peak discharge (m^3/s)	46.2	22.7	203.0	39.6	40.8	11.0	2.6	2.0
% of exceedance based on daily maximum flows from 2020 through 2022	1.1	2.3	0.2	1.5	1.3	0.3	1.5	0.9
Storm duration (hr)	21.5	15.5	65.8	36.8	53.5	67.0	38.8	72.0
Storm runoff (mm)	3.5	2.5	40.0	6.1	9.5	29.6	4.1	4.4
Flow-weighted SS concentration (mg/l)	294.4	300.2	525.5	212.4	165.4	124.8	71.5	44.0
SS export (kg/ha)	48.7	17.9	944.1	48.4	58.5	215.4	20.4	15.3
Flow-weighted DOC concentration (mg/l)	3.7	8.7	7.2	8.0	9.5	7.1	4.6	6.7
DOC export (g/ha)	127.4	216.6	2,868.4	488.6	897.3	2,090.1	189.2	292.2
Flow weighted NO_3N concentration (mg/l)	3.7	2.0	1.2	3.0	2.5	1.2	3.2	2.8
NO_3N export (g/ha)	129.8	49.6	471.8	184.2	241.1	367.4	130.7	124.2
Flow-weighted Sed-C concentration (mg/l)	12.1	15.1	33.5	13.3	11.1	10.9	5.0	2.6
Sed-C export (g/ha)	1,864	883	44,948	2,748	2,416	11,732	1,341	874
Flow-weighted Sed-N concentration (mg/l)	1.7	2.1	3.3	1.7	1.2	1.0	0.6	0.4
Sed-N export (g/ha)	254	124	5,000	366	299	1,132	179	119
U_{assim} (g/ha)	1.6 ± 1.9	0.7 ± 0.6	142.4 ± 70.9	17.5 ± 1.4	26.2 ± 2.9	46.6 ± 13.9	12.3 ± 2.7	26.6 ± 14.7
U_{den} (g/ha)	0.4 ± 0.2	5.1 ± 2.5	111.5 ± 108.8	128.3 ± 68.7	0.1 ± 0.1	459.6 ± 223.6	66.7 ± 22.1	34.5 ± 33.9
% of mean U_{assim}/Sed-N	0.6	0.6	2.9	4.8	8.8	4.1	6.9	22.4
% of mean U_{den}/Sed-N	0.1	4.1	2.2	35.0	0.0	40.6	37.3	29.0

ranged from 14.5 to 25.4 C and antecedent 7-days accumulated precipitation ranged from 0.80 to 40.1 mm. The spring/April event (E1) had the lowest water temperature (13.8°C) and no antecedent precipitation. Storm flows lasted from 38.8 h (E4) to 72.0 h (E5) at the upstream site, and from 15.5 h (E2) to 65.8 h (E3) for the downstream site. Not surprisingly, tropical storm Ida yielded the largest sediment export (944.1 kg/ha for the downstream site and 215.4 kg/ha for the upstream site) compared to other events (Table 1). This difference is also indicated by the average SS concentrations during storm events—for Ida, they were 525 mg/l and 124.8 mg/l for downstream and upstream sites, respectively, while for other events they ranged from 165.4 to 300.2 mg/l (downstream) and from 44.0 to 71.5 mg/l (upstream).

Biogeochemical fluxes across both sites

Carbon exports (DOC and Sed-C) were greater than corresponding nitrogen exports (NO_3-N and Sed-N) for all Sep-Oct storms, however, NO_3-N was slightly higher than DOC for E1. Nutrient fluxes increased with storm size and stream order with tropical storm Ida (E3) yielding the highest fluxes (Table 1). Flow-weighted stream water DOC concentrations were highest for the August-Oct storms, but NO_3-N concentrations were highest for the April (spring) event at the downstream site.

Comparison of U_{den}, U_{assim}, and Sed-N with storm events

Fluxes of U_{assim}, and Sed-N increased with size of storm events for both the upstream and downstream sites (Figure 2, Table 1). The increase in these fluxes, were however, not directly proportional to the magnitude of the events. Flux values for U_{den} were more variable than U_{assim} with respect to storm event magnitude, especially for the downstream site (Figure 2). Importantly, storm event Sed-N exports were 1–2 orders of magnitude greater than the corresponding U_{den} and U_{assim} fluxes (Table 1). As a % of the Sed-N exports, U_{assim} fluxes were consistently less than U_{den} for the upstream site and ranged from 4.1–22.4%. A mixed response was observed for the downstream sites with U_{assim} fluxes ranging between 0.6–8.8%. U_{den} varied between 0.1–40.6% for the study sites (Table 1). The April event (E1) measured at the downstream site yielded the lowest process fluxes.

Comparison of U_{den}, U_{assim}, and Sed-N with drainage area

Storm event Sed-N exports at the downstream site were 2–4 times the values measured at the upstream location (Figure 3). In comparison, the responses for N process fluxes (U_{den} and U_{assim}) were mixed (Table 1, Figure 3). Assimilatory N (U_{assim}) fluxes were greater at the downstream vs. the upstream site for events E3 (three times greater) and E4 (1.4 times greater), but similar for E5. In contrast, U_{den} flux was greater at the upstream site for two (E3 and E5) of the three common events. Tropical storm Ida in particular, produced a denitrification flux that was four times greater at the upstream vs. the downstream site (Table 1, Figure 3). U_{den} flux for the downstream site for E5 was unexpectedly very low (close to zero; Table 1), with low U_{den} rates in the rising limb and non-detectable denitrification during the falling limb of the storm.

Differences in U_{den}, U_{assim}, and Sed-N between the rising and falling limbs of the storm hydrographs

N process fluxes were consistently higher on the hydrograph falling limbs vs. the rising limbs regardless of storm size and drainage location (Figure 4). While Sed-N exports were also higher on falling limbs except for the tropical storm Ida at the upstream site, the differences between rising and falling for U_{den} and U_{assim} are much greater than for Sed-N. At the downstream site, U_{den}, and U_{assim} fluxes before peak flow were on average 71.4–99.8% and 98.6–99.8% smaller than those observed during the falling limb, respectively (Figure 4, Upstream). Similarly, rising limb values for U_{den} and U_{assim} fluxes at the upstream site were on average 95.3–99.8% and 96.9–99.9% smaller than mean fluxes in the falling limb (Figure 4, Downstream).

Discussion

This study provided the first important comparisons of storm-event fluxes of Sed-N and U_{assim} and U_{den}, with Sed-N fluxes substantially exceeding the U_{assim} and U_{den} values. Assimilatory N uptake and denitrification fluxes were also found to vary differentially with drainage area, storm magnitude, and rising and falling hydrograph limbs. We elaborate on these results further in the discussion below. We also discuss the implications of these results for watershed N modeling, budgets, and watershed management.

Variation of water column N uptake with drainage areas

We found that while the storm-event Sed-N exports were consistently greater at the downstream site, the same was not true for U_{den} and U_{assim} fluxes. U_{assim} fluxes were higher for downstream site for two events and similar for the third one. However, U_{den} (for two of the three events) were greater for the upstream drainage location. Previous studies have typically reported the rates, rather than watershed-scale fluxes [in M L^2] for denitrification (Christensen and Sørensen, 1988; Royer et al., 2004; Arango et al., 2008; Reisinger et al., 2015; Xia et al., 2017b; Wang et al., 2022). To allow for comparative analysis and evaluation with previous studies, we computed areal rates of U_{den} for our sites (Table 2). This was done by multiplying our volumetric rates with the average high flow depth estimated empirically from measured depths from USGS gage stations at those sites (we estimated high flow depth for the upstream site to be ~1.3 m and ~1.15 m for the downstream site). Our U_{assim} rates (0 to 5.82 mg m^{-3} hr^{-1} for the

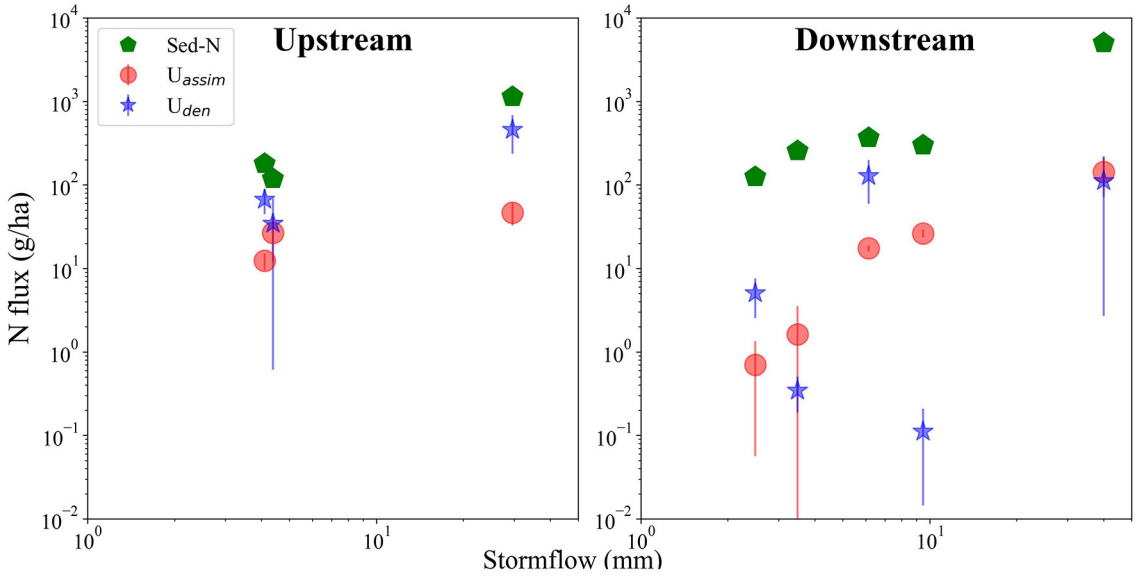

FIGURE 2
Comparison of Sed-N, U_{den}, and U_{assim} fluxes for the upstream and downstream sites with stormflow amounts (mm). Vertical bars indicate standard errors associated with the fluxes.

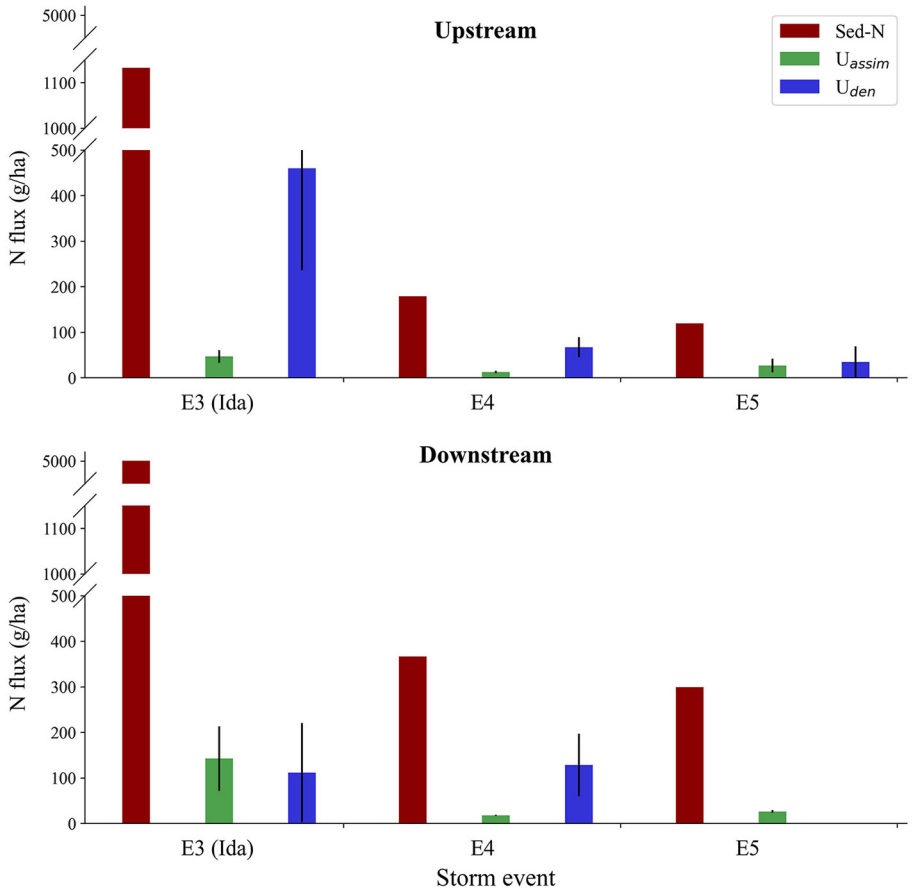

FIGURE 3
Comparison of Sed-N, $U_{assim,}$ and U_{den} fluxes with drainage location (upstream vs. downstream) for the three common events (E3-E5). Vertical bars indicate standard errors attached to corresponding fluxes.

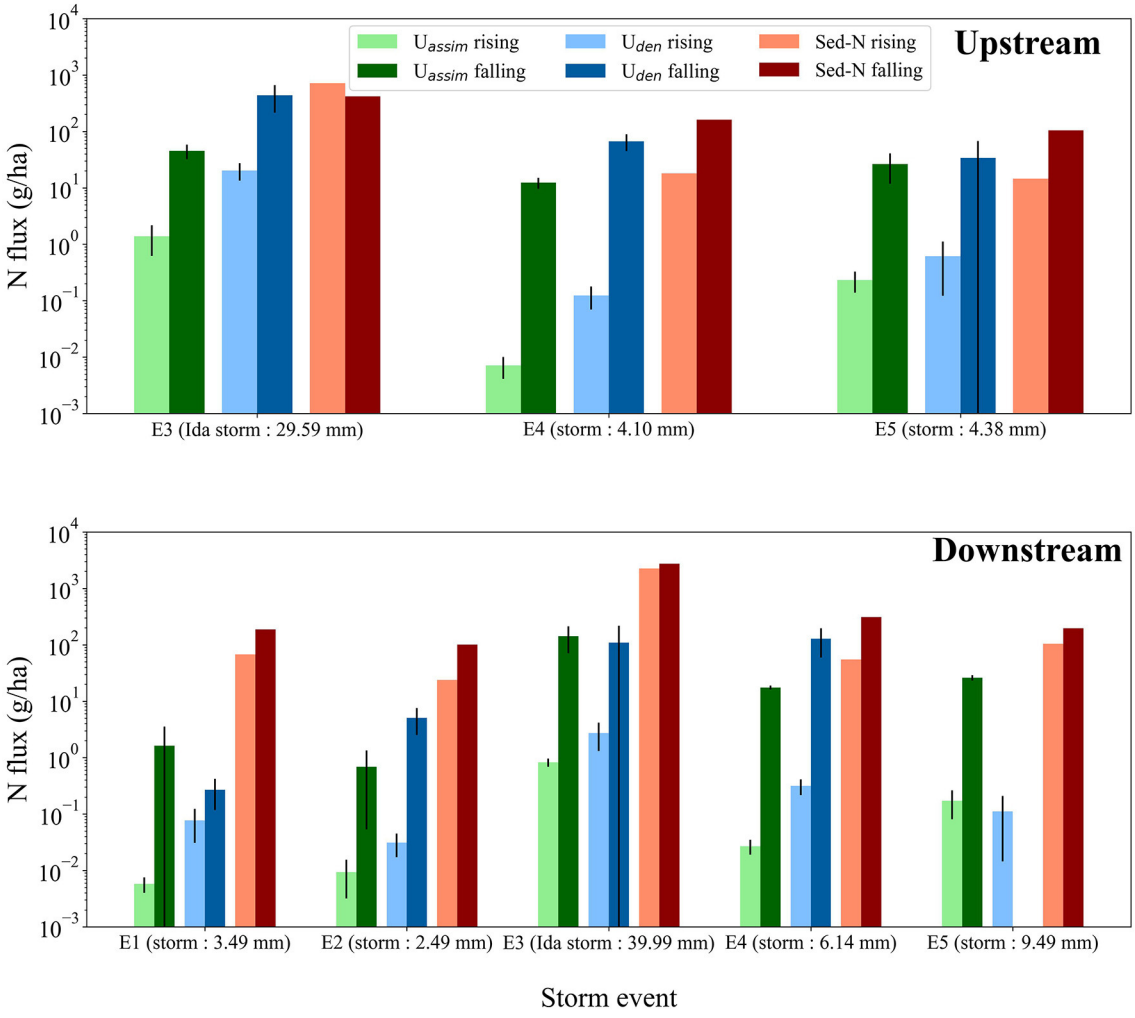

FIGURE 4
U_{den}, U_{assim}, and Sed-N fluxes for the rising and falling limbs of the storm hydrographs at the upstream site and at the downstream site. The black bars indicate errors in fluxes of U_{den} and U_{assim}.

downstream site, and 0 to 2.32 mg m^{-3} hr^{-1} for the upstream site) were within the range of rates (0.001–363 mg m^{-3} hr^{-1}) reported by Reisinger et al. (2015) across first to fifth order watersheds with contrasting landscapes in mid-West US.

Our water column U_{den} rates for both sites (0.00 to 6.08 mg m^{-3} hr^{-1} for the downstream site and 0.00 to 9.82 mg m^{-3} hr^{-1} for the upstream site) were within the broad range (−3.20 to 22.80 mg m^{-3} hr^{-1}) of those reported by Wang et al. (2022) for third to eighth order rivers in China. Wang et al. (2022) found that denitrification fluxes increased with stream order or drainage area and attributed it to increase in suspended sediment, total organic carbon, and water column depth. Reduced dissolved oxygen and increased microbial communities associated with the suspended sediments have also been identified as key factors in enhancing water column denitrification removal (Jia et al., 2016; Xia et al., 2018; Wang et al., 2022). In another study in China on the Yellow River, Xia et al. (2021) found that N_2 and N_2O fluxes from the river were highest in the middle reaches but lower in the upper and lower reaches (specific stream orders corresponding to "upper" and "lower" reaches were not provided). Xia et al. (2021) attributed the elevated N_2 and N_2O fluxes in the middle reach to the increased suspended sediment concentrations in this reach. Reisinger et al. (2016) also reported variable denitrification rates (range: 0.00 to 4.90 mg m^{-3} hr^{-1}) among five mid-Western rivers in the US.

Our denitrification rates were closer to the rates obtained by Reisinger et al. (2016) and did not increase with an increase in stream order (the upstream site had higher U_{den} rates compared to the downstream site). This was surprising given that suspended sediment and DOC concentrations were greater at the downstream vs. the upstream site while dissolved NO_3-N concentrations were comparable (Table 1). We speculate that greater fraction of agricultural land use providing more labile organic carbon and nitrogen in the upper watershed coupled with finer sediments could have played a potential role in the elevated denitrification rates/fluxes measured for the upstream site. Grain size distribution, was however, not available in our study. We also recognize here that these drainage scale comparisons were based on limited data from only three storm events (all in Sep-Oct time frame; Figure 3)

TABLE 2 Comparison of denitrification rates from this study against those reported previously in the literature.

References	U_{den} processes	Stream conditions	U_{den} mg m^{-2} hr^{-1}
Our study	Water column U_{den}	Storm events at WC Creek, downstream site	0.00 to 6.99
		Storm events at WC Creek, upstream site	0.00 to 12.77
Wang et al. (2022)	Water column U_{den}	Six river networks in China	−6.00 to 28.29
Xia et al. (2017b)	SS-water U_{den}	Rivers in China (with 1,000 mg/l\L SS conc.)	0.42
Reisinger et al. (2016)	Water column U_{den}	Five midwestern rivers, US	0.00 to 4.90
Royer et al. (2004)	Stream U_{den}	Headwater Streams, Illinois	0.08 to 8.33
Christensen and Sørensen (1988)	Stream U_{den}	Stream, Denmark	0.41 to 5.20
Arango et al. (2008)	Stream U_{den}	Kalamazoo River, Michigan (baseflow conditions)	2.4

and additional events across multiple years and multiple drainage locations are needed to make a robust assessment for the influence of drainage size on denitrification fluxes. Contrary to U_{den}, U_{assim} fluxes were however higher at the downstream site (Figure 3) and might be due to factors such as increased light, temperature, and algal biomass in the wider, downstream reaches (Rode et al., 2016). Indeed, mean stream water temperature was consistently higher at the downstream vs. the upstream site (Table 1).

Variation of sediment N and water column N uptake with storm events

Sed-N and assimilatory uptake fluxes displayed a pronounced increase with storm event magnitude (Figure 2), although the increase in Sed-N was greater than U_{assim}. The sharp increases in sediment bound N were not surprising given that the mobilization of suspended sediments and associated particulate N in storms is well recognized (Royer et al., 2006; Edwards and Withers, 2008; Inamdar et al., 2015; Jiang et al., 2020). The elevated values of U_{assim} and U_{den} during storms suggest that these fluxes are not trivial and need to be accounted for in reach and watershed scale N budgets and assessments. What was surprising though was that while U_{den} increased with storm magnitude at the upstream site, the same pattern was not repeated for the downstream site (Figure 2). Previous studies have typically observed U_{den} to increase with runoff amounts/depths and suspended sediment concentrations that provide valuable sediment surface area for microbial habitat and reactions that may facilitate denitrification and assimilatory processes (Xia et al., 2017b; Wang et al., 2022). Increased suspended sediment concentrations have also been found to enhance anoxic microsites that may support increasing denitrification loss (Beaulieu et al., 2009; Yu et al., 2013; Xia et al., 2021). Thus, the variable storm response at the downstream site suggests that additional unknown factors could influence the U_{den} process in the water column.

Temperature is also an important control that could influence the microbial growth processes responsible for water column assimilatory and denitrification fluxes (Xia et al., 2021; Wang et al., 2022). Elevated temperatures could also decrease the amount of dissolved oxygen in the water column making the environment more suitable for low oxygen nitrate reduction processes. Xia et al. (2021) reported higher N_2 and N_2O fluxes for summer vs. spring for the river network. While we did not specifically focus on seasonality and temperature differences across storms, our observations for the downstream site (Table 1) indicated that the U_{den} fluxes for the April/spring (E1) event were lower than those measured for most of the summer storms (except E5). Our sample size is however very small and additional storms across seasons need to be measured for a more thorough assessment.

This study provided important new insights on within-event patterns of (rising vs. falling hydrograph limb) U_{den} and U_{assim} fluxes which have not been reported before. Both N fluxes were greater on the falling limb of the discharge hydrograph as opposed to the rising limb (Figure 4). Duration and runoff volumes were both greater during the falling limbs of the storm hydrographs (Table 1) and likely contributed to the larger fluxes for this period. Previous studies have shown that hydrologic flow paths, sediment sources and characteristics, and nutrient concentrations could differ on the rising vs. falling limbs of the hydrograph (Buttle, 1994; McGlynn and McDonnell, 2003; Inamdar et al., 2013; Klaus and Mcdonnell, 2013; Johnson et al., 2018). Rainfall input and high erosive energy of runoff on the rising limb typically sustain greater grain size for suspended sediments vs. the falling limb (Walling et al., 2000). The flow turbulence on the rising limb could also facilitate well-mixed and more oxygenated conditions in the water column vs. the less turbulent flow on the recession limb of the hydrograph (Tabarestani and Zarrati, 2015). DOC, which is important energy source for heterotrophic denitrification, has also been typically reported to peak following the discharge peak (Inamdar et al., 2011; Dhillon and Inamdar, 2014). In a previous study in our upstream watershed in White Clay Creek (Kan, 2018), microbial communities involved in N processes were observed to vary across the storm hydrograph. Kan (2018) reported different microbial compositions as well as greater abundances of nitrification and denitrification genes on the recession limb vs. the rising limb of the discharge hydrograph. Terrestrial microbes flushing into a stream during storm flow might need time to adapt and thrive, showing up on the falling limb. We hypothesize that all or some of these factors likely contributed to the higher amounts of N fluxes that we observed on the falling limb of the discharge hydrograph. Future studies are needed to explicitly determine the influences of these factors on the N fluxes.

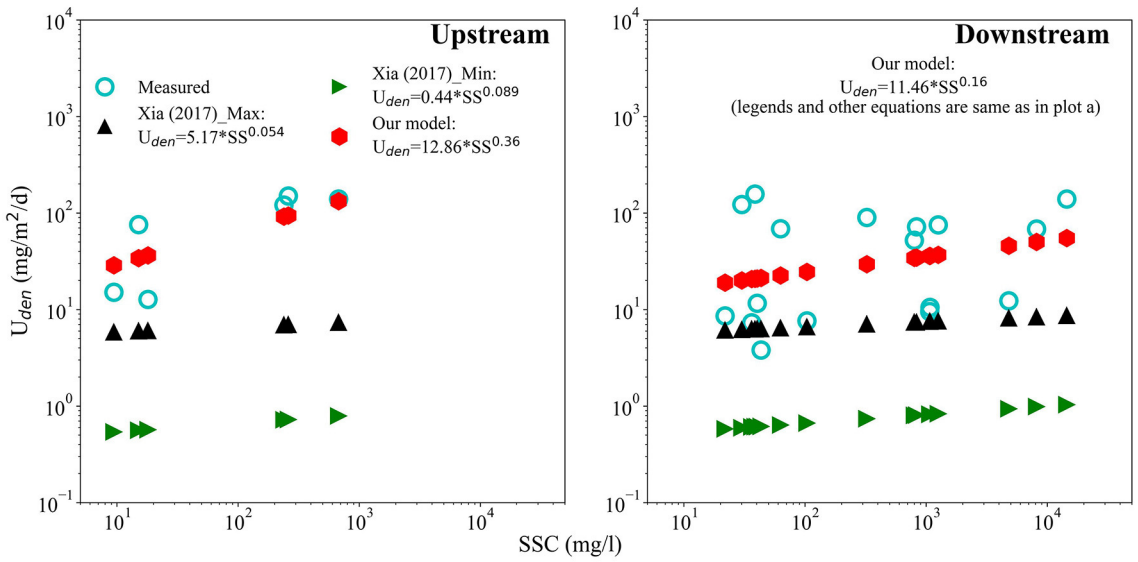

FIGURE 5
Comparison of measured U_{den} rates for White Clay Creek (Piedmont region watershed; empty circles) at the upstream site and the downstream site against values estimated from equations developed by other studies. Equations developed in other studies and fitted equations to our data are reported. The Xia (2017)_Max and Xia (2017)_Min indicate maximum and minimum estimates from Xia et al. (2017b).

Implications for N flux modeling and assessment and watershed management

Our results show that while the sediment bound N exports were much greater than U_{assim} and U_{den} during the large storms, the amounts of U_{assim} and U_{den} were not trivial and watershed N budgets and models would benefit from incorporating water column removal processes. Currently, most watershed-scale models for nutrient budgeting and management, including the more popular ones like the Soil Water Assessment Tool (SWAT; Arnold et al., 2012), and Storm Water Management Model (SWMM; Rossman and Huber, 2015) do not include water column denitrification processes (assimilatory uptake is simulated to various extent; Arnold et al., 2012; Rossman and Huber, 2015). This is an important knowledge gap. Models like SWAT and SWMM incorporate erosion and sediment transport algorithms that can describe sediment and sediment bound nutrient exports from the land surface into the stream (Arnold et al., 2012). The SWAT model already characterizes (via the In-channel module)—stream/river water depth and travel time for simulated reaches, dissolved oxygen, and suspended sediment concentration, transport, and particle size distribution. The model also has limited algorithms to characterize bacterial biomass (but not type) associated with channel sediments. These algorithms and sediment parameters can be leveraged and simplified equations linking water column denitrification to parameters such as water temperature, dissolved inorganic N, organic C, and suspended concentrations can be included. Such equations based on empirical data have already been developed by Xia et al. (2017b), Pang et al. (2022), and Wang et al. (2022) for various rivers in China. However, regression parameters for these equations likely vary with physiographic regions and climate and so region/climate specific values may be needed. For example, a comparison of our measured values (and fitted regression equations) against predicted estimates based on equations developed by Xia et al. (2017b) indicate that our measured fluxes were under predicted (Figure 5). Thus, accurate estimates of water column denitrification may be needed if we want to develop a robust estimate of these processes at the reach and watershed scales.

We also recognize that N process rates may vary with reach and watershed scales and algorithms and equations developed at the small mesocosm/microcosm scales may not necessarily apply as is at the larger scales. Addressing scaling issues for processes and their parameters has been an ongoing challenge across multiple disciplines (e.g., Blöschl and Sivapalan, 1995). This challenge stems from the inability to measure process rates and parameters at large scales. This applies here too given the practical challenges with measuring U_{den} and U_{assim} at the scale of the full stream reach. Currently, the best strategy in such situations is to collect as many N process measurements as possible and for a wide range of conditions (including discharges, suspended sediment concentrations, water temperatures, and dissolved oxygen) and assume that the relationships provide some representation of processes at the larger scales.

Additionally, climate change could further increase the frequency and intensity of the largest storms (Wuebbles et al., 2017). Increased intensity of storms is expected to increase sediments and sediment-bound nutrients from watersheds (Dhillon and Inamdar, 2013). This could increase the potential for water column denitrification losses as well as assimilatory uptake, particularly in combination with increasing air and water temperatures, thereby adding additional urgency to improving N fluxes in watershed budgets and models.

Conclusion

This study revealed that sediment bound N exports during storms exceeded the water column assimilatory and denitrification fluxes by a significant amount. This suggests that while the N sinks are not trivial, N removal by suspended sediment associated denitrification will likely be outpaced by sediment bound N exports during large stormflows. Our observations also revealed that the magnitude of the N fluxes varied with storm events and catchment drainage area. While it is challenging to sample storm events, future research should be targeted toward sampling multiple storm events of varying magnitudes, across seasons, and on the rising and falling limbs of the hydrograph. Ideally, *in-situ* measurements of water column N fluxes (e.g., Wang et al., 2022) with simultaneous measurements of suspended sediment size, concentrations, and nutrient (N, DOC) availability should be performed. Such measurements will further our ability to model water column N fluxes and better constrain the N cycle budgets for watersheds.

Data availability statement

The datasets presented in this study can be found in online repositories. The names of the repository/repositories and accession number(s) can be found below: https://github.com/BiseshJoshi/Storm-N-uptakes-data.

Author contributions

BJ: Data curation, Writing—original draft, Formal analysis, Investigation, Methodology, Visualization. EB: Methodology, Writing—review & editing, Data curation. EP: Writing—review & editing, Data curation. MP: Conceptualization, Funding acquisition, Supervision, Writing—review & editing, Resources. JK: Funding acquisition, Writing—review & editing. SI: Conceptualization, Funding acquisition, Supervision, Writing—review & editing, Resources.

Funding

The author(s) declare financial support was received for the research, authorship, and/or publication of this article. This research was financially supported by the US Department of Agriculture grant NIFA-12912936 to MP, SI, and JK.

Conflict of interest

The authors declare that the research was conducted in the absence of any commercial or financial relationships that could be construed as a potential conflict of interest.

Publisher's note

All claims expressed in this article are solely those of the authors and do not necessarily represent those of their affiliated organizations, or those of the publisher, the editors and the reviewers. Any product that may be evaluated in this article, or claim that may be made by its manufacturer, is not guaranteed or endorsed by the publisher.

Supplementary material

The Supplementary Material for this article can be found online at: https://www.frontiersin.org/articles/10.3389/frwa.2023.1254225/full#supplementary-material

SUPPLEMENTARY FIGURE 1
Upstream flood hydrograph for storm event E3 and sampling locations on rising and falling limbs.

SUPPLEMENTARY FIGURE 2
Upstream flood hydrograph for storm event E4 and sampling locations on rising and falling limbs.

SUPPLEMENTARY FIGURE 3
Upstream flood hydrograph for storm event E5 and sampling locations on rising and falling limbs.

SUPPLEMENTARY FIGURE 4
Downstream flood hydrograph for storm event E1 and sampling locations on rising and falling limbs.

SUPPLEMENTARY FIGURE 5
Downstream flood hydrograph for storm event E2 and sampling locations on rising and falling limbs.

SUPPLEMENTARY FIGURE 6
Downstream flood hydrograph for storm event E3 and sampling locations on rising and falling limbs.

SUPPLEMENTARY FIGURE 7
Downstream flood hydrograph for storm event E4 and sampling locations on rising and falling limbs.

SUPPLEMENTARY FIGURE 8
Downstream flood hydrograph for storm event E5 and sampling locations on rising and falling limbs.

References

Acharya, B., and Joshi, B. (2020). Flood frequency analysis for an ungauged Himalayan river basin using different methods: a case study of Modi Khola, Parbat, Nepal. *Meteorol. Hydrol. Water Manag.* 8, 46–51. doi: 10.26491/mhwm/131092

Alexander, R. B., Boyer, E. W., Smith, R. A., Schwarz, G. E., and Moore, R. B. (2007). The role of headwater streams in downstream water quality. *J. Am. Water Resour. Assoc.* 43, 41–59. doi: 10.1111/j.1752-1688.2007.00005.x

Alexander, R. B., Smith, R. A., Schwarz, G. E., Boyer, E. W., Nolan, J. V., and Brakebill, J. W. (2008). Differences in phosphorus and nitrogen delivery to the Gulf of Mexico from the Mississippi River Basin. *Environ. Sci. Technol.* 42, 822–830. doi: 10.1021/es0716103

APHA (2017). *Standard Methods for the Examination of Water and Wastewater*. 23rd Edition. Washington DC: American Public Health Association.

Arango, C.P., Tank, J. L., Johnson, L. T., and Hamilton, S. K. (2008). Assimilatory uptake rather than nitrification and denitrification determines nitrogen removal patterns in streams of varying land use. *Limnol. Oceanogr.* 53, 2558–2572. doi: 10.4319/lo.2008.53.6.2558

Arnold, J. G., Moriasi, D. N., Gassman, P. W., Abbaspour, K. C., White, M. J., Srinivasan, R., et al. (2012). SWAT: model use, calibration, and validation. *Trans. ASABE* 55, 1491–1508. doi: 10.13031/2013.42256

Bacmeister, E., Peck, E., Bernasconi, S., Inamdar, S., Kan, J., and Peipoch, M. (2022). Stream nitrogen uptake associated with suspended sediments: a microcosm study. *Front. Environ. Sci.* 10, 1043638. doi: 10.3389/fenvs.2022.1043638

Beaulieu, J. J., Arango, C. P., and Tank, J. L. (2009). The Effects of Season and Agriculture on Nitrous Oxide Production in Headwater Streams. *J. Environ. Quality* 38, 637–646. doi: 10.2134/jeq2008.0003

Blöschl, G., and Sivapalan, M. (1995). Scale issues in hydrological modelling: a review. *Hydrol. Proc.* 9, 251–290. doi: 10.1002/hyp.3360090305

Buttle, J. M. (1994). Isotope hydrograph separations and rapid delivery of pre-event water from drainage basins. *Progr. Phys. Geogr.* 18, 16–41. doi: 10.1177/030913339401800102

Canfield, D. E., Glazer, A. N., and Falkowski, P. G. (2010). The evolution and future of earth's nitrogen cycle. *Science* 330, 192–196. doi: 10.1126/science.1186120

Christensen, P. B., and Sørensen, J. (1988). Denitrification in sediment of lowland streams: Regional and seasonal variation in Gelbæk and Rabis Bæk, Denmark. *FEMS Microbiol. Lett.* 53, 335–344. doi: 10.1016/0378-1097(88)90499-5

Dhillon, G. S., and Inamdar, S. (2013). Extreme storms and changes in particulate and dissolved organic carbon in runoff: entering uncharted waters? *Geophys. Res. Lett.* 40, 1322–1327. doi: 10.1002/grl.50306

Dhillon, G. S., and Inamdar, S. (2014). Storm event patterns of particulate organic carbon (POC) for large storms and differences with dissolved organic carbon (DOC). *Biogeochemistry*. 118, 61–81. doi: 10.1007/s10533-013-9905-6

Diehl, T. H. (2008). *A Modified Siphon Sampler for Shallow Water*. US Geological Survey. doi: 10.3133/sir20075282

Dodds, W. K., Burgin, A. J., Marcarelli, A. M., and Strauss, E. A. (2017). *Nitrogen Transformations, Methods in Stream Ecology*. Third Edition. New York, NY: Elsevier Inc. doi: 10.1016/B978-0-12-813047-6.00010-3

Edwards, A. C., and Withers, P. J. A. (2008). Transport and delivery of suspended solids, nitrogen and phosphorus from various sources to freshwaters in the UK. *J. Hydrol.* 350, 144–153. doi: 10.1016/j.jhydrol.2007.10.053

Fowler, D., Coyle, M., Skiba, U., Sutton, M. A., Cape, J. N., Reis, S., et al. (2013). The global nitrogen cycle in the Twentyfirst century. *Philos. Trans. R Soc. Lond. B Biol. Sci.* 368, 368. doi: 10.1098/rstb.2013.0164

Galloway, J. N., Dentener, F. J., Capone, D. G., Boyer, E. W., Howarth, R. W., Seitzinger, S. P., et al. (2004). Nitrogen cycles: past, present, and future. *Biogeochemistry* 70, 153–226. doi: 10.1007/s10533-004-0370-0

Giles, M., Morley, N., Baggs, E. M., and Daniell, T. J. (2012). Soil nitrate reducing processes - Drivers, mechanisms for spatial variation, and significance for nitrous oxide production. *Front. Microbiol.* 3, 407. doi: 10.3389/fmicb.2012.00407

Hall, R. O., Baker, M. A., Rosi-Marshall, E. J., Tank, J. L., and Newbold, J. D. (2013). Solute-specific scaling of inorganic nitrogen and phosphorus uptake in streams. *Biogeosciences* 10, 7323–7331. doi: 10.5194/bg-10-7323-2013

Inamdar, S., Dhillon, G., Singh, S., Dutta, S., Levia, D., Scott, D., et al. (2013). Temporal variation in end-member chemistry and its influence on runoff mixing patterns in a forested, Piedmont catchment. *Water Resources Res.* 49, 1828–1844. doi: 10.1002/wrcr.20158

Inamdar, S., Dhillon, G., Singh, S., Parr, T., Qin, Z. (2015). Particulate nitrogen exports in stream runoff exceed dissolved nitrogen forms during large tropical storms in a temperate, headwater, forested watershed. *J. Geophys. Res.* 120, 1548–1566. doi: 10.1002/2015JG002909

Inamdar, S., Singh, S., Dutta, S., Levia, D., Mitchell, M., Scott, D., et al. (2011). Fluorescence characteristics and sources of dissolved organic matter for stream water during storm events in a forested mid-Atlantic watershed. *J. Geophys. Res.* 116, 1735. doi: 10.1029/2011JG001735

Jia, Z., Liu, T., Xia, X., and Xia, N. (2016). Effect of particle size and composition of suspended sediment on denitrification in river water. *Sci. Total Environ.* 541, 934–940. doi: 10.1016/j.scitotenv.2015.10.012

Jiang, G., Lutgen, A., Mattern, K., Sienkiewicz, N., Kan, J., Inamdar, S. (2020). Streambank legacy sediment contributions to suspended sediment-bound nutrient yields from a mid-atlantic, piedmont watershed. *J. Am. Water Resour. Assoc.* 56, 820–841. doi: 10.1111/1752-1688.12855

Johnson, E. R., Inamdar, S., Kan, J., and Vargas, R. (2018). Particulate organic matter composition in stream runoff following large storms: role of POM sources, particle size, and event characteristics. *J. Geophys. Res.* 123, 660–675. doi: 10.1002/2017JG004249

Kan, J. (2018). Storm events restructured bacterial community and their biogeochemical potentials. *J. Geophys. Res.* 123, 2257–2269. doi: 10.1029/2017JG004289

Katz, B. (2020). Exploring the widespread impacts of ongoing nitrogen pollution. *Eos* 101, e10654. doi: 10.1029/2020EO149413

Kim, H., Bae, H.-S., Reddy, K. R., and Ogram, A. (2016). Distributions, abundances and activities of microbes associated with the nitrogen cycle in riparian and stream sediments of a river tributary. *Water Res.* 106, 51–61. doi: 10.1016/j.watres.2016.09.048

Klaus, J., and Mcdonnell, J. J. (2013). Hydrograph separation using stable isotopes: Review and evaluation. *J. Hydrol.* 505, 47–64. doi: 10.1016/j.jhydrol.2013.09.006

Liu, T., Wang, F., Michalski, G., Xia, X., and Liu, S. (2013). Using 15N, 17O, and 18O to determine nitrate sources in the Yellow River, China. *Environ. Sci. Technol.* 47, 13412–13421. doi: 10.1021/es403357m

Lowrance, R., Altier, L., Newbold, J., Schnabel, R., Groffman, P., Denver, J., et al. (1997). Water quality functions of riparian forest buffers in Chesapeake Bay watersheds. *Environ. Manage.* 21, 687–712. doi: 10.1007/s002679900060

McGlynn, B. L., and McDonnell, J. J. (2003). Quantifying the relative contributions of riparian and hillslope zones to catchment runoff. *Water Resour. Res.* 39, 1310–1330. doi: 10.1029/2003WR002091

Menzel, D. W., and Vaccaro, R. F. (1964). The measurement of dissolved organic and particulate carbon in seawater. *Limnol. Oceanogr.* 9, 138–142. doi: 10.4319/lo.1964.9.1.0138

Merill, L., and Tonjes, D. (2014). A review of the hyporheic zone, stream restoration, and means to enhance denitrification. *Taylor Francis* 44, 2337–2379. doi: 10.1080/10643389.2013.829769

Meybeck, M. (1982). Carbon, nitrogen, and phosphorus transport by world rivers. *Am. J. Sci.* 282, 401–450. doi: 10.2475/ajs.282.4.401

Montgomery, D. C., Peck, E. A., and Vining, G. G. (2012). *Introduction to Linear Regression Analysis*. Fifth Edition. London: John Wiley and Sons.

Mulholland, P. J., Helton, A. M., Poole, G. C., Hall, R. O., Hamilton, S. K., Peterson, B. J., et al. (2008). Stream denitrification across biomes and its response to anthropogenic nitrate loading. *Nature* 452, 202–205. doi: 10.1038/nature06686

Mulholland, P. J., Tank, J. L., Sanzone, D. M., Wollheim, W. M., Peterson, B. J., Webster, J. R., et al. (2000). Nitrogen cycling in a forest stream determined by a 15N tracer addition. *Ecol. Monogr.* 70, 471–493. doi: 10.1890/0012-9615(2000)070[0471:NCIAFS]2.0.CO;2

National Weather Service (2023a). Available online at: https://www.weather.gov/wrh/Climate?wfo=phi (accessed May 2, 2023).

National Weather Service (2023b). Available online at: https://www.weather.gov/tae/event-200911_ida (accessed May 2, 2023).

Nielsen, L. P. (1992). Denitrification in sediment determined from nitrogen isotope pairing. *FEMS Microbiol. Ecol.* 86, 357–362. doi: 10.1111/j.1574-6968.1992.tb04828.x

Pang, L., Sun, Y., Yue, Y., Liu, C., An, C., Yang, T., et al. (2022). Stability of aquatic nitrogen cycle under dramatic changes of water and sediment inflows to the three gorges reservoir. *GeoHealth* 6, e2022GH000607. doi: 10.1029/2022GH000607

Pennsylvania Geological Survey (2017). Available online at: https://www.dcnr.pa.gov/Geology/GeologyOfPA/CountyRockMaps/Pages/default.aspx (accessed January 24, 2023).

Randall, C. W. (2004). The environmental, economic and societal consequences of inadequate nitrogen pollution controls. *Water Sci. Technol.* 49, 23–33. doi: 10.2166/wst.2004.0733

Rashleigh, B., Paulsen, S., Flotemersch, J., and Pelletier, M. (2013). Biological assessment of streams and rivers in the U.S.: design, methods, and analysis. *J. Ecol. Environ.* 36, 2288–1220. doi: 10.5141/ecoenv.2013.010

Reisinger, A. J., Tank, J. L., Hoellein, T. J., and Hall, J.r., RO. (2016). Sediment, water column, and open-channel denitrification in rivers measured using membrane-inlet mass spectrometry. *J. Geophys. Res.* 121, 1258–1274. doi: 10.1002/2015JG003261

Reisinger, A. J., Tank, J. L., Rosi-Marshall, E. J., and Hall, J.r,., R. O., Baker MA (2015). The varying role of water column nutrient uptake along river continua in contrasting landscapes. *Biogeochemistry* 125, 115–131. doi: 10.1007/s10533-015-0118-z

Revsbech, N. P., Jacobsen, J. P., and Nielsen, L. P. (2005). Nitrogen transformations in microenvironments of river beds and riparian zones. *Ecol. Eng.* 24, 447–455. doi: 10.1016/j.ecoleng.2005.02.002

Rode, M., Halbedel Née Angelstein, S., Anis, M. R., Borchardt, D., and Weitere, M. (2016). Continuous In-stream assimilatory nitrate uptake from high-frequency sensor measurements. *Environ. Sci. Technol.* 50, 5685–5694. doi: 10.1021/acs.est.6b00943

Rossman, L. A., and Huber, W. C. (2015). Storm water management model reference manual. *U.S. Environ. Protect. Ag.* I, 231. Available online at: www.epa.gov/water-research (accessed June 26, 2023).

Royer, T. V., David, M. B., and Gentry, L. E. (2006). Timing of riverine export of nitrate and phosphorus from agricultural watersheds in Illinois: Implications for reducing nutrient loading to the Mississippi River. *Environ. Sci. Technol.* 40, 4126–4131. doi: 10.1021/es052573n

Royer, T. V., Tank, J. L., and David, M. B. (2004). Transport and fate of nitrate in headwater agricultural streams in illinois. *J. Environ. Quality* 33, 1296. doi: 10.2134/jeq2004.1296

Scheidegger, A. E. (1965). The algebra of stream-order numbers. *US. Geol. Surv.* 525, 187–189.

Seitzinger, S. P., Styles, R. V., Boyer, E. W., Alexander, R. B., and Billen, G., Howarth, R. W. et al. (2002). Nitrogen retention in rivers: model development and application to watersheds in the northeastern U.S.A. *Biogeochemistry* 57, 199–237. doi: 10.1023/A:1015745629794

Steinman, A. D., Lamberti, A. G., and Leavitt, P. R. (2006). "Biomass and pigments of benthic algae," in *Methods in Stream Ecology,* eds. F.R. Hauer

and G.A. Lamberti (Amsterdam, Boston: Elsevier Academic Press), 357–380. doi: 10.1016/B978-012332908-0.50024-3

StreamStats/US Geological Survey (2023). Available online at: https://www.usgs.gov/streamstats (accessed May 2, 2023).

Sweeney, B. W. (1993). Effects of streamside vegetation on macroinvertebrate communities of white clay creek in Eastern North America. *Acad. Natur. Sci.* 144, 291–340.

Tabarestani, M. K., and Zarrati, A. R. (2015). Sediment transport during flood event: a review. *Int. J. Environ. Sci. Technol.* 12, 775–788. doi: 10.1007/s13762-014-0689-6

Trevor, H., Robert, T., and Jerome, F. (2008). "The elements of statistical learning || linear methods for regression," in *Springer Series in Statistics* 43–99. doi: 10.1007/978-0-387-84858-7_3

USEPA (2023). *U.S. Environmental Protection Agency|The Effects: Economy*. Available online at: https://www.epa.gov/nutrientpollution/effects-economy (accessed May 2, 2023).

USGS Water Data for the Nation (2023a). Available online at: https://waterdata.usgs.gov/monitoring-location/01478100/#parameterCode=00065&period=P7D&showMedian=true (accessed May 2, 2023).

USGS Water Data for the Nation (2023b). Available at: https://waterdata.usgs.gov/monitoring-location/01478245/#parameterCode=00065&period=P7D&showMedian=true (accessed May 2, 2023).

Walling, D., Owens, P., Waterfall, B., Leeks, G., and Wass, P. (2000). The particle size characteristics of fluvial suspended sediment in the Humber and Tweed catchments, UK. *Sci. Total Environ.* 251, 205–22. doi: 10.1016/S0048-9697(00)00384-3

Wang, J., Xia, X., Liu, S., Zhang, S., Zhang, L., Jiang, C., et al. (2022). The dominant role of the water column in nitrogen removal and N_2O emissions in large rivers. *Geophys. Res. Lett.* 49, 1–12. doi: 10.1029/2022GL098955

Wuebbles, D. J., Fahey, D. W., Hibbard, K. A., Dokken, D. J., Stewart, B. C., and Maycock, T. K. (2017). *Climate Science Special Report: 4 th US National Climate Assessment*. Washington, DC. doi: 10.7930/J0J964J6

Xia, X., Jia, Z., Liu, T., Zhang, S., and Zhang, L. (2017a). Coupled nitrification-denitrification caused by suspended sediment (SPS) in rivers: importance of SPS size and composition. *Environ. Sci. Technol.* 51, 212–221. doi: 10.1021/acs.est.6b03886

Xia, X., Liu, T., Yang, Z., Michalski, G., Liu, S., Jia, Z., et al. (2017b). Enhanced nitrogen loss from rivers through coupled nitrification-denitrification caused by suspended sediment. *Sci. Total Environ.* 579, 47–59. doi: 10.1016/j.scitotenv.2016.10.181

Xia, X., Liu, T., Yang, Z., Zhang, X., and Yu, Z. (2013). Dissolved organic nitrogen transformation in river water: effects of suspended sediment and organic nitrogen concentration. *J. Hydrol.* 484, 96–104. doi: 10.1016/j.jhydrol.2013.01.012

Xia, X., Yang, Z., and Zhang, X. (2009). Effect of suspended-sediment concentration on nitrification in river water: importance of suspended sediment - Water interface. *Environ. Sci. Technol.* 43, 3681–3687. doi: 10.1021/es8036675

Xia, X., Zhang, L., Wang, G., Wang, J., Zhang, L., Zhang, S., et al. (2021). Nitrogen loss from a turbid river network based on N2 and N2O fluxes: importance of suspended sediment. *Sci. Total Environ.* 757, 143918. doi: 10.1016/j.scitotenv.2020.143918

Xia, X., Zhang, S., Li, S., Zhang, L., Wang, G., Zhang, L., et al. (2018). The cycle of nitrogen in river systems: sources, transformation, and flux. *Environ. Sci.* 20, 863–891. doi: 10.1039/C8EM00042E

Xin, J., Liu, Y., Chen, F., Duan, Y., Wei, G., Zheng, X., et al. (2019). The missing nitrogen pieces: A critical review on the distribution, transformation, and budget of nitrogen in the vadose zone-groundwater system. *Water Res.* 165, 114977. doi: 10.1016/j.watres.2019.114977

Yu, Z., Deng, H., Wang, D., Ye, M., Tan, Y., Li, Y., et al. (2013). Nitrous oxide emissions in the Shanghai river network: implications for the effects of urban sewage and IPCC methodology. *Global Change Biol.* 19, 2999–3010. doi: 10.1111/gcb.12290

frontiers | Frontiers in Water

TYPE Original Research
PUBLISHED 08 January 2024
DOI 10.3389/frwa.2023.1306481

OPEN ACCESS

EDITED BY
Ronald Erwin Pöppl,
University of Vienna, Austria

REVIEWED BY
Katherine B. Lininger,
University of Colorado Boulder, United States
Hossein Hamidifar,
Shiraz University, Iran

*CORRESPONDENCE
Paola Passalacqua
✉ paola@austin.utexas.edu

RECEIVED 03 October 2023
ACCEPTED 01 December 2023
PUBLISHED 08 January 2024

CITATION
Tull N, Moodie AJ and Passalacqua P (2024) River-floodplain connectivity and residence times controlled by topographic bluffs along a backwater transition. *Front. Water* 5:1306481. doi: 10.3389/frwa.2023.1306481

River-floodplain connectivity and residence times controlled by topographic bluffs along a backwater transition

Nelson Tull[1], Andrew J. Moodie[1,2] and Paola Passalacqua[1]*

[1]Maseeh Department of Civil, Architectural and Environmental Engineering, Center for Water and the Environment, The University of Texas at Austin, Austin, TX, United States, [2]Department of Geography, Texas A&M University, College Station, TX, United States

The morphology of river levees and floodplains is an important control on river-floodplain connectivity within a river system under sub-bankfull conditions, and this morphology changes as a river approaches the coast due to backwater influence. Floodplain width can also vary along a river, and floodplain constrictions in the form of bluffs adjacent to the river can influence inundation extent. However, the relative controls of backwater-influenced floodplain topography and bluff topography on river-floodplain connectivity have not been studied. We measure discharge along the lower Trinity River (Texas, USA) during high flow to determine which floodplain features are associated with major river-floodplain flow exchanges. We develop a numerical model representing the transition to backwater-dominated river hydraulics, and quantify downstream changes in levee channelization, inundation, and fluxes along the river-floodplain boundary. We model passive particle transport through the floodplain, and compute residence times as a function of location where particles enter the floodplain. We find that bluff topography controls flow from the floodplain back to the river, whereas levee topography facilitates flow to the floodplain through floodplain channels. Return flow to the river is limited to locations just upstream of bluffs, even under receding flood conditions, whereas outflow locations are numerous and occur all along the river. Residence times for particles entering the floodplain far upstream of bluffs are as much as two orders of magnitude longer than those for particles entering short distances upstream of bluffs. This study can benefit floodplain ecosystem management and restoration plans by informing on the key locations of lateral exchange and variable residence time distributions in river-floodplain systems.

KEYWORDS

floodplains, hydrological connectivity, lateral exchange, residence times, particle routing, levees, bluffs

1 Introduction

River floodplains are often associated with flood hazard zones, but when preserved and healthy, they represent critical ecosystems and landforms as well (Ward et al., 1999; Melack and Forsberg, 2001; Kondolf et al., 2006; Roley et al., 2012; Noe et al., 2013; Kufel and Leśniczuk, 2014). Seasonal and storm-driven inundation from the river brings nutrients to floodplain ecosystems as solutes and particulates attached to suspended sediment, and widespread inundation provides a wetland environment that stores large amounts of carbon (Battin et al., 2009; Aufdenkampe et al., 2011; Mitsch et al., 2013; Sutfin et al., 2016). The deposition of sediment in floodplain ponds and on river levees is another crucial component

of nutrient and organic carbon transport into the floodplain, where saturated soils and long-term inundation enable processing and sequestering of these solutes (Walling et al., 1998; Walling and Owens, 2003; Noe and Hupp, 2005, 2009). Furthermore, floodplains provide both flood attenuation and a record of flood history through periodic sediment deposition (Shen et al., 2015).

While these processes are important components of a healthy river environment, they depend on a river bank structure that allows water, solids, and solutes to flow between the river and floodplain, particularly in the absence of overbank inundation. Gaps in the levee, such as lateral floodplain channels, are an example of system "structural connectivity," which has been defined as the extent to which adjacent landscape units (e.g., a river and its floodplain) are physically linked with one another (Wainwright et al., 2011; Bracken et al., 2013; Passalacqua, 2017; Wohl et al., 2019). To varying degrees, lateral floodplain channels can be conduits for mass and momentum exchange between the river and floodplain even when stage is less than bankfull (Byrne et al., 2019; Czuba et al., 2019; Lindroth et al., 2020; Tull et al., 2022; van der Steeg et al., 2023). We consider fluxes through these landscape pathways as examples of "functional connectivity," which is defined in the context of the present study as the movement of water, sediment, and solutes between adjacent landscape units that are connected structurally (Wainwright et al., 2011; Bracken et al., 2013; Passalacqua, 2017; Wohl et al., 2019). The extent to which a system is connected can be a major control on flood attenuation and the development of wetland conditions that store nutrients and carbon (Tockner et al., 1999; Hughes et al., 2001; Thoms, 2003; Welti et al., 2012; Harvey and Gooseff, 2015; Gurnell et al., 2016; Covino, 2017).

The relationship between hydrological connectivity and ecosystem health in floodplain systems has been established, and studies have shown how complex floodplain topography can lead to downstream variability in hydrological connectivity in both fluvial environments (Croke et al., 2013; Byrne et al., 2019) and deltaic environments (Hiatt and Passalacqua, 2015; Wright et al., 2022a). However, variability in hydrological river-floodplain connectivity as a coastal river transitions from a fluvial to a deltaic environment has not been evaluated, even though a river's topographic and hydraulic characteristics may change dramatically under the backwater influence. Within the backwater reach of the Trinity River (Texas, USA; Figure 1), for example, the difference in water surface elevations during low and high flows is less than in the upstream reach, and the normal water surface elevation approaches the average bank elevation closer to the delta (Smith et al., 2020; Hassenruck-Gudipati et al., 2022). The river also exhibits changes in channel and bank morphology under the backwater influence, with a dramatic increase in levee size (Smith et al., 2020; Hassenruck-Gudipati et al., 2022) and reduction in channel migration rates and associated morphological features in the downstream direction (Mason and Mohrig, 2019; Smith et al., 2020). So although changes in topography through a backwater transition have been studied, we have a very limited understanding of how those topographic changes translate to functional river-floodplain connectivity.

Variations in floodplain width can also influence river-floodplain connectivity, particularly inundation extent (Croke et al., 2013). River reaches with wide floodplains generally provide more space for expansive inundation, while reaches that are bounded by bluffs or terraces have greater channel capacity that compensates for the reduced floodplain inundation. Floodplain expansions and contractions along a reach are important controls on the development of floodplain channels (David et al., 2017), organic carbon storage in floodplains (Wohl et al., 2018), sediment connectivity between the river and the floodplain (Croke et al., 2013), sediment connectivity between the floodplain and upland tributary basins (Rathburn et al., 2018), and channel mobility (Mertes et al., 1996). However, the relationship between bluff topography and hydrological river-floodplain connectivity has not been quantified.

Downstream changes in river hydraulics and floodplain topography may have an impact on the time water spends in the floodplain, commonly referred to as the "floodplain residence time." Significant removal of nutrients is dependent on floodplain residence times (Tockner et al., 1999; Yu et al., 2006; Noe and Hupp, 2009; Noe et al., 2013; Cheng and Basu, 2017; Hiatt et al., 2018), and although there is limited guidance in the literature on optimal residence times for nutrient removal in wetlands, longer surface-water residence times can drastically increase the productivity of these environments (Seitzinger et al., 2006; Sheibley et al., 2006; Kaushal et al., 2008). Residence times, however, can be difficult to quantify due to complex floodplain geometry, topography, and flow patterns. Tracer studies are a possibility, but they are typically performed only in a small area of interest with unique characteristics, such as a constructed wetland (Holland et al., 2004) or delta island (Hiatt and Passalacqua, 2015). Similarly, hydrodynamic models that incorporate particle tracking have been used to estimate floodplain residence times, but those models have used either relatively coarse spatial resolution (Helton et al., 2014; Hiatt et al., 2018) or focused on a localized floodplain domain (Tull et al., 2022). A comprehensive assessment of residence time distributions across river reaches spanning the backwater length has not been performed.

This study combines discharge data collected on the lower Trinity River and a calibrated hydrodynamic model to analyze how lateral water exchange and floodplain inundation patterns change as the river approaches its delta. We run steady flow models at various discharges and quantify how hydrological connectivity changes along the length of the river reach. We utilize a Lagrangian particle routing model to track flow paths through the floodplain, including the origins, termini, and travel times for all particles, and describe how those flow characteristics change with distance downstream. The results of this study characterize topographic controls on hydrological connectivity along a backwater transition and within a valley containing several bluffs along the river. Understanding this transition is critical for understanding ecological and geomorphic processes and water resources in both riverine and deltaic environments.

2 Study area: the lower Trinity River

Our study reach on the lower Trinity River includes 65 river kilometers (rkm) between its mouth at Trinity Bay and the city of Liberty, TX in the upstream reach (Figure 1). We chose this study site because upstream of Wallisville, TX it is mostly free of engineered modifications such as containment levees and

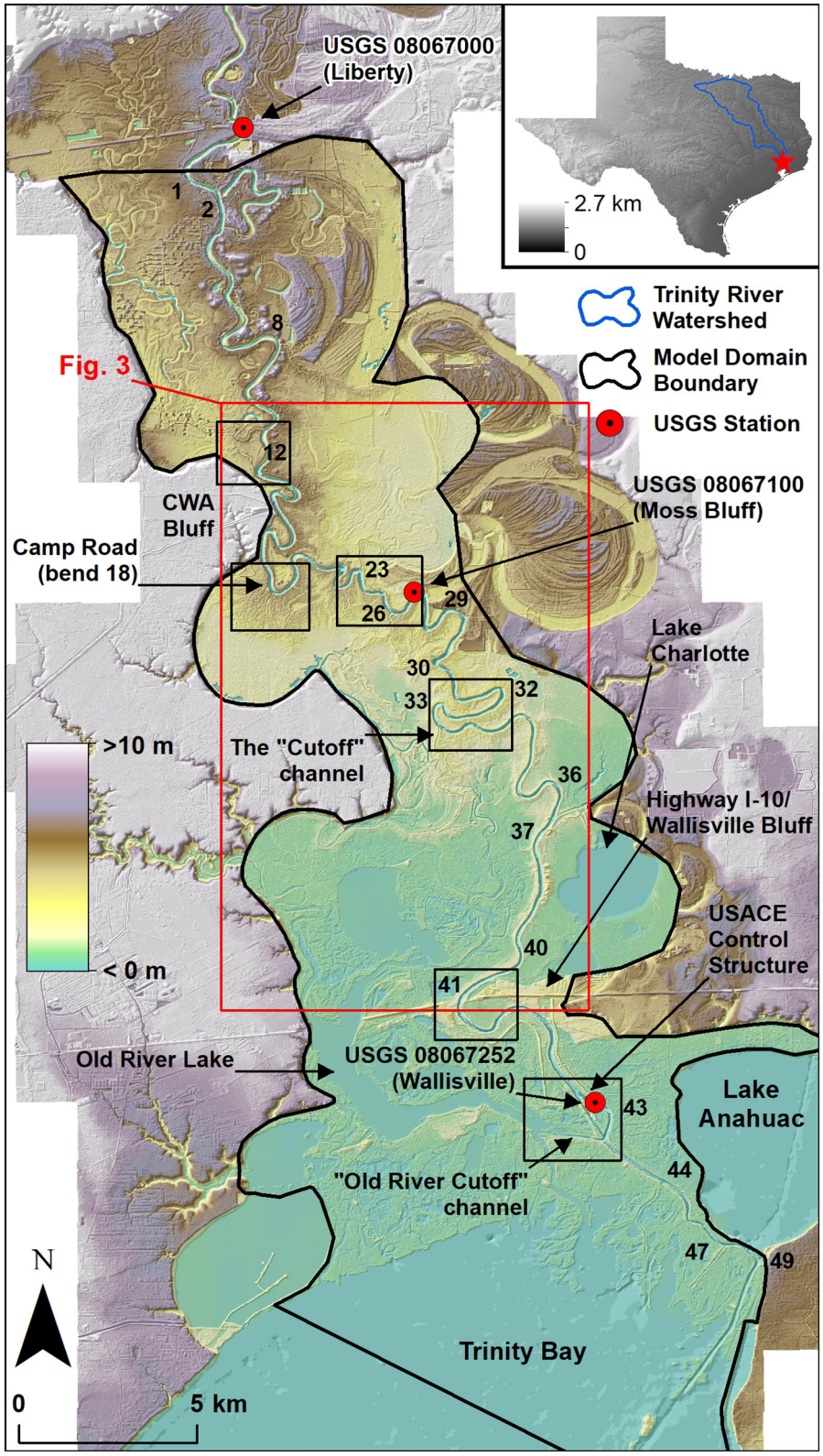

FIGURE 1
Study region on the lower Trinity River. The labeled locations refer to locations that are referenced in the manuscript. Numbers along the river refer to bend (zone) numbers that are referenced in the manuscript. Small black boxes represent the extents of the panels shown in Figure 2.

revetments and the floodplain is largely undeveloped; thus, the floodplain topography is the result of natural meandering and flooding processes. Furthermore, the geomorphology of the lower Trinity River has been well-studied (Phillips et al., 2004, 2005; Phillips and Slattery, 2007; Phillips, 2010; Mason and Mohrig, 2018; Smith et al., 2020; Hassenruck-Gudipati et al., 2022). The transition to fully backwater-dominated flow occurs just upstream of river bend 12 (as depicted in Figure 1). Upstream of this point, the river bend migration rates and point bar sizes increase as the river transitions to a quasi-normal flow reach. The floodplain within this region consists of geomorphic features associated with active migration, such as oxbow lakes and relict channels. Natural river levees grow in size within the backwater region, as do the floodplain channels that move through them. Farther downstream, the presence of several large floodplain lakes marks the transition to a coastal wetland environment. Floodplain width is highly variable throughout the study region, with some deep floodplain basins up to 7 km wide, while in other locations topographic bluffs or terraces exist adjacent to the river with no floodplain present at all (Figure 1).

Within the study reach are three USGS gaging stations located at Liberty (USGS 08067000), Moss Bluff (USGS 08067100), and Wallisville (USGS 08067252). Discharge data derived from a rating curve are available at the Liberty gage, while the other two stations measure river stage and several other parameters. The Wallisville gage is located adjacent to a run-of-river dam and gate (Figure 2F) that are operated by the U.S. Army Corps of Engineers (USACE) for the purpose of preventing saltwater intrusion into the Trinity River National Wildlife Refuge upstream. The gate is closed only during low flows, and remains open during periods of higher flow, including all flow conditions within the scope of this study. The USACE compound contains embankments on either side of the river that extend upstream about 6 km until the highway I-10 bridge, where there is a bluff on the east side of the river that we refer to as "Wallisville Bluff" (Figures 2E, F). The Moss Bluff gage is adjacent to a set of pumps and an elevated canal that draws water from the river for agricultural use (Figure 2C), where past flow measurements indicate an average withdrawal rate of 3 m^3/s (Lucena and Lee, 2022). Between Moss Bluff and Liberty is another pump station operated by the Coastal Water Authority (CWA) situated on a bluff along the river, which we refer to as "CWA Bluff," that withdraws water at an average rate of 26 m^3/s (USGS 08067070). The river hydraulics within the study area are affected by tides with amplitudes in Trinity Bay between 15 and 50 cm. Upstream of the USACE compound at Wallisville, however, tidal influence is limited by river discharge during high-flow conditions and by the control of the USACE gate during low-flow conditions. The tidal signal is only detectable at the Moss Bluff gage under low-flow conditions. Even though the USACE gate remains closed during low flows, the tidal signal reaches the Trinity River via the Old River Lake and the connected network of floodplain channels to the west of the river, including the "Cutoff" floodplain channel (Figures 2D, F).

The river upstream and downstream of the USACE embankment and control structure is fundamentally different. We consider the Trinity River delta to begin downstream of the control structure. There is a particularly large distributary to the main channel called the "Old River Cutoff" that is located just past the end of the USACE embankment (Figure 2F), and this channel connects the Trinity River with the floodplain lakes to the west. The geometry of the delta is somewhat atypical, as the left bank of the main channel is much more confined than the right bank due to the presence of Lake Anahuac (a water storage reservoir); all of the delta distributaries are located along the right bank. The USACE compound between Wallisville Bluff and the Old River Cutoff is a significant discontinuity of the Trinity river, and is relevant to our study that seeks to quantify topographic and hydraulic changes from the normal flow reach to the delta. Thus, our analysis considers this compound to be the delineation between the river and its delta, and our results are discussed with its influence and this delineation in mind.

3 Methods

3.1 Collecting river discharge data

On 13 April 2023 we measured river discharge at 25 transects on the Trinity River with an Acoustic Doppler Current Profiler (ADCP), to understand where and how much lateral flow exchange occurs along the river and how the topography controls those flow exchanges (Figure 3). We collected measurements using RiverRay ADCP from Teledyne Marine mounted to the bow of the R/V Scott Petty, a research vessel operated by the University of Texas Institute for Geosciences. We collected and processed the data using the WinRiver II software. The start and end positions of each transect were located on average about 10 m from the adjacent river bank, to avoid getting stuck in vegetation and shallow waters. We used a Laser Rangefinder to estimate the horizontal distance from the end of the transect to the river bank. We accounted for each missing edge of the cross section using the triangular extrapolation method from WinRiver, and used the power law method from WinRiver to estimate the discharge in the top and bottom layers of the cross section where the ADCP is not able to measure velocities. We took between two and four transect measurements at each location. At transects where three measurements were taken, we averaged together the two measurements taken in the same direction prior to averaging with the third measurement, to remove directional bias.

We positioned transects upstream and downstream of each location where flow exchange between the river and the floodplain was evident or where we expected floodplain channel locations based on visual inspection of lidar data (Figure 3). We measured the first transect (transect A, Figure 2A, 11 rkm downstream of Liberty) upstream of CWA Bluff at 10:50 CDT (all times are local, central daylight time), and the final transect (transect Y, Figure 2E, 47 rkm downstream of Liberty) just upstream of Wallisville Bluff at 16:45 CDT. River flows were declining over the course of the day from an earlier peak of 800 m^3/s at the Liberty gage on 10 April. During the six hours it took to collect measurements from transect A to transect Y, the discharge measured at the Liberty gage had fallen from 515 to 467 m^3/s.

3.2 Numerical model development

We used the Australian National University and Geosciences Australia (ANUGA) hydrodynamic model to quantify functional connectivity along the river

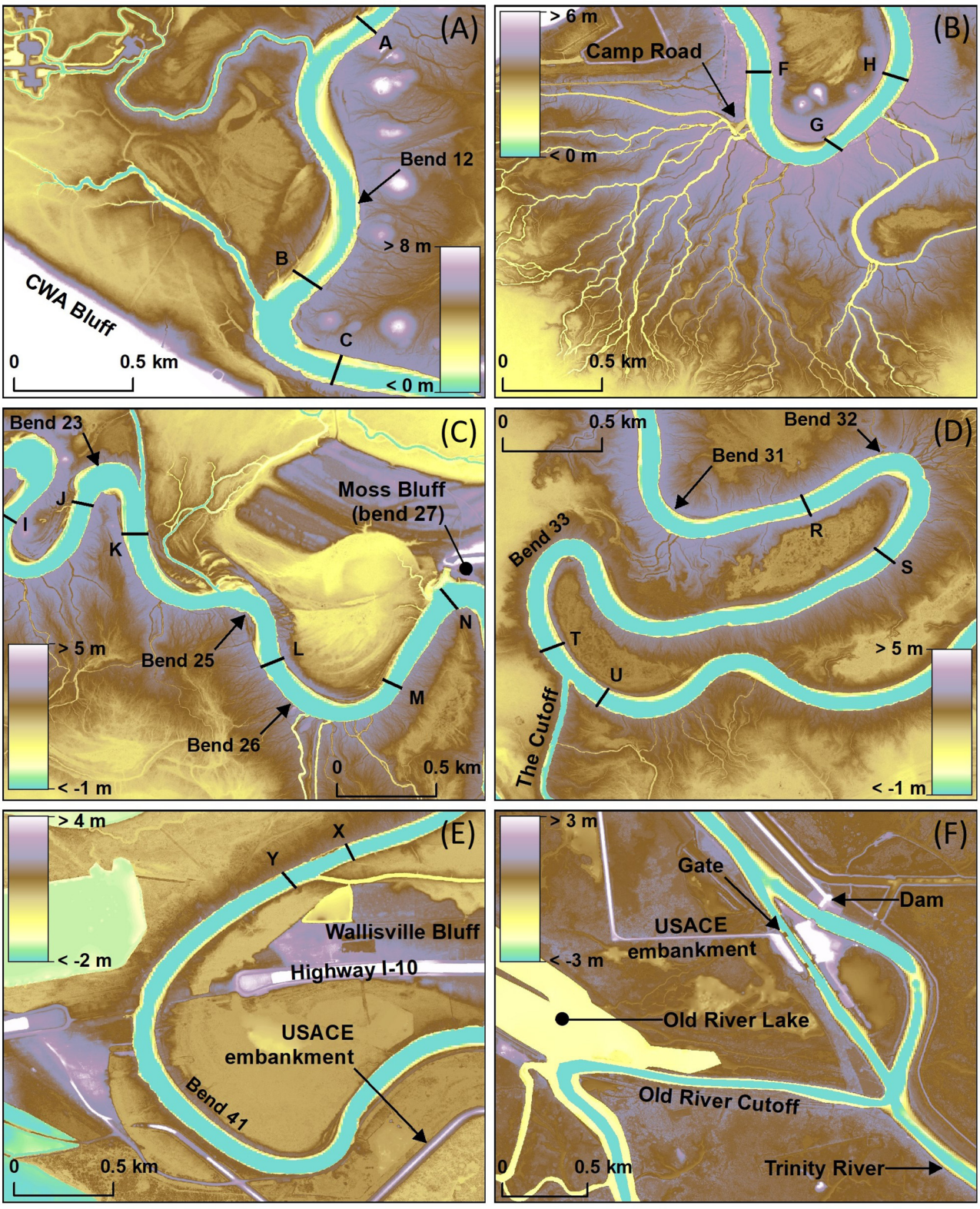

FIGURE 2
Elevation maps for locations within the study area that are referenced frequently in the manuscript. **(A)** Area upstream of CWA Bluff, **(B)** large network of floodplain channels at Camp Road, **(C)** area upstream of Moss Bluff, **(D)** highly sinuous bend and location of the "Cutoff" channel, **(E)** Wallisville Bluff and the upstream end of the USACE embankments, and **(F)** USACE structures and the "Old River Cutoff" channel. Locations of each panel are shown in Figure 1, from **(A)** upstream to **(F)** downstream. Capital letters shown along the river are labels for the ADCP transect locations shown in Figure 3 and data shown in Figure 5.

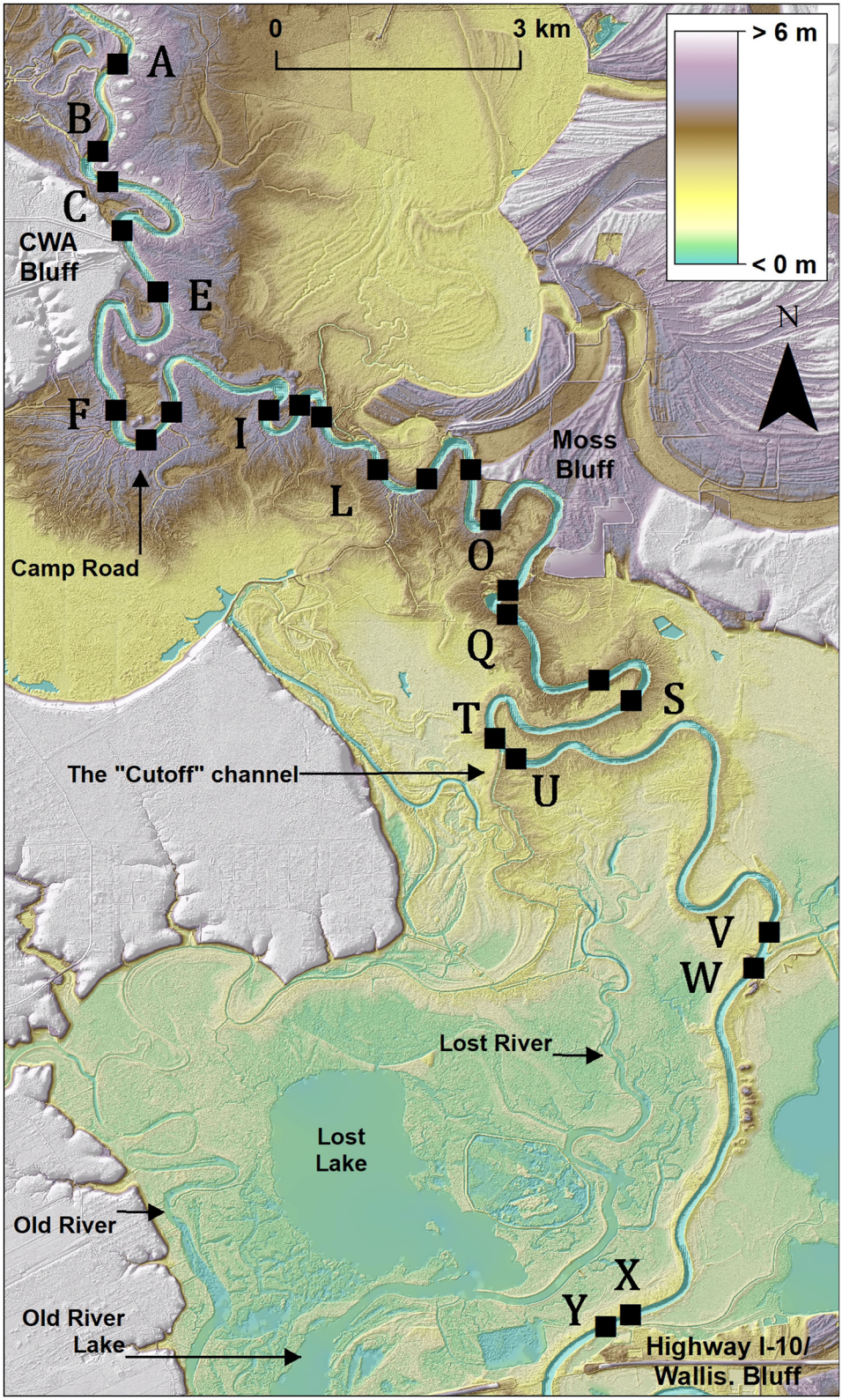

FIGURE 3
Location of ADCP transects. Labels are in order from A to Y (25 total transects) from upstream to downstream, as shown in Figure 5.

(Nielsen et al., 2005; Mungkasi and Roberts, 2011, 2013). ANUGA is an open-source model that uses a finite-volume method to solve the shallow-water equations on unstructured meshes. ANUGA was originally developed for coastal applications such as tsunami modeling and has been validated for such applications (Nielsen et al., 2005; Mungkasi and Roberts, 2013). In recent years, ANUGA

has been used for delta and coastal river systems along the U.S. Gulf Coast and other similar applications (Tull et al., 2022; Wright et al., 2022a,b; Hariharan et al., 2023). Additional information on this model and its application to the Trinity River can be found in Tull et al. (2022).

We calibrated the numerical model using the discharge data collected during the April 2023 campaign and local USGS gage data. We validated the model using discharge data collected during a separate campaign on 11–12 May 2022 at various locations between CWA Bluff and Wallisville Bluff (Supplementary Figures S1, S2), under lower flow conditions than those of April 2023. A description of the May 2022 data and the calibration (Supplementary Figure S3) and validation (Supplementary Figure S4) processes and results can be found in the Supporting Information.

The model domain for the present study extends from just south of Liberty, TX at the upstream end to Trinity Bay at the downstream end (Figure 1). The side boundaries of the domain represent the valley walls. The average mesh resolution, or average mesh element edge length, in the main channel is about 18 m, while along the breakline representing the river-floodplain boundary the resolution is 12 m. In general, the average mesh resolution in the floodplain is 50 m. However, along floodplain channels and lake margins, we increased the mesh resolution to capture the geometry of those features. Floodplain channels contain mesh elements whose sizes are commensurate with the width of the channels they represent, such that there are at least two elements across the width of each channel. In Trinity Bay, we relaxed the mesh resolution to 200 m. The final mesh contains 670,826 elements and 336,952 nodes. We provide a full description of the mesh development process, including the detection and extraction of floodplain features using elevation data, in the Supporting Information.

For the model elevation data, we used a Digital Elevation Model (DEM) with 1-m resolution, consisting of a combination of lidar and surveyed bathymetry; more information on the acquisition and processing of the DEM can be found in Tull et al. (2022). We modified the DEM to improve the bathymetry of certain channels in the system, namely those where bathymetry data were unavailable due to the presence of water during lidar collection (we provide a description of the modifications made to the DEM during the model calibration process in the Supporting Information). We interpolated the DEM to mesh element centroids via a least-squares fit. We applied friction forcing to the domain based on our calibration of the model using the high-flow conditions measured in April 2023, with a Manning's n value of 0.02 in the main channel, lakes, and bay, a value of 0.05 in floodplain channels, and a value of 0.1 over the rest of the floodplain. The upstream and side boundaries of the domain are no-flow boundaries. We modeled the downstream boundary as a tidal boundary during the calibration process, but for the steady discharge scenarios modeled in this study, we imposed a constant water level boundary equal to the average water level in the bay over a 30-day period (0.3 m, NAVD88).

We ran three steady flow simulations at discharges of 500, 800, and 1,100 m^3/s. A discharge of 500 m^3/s is similar to the river discharge measured in the field in April 2023 (Section 3.1), and represents a stage where the largest floodplain channels convey water from the river, but many of the smaller channels remain dry. A discharge of 1,100 m^3/s is near the bankfull discharge. We applied the constant discharges in the river at the upstream end, just south of Liberty, TX. We ran the models until they reached steady-state conditions based on an analysis of the rate of change of total water volume in the domain. Although the rising and falling flood wave dynamics associated with an unsteady flow event are important and not fully represented by a steady flow model, the objective of this study is to quantify *spatial* changes in connectivity and hydrodynamics over a large domain, and adding a temporal dimension would bring unnecessary complexity to the analysis and presentation of results related to our objective. We consider the steady modeling approach to be a representation of the long-lasting flood events (1–2 months) that can occur on the Trinity River, such as, for example, the flooding that occurred during the period between November 2015 and June 2016 (see USGS 08067000).

3.3 Defining analysis zones along the river

This study is centered around quantifying changes in structural and functional connectivity as a river approaches the coast. Within a defined strip of overbank area directly abutting the river, we quantified the degree of floodplain channelization using lidar data, and using model results at various discharges (as described in Section 3.2), we quantified the fractional inundated area, inundation volume, water fluxes, and floodplain residence times associated with those fluxes. Therefore, we delineated analysis boundaries, or "zones," for each side of the river, which we refer to as "river bank zones." Each river bank zone consists of a 200-m buffer from the main channel, and successive zones in the along-stream direction are delineated at the inflection point between successive river bends. For particularly sinuous parts of the river where neighboring bends are less than 400 m from each other (e.g., bend 23 in Figure 1), the buffer distance is reduced such that the dividing line between the two river bank zones is equidistant from the edges of each river bend.

These river bank zones represent the boundary between the river and the floodplain. Pathways across this boundary, such as floodplain channels, are an example of structural connectivity, while fluxes across this boundary represent functional connectivity. The 200-m buffer distance encompasses the typical width of the wider levees along the river, and therefore encompasses the floodplain channels that run through them. Even though levee width varies within the study region, we chose the 200-m buffer distance for consistency. A smaller buffer (say, 100 m) would not extend out to the levee crest for many of the larger levees, and would increase noise in our quantification of river-floodplain water exchanges by including fluxes that enter the river bank zone but quickly return to the source. A larger buffer would include more of the deeper floodplain beyond the levee, which would include significantly more inundated area for almost all river bank zones. Since the purpose of these zones is to quantify inundated area, inundation volume, and water fluxes within and through the adjacent river bank areas, we aimed to limit the zones to encompass the levee topography as best as possible. We numbered river bank zones by the river bend at which they are located. The first river

bank zone is located just south of Liberty at bend 1, while the final zone at bend 49 is at the end of the Trinity River delta.

3.4 Quantifying structural connectivity

Structural connectivity in the context of this study is quantified by the degree to which the river is connected to the adjacent floodplain via secondary (or floodplain) channels (Passalacqua, 2017). We identified the presence of channels in river bank zones by filtering the DEM described in Section 3.2 and computing the curvature using the GeoNet approach (Passalacqua et al., 2010). The Laplacian curvature has been shown to be effective in highlighting channel features, particularly in flat landscapes and environments where increased selectivity of those features is needed (Passalacqua et al., 2012). We applied a curvature threshold of 0.3 m^{-1} across the landscape, as this value captures the most channelized pixels while also limiting noise. This method does not capture the centerline of the channels nor the entire channel area; instead, it captures the pixels along the boundary between the channel wall and the channel bottom. So there are two lines of pixels for each captured channel, one on each side of the channel.

We used the "Zonal Statistics as Table" tool in ArcGIS to compute the total number of channelized pixels in each river bank zone, where each pixel is 1 square meter. Then we divided the number of channelized pixels by the total zone area to obtain a percent channelization metric. For this analysis, we did not consider the zones within the USACE compound and in the delta downstream, as there is no channelization within the compound, and in the delta the hydraulics are unconfined and the distributary channels are much different structurally than the floodplain channels upstream.

3.5 Quantifying functional connectivity

We analyzed the functional connectivity of the lower Trinity River using ANUGA, the numerical model described in Section 3.2, and the river bank zones defined in Section 3.3 to quantify changes in hydrodynamic characteristics with distance downstream. Within each river bank zone, we quantified inundated area and inundation volume from the model results, normalized by the area of each zone. We applied `dorado`, a Lagrangian particle tracking tool that runs on flow fields generated by the model, to quantify fluxes between the river and the floodplain through each zone. We also tracked particle paths through the floodplain, calculated their residence times, and tied those residence times to the river bank zones where the particles entered the floodplain, as a way of quantifying residence time dependence on flux location and proximity to the coast.

3.5.1 "Static" metrics of functional connectivity

We queried the model results to determine both the inundated area and inundation volume within each river bank zone (Figure 4). We expect both metrics to be affected by the changes in topography and hydraulics as the river approaches the coast. Because the zones represent the overbank area within 200 m of the river, these measures of inundation do not represent overall flooding in the floodplain but rather water connectivity along the river bank. At sub-bankfull discharges, inundated area in particular is an indicator of bank line topography, where more inundated area indicates a lower-lying, relatively flatter river bank. In contrast, inundation volume in a river bank zone describes river bends with more bank line variability, as banks containing both high levees and deep floodplain channels would likely have less inundated area but more inundation volume. We expect that inundated area will increase toward the coast as the water surface profile flattens and approaches the average bank elevation. We do not expect inundation volumes to increase downstream, but instead be correlated with river bank structure. Each of these inundation metrics is a form of hydrological connectivity, but neither describes the transfer of mass or energy between the river and the floodplain. These metrics represent static quantities of water present within 200 m of the river, under steady-state conditions. We describe fluxes through river bank zones in the following subsection.

We interpolated modeled flow depths for each simulation from mesh element centroids to a 2-m grid using an inverse-distance weighting method with the three nearest neighbors. Again using the "Zonal Statistics as Table" tool in ArcGIS, we computed the total number of grid cells in each river bank zone with depths greater than 1 cm, which is an arbitrary threshold selected to eliminate model noise from the analysis, although increasing this threshold above 1 cm did not change the results. We computed the percent inundated area for each zone by dividing the number of inundated cells by the total number of cells in the zone. We computed and normalized the inundation volume by taking the mean depth in each zone (for cells with depths greater than 1 cm) and multiplying it by the ratio of wet cell area to total zone area. Normalizing the inundation volume accounts for the wide range of zone sizes, which vary based on river bend geometry.

3.5.2 Flux and residence time quantification with dorado

We used the `dorado` Lagrangian particle routing package (Hariharan et al., 2020) for computing fluxes, flow paths, and residence times in the model domain. `dorado` uses a weighted random walk algorithm adapted from DeltaRCM (Liang et al., 2015a,b) to simulate passive particle transport through model flow fields on a regular grid. It has been used recently in several modeling studies of coastal river and delta systems (Tull et al., 2022; Wright et al., 2022a; Hariharan et al., 2023); more detail on the routing algorithm can be found in the Methods sections of those studies as well as in the software documentation online.

We interpolated model outputs of water stage, depth, and depth-averaged momentum at the end of each simulation (i.e., at steady-state) to a 5-m grid using three-neighbor inverse distance weighting. Particle routing results showed little sensitivity to changes in the interpolated grid size between 2-m and 10-m resolution. We applied a dry-depth limit such that particles were limited to cells with at least 1 cm of depth. `dorado` routes particles as passive tracers of water movement, where routing is weighted proportional to water depth in the downstream direction ($\theta = 1$;

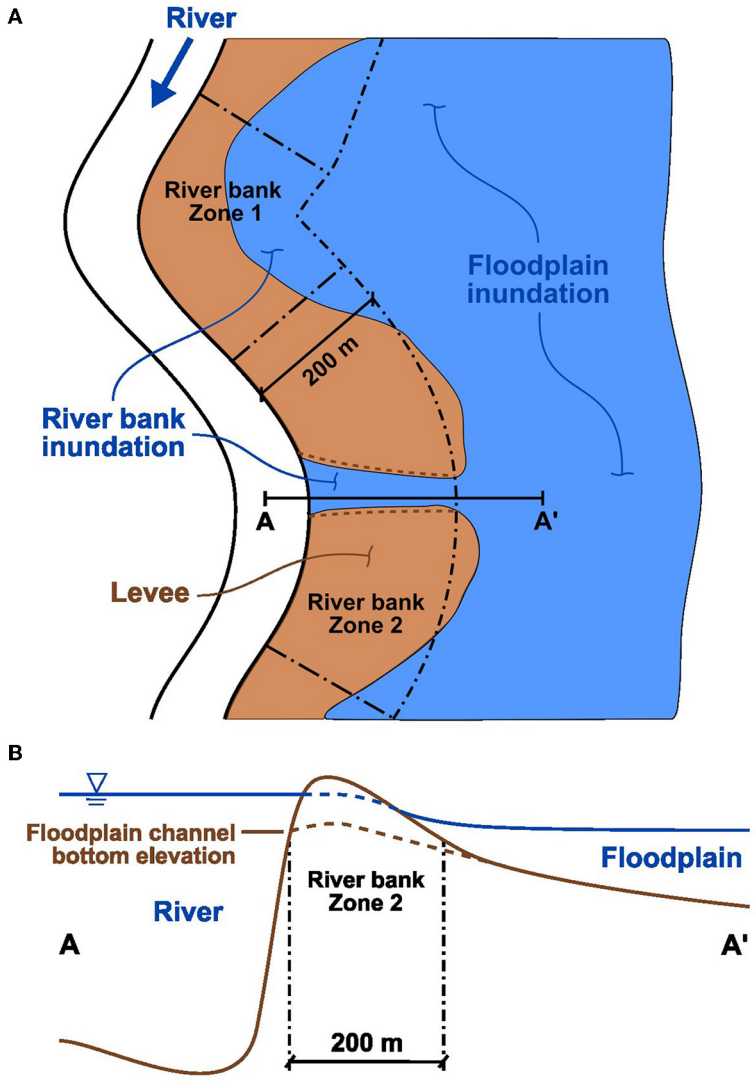

FIGURE 4
Illustration of inundation within river bank zones. In this manuscript, "inundated area" refers to the fractional area within each river bank zone that contains water, as in the simple example shown in plan view **(A)**. To calculate normalized "inundation volume" within each river bank zone, we multiply the average depth in the zone by the inundated area fraction. For zones with deep levee channels, such as Zone 2 in cross-section view **(B)**, the inundation volume can be greater than those with higher inundated area if the average depth of the latter is shallow.

Hariharan et al., 2020; Wright et al., 2022a). Thus, particle transport in this study represents transport of neutrally buoyant materials.

Because particles approximate water and neutrally buoyant material transport through the domain, and total water volume on the floodplain scales with discharge, we routed a large number of particles proportional to the steady discharge in each model simulation. For discharges of 500, 800, and 1,100 m^3/s, we initialized 50,000, 80,000, and 110,000 particles, respectively, at the inlet of the domain. Particles traveled through the model flow fields for 50 days, at which point the vast majority of particles had reached the distal domain edge in the bay, which we defined as the stopping criteria for the particle routing.

To quantify fluxes into and out of the river through river bank zones, we converted the zone polygons to a raster of the same shape as those used for the particle simulations. We assigned a unique integer value to raster area covered by each river bank zone, the river itself, the floodplain, and the bay. For each particle that steps into a floodplain cell, we tracked its path to find the river bank zone it entered when it last left the river. If that same particle re-entered the river somewhere downstream, we recorded the river bank zone where the re-entry occurred. The floodplain residence time of that particle is the total travel time between the river exit point and the river re-entry point, where travel time per step is computed based on the step distance, local flow velocities, and a diffusivity modifier (Hariharan et al., 2020). For particles that did not re-enter the river, we considered the residence time calculation complete once they reached the bay.

For the range of modeled discharges we can determine the magnitude of flux to the floodplain occurring at each river bank zone, the magnitude of flux re-entering the river at each zone

including the distribution of bends where those fluxes originated, and the residence times associated with fluxes from each river zone. Within the Eulerian framework of the numerical model, it is possible to achieve a first-order estimate of flow into the floodplain from a given river bend. However, it is impossible to get information on the fate of those specific flows once they enter the floodplain and mix with other sources of water. Likewise, it is possible (and common) to measure the residence time of a body of water by considering the total volume of water and flow rate through the system, but computing a distribution of residence times is only possible within a Lagrangian framework. Particle routing with `dorado` allows us to track the fate of specific river-floodplain fluxes, and study the influence of specific river bends on transport through the floodplain.

4 Results

4.1 Field measurements of lateral exchange

Discharge measurements taken in the backwater reach of the Trinity River show that there can be a systematic decrease in river flow approaching the coast, even in a reach upstream of the delta (Figure 5). We collected the data during the falling limb of a minor flood event that lasted 5–6 days, when water in the floodplain was returning back to the river. Many locations continued to convey flow from the river to the floodplain, though, even as river stage decreased.

The first three measurements (transects A–C, Figure 5) located upstream of CWA Bluff (Figure 2A) show that the flow increased from 480 to 520 m^3/s over a short distance (1.8 rkm) in the downstream direction. The measured discharge of 480 m^3/s at transect A was lower than the discharge at Liberty at the same time the transect A measurement was taken (515 m^3/s at 10:50 CDT), even though the falling river stage would have indicated that Liberty would have a lower discharge than points downstream at a given time. However, the flow increased from transects A to B and from transects B to C corresponding to two large floodplain channels upstream of CWA Bluff that were flowing toward the river (Figure 3). This location is one of the few within the study area where flow was returning to the river during the field campaign.

Downstream of CWA Bluff is a bend (bend 18) with one of the largest levee extents on the river, along with the largest network of floodplain channels within the levee, referred to here as Camp Road, which is a name given to the unmaintained path that runs along the levee crest (Figure 2B). Transects F and G were located upstream and downstream of this bend, respectively, where measurements indicated a flow loss of about 40 m^3/s through this levee, or 8% of the total river discharge at Liberty at the time of measurement. This bend has one of the highest and widest levees on the Lower Trinity River, and at the same time functions as one of the major points of flow loss from the river during high flows.

Between transects I and O (Figures 2C, 3), flows in the river did not change significantly but instead alternated between small increases and decreases along the river. There are both large and small floodplain channels connected to the river between these transects. Flow was moving to the floodplain through a deep connecting channel between transects J and K (bend 23), but came back to the river at the next bend downstream between transects K and L. After transect L, more flow was moving out of the river through the set of floodplain channels at the next river bend (bend 26). The left bank between transects M and N was completely inundated, and the small increase in measured discharge at transect N indicates that the net water flux at this location was toward the river. This increase is in spite of the fact that the Moss Bluff pump station was likely removing a small amount of water from the river upstream of transect N (bend 27). At transect P (bend 30), there was a flow increase of 16 m^3/s, however there are no natural features between transects O and P that would indicate an inflow. There is a community living along the left river bank here as well as a large engineered pond, which could be the source of the flow increase, but we are unsure of the mode by which water was entering the river at this location.

The largest floodplain channel in the study area, the "Cutoff," is located at bend 33 between transects T and U (Figure 2D), representing the largest measured flow loss from the river of 72 m^3/s, or 15% of the Liberty discharge at the time of measurement. Downstream of the Cutoff the river-right floodplain becomes dominated by large floodplain lakes and eventually tidal estuaries. River water moving through the Cutoff is one of the primary sources of freshwater to these lakes, even at low flows.

Transects V–Y represent measurements upstream and downstream of two separate floodplain channels connected to the river on the left bank (Figure 3). Each of these channels currently functions to bring water to and from the large floodplain lakes near the river on that side. Under most conditions, the first channel (between transects V–W at bend 36) brings flow to the floodplain while the second channel (between transects X–Y at bend 41, Figure 2E) returns flow to the river just upstream of Wallisville Bluff (Figure 5).

4.2 Downstream changes in bank channelization

The degree of river bank channelization varies greatly along the river (Figure 6). Features contributing to high channelization on the east side of the river include the oxbow lake and tie channel at bend 2, a floodplain channel that begins at bend 8 and connects back to the river at bend 23, and another channel that passes through bend 24 but connects to the river at bend 25 (Figure 2C). The channels at bends 36 and 41 on the east side correspond to the location of the downstream-most discharge measurements in Figure 5, transects V–W and X–Y, respectively. On the west side, the largest total channelized area was computed at bend 18, which is the Camp Road bend associated with discharge measurements taken at transects F–G (Figure 5).

Bend 33 on the west side contains the largest floodplain channel upstream of the delta (the Cutoff, Figure 2D), but this channel does not translate to a high channelized pixel count in Figure 6A. Its signal is even less prominent as a percentage of the zone area (Figure 6B), because this bend is by far the most sinuous in the study region, and its river bank zone is the largest as a result.

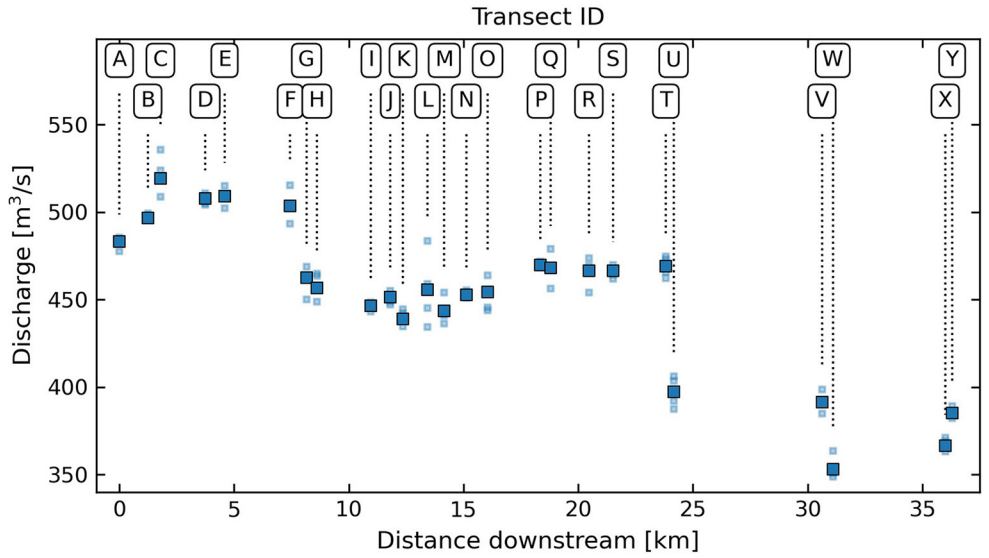

FIGURE 5
Measured discharge data during the falling limb of a minor flood event on 13 April 2023. Transect labels correspond to those labeled in Figure 3. Smaller, lighter squares indicate individual measurements, while large, solid squares indicate the average value.

This channel is a known location of high outflow (transects T–U in Figure 5). Figure 6 gives a sense of the bank line variability of the system and the presence of channels. Many bends have no identifiable channels at all; however, the presence of floodplain channels is not a requirement for lateral fluxes. For example, there is a long distance on the upstream side of bend 33 over which the river is mostly unbounded by a levee. This particular river bank is prone to overtopping at sub-bankfull discharges, and these wider, unchannelized gaps in the levee can be an important control on lateral exchange (Tull et al., 2022).

4.3 Downstream changes in functional connectivity

Model outputs show the differences in extent and depth of flooding in the domain for the lower discharge scenario (500 m^3/s, Figure 7A) and the higher discharge scenario (1,100 m^3/s, Figure 7B). At 500 m^3/s, the overall increase in water in the floodplain with distance downstream is evident. The deeper lakes and floodplain basins are inundated, particularly closer to the bay. However, many parts of the upstream floodplain remain dry, while the higher levees along the length of the river remain much drier than the deeper parts of the floodplain along the valley walls. At 1,100 m^3/s, the river stage is just below bankfull and nearly the entire valley is inundated. Exceptions include a few of the high elevation, Pleistocene scroll bars just south of Liberty, TX, the highest levees in the system, and some of the island topography in the delta. The presence of dry land in the delta even at a much higher discharge illustrates how flows are attenuated and spread out as they approach the bay. The diversity in floodplain topography is evident under the high discharge conditions, which is part of the motivation behind studying unique flow paths and residence times through the floodplain.

4.3.1 Inundated area and volumes within river bank zones

For a steady discharge of 500 m^3/s, inundated area in river bank zones generally increases with distance downstream (Figure 8A). However, the increase is not monotonic, and instead exhibits several distinct groups of consecutive bends with similar inundated river bank area, with lower inundated area upstream and downstream of the bend group. On the west side of the river in particular (right bank), the bend with the highest percent inundated area is located just upstream of CWA Bluff (bend 12), far upstream from the delta and almost outside of the backwater reach entirely. It was at this location where we had measured significant return flows in the field. Just after this bluff, though, the inundated area is reduced drastically at river bend 18 (Camp Road) where the levee is massive and there are many deep floodplain channels within the levee. We know from measured discharge data that this bend conveyed a significant fraction of river flow to the floodplain through the network of floodplain channels (Figure 5), and so it is notable that this bend is a major location of lateral exchange even when most of the levee above the channelized portion remains dry.

At higher discharges, the pattern of increasing inundated area downstream is less apparent (Figures 8B, C). Groups of bends with high inundated area are still present at a discharge of 800 m^3/s (Figure 8B), and many of the river bank zones that had relatively less inundated area at 500 m^3/s remain with less inundated area. Notably though, many river bank zones that previously had very little to no inundated area show significant inundated area at this higher discharge. The increase in inundated river bank zones in the upstream reach lessens the overall trend of increasing inundated area toward the delta. At 1,100 m^3/s (Figure 8C), inundated area

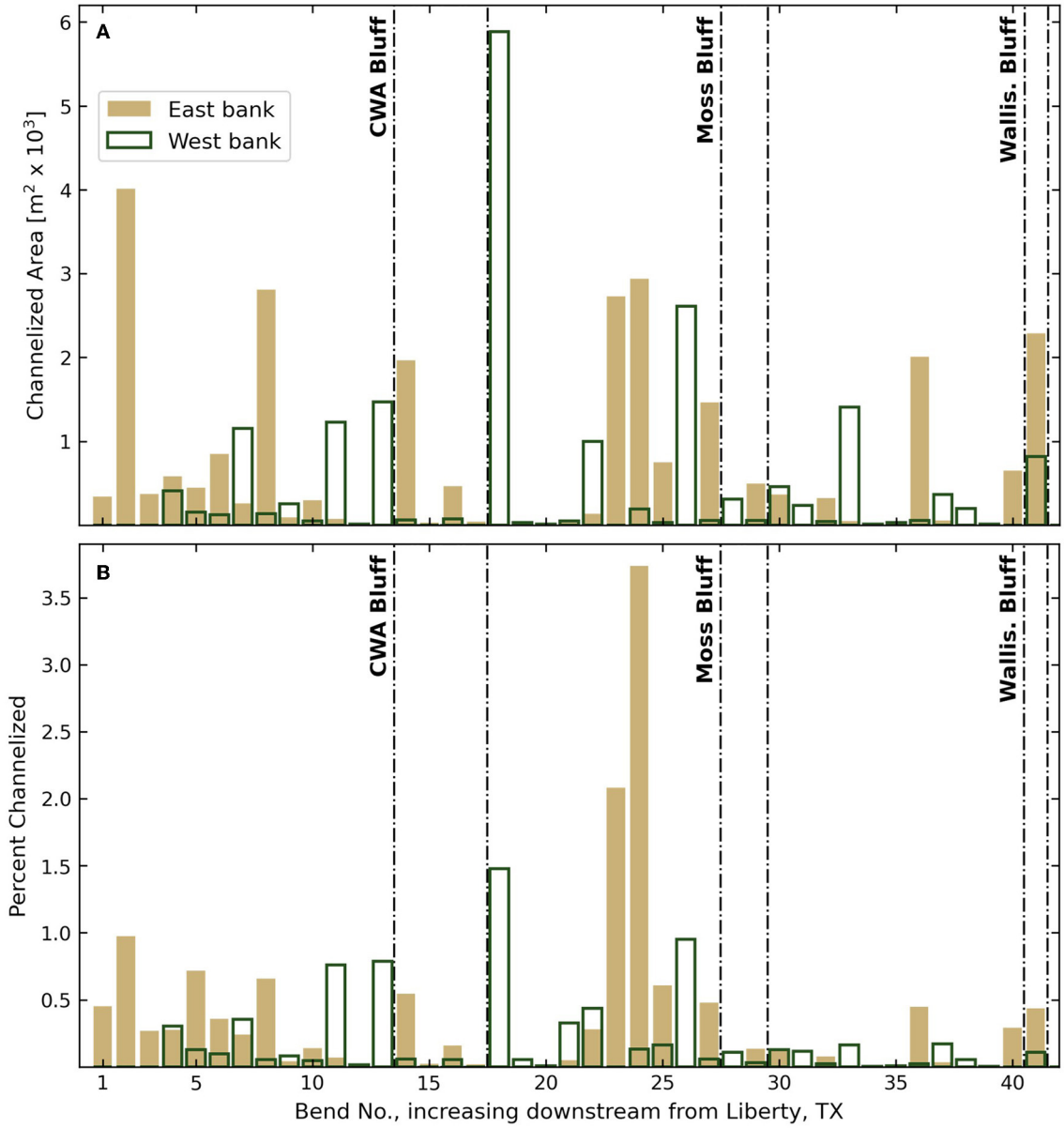

FIGURE 6
(A) Total channelized pixel area and **(B)** percent channelization within the river bank zone at each river bend. CWA Bluff is located on the west bank of the river, while Moss Bluff and Wallisville Bluff are on the east bank.

in river bank zones approaches a bankfull condition, and almost all zones are mostly inundated, with only slightly less inundated area in the upstream reach. One exception is the east side of bend 29. Low inundation at this bend is attributed to the presence of Moss Bluff, which maintains elevations too high for nearly any flood level to reach. Another exception is within the delta (bends 44–49), where inundated area on the west side (the unconfined side) changes only slightly over the range of discharges studied. At higher discharges, excess river flow lost to the floodplain via the Cutoff and Old River Cutoff channels modulates the flow that reaches the delta. Furthermore, the water surface elevation of the bay controls water levels in the delta, preventing significant variation in river bank inundation in the delta over the range of modeled discharges.

Whereas inundated area provides an understanding of river bank topography, the inundation volume metric incorporates information on flow depths within river bank zones, and represents an additional step toward a description of functional connectivity along the river. While inundated area increases with distance downstream for the 500 m^3/s scenario, there is no similar increase in inundation volume in river bank zones (Figure 9A). Instead, inundation volumes along the river bank are substantially higher just upstream of each of the three bluffs in the system: CWA Bluff on the west side, and Moss Bluff and Wallisville Bluff on the east side. This pattern of maximum inundation volume just upstream of bluffs is present across all discharges. These locations upstream of the bluffs are those that were measured in the field as being

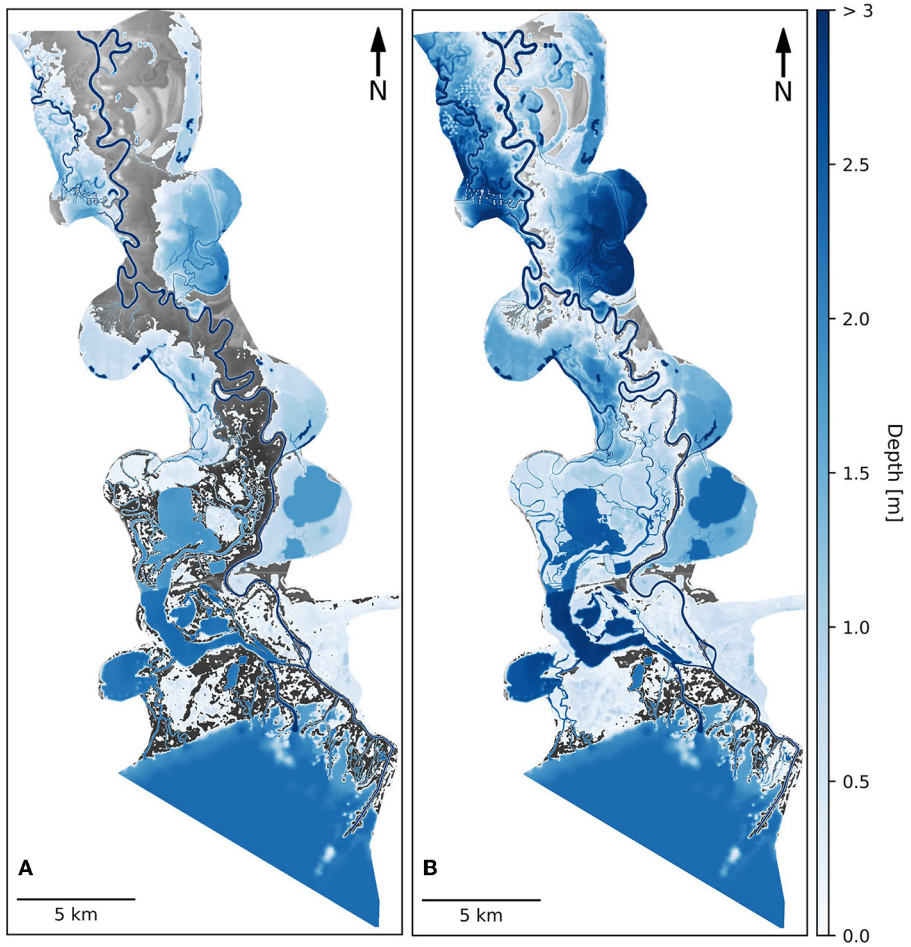

FIGURE 7
Depth maps for model simulations with discharges of **(A)** 500 m^3/s and **(B)** 1,100 m^3/s.

the major locations of return flow back to the river. Interestingly, inundation volumes immediately across the river from the zones of maximum inundation volume are consistently among the lowest in the system. There are almost no locations along the river where inundation volumes are high on both sides.

4.3.2 River-floodplain fluxes through river bank zones

Locations of lateral exchange between the river and the floodplain are also dependent on river bank structure (Figure 10). At a discharge of 500 m^3/s (Figure 10A), lateral exchange only occurs at a few river bends. For example, bends 33 and 36 (corresponding to transects T–U and V–W, Figure 5) include large floodplain channels on the west and east side of the river, respectively, which convey about 1,800 particles (18 m^3/s) and 3,100 particles (31 m^3/s), respectively, to the floodplain under these conditions. Bend 18 on the west side (Camp Road) conveys about 2,700 particles (27 m^3/s) through the network of channels south of CWA Bluff. The largest flux from the river occurs downstream of the USACE control structure on the west side of the river (river right), through the Old River Cutoff (bend 43, see Section 2). The flow through this channel (22,600 particles, or 226 m^3/s) is nearly half of the flow rate moving through the entire domain. Some flow also leaves the river through the passes in the delta ("bend" 47), but not nearly as much as the flow through the larger Old River Cutoff upstream.

It is evident that the locations of flow to the floodplain do not correspond to locations with high or low degrees of river bank zone inundation (Figures 8, 9). Return flows to the river (negative fluxes, Figure 10), however, have a strong correspondence to river bank zones with high inundation volumes, and thus are highly dependent on changes in valley width and proximity to bluffs. At all discharges, locations of return flow are clustered at or just upstream of one of the three bluffs along the river. These locations correspond to the return flow locations observed in the field. Upstream of each bluff there is at least one floodplain channel connected to the river, and the apparent function of these channels is to return water to the river, both for long-lasting "steady" flood events and during the falling limb of a shorter flood event like the one measured in April 2023. The high inundation volumes upstream of each bluff indicate that floodplain water accumulates at these locations, and the modeled fluxes show that this water is forced by the constriction imposed by the bluffs to return to the river. The combination of

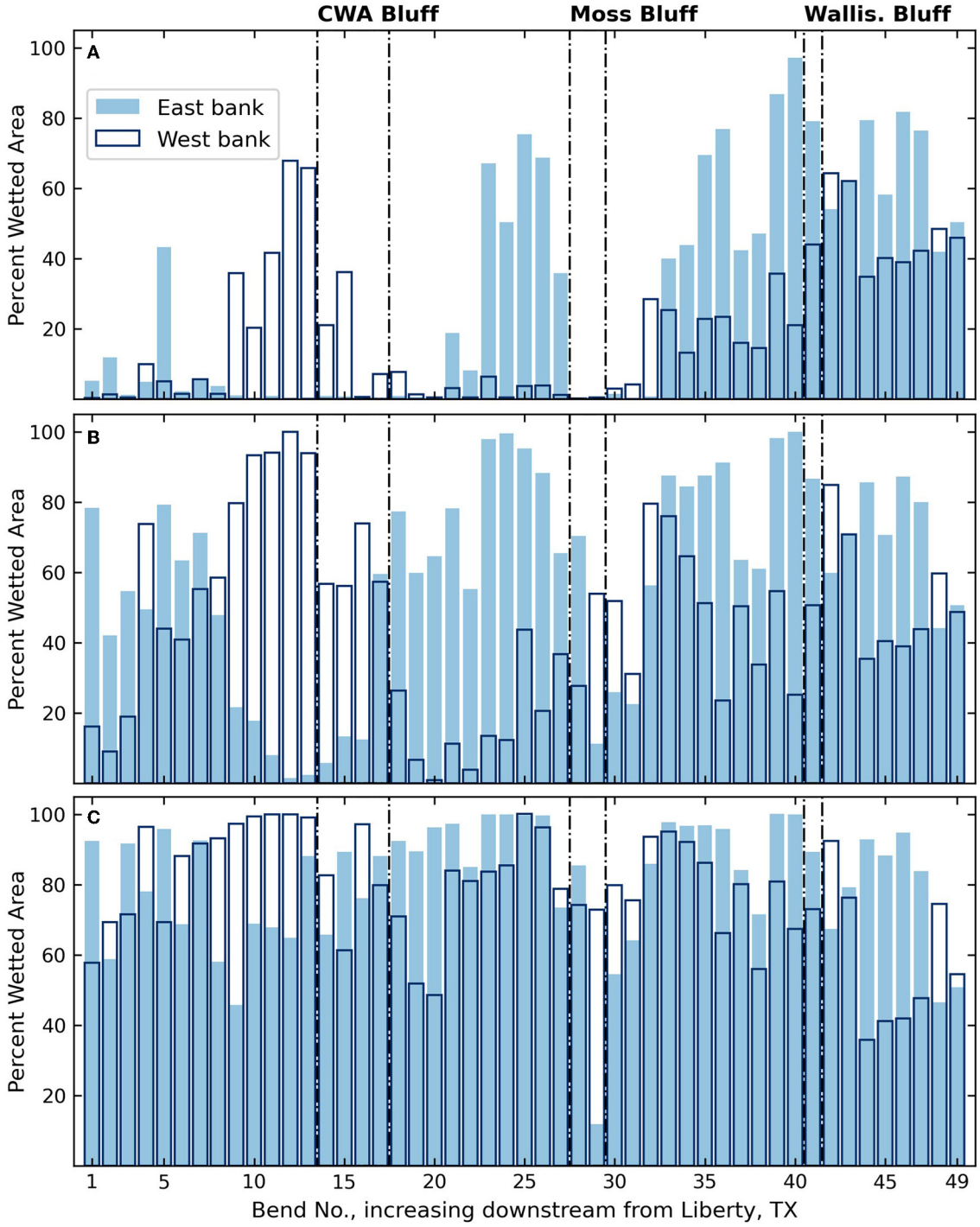

FIGURE 8
Percent inundated area within the river bank zone of each river bend for discharges of **(A)** 500 m^3/s, **(B)** 800 m^3/s, and **(C)** 1,100 m^3/s. CWA Bluff is located on the west bank on the river, while Moss Bluff and Wallisville Bluff are on the east bank.

these two results highlights the importance of the bluffs as major controls on lateral exchange along the river.

At a discharge of 1,100 m^3/s (Figure 10C), lateral exchange occurs at almost every river bend. The flow rates to the floodplain are highly variable, though, and there is a degree of spatial heterogeneity that is not seen in the patterns of inundated area or inundation volume. As discharge approaches bankfull, the inundated area in river bank zones approaches 100 percent (Figure 8C). Even with a nearly full overbank flood event, it is clear that flow into the floodplain is still controlled by the bank line topography. Flow to the floodplain occurs at most river bends, but those with the largest floodplain channels (e.g., west side bends 18

10.3389/frwa.2023.1306481

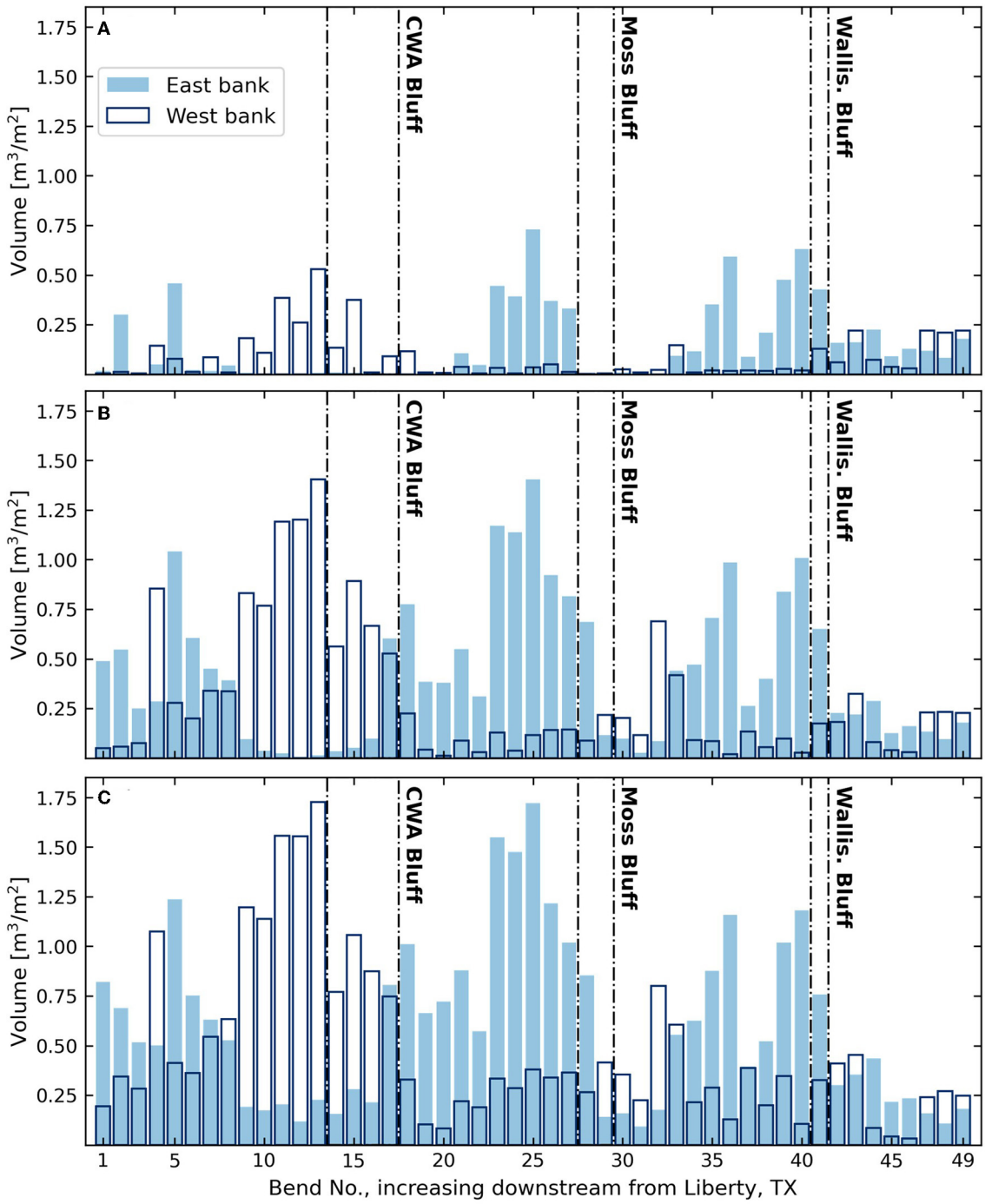

FIGURE 9
Normalized inundation volume within the river bank zone of each river bend (total water volume divided by zone area) for discharges of **(A)** 500 m^3/s, **(B)** 800 m^3/s, and **(C)** 1,100 m^3/s. CWA Bluff is located on the west bank on the river, while Moss Bluff and Wallisville Bluff are on the east bank.

and 33 and east side bend 8) continue to contribute a substantial portion of this flow. In contrast, locations of return flow are fewer, and are controlled less by bank line topography and more by bluffs. These return flow locations are associated with large floodplain channels as well, but we hypothesize that those channels exist in that location because of carving by outflow upstream of the bluffs.

At all discharges, the Old River Cutoff is the location with the largest outward flow (bend 43). The flow through the Old River Cutoff increases with increasing overall discharge, but only slightly. At higher overall discharges, the increased flow to the floodplain at upstream locations reduces the flow in the river at the USACE control structure, and therefore limits the difference in flows moving through the delta among the various discharge scenarios. Therefore, as river discharge at Liberty increases, it is likely that flow would increase more through the Old River Lake to the west of the Trinity

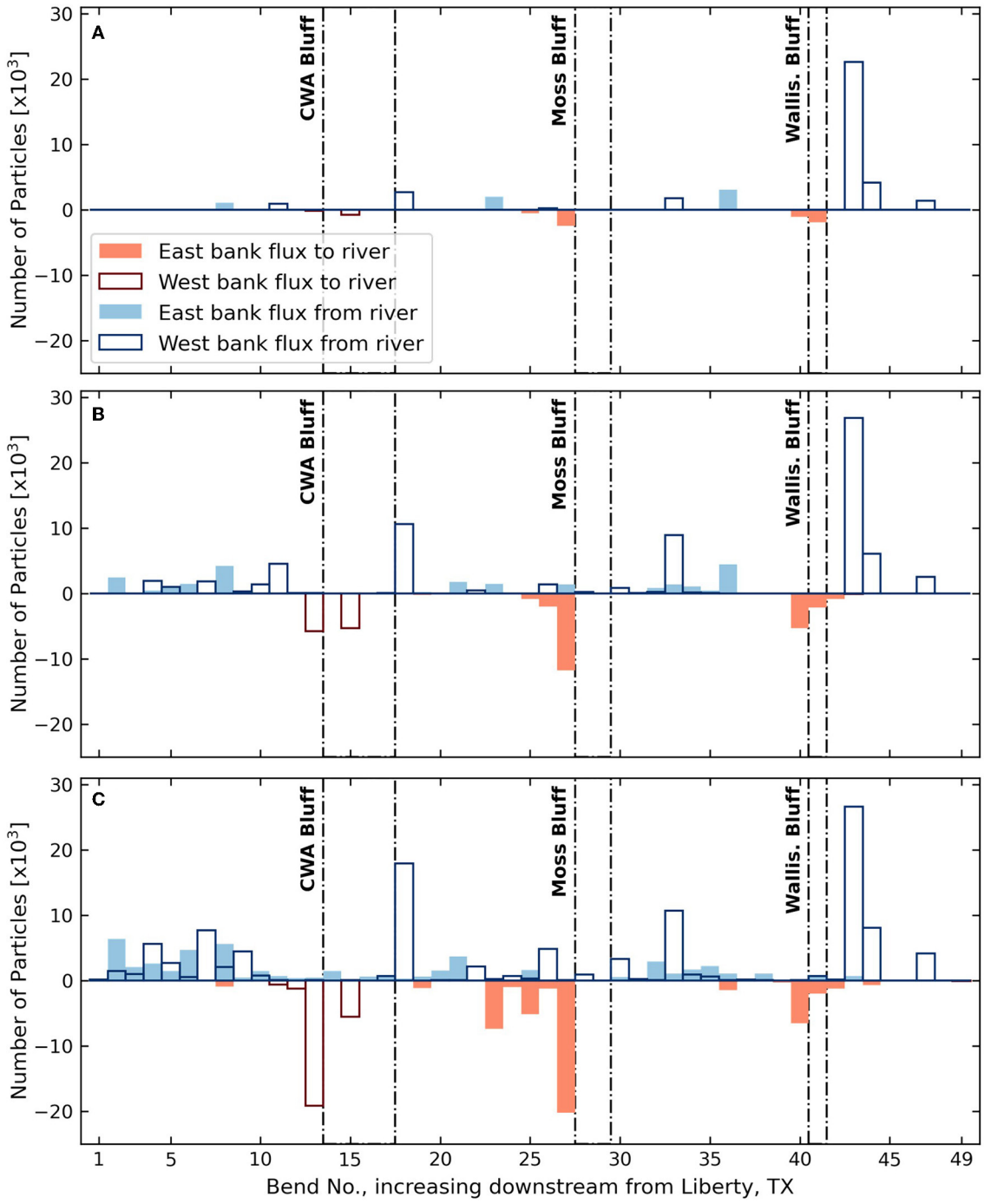

FIGURE 10
Particle fluxes into (negative) and out of the river (positive) through the river bank zone of each river bend for discharges of **(A)** 500 m^3/s, **(B)** 800 m^3/s, and **(C)** 1,100 m^3/s. Particle fluxes are approximately proportional to discharge; an equivalent water flux in m^3/s can be calculated by dividing the number of particles by 100. CWA Bluff is located on the west bank on the river, while Moss Bluff and Wallisville Bluff are on the east bank.

River, rather than continuing to increase in the Trinity River delta.

4.3.3 Floodplain residence times as function of flux location

At 500 m^3/s, lateral exchange on both the east (Figure 11A) and west (Figure 12A) sides of the river is limited to certain bends. But for water that does reach the floodplain, residence times are longer on average than those under higher discharge conditions. One exception is within the delta (bends 43–49, Figure 12A), where residence times are shorter than for those fluxes entering the floodplain farther upstream. Short "residence times" in the delta are to be expected, though, as the residence time definition for these particles is the travel time from when they leave the river to when they reach the bay, which is a relatively short distance. The high

positive skew for these delta particle distributions may be a result of the faster travel times directly to the bay through the distributaries compared to the longer and less frequently traveled paths through the delta islands and estuaries.

With increasing discharge, residence times become more strongly a function of the location where the water (or particles) entered the floodplain. The three bluffs in the study area have been shown to control the locations of return flow to the river, and these return flow locations are less numerous than the number of outflow locations. It follows, then, that for a given particle, the residence time of that particle is dependent on how far upstream of a bluff it entered the floodplain. On the east side of the river, for example, we see more than an order of magnitude difference in residence times among particles entering the floodplain close to the bluff compared to those entering farther upstream (Figures 11B, C). The range of residence times is similar for the floodplain upstream of Moss Bluff and the floodplain upstream of Wallisville Bluff, even though the adjacent river distance is more than twice as long for the former.

The residence time decrease closer to bluffs is not always consistent, though, as the signal of some of the large floodplain channels remains evident within this transition. For example, at 800 m^3/s there is a discontinuity in the decreasing trend of residence times at bend 37 (east side, Figure 11B, transects V–W in Figure 5). Particles entering the floodplain through this channel or upstream of it must flow through Lake Charlotte (Figure 1), which will cause them to take much longer to re-enter the river at the return flow location just upstream of Wallisville Bluff. Particles entering the floodplain downstream of bend 37 via overbank flow (rather than channelized flow) have residence times an order of magnitude less than those of particles from bend 37. Meanwhile, at 500 m^3/s there is no lateral exchange at all downstream of bend 37 (Figure 11A). In this scenario, residence times for particles entering between bends 32 and 37 are significantly longer than those of particles entering via the same bends at higher discharges, as the velocities in the floodplain at lower discharges are lower. The difference in residence times at 500 m^3/s for east side bends 23 and 25 is also notable, where each bend contains a large floodplain channel; particles from bend 23 have an opportunity to circulate through the deep floodplain upstream of Moss Bluff before returning to the river, while those from bend 25 return almost immediately to the river (Figure 11A). This difference is limited at 800 m^3/s, and the outward flux at bend 23 is completely eliminated at 1,100 m^3/s, as the flow direction is reversed due to the greater floodplain flows returning to the river upstream of Moss Bluff.

Upstream of CWA Bluff on the west side of the river, there is a decrease in residence time over two orders of magnitude for discharges between 800 and 1,100 m^3/s (Figures 12B, C). CWA Bluff is the only bluff on this side of the river, and downstream of this bluff there is no such systematic decrease in residence times. In fact, particles that move to the west floodplain downstream of CWA Bluff never return to the river (no negative fluxes on the west side in Figure 10), and instead flow through the Old River Lake and into Trinity Bay. At a discharge of 1,100 m^3/s, particles entering the floodplain from bend 18 (Camp Road, transects F–G in Figure 5) took an average of 71 hours to reach the bay, while those from bend 41 just upstream of the USACE compound spent an average of 76 hours in the floodplain (Figure 12C). While the total distance traveled for particles originating from bend 18 is substantially longer, their shared path through the system of large lakes and estuaries near the bay is likely where net movement toward the bay is the slowest, and so the residence times are similar. For particles leaving the river at bend 43 (within and just downstream of the USACE compound, including the Old River Cutoff), the average residence time drops to 3 h, indicating that the path through the Old River Cutoff is likely the fastest path in the delta. At the very next bend downstream of Old River Cutoff (bend 44), the average jumps back up to 30 hours, as some of the less-frequented paths through the delta islands can be slower.

5 Discussion and conclusions

5.1 Directionality of lateral exchange

The discharge data measured under sub-bankfull conditions (Figure 5) show that there are certain locations along the Trinity River that are largely responsible for bringing flow to the floodplain, and others that are predominantly locations of return flow. We had expected that many floodplain channels and other gaps in the levee where water moved to the floodplain during the rising limb would then bring water back to the river as the flood receded. While we do not know where flow moved to the floodplain prior to our field campaign in April 2023, we did observe only two or three locations where flow was re-entering the river, even as the flood receded. The biggest measured changes in river flow were all flows to the floodplain. Within the backwater reach of the Trinity River, the expected return flows associated with a falling flood wave are counteracted by the increased opportunities for lateral exchange as the normal water surface elevation approaches the elevation of the river bank closer to the bay. In effect, the majority of locations with large pathways between the river and floodplain are predominantly outflow locations. Locations of return flow exist but they are fewer than outflow locations. Furthermore, the magnitude of return flows from the floodplain is significantly less than the flows leaving the river elsewhere (under unsteady conditions).

Model simulations of steady flow conditions illustrate a similar finding, where lateral exchange is dominated by the number of outflow locations, and the return flow locations are limited. Of course, under steady conditions the flow into a floodplain segment must equal the flow out. Only in the floodplain west of the Trinity River and south of CWA Bluff is there a net flow loss, as these flows do not return to the river at any point downstream.

We have identified locations along the river where return flow occurs, in situations where the river stage is falling (Figure 5) and under steady flow conditions (Figure 10). However, it is not certain how these channels would function during the rising limb of a flood event, and whether they would reverse direction after the river-floodplain gradient equalizes or if they would always function as return flow channels. The return flux just upstream of Moss Bluff is the largest single return flux in any of the simulations (bend 27 on east bank, Figure 10), but discharge measurements showed that the return flux here was the least of the three bluff locations (transect N, Figure 5). This discrepancy is partly explained by the presence of other features at this bend that were removing river flow, including the pump station at Moss Bluff and a few nearby floodplain channels. A bigger factor, though, could be the difference

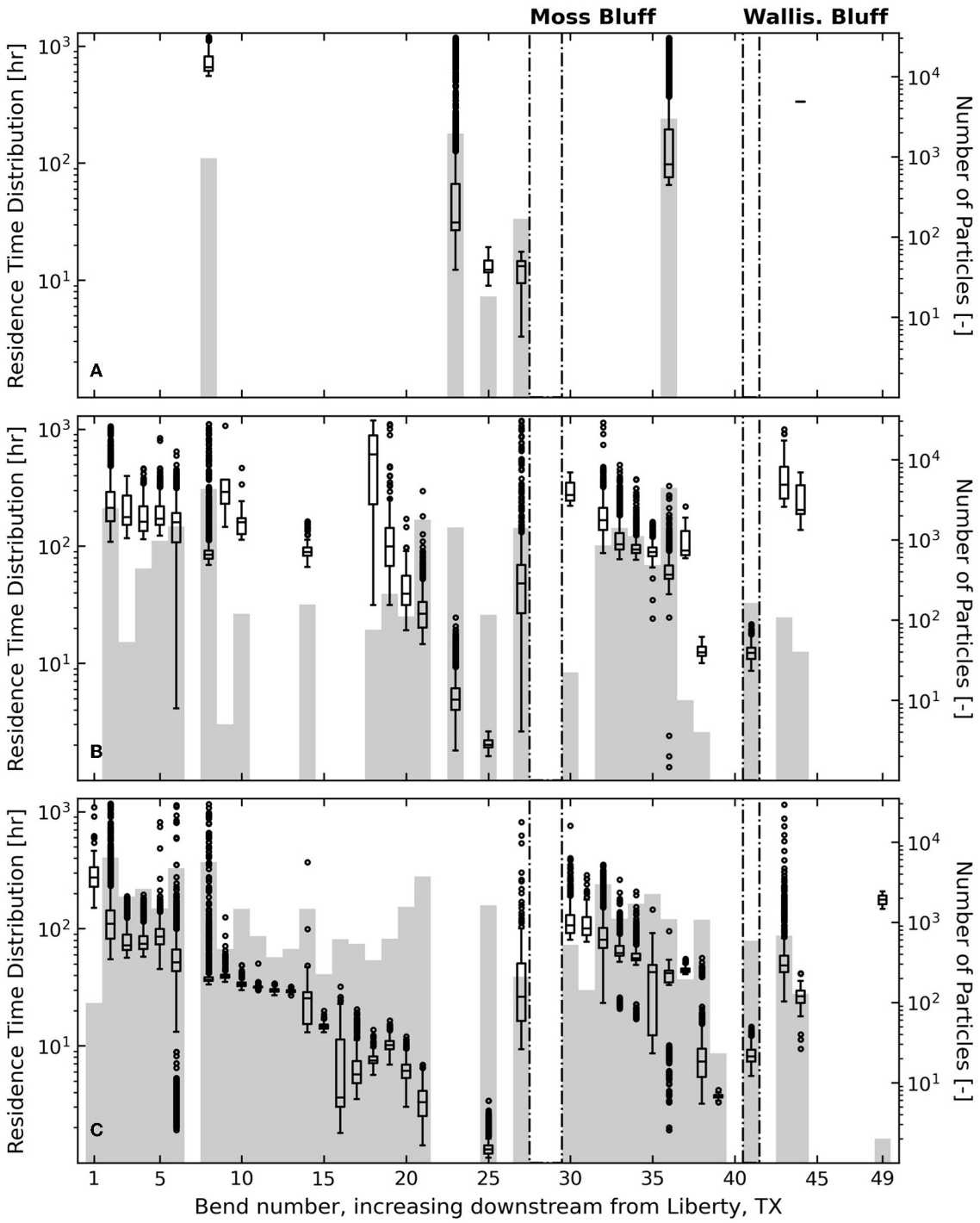

FIGURE 11
Residence time distributions (box plots) for particles that leave the river through the river bank zone of each river bend on the *east* side of the river for discharges of **(A)** 500 m^3/s, **(B)** 800 m^3/s, and **(C)** 1,100 m^3/s. Gray bars underneath indicate the number of particles associated with each distribution.

in the river-floodplain hydraulics at steady-state compared to the falling limb of a flood of shorter duration. The steady flow models give insight into lateral exchange dynamics under a given set of conditions; future work could explore how lateral flow directions and magnitudes transition from the rising limb to the falling limb of a flood event.

5.2 Controls imposed by bluffs

While river bank topography has been shown in many contexts to be an important control on lateral exchanges during sub-bankfull flows (Byrne et al., 2019; Czuba et al., 2019; Lindroth et al., 2020; Tull et al., 2022; van der Steeg et al., 2023), this study is the first

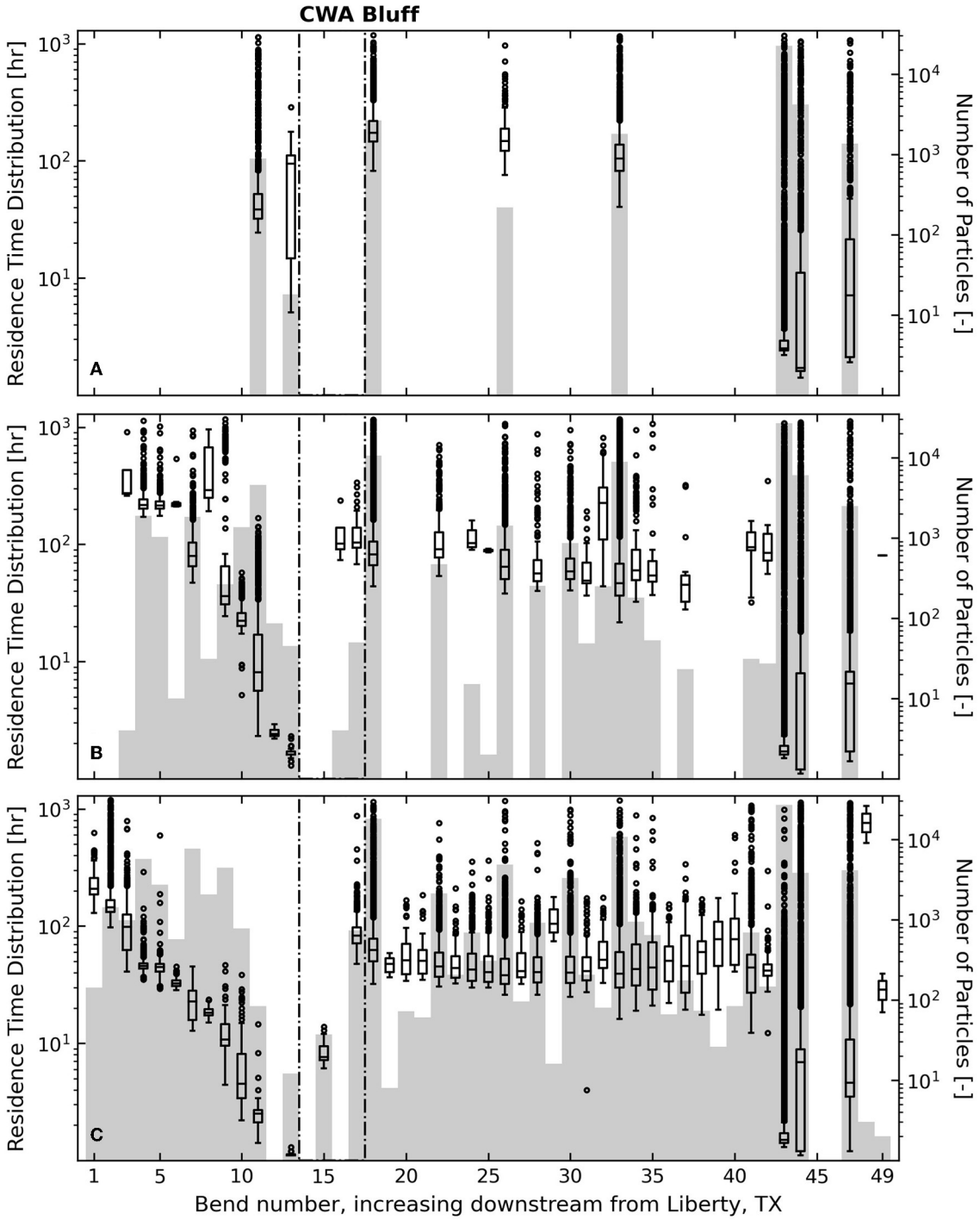

FIGURE 12
Residence time distributions (box plots) for particles that leave the river through the river bank zone of each river bend on the *west* side of the river for discharges of **(A)** 500 m^3/s, **(B)** 800 m^3/s, and **(C)** 1,100 m^3/s. Gray bars underneath indicate the number of particles associated with each distribution.

to show that bluffs along the river are even stronger controls on where and how much water moves between the river and the floodplain. The bluffs function as break points for the floodplain, as no floodplain exists between the high bluff topography and the river. Thus, any water that does not infiltrate or leave the floodplain via other means is forced to return back to the river upstream of the bluff (Figures 5, 10). Furthermore, these return locations are typically adjacent to deep floodplain basins where water collects upstream of the bluff (Figures 7, 9, 10).

Along the Trinity River, including the reaches upstream of the study region, the valley width oscillates in such a way that there is no instance of two bluffs directly across from each other. At the northern boundary of the model domain, the city of Liberty is located on a bluff on the east side of the river while the west

floodplain continues north from the domain (there is a highway embankment at the domain boundary, but there are several culverts that pass floodwaters underneath). The uneven distribution of bluffs along the river is counterbalanced by an uneven distribution of deep floodplain basins. These basins represent vast reservoirs that support ecosystems and remove nutrients from river water (Castillo, 2020), and the travel times through these basins can be several hundreds of hours (Figures 11, 12). This oscillatory pattern is extremely evident from the model results of inundation volume in river bank zones (Figure 9), where there are no locations where inundation volumes are high on both sides of the river. The high water volumes at these return flow locations are in contrast to the lesser volumes in the river bank zones where water moves to the floodplain. This discrepancy highlights the different flow mechanisms associated with outflow and return flow locations, where the former tends to be channelized flow or flow through smaller gaps in the levee and the latter tends to be unchannelized flow. Although there are large floodplain channels at each of the return flow locations within the study area, it is likely that these channels function as simple tributaries under non-flood conditions, bringing direct runoff from the floodplain to the river. Of course, water also flows into the river through these channels under flood conditions, but high inundation volumes associated with these locations during flood conditions indicate that return flow occurs over a wider area and not just through the channels themselves.

At higher discharges, floodplain residence times vary over two orders of magnitude, depending on the proximity to a bluff that a particle enters the floodplain. For the section of floodplain downstream of the last bluff, residence times are much less dependent on lateral flux location. Deep water that collects just upstream of bluffs creates a slow moving environment that increases residence times, and therefore particles entering upstream of those basins spend several hundreds of hours in the floodplain, while those entering much closer to the return flow location spend less than ten hours in the floodplain. This finding shows that two locations of lateral connectivity along a river reach may have very different functions. For example, a flux occurring far upstream from a bluff could have a disproportionate contribution to important floodplain processes like flood attenuation, water treatment, and fine sediment deposition. It is possible that a lateral connection closer to a bluff could have an equivalent flux magnitude toward the floodplain, but those waters "short-circuit" the floodplain basin too quickly to contribute meaningfully to the ecosystem.

5.3 Controls imposed by river bank topography

Bluffs are a major control on the locations of return flow to the river, and by extension, residence times in the floodplain. Still, variable river bank topography plays an important role in facilitating river-floodplain connectivity. While it is understood that gaps in the levee allow flow to move between the river and the floodplain at sub-bankfull river discharge, the results of this study show that there can be floodplain channels or other bank line gaps that impose more of a control on floodplain hydrodynamics than others. For example, the floodplain channel on the east side of bend 36 is a sort of break point feature that modifies the residence times for fluxes entering the floodplain downstream of that point (Figure 11). The Old River Cutoff remains a major control on the circulation in the delta (Figure 12, although this dynamic is partly a result of the influence of the USACE compound, see Section 5.4). Lastly, the largest gaps in the levee remain a first-order control on river-floodplain connectivity under lower discharge conditions, such as at 500 m^3/s. Return flow locations are still bluff-adjacent under these conditions, but the distribution of outflow locations is limited to only the largest openings along the river bank. It is these features that extend the range of discharges at which the river is connected to its floodplain.

Furthermore, inundated area is not necessarily indicative of functional connectivity, whether the inundation is in the river bank zones or deeper in the floodplain. Fluxes between the river and floodplain can occur through narrow channels within high levees that otherwise remain mostly dry. In other words, the areal extent of inundation in a river valley may not be indicative of active transport across the river-floodplain boundary, especially when water can arrive to the floodplain from other sources (Mertes, 1997; Tull et al., 2022). For almost all applications, it is critical to quantify the fluxes through or over the bank when evaluating the hydrological connectivity of a system.

5.4 Abrupt transition points in the system

The similarity in residence times for fluxes occurring downstream of CWA Bluff on the west side (Figures 12B, C) stands in stark contrast with the residence time distributions upstream of each of the three bluffs. CWA Bluff marks the point along the Trinity River where flow never returns to the main river, at least not for sub-bankfull discharges. Downstream of this point, the floodplain transitions to a connected system of rivers, lakes, and estuaries (Old River Lake, Figure 1), which represents an alternate conveyance pathway to the bay. In fact, this estuary has built out its own delta in the bay.

The existence of this delta that is somewhat separate from the main-thread Trinity River highlights two transition points within the system: CWA Bluff and the USACE control structure at Wallisville. The deltas formed by the Trinity River and the Old River are connected hydraulically via the Old River Cutoff, but the constriction at the control structure represents a discontinuity along the river that has likely prevented the delta from growing as a single system. Instead, a fraction of the flow exiting the control structure moves west through the Old River Cutoff, and at higher discharges, this flow diversion is significantly greater than the flow that continues through the Trinity River. This observation implies that there is a limited hydraulic capacity through the USACE compound and that the Old River Cutoff is a necessary feature for equalizing the discharge just downstream of the compound. The capacity of the channel here is also notable because the compound begins just downstream of one of the three major return flow locations along the river (Wallisville Bluff). Whereas just downstream of CWA Bluff and Moss Bluff there are locations where water can leave the river again, downstream of Wallisville

Bluff the USACE compound embankments do not allow water to freely leave the river. In other words, water that returns to the river upstream of Wallisville Bluff cannot leave the river until it reaches the Old River Cutoff, where there is a high proportion of flow that leaves the river (Figure 10, bend 43, west side). Thus, the 6-rkm constriction of the channel through the USACE compound represents an abrupt system transition. Meanwhile, CWA Bluff represents a different kind of abrupt transition: a major change in topography where levees are larger downstream and outflows from the river eventually reach the Old River delta rather than the Trinity River delta.

The combination of a limited capacity through the USACE compound and the increased floodplain flows downstream of CWA Bluff compared to other points along the river (Figures 10B, C) results in a system where excess flow is diverted to the Old and Lost Rivers. As discharge increases, we see minimal changes in river bank inundation and lateral fluxes in the delta reach (Figures 8–10). This result is consistent with earlier findings that discharges of approximately 600 to 1,100 m^3/s convert the Old River Lake into the primary pathway for freshwater to enter the bay (Lucena and Lee, 2022).

5.5 Insights for floodplain management

The findings from this study provide insights for the management of floodplain ecosystems. The oscillatory, down-valley pattern of river-floodplain fluxes and inundation (Figure 9, Section 5.2) illustrates a need to quantify connectivity on both sides of the river. Floodplain basins directly upstream of bluffs are deep and contain large volumes of water, but there are no locations were those deep basins are situated directly across the river from each other, because there are no bluffs situated directly across the river from each other. We also assume that floodplain ecosystems, including types of vegetation, soil types, and quantities of sequestered carbon, vary in the downstream direction. It is likely that the ecosystems in deep floodplain basins upstream of bluffs differ from those in drier areas farther upstream. This ecosystem heterogeneity in relation to the river valley structure is going to be dependent on a river bank with sufficient lateral connections on both sides of the river. Distinguishing floodplain ecosystems adjacent to bluffs with those farther upstream, as well as locations of river-floodplain fluxes along the river, should be considered in river restoration designs as an important feature of natural river systems.

The relationship between bluff proximity and residence times also has implications for the management of floodplains. Our results show that floodplain ecosystem services, such as nutrient removal, do not occur uniformly. Moreover, inundation and water movement through the floodplain depend critically on the location of valley constrictions, or bluffs. Certain areas of floodplains can be responsible for a disproportionate amount of water treatment and flood storage, as some locations of lateral exchange produce longer residence times in the floodplain while exchanges at other locations enter and leave the floodplain quickly. We recommend that these spatial differences be a factor in the decision-making process when development or other activity on the floodplain is under consideration.

5.6 Insights for river systems with similar characteristics

This study focuses on the hydraulics and topography of the lower Trinity River, but many other river systems share similar characteristics. The Sabine and Neches Rivers and even the smaller San Antonio and Mission Rivers are examples of other systems along the Texas coast where the main channel flows from one edge of the floodplain to the other as it moves downstream, and is bounded by oscillating floodplain segments and bluffs. It is likely that the delivery of water, sediment, and nutrients to the bays along the Texas coast is controlled by these similar topographic constraints. The location of the river with respect to the valley walls should be an important consideration for the management and study of many rivers in the region.

The results of this study have implications for systems outside of the region as well, including inland rivers and floodplains that were formed under very different geologic conditions. Recently studied floodplains in the midwest U.S. (East Fork White River, Indiana and Upper Sangamon River, Illinois) exhibit a similar dynamic of river positioning within the valley that certainly plays a role in how floodplain flow returns to the river (Czuba et al., 2019; Lindroth et al., 2020). Even though the East Fork White River floodplain consists of topography formed by glacial retreat (David et al., 2017), it remains a low-gradient river with similar variability in floodplain width. The management goals of this predominately agricultural floodplain may be different from those of the lower Trinity River, but the return flow and residence time dynamics are likely similar and of critical importance in each system. River valley structure is an important geomorphic control in many other river systems as well, such as the Lockyer Creek in Australia (Croke et al., 2013) and the Solimões-Amazon River in Brazil (Mertes et al., 1996); the current study provides an understanding of how floodplain flow dynamics change based on proximity to valley contractions.

Data availability statement

The models used in this study are open source and available freely. ANUGA is available at https://github.com/GeoscienceAustralia/anuga_core and `dorado` is available at https://github.com/passaH2O/dorado. Raw data and model files supporting the conclusions of this article will be made available by the authors, without undue reservation.

Author contributions

NT: Conceptualization, Data curation, Investigation, Methodology, Writing – original draft, Writing – review & editing. AM: Conceptualization, Writing – review & editing, Methodology. PP: Conceptualization, Writing – review & editing, Funding acquisition, Supervision.

Funding

The author(s) declare financial support was received for the research, authorship, and/or publication of this

article. This work was supported by the National Science Foundation (grant no. EAR-2150975) and Texas Water Development Board (contract no. 2000012435). AM was supported by National Science Foundation Postdoctoral Fellowship (grant no. EAR-1952772). All modeling was performed using resources provided by the Extreme Science and Engineering Discovery Environment (XSEDE), which was supported by the National Science Foundation (grant no. ACI-1548562).

Acknowledgments

The authors acknowledge the Texas Advanced Computing Center (TACC) at the University of Texas at Austin for providing HPC resources that have contributed to the research results reported within this paper (http://www.tacc.utexas.edu). The authors would also like to acknowledge Jayaram Hariharan, Kyle Wright, Mariel Nelson, Hima Hassenruck-Gudipati, David Mohrig, Ben Hodges, and Tian Dong for their feedback on this research, as well as Dan Duncan, Marcy Davis, and Mariel Nelson for their help with field data collection.

Conflict of interest

The authors declare that the research was conducted in the absence of any commercial or financial relationships that could be construed as a potential conflict of interest.

Publisher's note

All claims expressed in this article are solely those of the authors and do not necessarily represent those of their affiliated organizations, or those of the publisher, the editors and the reviewers. Any product that may be evaluated in this article, or claim that may be made by its manufacturer, is not guaranteed or endorsed by the publisher.

Supplementary material

The Supplementary Material for this article can be found online at: https://www.frontiersin.org/articles/10.3389/frwa.2023.1306481/full#supplementary-material

References

Aufdenkampe, A. K., Mayorga, E., Raymond, P. A., Melack, J. M., Doney, S. C., Alin, S. R., et al. (2011). Riverine coupling of biogeochemical cycles between land, oceans, and atmosphere. *Front. Ecol. Environ*. 9, 53–60. doi: 10.1890/100014

Battin, T. J., Luyssaert, S., Kaplan, L. A., Aufdenkampe, A. K., Richter, A., and Tranvik, L. J. (2009). The boundless carbon cycle. *Nat. Geosci*. 2, 598–600. doi: 10.1038/ngeo618

Bracken, L. J., Wainwright, J., Ali, G., Tetzlaff, D., Smith, M. W., Reaney, S. M., et al. (2013). Concepts of hydrological connectivity: Research approaches, pathways and future agendas. *Earth-Sci. Rev*. 119, 17–34. doi: 10.1016/j.earscirev.2013.02.001

Byrne, C. F., Stone, M. C., and Morrison, R. R. (2019). Scalable flux metrics at the channel-floodplain interface as indicators of lateral surface connectivity during flood events. *Water Resour. Res*. 55, 9788–9807. doi: 10.1029/2019WR026080

Castillo, M. M. (2020). Suspended sediment, nutrients, and chlorophyll in tropical floodplain lakes with different patterns of hydrological connectivity. *Limnologica* 82, 125767. doi: 10.1016/j.limno.2020.125767

Cheng, F. Y., and Basu, N. B. (2017). Biogeochemical hotspots: Role of small water bodies in landscape nutrient processing. *Water Resources Research* 53, 5038–5056. doi: 10.1002/2016WR020102

Covino, T. (2017). Hydrologic connectivity as a framework for understanding biogeochemical flux through watersheds and along fluvial networks. *Geomorphol*. 277, 133–144. doi: 10.1016/j.geomorph.2016.09.030

Croke, J., Fryirs, K., and Thompson, C. (2013). Channel-floodplain connectivity during an extreme flood event: Implications for sediment erosion, deposition, and delivery. *Earth Surf. Proc. Landf*. 38, 1444–1456. doi: 10.1002/esp.3430

Czuba, J. A., David, S., Edmonds, D. A., and Ward, A. S. (2019). Dynamics of surface-water connectivity in a low-gradient meandering river floodplain. *Water Resourc. Res*. 55, 1849–1870. doi: 10.1029/2018WR023527

David, S. R., Edmonds, D. A., and Letsinger, S. L. (2017). Controls on the occurrence and prevalence of floodplain channels in meandering rivers. *Earth Surf. Proc. Landf*. 42, 460–472. doi: 10.1002/esp.4002

Gurnell, A. M., Corenblit, D., de Jalón, D. G., del Tánago, M. G., Grabowski, R. C., O'Hare, M. T., et al. (2016). A conceptual model of vegetation–hydrogeomorphology interactions within river corridors. *River Res. Applic*. 32, 142–163. doi: 10.1002/rra.2928

Hariharan, J., Wright, K., Moodie, A., Tull, N., and Passalacqua, P. (2023). Impacts of human modifications on material transport in deltas. *Earth Surf. Dyn*. 11, 405–427. doi: 10.5194/esurf-11-405-2023

Hariharan, J., Wright, K., and Passalacqua, P. (2020). *dorado*: a Python package for simulating passive Lagrangian particle transport in shallow-water flows. *J. Open Source Softw*. 5, 2585. doi: 10.21105/joss.02585

Harvey, J., and Gooseff, M. (2015). River corridor science: Hydrologic exchange and ecological consequences from bedforms to basins. *Water Resour. Res*. 51, 6893–6922. doi: 10.1002/2015WR017617

Hassenruck-Gudipati, H. J., Passalacqua, P., and Mohrig, D. (2022). Natural levees increase in prevalence in the backwater zone: Coastal Trinity River, Texas, USA. *Geology* 50, 1068–1072. doi: 10.1130/G50011.1

Helton, A. M., Poole, G. C., Payn, R. A., Izurieta, C., and Stanford, J. A. (2014). Relative influences of the river channel, floodplain surface, and alluvial aquifer on simulated hydrologic residence time in a montane river floodplain. *Geomorphology* 205, 17–26. doi: 10.1016/j.geomorph.2012.01.004

Hiatt, M., Castaneda-Moya, E., Twilley, R., Hodges, B. R., and Passalacqua, P. (2018). Channel-island hydrological connectivity affects exposure time distributions in a coastal river delta. *Water Resourc. Res*. 54, 2212–2232. doi: 10.1002/2017WR021289

Hiatt, M., and Passalacqua, P. (2015). Hydrological connectivity in river deltas: The first-order importance of channel-island exchange. *Water Resourc. Res*. 51, 2264–2282. doi: 10.1002/2014WR016149

Holland, J. F., Martin, J. F., Granata, T., Bouchard, V., Quigley, M., and Brown, L. (2004). Effects of wetland depth and flow rate on residence time distribution characteristics. *Ecol. Eng*. 23, 189–203. doi: 10.1016/j.ecoleng.2004.09.003

Hughes, F. M. R., Adams, W. M., Muller, E., Nilsson, C., Richards, K. S., Barsoum, N., et al. (2001). The importance of different scale processes for the restoration of floodplain woodlands. *Regul. Riv*. 17, 325–345. doi: 10.1002/rrr.656

Kaushal, S. S., Groffman, P. M., Mayer, P. M., Striz, E., and Gold, A. J. (2008). Effects of stream restoration on denitrification in an urbanizing watershed. *Ecol. Applic*. 18, 789–804. doi: 10.1890/07-1159.1

Kondolf, G. M., Boulton, A. J., O'Daniel, S., Poole, G. C., Rachel, F. J., Stanley, E. H., et al. (2006). Process-based ecological river restoration: Visualizing three-dimensional connectivity and dynamic vectors to recover lost linkages. *Ecol. Soc*. 11, 17. doi: 10.5751/ES-01747-110205

Kufel, L., and Leśniczuk, S. (2014). Hydrological connectivity as most probable key driver of chlorophyll and nutrients in oxbow lakes of the Bug River (Poland). *Limnologica* 46, 94–98. doi: 10.1016/j.limno.2013.10.008

Liang, M., Geleynse, N., Edmonds, D. A., and Passalacqua, P. (2015a). A reduced-complexity model for river delta formation - Part II: Assessment of the flow routing scheme. *Earth Surf. Dyn*. 3, 87–104. doi: 10.5194/esurf-3-87-2015

Liang, M., Voller, V. R., and Paola, C. (2015b). A reduced-complexity model for river delta formation - Part I: Modeling deltas with channel dynamics. *Earth Surf. Dyn.* 3, 67–86. doi: 10.5194/esurf-3-67-2015

Lindroth, E. M., Rhoads, B. L., Castillo, C. R., Czuba, J. A., Güneralp, I., and Edmonds, D. (2020). Spatial variability in bankfull stage and bank elevations of lowland meandering rivers: relation to rating curves and channel planform characteristics. *Water Resour. Res.* 56, e2020WR027477. doi: 10.1029/2020WR027477

Lucena, Z., and Lee, M. T. (2022). *Distribution of streamflow, sediment, and nutrients entering Galveston Bay from the Trinity River, Texas, 2016-19*. Technical report, US Geological Survey. doi: 10.3133/sir20225015

Mason, J., and Mohrig, D. (2018). Using time-lapse lidar to quantify river bend evolution on the meandering coastal Trinity River, Texas, USA. *J. Geophys. Res.* 123, 1133–1144. doi: 10.1029/2017JF004492

Mason, J., and Mohrig, D. (2019). Scroll bars are inner bank levees along meandering river bends. *Earth Surf. Proc. Landf.* 44, 2649–2659. doi: 10.1002/esp.4690

Melack, J. M., and Forsberg, B. (2001). "Biogeochemistry of Amazon floodplain lakes and associated wetlands," in *Biogeochemistry of the Amazon Basin and its Role in a Changing World*, eds. M. E. McClain, R. L. Victoria, and J. E. Richey (New York: Oxford University Press), 235–276. doi: 10.1093/oso/9780195114317.003.0017

Mertes, L. A. K. (1997). Documentation and significance of the perirheic zone on inundated floodplains. *Water Resourc. Res.* 33, 1749–1762. doi: 10.1029/97WR00658

Mertes, L. A. K., Dunne, T., and Martinelli, L. A. (1996). Channel-floodplain geomorphology along the Solimões-Amazon River, Brazil. *Geol. Soc. Am. Bull.* 108, 1089–1107. doi: 10.1130/0016-7606(1996)108<1089:CFGATS>2.3.CO;2

Mitsch, W. J., BBernal, B., Nahlik, A. M., Mander, Ü., Zhang, L., Anderson, C. J., et al. (2013). Wetlands, carbon, and climate change. *Landscape Ecol.* 28, 583–597. doi: 10.1007/s10980-012-9758-8

Mungkasi, S., and Roberts, S. G. (2011). "A finite volume method for shallow water flows on triangular computational grids," in *Proceedings 2011 International Conferences Advanced Computer Science and Information System (ICACSIS)* (IEEE), 79–84.

Mungkasi, S., and Roberts, S. G. (2013). "Validation of ANUGA hydraulic model using exact solutions to shallow water wave problems," in *Journal of Physics: Conference Series* 423. doi: 10.1088/1742-6596/423/1/012029

Nielsen, O., Roberts, S., Gray, D., McPherson, A., and Hitchman, A. (2005). "Hydrodynamic modelling of coastal inundation," in *Proceedings of MODSIM 2005*.

Noe, G. B., and Hupp, C. R. (2005). Carbon, nitrogen, and phosphorus accumulation in floodplains of Atlantic Coastal Plain rivers, USA. *Ecol. Applic.* 15, 1178–1190. doi: 10.1890/04-1677

Noe, G. B., and Hupp, C. R. (2009). Retention of riverine sediment and nutrient loads by coastal plain floodplains. *Ecosystems* 12, 728–746. doi: 10.1007/s10021-009-9253-5

Noe, G. B., Hupp, C. R., and Rybicki, N. B. (2013). Hydrogeomorphology influences soil nitrogen and phosphorus mineralization in floodplain wetlands. *Ecosystems* 16, 75–94. doi: 10.1007/s10021-012-9597-0

Passalacqua, P. (2017). The *Delta* Connectome: a network-based framework for studying connectivity in river deltas. *Geomorphology* 277, 50–62. doi: 10.1016/j.geomorph.2016.04.001

Passalacqua, P., Belmont, P., and Foufoula-Georgiou, E. (2012). Automatic geomorphic feature extraction from lidar in flat and engineered landscapes. *Water Resour. Res.* 48, W03528. doi: 10.1029/2011WR010958

Passalacqua, P., Do Trung, T., Foufoula-Georgiou, E., Sapiro, G., and Dietrich, W. E. (2010). A geometric framework for channel network extraction from LiDAR: Nonlinear diffusion and geodesic paths. *J. Geophys. Res.* 115, F01002. doi: 10.1029/2009JF001254

Phillips, J. D. (2010). Relative importance of intrinsic, extrinsic, and anthropic factors in the geomorphic zonation of the Trinity River, Texas. *J. Am. Water Resour. Assoc.* 46, 807–823. doi: 10.1111/j.1093-474X.2010.00457.x

Phillips, J. D., and Slattery, M. C. (2007). Downstream trends in discharge, slope, and stream power in a lower coastal plain river. *J. Hydrol.* 334, 290–303. doi: 10.1016/j.jhydrol.2006.10.018

Phillips, J. D., Slattery, M. C., and Musselman, Z. A. (2004). Dam-to-delta sediment inputs and storage, lower Trinity River, Texas. *Geomorphology* 62, 17–34. doi: 10.1016/j.geomorph.2004.02.004

Phillips, J. D., Slattery, M. C., and Musselman, Z. A. (2005). Channel adjustments of the lower Trinity River, Texas, downstream of Livingston Dam. *Earth Surf. Proc. Landf.* 30, 1419–1439. doi: 10.1002/esp.1203

Rathburn, S. L., Shahverdian, S. M., and Ryan, S. E. (2018). Post-disturbance sediment recovery: implications for watershed resilience. *Geomorphology* 305, 61–75. doi: 10.1016/j.geomorph.2017.08.039

Roley, S. S., Tank, J. L., and Williams, M. A. (2012). Hydrologic connectivity increases denitrification in the hyporheic zone and restored floodplains of an agricultural stream. *J. Geophys. Res.* 117, 1950. doi: 10.1029/2012JG001950

Seitzinger, S., Harrison, J. A., Böhlke, J., Bouwman, A., Lowrance, R., Peterson, B., et al. (2006). Denitrification across landscapes and waterscapes: a synthesis. *Ecol. Applic.* 16, 2064–2090. doi: 10.1890/1051-0761(2006)016[2064:DALAWA]2.0.CO;2

Sheibley, R. W., Ahearn, D. S., and Dahlgren, R. A. (2006). Nitrate loss from a restored floodplain in the lower Cosumnes River, California. *Hydrobiologia* 571, 261–272. doi: 10.1007/s10750-006-0249-2

Shen, Z., Törnqvist, T. E., Mauz, B., Chamberlain, E. L., Nijhuis, A. G., and Sandoval, L. (2015). Episodic overbank deposition as a dominant mechanism of floodplain and delta-plain aggradation. *Geol.* 43, 875–878. doi: 10.1130/G36847.1

Smith, V. B., Mason, J., and Mohrig, D. (2020). Reach-scale changes in channel geometry and dynamics due to the coastal backwater effect: the lower Trinity River, Texas. *Earth Surf. Proc. Landf.* 45, 565–573. doi: 10.1002/esp.4754

Sutfin, N. A., Wohl, E. E., and Dwire, K. A. (2016). Banking carbon: a review of organic carbon storage and physical factors influencing retention in floodplains and riparian ecosystems. *Earth Surf. Proc. Landf.* 41, 38–60. doi: 10.1002/esp.3857

Thoms, M. C. (2003). Floodplain-river ecosystems: lateral connections and the implications of human interference. *Geomorphology* 56, 335–349. doi: 10.1016/S0169-555X(03)00160-0

Tockner, K., Pennetzdorfer, D., Reiner, N., Schiemer, F., and Ward, J. V. (1999). Hydrological connectivity, and the exchange of organic matter and nutrients in a dynamic river-floodplain system (Danube, Austria). *Freshwater Biol.* 41, 521–535. doi: 10.1046/j.1365-2427.1999.00399.x

Tull, N., Passalacqua, P., Hassenruck-Gudipati, H. J., Rahman, S., Wright, K., Hariharan, J., et al. (2022). Bidirectional river-floodplain connectivity during combined pluvial-fluvial events. *Water Resour. Res.* 58, e2021WR030492. doi: 10.1029/2021WR030492

van der Steeg, S., Torres, R., Viparelli, E., Xu, H., Elias, E., and Sullivan, J. C. (2023). Floodplain surface-water circulation dynamics: Congaree River, South Carolina, USA. *Water Resour. Res.* 59, e2022WR032982. doi: 10.1029/2022WR032982

Wainwright, J., Turnbull, L., Ibrahim, T. G., Lexartza-Artza, I., Thornton, S. F., and Brazier, R. E. (2011). Linking environmental regimes, space and time: interpretations of structural and functional connectivity. *Geomorphology* 126, 387–404. doi: 10.1016/j.geomorph.2010.07.027

Walling, D., and Owens, P. (2003). The role of overbank floodplain sedimentation in catchment contaminant budgets. *Hydrobiologia* 494, 83–91. doi: 10.1023/A:1025489526364

Walling, D. E., Owens, P. N., and Leeks, G. J. (1998). The role of channel and floodplain storage in the suspended sediment budget of the River Ouse, Yorkshire, UK. *Geomorphology* 22, 225–242. doi: 10.1016/S0169-555X(97)00086-X

Ward, J. V., Tockner, K., and Schiemer, F. (1999). Biodiversity of floodplain river ecosystems: Ecotones and connectivity. *Regul.Rivers* 15, 125–139. doi: 10.1002/(SICI)1099-1646(199901/06)15:1/3<125::AID-RRR523>3.0.CO;2-E

Welti, N., Bondar-Kunze, E., Singer, G., Tritthart, M., Zechmeister-Boltenstern, S., Hein, T., et al. (2012). Large-scale controls on potential respiration and denitrification in riverine floodplains. *Ecol. Eng.* 42, 73–84. doi: 10.1016/j.ecoleng.2012.02.005

Wohl, E., Brierley, G., Cadol, D., Coulthard, T. J., Covino, T., Fryirs, K. A., et al. (2019). Connectivity as an emergent property of geomorphic systems. *Earth Surf. Proc. Landf.* 44, 4–26. doi: 10.1002/esp.4434

Wohl, E., Lininger, K. B., and Scott, D. N. (2018). River beads as a conceptual framework for building carbon storage and resilience to extreme climate events into river management. *Biogeochemistry* 141, 365–383. doi: 10.1007/s10533-017-0397-7

Wright, K., Hariharan, J., Passalacqua, P., Salter, G., and Lamb, M. P. (2022a). From grains to plastics: Modeling nourishment patterns and hydraulic sorting of fluvially transported materials in deltas. *J. Geophys. Res.* 127, e2022JF006769. doi: 10.1029/2022JF006769

Wright, K., Passalacqua, P., Simard, M., and Jones, C. E. (2022b). Integrating connectivity into hydrodynamic models: an automated open-source method to refine an unstructured mesh using remote sensing. *J. Adv. Model. Earth Syst.* 14, 3025. doi: 10.1029/2022MS003025

Yu, K., DeLaune, R. D., and Boeckx, P. (2006). Direct measurement of denitrification activity in a Gulf coast freshwater marsh receiving diverted Mississippi River water. *Chemosphere* 65, 2449–2455. doi: 10.1016/j.chemosphere.2006.04.046

frontiers | Frontiers in Water

TYPE Original Research
PUBLISHED 15 March 2024
DOI 10.3389/frwa.2024.1255883

OPEN ACCESS

EDITED BY
Dipankar Dwivedi,
Berkeley Lab (DOE), United States

REVIEWED BY
Allen Hunt,
Wright State University, United States
Boris Faybishenko,
Berkeley Lab (DOE), United States

*CORRESPONDENCE
Kyungdoe Han
✉ doe.han@wisc.edu

RECEIVED 10 July 2023
ACCEPTED 05 March 2024
PUBLISHED 15 March 2024

CITATION
Han K and Wilson JL (2024) Deciphering the interplay between tectonic and climatic forces on hydrologic connectivity in the evolving landscapes. *Front. Water* 6:1255883. doi: 10.3389/frwa.2024.1255883

Deciphering the interplay between tectonic and climatic forces on hydrologic connectivity in the evolving landscapes

Kyungdoe Han[1,2]* and John L. Wilson[2]

[1]Department of Civil and Environmental Engineering, University of Wisconsin-Madison, Madison, WI, United States, [2]Department of Earth and Environmental Science, New Mexico Institute of Mining and Technology, Socorro, NM, United States

The intricate interplay between climate and tectonics profoundly shapes landscapes over time frames surpassing 10 million years. Active tectonic processes and climatic shifts unsettle established drainage systems, instigating fragmentation or amalgamation of watersheds. These activities yield substantial transformation in surface hydrologic connectivity, thereby underlining the profound influence of these tectonic and climatic forces on the evolution of both landscape and hydrology. Such transformations within the hydrological landscape have direct implications for the evolution of aquatic species. As connections among aquatic habitats undergo reconfiguration, they incite shifts in species distribution and adaptive responses. These findings underscore the role of tectonics and climate in not only sculpting the physical landscape but also steering the course of biological evolution within these dynamically changing aquatic ecosystems relying on hydrologic connections. Despite the significance of these interactions, scholarly literature seldom examines alterations in hydrologic connectivity over tectonic, or orogen-scale, timescales. This study aims to bridge this gap, exploring changes in hydrologic connectivity over extended periods by simulating a continental rift system akin to the Rio Grande Rift, USA, subject to various tectonoclimatic scenarios. Multiple rift basins hosting large lakes, brought into existence by active tectonic extension, are further molded by tectonic extension and post-rift climatic changes. The study focuses on phenomena such as interbasin river breakthroughs and knickpoint generation, assembling a time-series of connectivity metrics based on stream network characteristics such as flow rate, flow distance, and captured drainage areas. We anticipate that the insights gleaned from this study will enhance our comprehension of the enduring impact of tectonic and climate processes on hydrologic connectivity and the subsequent evolution of aquatic species.

KEYWORDS

surface hydrologic connectivity, landscape evolution, tectonics, climate change, aquatic species evolution

1 Introduction

Tectonic and climatic forces are key drivers of landscape transformation and changes in surface hydrologic connectivity (SHC), which in turn significantly impact the dispersal of aquatic species and can cause habitat fragmentation and species isolation. Understanding the historical changes in SHC is therefore essential for studying the evolutionary history of aquatic species. This research examines SHC changes over 30 *Myrs* in a hypothetical,

semiarid geological rift system, aiming to provide insights into long-term SHC variations and their implications for the evolution of aquatic species.

The concept of SHC and its derived metrics function as indicators of the degree of interconnectedness within a given hydrologic system (e.g., Fullerton et al., 2010; Bracken et al., 2013). Spanning millions of years, tectonic events such as uplift and faulting, along with surface processes like erosion and sediment transport and deposition, are integral in shaping landscapes. These actions develop topographic relief and govern the trajectory of water and sediment movement (e.g., Whipple, 2009; Willett et al., 2014), resulting in alterations in SHC. In parallel, climatic variations, including shifts in atmospheric temperature and precipitation levels, profoundly influence surface processes. These variations impact soil development, vegetation distribution, erosion rates, and the overall hydrologic cycle. The roles of tectonic and climatic processes in landscape evolution have been substantiated through extensive research. For instance, the work of Molnar and England (1990) provides a prime example of how tectonic uplift and subsidence have altered the topography and drainage patterns of the Tibetan Plateau. The interplay between tectonic and climatic processes has been explored in studies like Whipple and Tucker (1999), which investigates the feedback loop between tectonic uplift, erosion, and climate in the Himalayas.

Understanding how tectonic and climatic forces interact with landscape evolution is essential for reconstructing changes in SHC over time. This study investigates the impact of tectonoclimatic forcings on landscape evolution and SHC changes over 30 *Myrs* in a hypothetical rift scenario, paralleling the Rio Grande Rift system (Figure 1). The Rio Grande Rift is segmented, forming a series of rift basins with opposite structural asymmetries (van Wijk et al., 2018). The basins were hydrologically disconnected through most of the rift evolution but since the Late Miocene a through-going river (Rio Grande; Figure 1) has gradually connected the basins (Repasch et al., 2017).

The complex history of hydrologic changes in the evolving rift system is studied using established landscape evolution principles (Willgoose, 2018) through a well-known computer program. Among its other strengths, landscape evolution modeling has been shown to realistically model hydrologic stream networks (e.g., Rodriguez-Iturbe and Rinaldo, 1997), which is essential to the study of HC. The model domain has an area of 40,000 km^2 with 1-*km* resolution to assess the tectonic, topographic, and hydrologic evolution of the landscape. This study analyzes a series of quasi-steady-state snapshots over a 30-*Myr* simulation period, focusing on hydrologically persistent and irreversible conditions rather than short-term transient and event-based simulations. This approach provides insights into the extent of hydrologic disconnections and the resultant divergence of aquatic species over geological timescales, facilitating the simulation of long-term processes. The models developed track significant changes in SHC, such as the formation of a through-going river and the reorganization of drainage basins. The model results provide information on surface water flow, erosion of bedrock and sediment, and transport and deposition of sediment, as well as tectonic processes including faulting and crustal block movement.

The rift extension phase accompanies hydrologic fragmentation (Repasch et al., 2017). Key metrics quantify such sudden shifts in hydrologic connections (i.e., fragmentation). The focus is on how SHC changes, driven by tectonics and climate, influence aquatic species evolution by disconnecting and rerouting aquatic pathways between habitats. We outline four steps of a six-step research framework, tectonoclimatic conceptualization, numerical modeling, statistical analysis, and SHC metric development (red dashed box in Figure 2). These steps help understand the initiation and development of SHC and their impact on the evolution of endemic aquatic species (i.e., a species that is native and restricted to a specific area), exemplified by the Rio Grande cutthroat trout (*Oncorhynchus clarkii virginalis*; Kalb and Caldwell, 2014).

2 Methodology

2.1 Tectonoclimatic landscape evolution model

To simulate changes in surface hydrologic connectivity (SHC) over time, this study employs the landscape evolution software package TISC (Garcia-Castellanos, 2002; Garcia-Castellanos and Jimenez-Munt, 2015), which models tectonic extension and surface processes like erosion and sediment transport. TISC is a quasi-3D, finite-difference code capable of modeling surface hydrology, tectonic motion of crustal bocks, surface erosion, sediment transport and deposition, and isostasy. TISC effectively addresses long-term tectonic evolution and corresponding landscape development, offering a versatile modeling platform tailored to the objectives of this study. Owing to the scarcity of climate data from the distant past and the requirement for substantial computational resources, several simplistic climate scenarios are devised. First, a range of constant climates with different mean annual precipitation (*MAP*), representing dry to wet climates are simulated. Second, climate variations in the post-rift period are modeled by progressively decreasing MAP (see Supplementary material S1).

The general configuration of the model domain builds on the landscape-evolution study conducted by Berry et al. (2019) on endorheic to exorheic transition of a rift basin. In this study, the model is extended to two rift basins (Figure 3). The initial topography has a gentle south or southeast slope of 0.8%–1.2% to represent a hypothetical pre-rift state (Figure 4 and Supplementary Figure S2b), with the initial slope oriented from NW to SE at a 1% gradient in the base case scenario (Figure 4A).

The model domain undergoes an initial spin-up period of 2 *Myrs*, allowing for the establishment of drainage networks prior to the onset of tectonic activity. This is followed by 15–25 *Myrs* of rifting, during which two sedimentary basins form. During this interval, syn-rift changes in SHC due to tectonic processes are analyzed. In the subsequent 5 *Myrs*, changes in connectivity originating from climatic variations are examined. Including the spin-up period, the maximum simulation time is 32 *Myrs*.

The tectonic timestep for simulating isostasy and crustal block movement is set at 0.5 *Myrs*, whereas the surface process timestep, which handles surface flow routing, erosion of bedrock and sediment, and sediment transport, is set at 1,000 *kyrs*. These are typical TISC time steps for the space and time scales of this study.

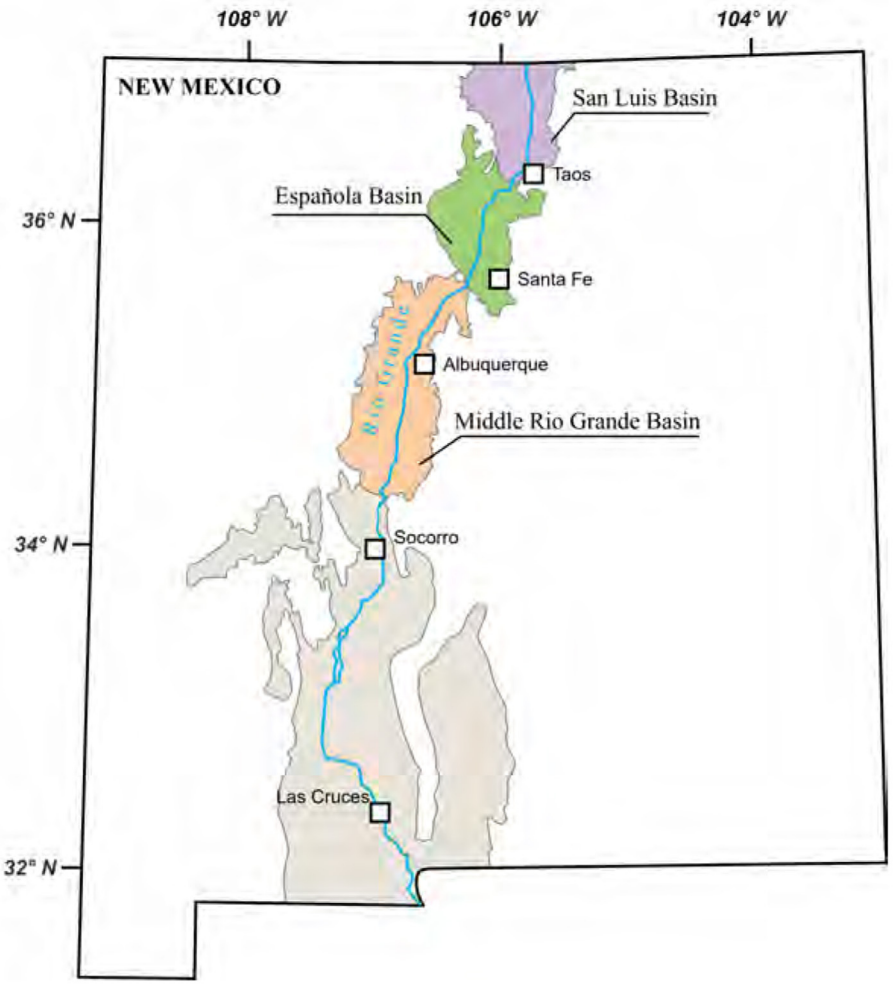

FIGURE 1
An illustrative map depicting the distinct basins within the Rio Grande Rift system, located in New Mexico, USA. Redrawn and modified after Kellogg et al. (2017).

Supplementary materials S1, S2 contain additional information about the model settings (see Supplementary Table S2 for model parameters).

2.2 Construction of rift model and sensitivity cases

A continental rift system is a complex geologic feature that develops due to extensional tectonic forces that cause the lithosphere to stretch and undergo thinning (McKenzie, 1978). These processes give rise to a complex structure characterized by faults, horsts, and grabens, often associated with volcanism (e.g., Corti, 2009). The structure of a rift system can be divided into three principal domains, including the axial, shoulder (e.g., Van Balen et al., 1995), and rift flank (e.g., Masek et al., 1994) domains, each displaying distinct geologic features and vertical motions.

In the model, lakes naturally emerge within rift basins, becoming critical hubs for the interplay between tectonoclimatic forcings. The lakes significantly influence the distribution and cycling of water, nutrients, and energy across their encompassing landscapes (e.g., Downing et al., 2006; Carpenter et al., 2011). The landscape evolution paper by Berry et al. (2019) explores half-graben geometry in a comparable model domain that includes a single rift basin, focusing on the transition from an internal to an external drainage system. Like Berry et al. (2019), we concentrate on analyzing the surface hydrology that arises from tectonic extension (Supplementary material S3). Our primary objective does not lie in the pursuit of producing a precise representation of the tectonic and geological phenomena *per se*, but rather in extracting pertinent information pertaining to the hydrologic system evolution.

The model domain has an area of 200 × 200 km^2, discretized into 1 × 1 km^2 cells. Within this area, there are two rift basins that are positioned in an en-echelon pattern (Figure 3B), which is reminiscent of the San Luis Basin in the northern Rio Grande Rift and the Española Basin located further south (Figure 2). The unique positioning of the two rift basins in the model domain gives rise to a landscape that has distinct geological, hydrological, and ecological characteristics compared to other regions. Basin opening, or syn-rift extension of the

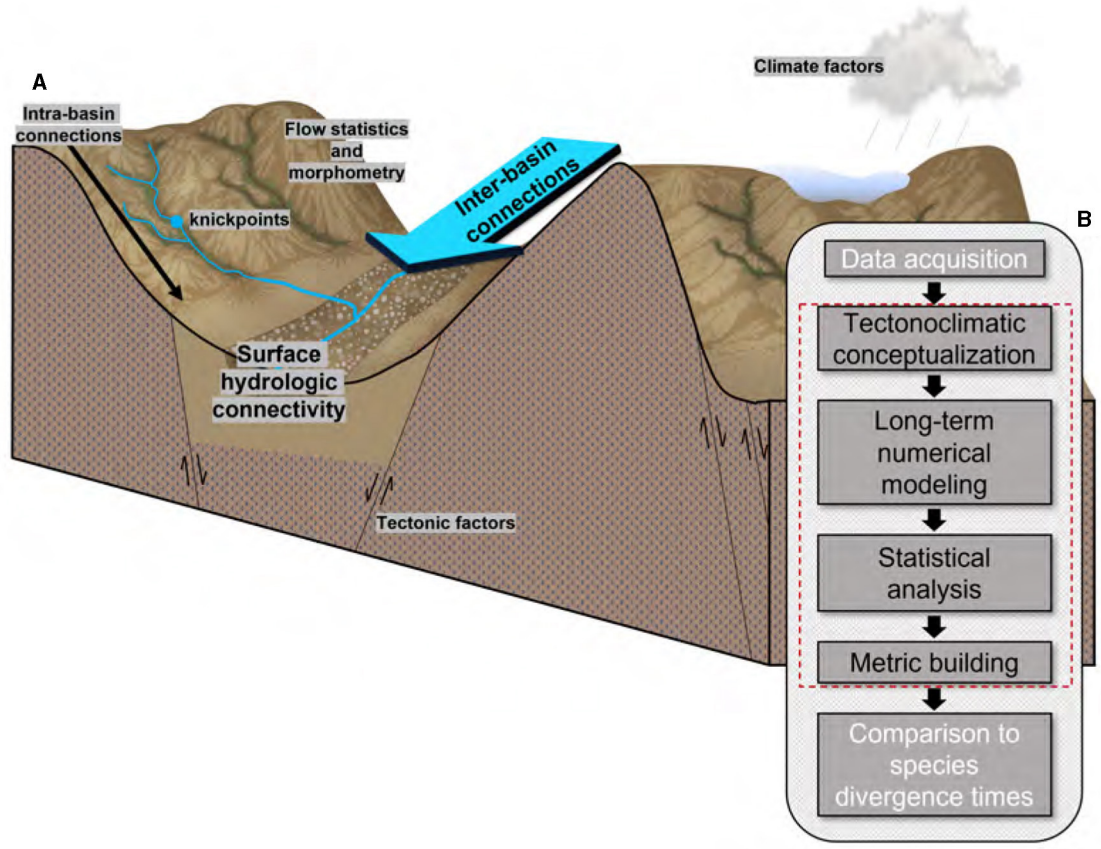

FIGURE 2
Conceptual model of this study. **(A)** Factors considered and examples of connectivity metrics examined; **(B)** a schematic diagram illustrating the sequential steps involved in reconstructing the evolutionary history of aquatic species in response to tectonic and climate forcings.

crust, begins at 0 *Myr*, following a 2-*Myr* spin-up period during which a drainage pattern "imprint" forms on the domain surface. The spin-up step is crucial for establishing antecedent drainage patterns. The accommodation zone, the area between two basins, spans a width ranging from 10 to 20 *km* (Figure 1) and is modeled as a transfer zone. The basin opening rates vary between 1 and 5 *mm/year*, equivalent to 1–5 *km* per *Myr*, depending on the scenario. The opening rates are held constant over time. The opening of the two basins exhibits an alternating asymmetric pattern, with one opening eastward and the other westward. The overlap across the accommodation zone, another sensitivity parameter, varies between 10 and 30 *km* (Figure 1).

This study presents a base-case scenario, conducting a simulation of rift extension over a duration of 20 *Myrs*, resulting in a cumulative basin width of 60 *km*. The tectonic block displacement rate chosen for this scenario is 3 *mm/year*, and the width of the accommodation zone in the base-case scenario is 10 km. Throughout the simulation period of the base-case, the climate is assumed to remain constant, with mean annual precipitation (*MAP*) fixed at 1,000 *mm/year*. To explore the sensitivity of the results, additional models are constructed by individually varying parameters or climate scenarios, as presented in Supplementary Table S1.

2.3 Connectivity metrics

Metrics acquired through an analysis of each cell at discrete 0.5 *Myrs* intervals, form the cornerstone of the analysis. The metrics are calculated immediately after each timestep is completed, and interpreted through the creation of spatiotemporal visualizations, a selection of which are incorporated within the Supplementary Figures S1–S7. The primary analytical method, however, involves the application of statistical analysis to the data from each time step, resulting in multiple scalar metrics that are tracked over time. This approach uses statistical tools such as moments (e.g., spatial mean), quantiles, and extreme values to derive representative, consolidated values. Several of these metrics inherently require summation across cell values. This approach condenses vast arrays of data into a more manageable form, enabling us to draw meaningful conclusions over an expansive temporal scale.

TISC is an indiscriminate landscape evolution model that treats hillslopes and stream channels together. It computes the volumetric streamflow for each 1-*km* cell, ensuring every cell contains a measurable quantity of flowing water. The ensuing spatial variability in cell streamflow provides information about SHC. Cells with little streamflow represent areas that are unlikely to sustain aquatic life, in contrast to those with consistently high flow

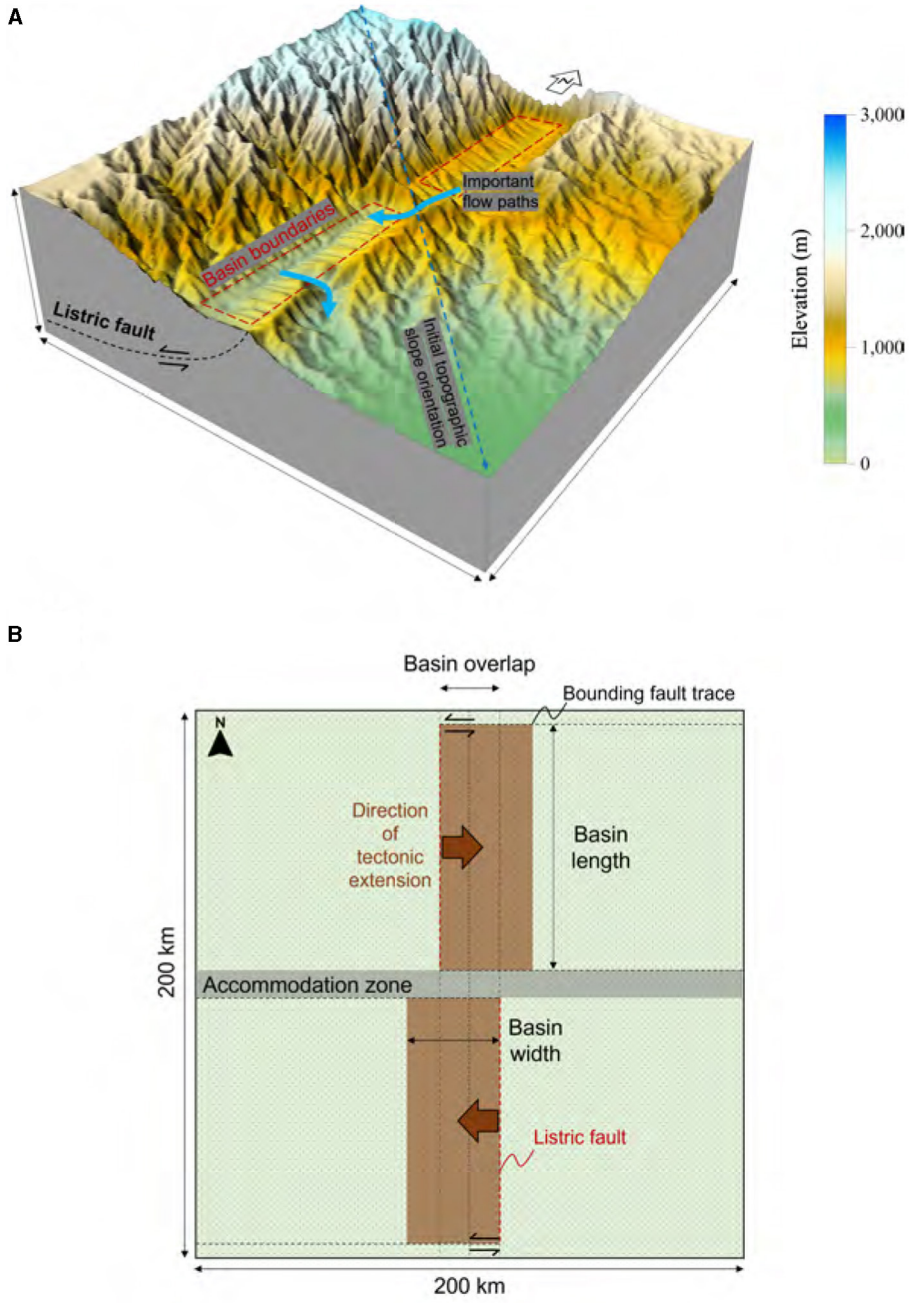

FIGURE 3
Conceptual model diagrams. **(A)** A conceptual model diagram of a base-case depicting 10 *Myrs* after rift initiation. **(B)** A planimetric view of the model depicting basin positions and opening directions. Each fault block is bounded below and updip by a listric fault, and on sides by strike-slip bounding faults.

rates. The spatial frequency of these flow rates serves as a window into connectivity, raising a pertinent question: Is flow uniformly distributed across numerous cells, or is it sequestered within the confines of major channels and a select few cells? Insights into these phenomena are glimpsed through the prism of cell flow-rate statistics. A broad suite of streamflow statistics, incorporating measures of variance, skewness, and kurtosis of the surface flow (or volumetric discharge) are analyzed here. Time-series data for these statistical parameters are generated, endowing us with the capacity to probe the temporal dynamics inherent within the surface hydrological system.

Morphometrics are produced for each model snapshot. These include the Terrain Ruggedness Index (TRI; Riley et al., 1999), which quantifies the amount of elevation change between adjacent cells and thus indicates the roughness of the terrain, and the Topographic Wetness Index (TWI; Beven and Kirkby, 1979; Moore et al., 1991; Boehner and Selige, 2006), which is a hydrologic indicator that combines slope and upstream contributing area

to predict areas of saturation, among other conditions. Both metrics assess the suitability of the evolving topography (landscape) for aquatic species migration. The TRI reveals the degree of hydrological fragmentation of the domain surface, while the TWI indicates how conducive the surface is to water flow. These metrics play a crucial role in enhancing the understanding of the magnitude of changes occurring at each time step by offering quantified measures of the topographic controls on SHC.

The investigation includes monitoring the dynamics of knickpoints, which represent sudden transitions in the longitudinal profile of streams or rivers. Knickpoints play a crucial role in species migration since these locations with rapid slope change usually prevent aquatic species to migrate upstream (e.g., Rice et al., 2001), and possibly lead to desiccation of downstream habitats (e.g., Larsen et al., 2016). Shifts in location and occurrence of knickpoints are tracked. Knickpoints are pinpointed based on an along-stream slope exceeding 10% and a flow rate above 0.03 m^3/s. The slope value factors in the requirements of weak-swimming aquatic species, referencing prior studies that have constructed anthropogenic passages for various aquatic species (Powers and Orsborn, 1985; Behlke et al., 1991; Adams et al., 2000).

Entropy metrics are calculated to capture the timings of abrupt hydrologic changes. In this study, entropy is used to indicate the spatial variability of streamflow across consecutive timesteps. These metrics include joint entropy (JE), conditional entropy (CE), and mutual information (MI). For more details of entropy metrics, see Supplementary material S5.4. Calculations are conducted over intervals of 0.5 *Myr* (one tectonic timestep), creating a chronologically ordered sequence of entropy values. This sequence illustrates the evolving degree of changes in streamflow distribution over time. Such a time-series offers insights into the spatial organization and reorganization of drainage networks, aiding in various applications like assessing the impact of different factors on the system's dynamics. A higher JE value, in particular, indicates a greater degree of combined spatial variability in the two systems.

Monitoring the progression of entropy metrics helps track the temporal changes in spatial variability in streamflow. High JE values indicate increased spatial variability between consecutive streamflow snapshots, reflecting a complex spatial organization. CE measures informational continuity between timeframes, with high values indicating little carryover and greater spatial variability. MI assesses the reduction in variability achieved by knowing the previous streamflow state, where high MI suggests strong informational correlation and reduced variability. Fluctuations in these metrics over time signal changes in the system's variability, with abrupt shifts indicating rapid changes and gradual variations pointing to a slower evolution. This analysis enables understanding the rate and nature of variability evolution within the system.

In rift systems with distinct terrains like basins, shoulders, and flanks, using region-specific metrics, especially for rift basins, aids in focusing analyses on the unique characteristics and dynamics of these areas.

This study analyzes the contributing area of each rift basin, which delineates the flow into each basin. The continuous spatial translation of portions of the model domain's land surface due to tectonic extension implies that some elements of the land surface exit the model domain at its boundaries (Figure 3B), and the fluvial catchment systems nested within the shifting crustal subdomains adhere to their specified trajectories. Movement of crustal blocks subsequently leads to a portion of watershed being displaced by rift basins or ultimately conveyed beyond the confines of the model domain. Therefore, the metrics account for the movements of two listric faults and the overlying tectonic blocks. To depict these overall changes, most of the metrics encompass the analysis of the entire model domain. The derivation of all metrics is documented in Supplementary material S5.

3 Results

3.1 Co-evolution of overall drainage network with the rift system

The formation of two rift basins (northern and southern) above listric faults incites substantial alterations in surface topography, consequently disrupting the efficient transportation of water to downstream areas (Figure 4). These rift basins serve to segment the pre-existing drainage network into several distinct sections, potentially inhibiting the preservation of their original connectivity through the antecedent drainage (as further discussed later and demonstrated in Figure 4). Basins formed during the syntectonic phase exhibit dimensions of up to 60 *km* in width (Figure 3B) and 6 *km* in depth, corresponding to the base of listric faults. Depending on the specific scenario, the sediment stored in each basin can reach depths of up to 6 *km*, though this is decreased during syntectonic activities as a result of lithospheric, isostatic rebound. Rift flanks form that, dependent on their height and uplift rate, may form the boundaries between adjacent watersheds (Figures 3, 4). In the base-case model, an inherited drainage in the lower basin continues its NW-SE course throughout the rift opening phase.

As a consequence of flow accumulation, lakes are formed within the basins, creating potential intra-basin pathways for aquatic species (refer to Figures 4, 5). The overall SHC across the entire domain is primarily influenced by the size and connectivity of each basin, particularly the connection between the two basin lakes (see Supplementary material S5.3 for more details). In contrast to the study conducted by Berry et al. (2019), rift basins in the base-case are inherently exorheic, meaning they drain water and sediment out of the system (Figure 4). The lower basin is exorheic because its rift flank uplifts are not as pronounced as in the Berry et al. (2019) study. The upper basin is exorheic because it utilizes an inherited drainage to connect the lower basin. When the interbasin river breakthrough (i.e., a river that connects two basins through the accommodation zone; IB) is active, two distinct major watersheds combine into a single system. However, when IB ceases to exist, a significant division occurs, resulting in the separation of the two distinct major watersheds, one for the upper rift basin and another for the lower rift basin.

The presence of an accommodation zone serves as a barrier, effectively isolating two basins from one another until an IB event occurs (marked by the red dashed lines in Figures 4D–F), resulting in the creation of a pathway between the basins. The damming wall arises due to the strike-slip movement occurring along the boundaries of the two rift basins (Figure 3B). In the base-case scenario, IB occurs at 3 *Myrs* after rift initiation (Figure 4D),

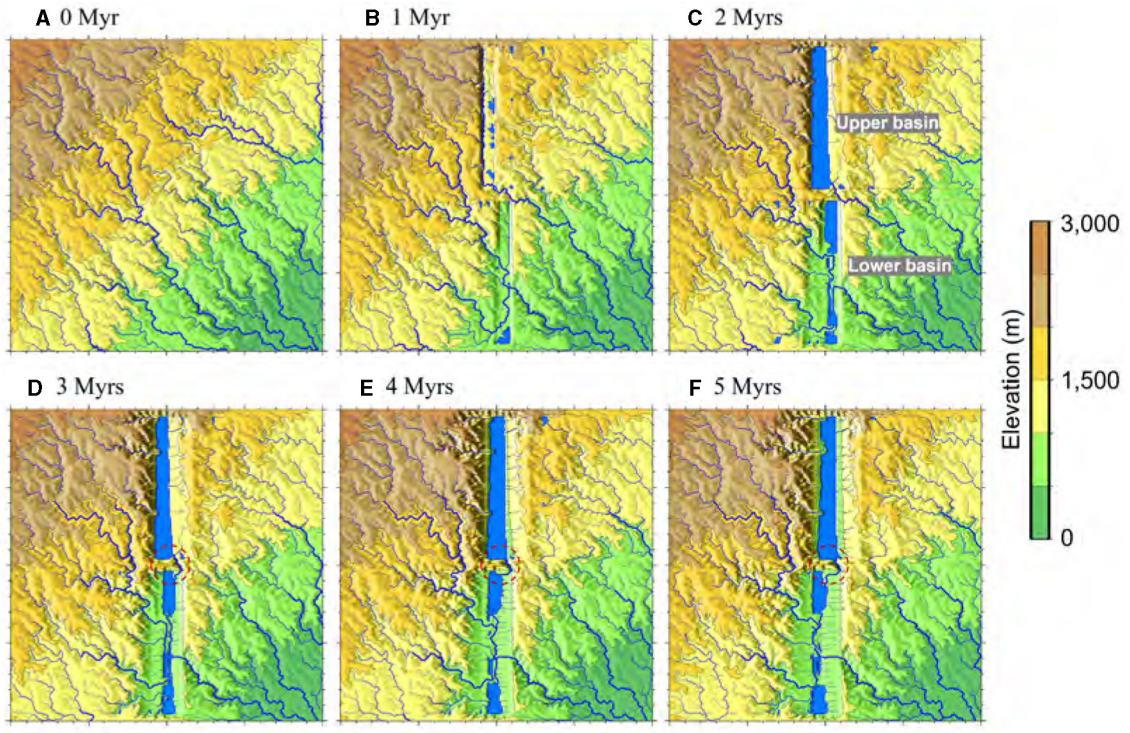

FIGURE 4
Temporal evolution of drainage patterns over a span of 5 *Myrs*. **(A)** Illustrates the initial condition, after 2-*Myr* spin-up and prior to tectonic extension, marked as 0 *Myr*. **(B–F)** Show basin openings at successive 1 *Myr* steps. The circles denoted by red dashed lines in **(D–F)** indicate the inter basin surface-drainage breakthrough, IB.

facilitating the overflow of water and sediment into the lower basin. The pathway takes advantage of the initial exorheic (i.e., outflow of water from the basin) drainage route (cf. Figures 4B, C), gradually cutting deeper into the lower basin to form a connecting river (Figures 4D–F, 5). In the model results, it is evident that IB acts as the sole pathway that establishes a connection between the northern (higher elevation) and southern (lower elevation) rift basins.

As the process of rift extension in each basin persists, the depocenter, which represents the primary sediment and water accumulation zone, progressively shifts away from the initial surface trace of the listric fault. As rift basins move farther apart due to extension, the depocenter also shifts (Figure 6). Continuous sedimentation focused on the depocenter causes the basin to overfill, raising the lake stage (not shown visually) and eventually leading to exorheic spillage. Following the cessation of interbasin (IB) flow, sediment and water transport in the northern rift basins are redirected toward the exorheic drain located at the southwestern corner (Figures 6E, F). Due to the blockage of the previous IB flowpath by basement hills in each rift basin, water in the northern basin reverts to its antecedent drainage pattern near its SE corner instead of using the IB path. This leads to the fragmentation and abandonment of the established interbasin connection, lowering the SHC. The depiction of drainage evolution within the rift system through an animation is available in a GitHub repository (https://github.com/hanhydro/Frontiers2023).

In the initial few *Myrs* of rift extension, there is a substantial surge in the number of knickpoints (Figure 7). These primarily form on the rift flanks, as the rift basins rapidly subside and the steep topography of the flanks develop. As the extension continues, these knickpoints gradually dissipate due to a combination of local baselevel changes, as well as erosional and depositional processes (Figures 7D, 8A).

Over time, the number of watersheds reduces, signaling a reorganization of the flow regime that increasingly centers on rift basins (Figure 8A). This consolidation incorporates the drainage area external to the rift basins, thus transforming the area into rift-basin-centric hydrographic systems (Figures 5–7). As a result, the rivers within the model domain ultimately fall into one of two categories: those that are connected to the rift basins, and those that are not.

3.2 Water discharge statistics and basin-centered metrics

Topography and water discharge at each timestep are analyzed statistically to gain an understanding of rift system evolution (Supplementary material S5). Figure 8 shows various metrics that can serve as connectivity metrics. From the perspective of flow (discharge) statistics, the time-series plots (Figures 8D, E) reveal that the most decisive factor influencing these statistics is the process of rift extension itself, followed by the IB, and subsequently, the cessation of rift extension. The commencement of rift extension triggers a significant increase in the number of knickpoints,

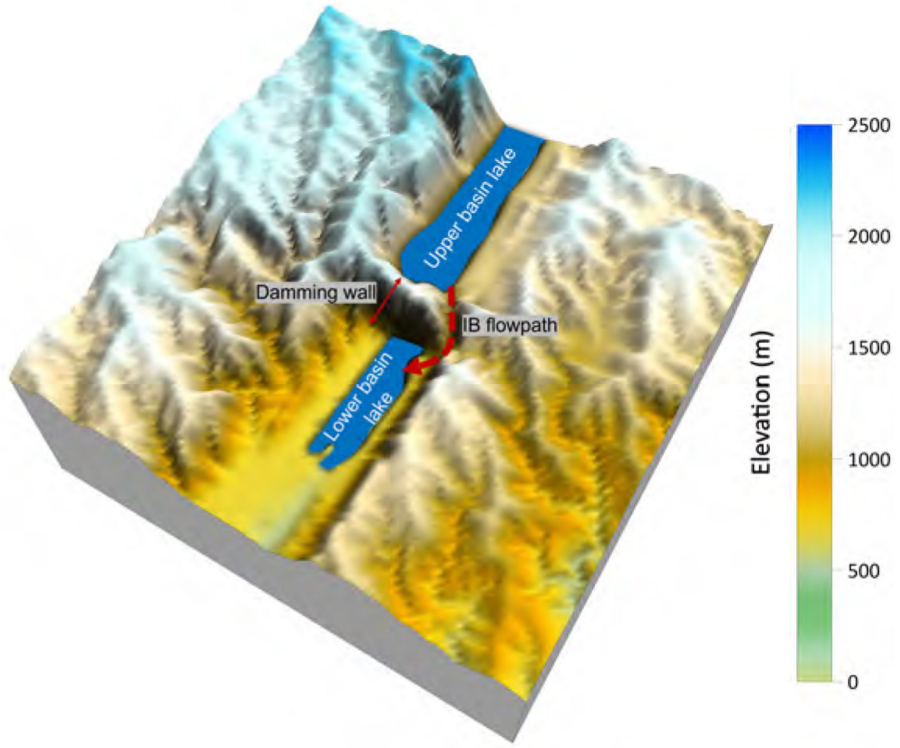

FIGURE 5
IB flowpath and the shape of the damming wall. The domain in the figure represents 50 × 50 km^2 around the IB location, and generated using the snapshot of 3 *Myrs* after rifting initiation.

attributable to the alteration of the initial landscape and the formation of rift basins (i.e., lowering baselevel; Figure 8A). Subsequently, a gradual decrease in the number of knickpoints is observed over time as the rift-basin depocenters shift and sediment deposition smoothens the topography around the transition zone between the mountains and sedimentary basins (specifically, the abrupt accommodation space delineating the surrounding mountains and rift basins). The presence of knickpoints serves as a potential barrier to functional SHC, particularly impacting the migration and dispersal of aquatic species. Therefore, an increase in the number of knickpoints can be regarded as an indication of the extent of intra-basin fragmentation, which is characterized by lower SHC. This concept has been discussed in various studies (e.g., Pringle, 1997; Muehlbauer and Doyle, 2012; Lyons et al., 2020). The role of knickpoints thus highlights the influence of landscape features on the patterns of water movement and the biological processes they support.

Following the onset of rift extension, which begins after 0 *Myr* as depicted in Figures 8B, C, there is an observed increase in both Terrain Ruggedness Index (TRI) and Topographic Wetness Index (TWI) until interbasin breakthrough (IB) begins, except the case of mean TWI. This suggests that there is a heightened variation in elevation changes, accompanied by an expansion of water-saturated areas characterized by high flow accumulation. However, simultaneously, there is a decrease in discharge within the downstream regions situated in the Southeast quadrant due to the interception of water by rift basins, which is observed as a decline in the mean TWI from 0 *Myr* to the occurrence of IB. In the presence of IB, a rising trend in the maximum TWI, coupled with a general decrease in the mean TWI, becomes evident. The pattern observed from 3 to 17 *Myrs* (Figures 8B, C) indicates the expansion of rift basins, which accumulate more water compared to surrounding areas like rift flanks and external drainage regions. This condition bifurcates the domain into areas of relative wetness (within the rift basins) and dryness (beyond the basin peripheries). Such a shift in hydrologic conditions is largely ascribed to the emergence and growth of rift basins. The basins act as natural water collectors, channeling and holding a large part of the area's water within their boundaries. Consequently, this concentration of water within the basins leads to comparatively drier conditions in the areas beyond their confines, setting the stage for a distinct partition of wet and dry zones across the landscape.

The level of fragmentation in drainage network can be surmised indirectly from the comparison between maximum and mean TWI (Figures 8B, C). An increase in maximum TWI coupled with a decrease in mean TWI suggests the presence of areas accumulating significantly more water relative to others, indicating more fragmentation in the surface flow regime. Upon the disconnection of the IB pathway at 17 *Myrs* (Figure 6B), an almost monotonous escalation in mean TWI is observed. This augmentation does not appear to be directly tied to the IB's flow distribution effects. Rather, it is attributable to the cumulative impact of sediment accumulation (and the consequent rise in base level) in rift basins, the cessation of IB, and the

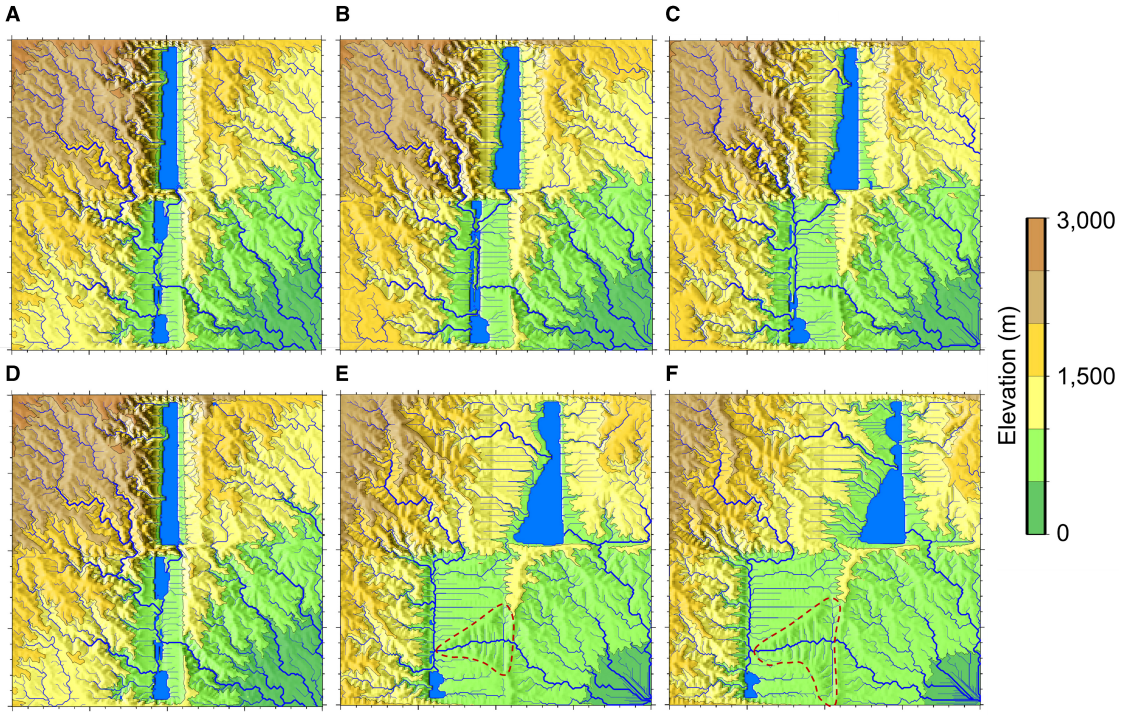

FIGURE 6
Late stages of rift surface hydrologic evolution. Topography and drainage patterns from **(A)** 7.5 *Myrs*; **(B)** 10 *Myrs*; **(C)** 12.5 *Myrs*; **(D)** 15 *Myrs*; **(E)** 17.5 Ma; **(F)** 20 *Myrs*. IB disappears around 17 *Myrs* [between **(D)** and **(E)**].

intensified erosion in the southeastern corner of the model domain. These multifaceted factors contribute to the overall smoothing of the topography and flow distribution, suggesting a reduction in hydrologic fragmentation across the two principal watersheds (Figures 6B, C). Hence, these findings highlight the erosion and deposition with tectonoclimatic forcings in shaping the drainage network's structure and fragmentation level.

Insights gleaned from the 95-th and 99-th percentile flow rate plots indicate that the reorganization of watersheds, triggered by rift extension, markedly disrupts the antecedent surface-flow regime (Figure 8D). The initial impact of this disruption fragments the extensive, continuous flow of rivers into discrete hydrologic units, which are subsequently redistributed into stream fragments oriented toward rift basins. Following the cessation of rifting, these fragments experience increased longitudinal connectivity, resulting in a higher flow rate. An increase in skewness signals that the majority of flow rates are decreasing, while certain locations, such as confluences, experience significantly higher flow rates. This indicates that watersheds are undergoing a process of combination (Figure 8A), showing a decreasing trend in the number of watersheds. An elevated kurtosis, on the other hand, indicates a higher frequency of extreme flow rates-either exceptionally high or low-within the domain, which echoes the implications drawn from the skewness. Furthermore, a heightened coefficient of variation (CV) reveals a substantial degree of variability in the flow rates in comparison to the mean flow rate. This is indicative of a domain characterized by increased topographic roughness. While not explicitly represented in the plots, there was an observed increase in the stream order according to the Strahler system (Strahler, 1957), rising from six (at rift initiation) to eight during rift extension, and then stabilizing at seven post-rifting. The distribution of water discharge and its corresponding statistical characteristics are influenced by the manifestation of IB. As evident in Figure 8E, IB mediates the asymmetry in the flow distribution, fostering a more balanced dispersal of flow across the region. This redistribution consolidates the flow into a rift-centric system characterized by a central, axial river.

The metrics centered around the rift basins, specifically the upper and lower contributing areas, serve as tools in delineating the evolution of stream and watershed capture over time (Figure 8F). As time progresses, there is a steady expansion in the contributing area of the upper basin. Conversely, the contributing area of the lower basin demonstrates modest fluctuations throughout the simulation period. This behavior results from a combination of factors: the initial orientation of the domain slope (northwest-southeast) and the directions in which the rift opens. These factors selectively influence the organization of watershed and stream captures. The time-series trends for the lower contributing area result from the watershed expansion downstream of the lake outlet. As more watersheds and streams are captured by the watershed extending from the southern basin outlet, the contributing area of the southern rift basin decreases (compare the areas enclosed by red dash lines in Figures 5, 6E, F). This lake outlet watershed is not part of the lower rift basin (Figure 6).

The analysis of JE, CE, and MI streamflow-entropy metrics is illustrated in Figure 9. The time-series representation of each

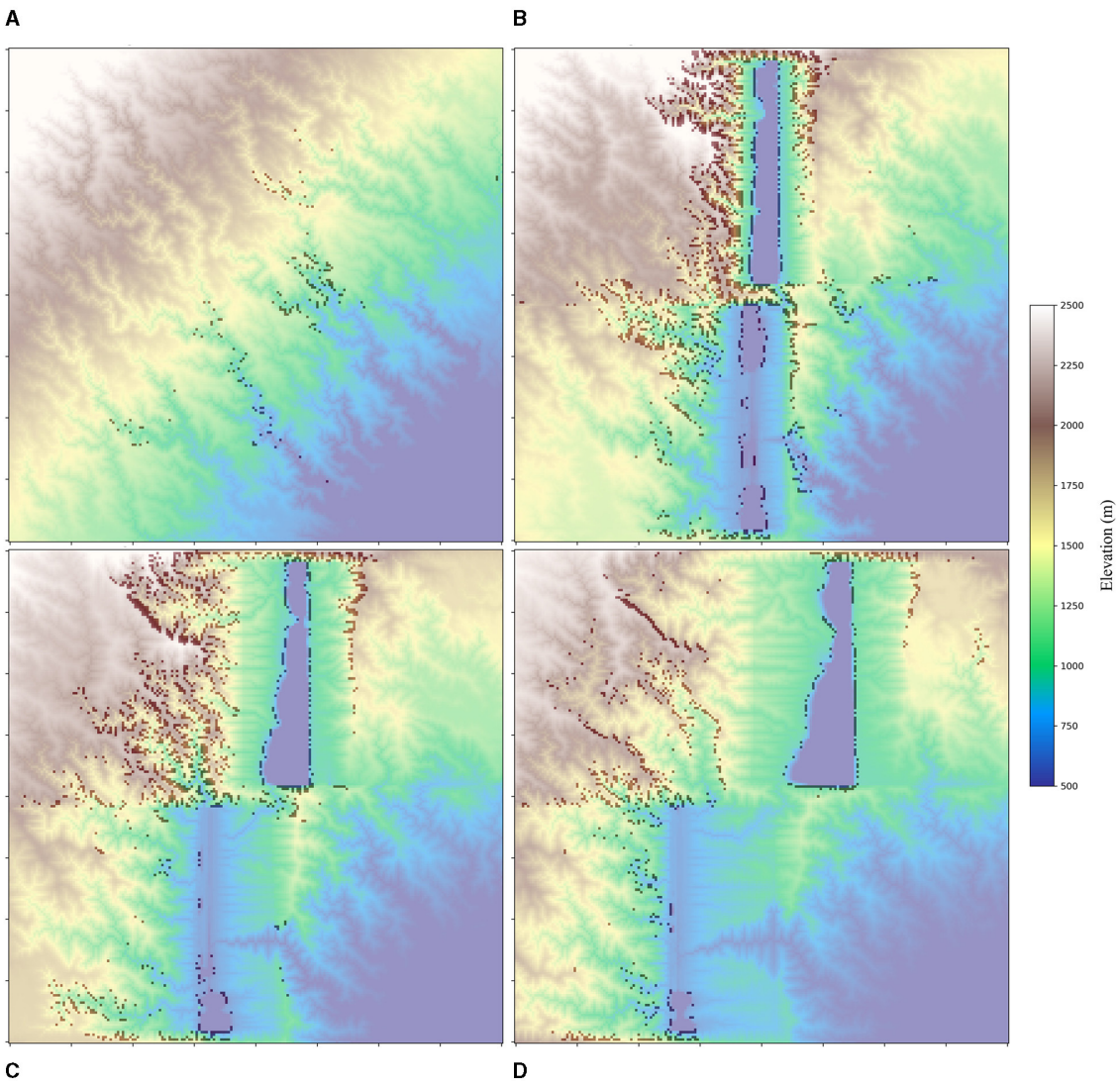

FIGURE 7
Knickpoints (darker spots) identified from different timesteps. **(A)** 0 *Myr* (at the initiation of rift); **(B)** 5 *Myrs*; **(C)** 10 *Myrs*; **(D)** 15 *Myrs*.

entropy value captures the beginning and cessation of rift extension. However, it does not offer insights into the timings of IB as do other flow statistics. Examining the overall shape of each time-series plot (Figure 9), the spatial variability of discharge distribution across the domain undergoes a sudden increase due to the effects of rift extension. Likewise, it experiences a rapid decline once the extension stops (20 *Myrs*). The smaller peaks in the time-series signify significant stream or watershed capture events between two time steps, amplifying the spatial variability of streamflow of the preceding step.

3.3 Climatic effects

Two different kinds of climate sensitivity analyses were conducted. (1) scenarios using different constant mean annual precipitation (*MAP*) values throughout the simulation period including the post-rift phase, and (2) cases considering only post-rift climate change dynamics. This study focuses on investigating IB, a key feature in rift systems leading to axial rivers, to structure the results. Across the studied models, the occurrence of IB is primarily influenced by mean annual precipitation, *MAP*. IB connections fail to develop when the *MAP* exceeds or equals 1,250 mm/year (Figure 10D). Conversely, decreasing *MAP* accelerates the onset of IB, taking ~1.5 *Myrs* for a *MAP* of 500 *mm/year*, and around 3 *Myrs* for *MAP* values of 750 and 1,000 *mm/year* (Figure 10). The absence of IB at higher *MAP* is attributed to the erosion of the riverbed resulting from the initial spillage of exorheic lake water. This spillage prompts further incision of pre-existing stream channels, thus enhancing antecedent pathways rather than facilitating the connection between the two basins. At lower *MAP* levels, lake water tends to be contained in the basin.

Post-rift climate change scenarios have minimal impact on the overall drainage patterns, as the landscape has already adapted to higher precipitation levels (represented by the black solid line at

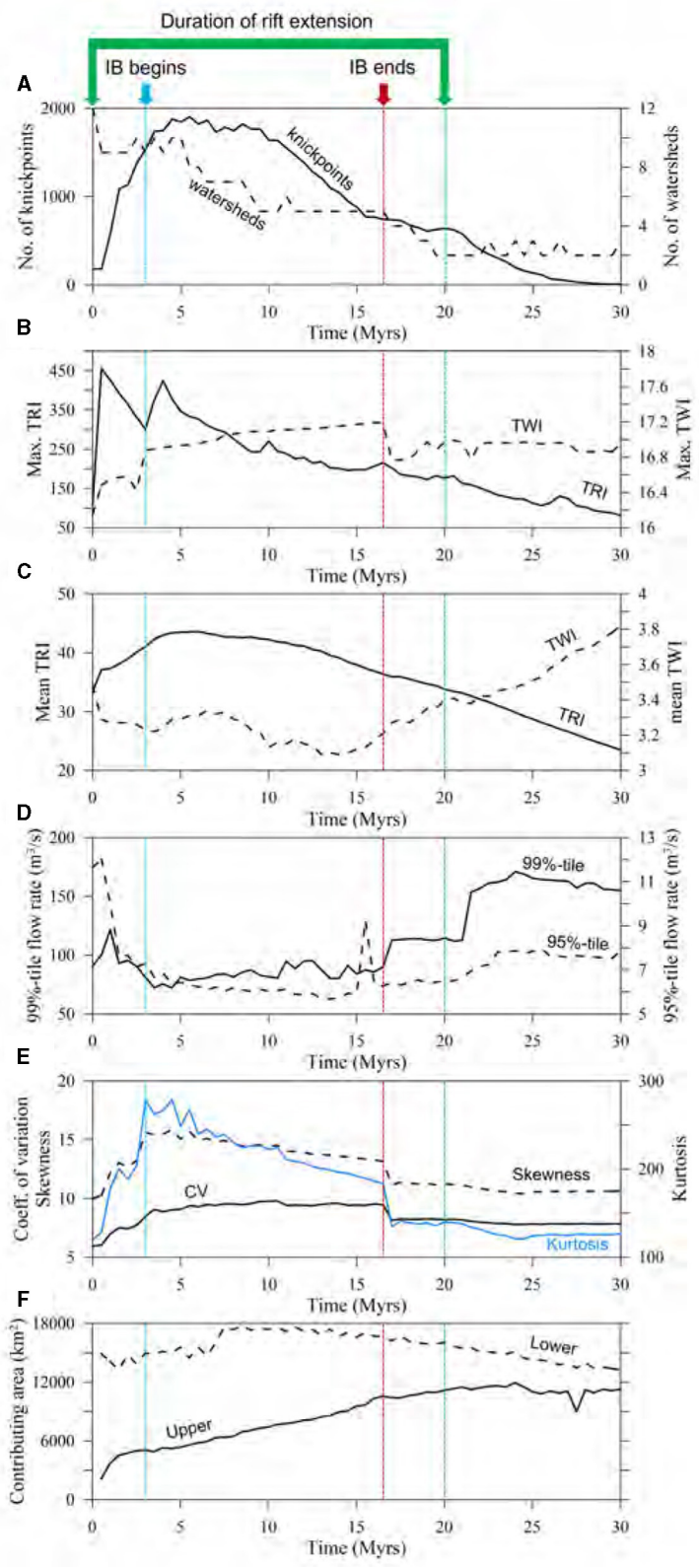

FIGURE 8
Time series of flow and morphometrics. **(A)** Changes in number of knickpoints and watersheds during the simulation period; **(B)** maximum TRI and TWI; **(C)** mean TRI and TWI; **(D)** 95 and 99%-tile flow rate; **(E)** coefficient of variation, skewness, and kurtosis of flow rate; **(F)** contributing area of each upper and lower rift basin. All metrics are obtained from data over the whole model domain of 200 × 200 km^2. 0 *Myr* refers to the moment of rift initiation. TRI and TWI represent terrain ruggedness index and topographic wetness index, respectively. The plotting interval is 0.5 *Myrs*.

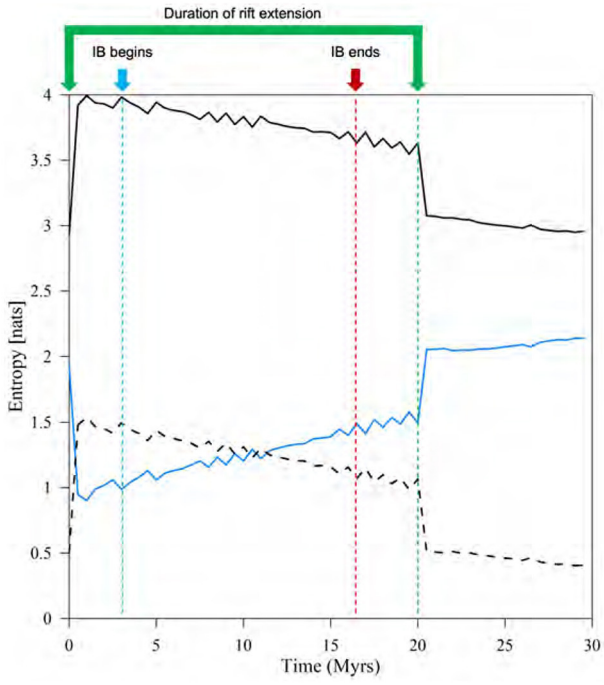

FIGURE 9
The time series of joint entropy (black solid line), conditional entropy (black dashed line), and mutual information (blue solid line). These metrics were calculated using two consecutive snapshots of water discharge over the entire simulation period.

1,000 mm/year in Figure 11A). The only notable change observed is in the number of knickpoints (Figure 11B). Knickpoints decrease faster in the cases with faster reduction rate in *MAP*, indicating less headwater migration of the knickpoints. There were no significant alterations observed in the spatial distribution characteristics of water discharge over time, as indicated by the absence of major changes in flow statistics (not shown). Despite the drying climate conditions associated with decreasing *MAP*, flow routing and SHC remain relatively stable. This is due to deeper stream incisions under past high mean annual precipitation (1,000 *mm/year*) and slower erosion and incision under drier climate conditions that cannot change antecedent drainage patterns.

3.4 Effect of initial conditions and physical parameters

Initial conditions and physical parameters, particularly the orientation of the initial slope, play a crucial role in determining the final SHC. Especially, the initial slope significantly influences the drainage pattern, as well as the timing and location of IB and lake overflow (Figures 3, 4). When the slope orientation aligns along a North-South axis (Supplementary Figure S3a; contrasting with the base-case of a Northwest-Southeast orientation), the potential for an IB becomes universal across all cases. The basins are then aligned with natural drainage direction and the accommodation zone (AZ; Figure 3) dam between the basins is more easily eroded, being oriented perpendicular to the slope.

Considering Northwest-Southeast oriented cases, including the base-case scenario, the occurrence of an IB is contingent upon factors such as basin opening rates, the overlap (initial positioning of the basin), and *MAP*. The extent of basin overlap, as depicted in Figure 3B, primarily influences the timing of the IB event, rather than the actual occurrence of the IB itself. The basin opening rate is the most important factor controlling IB and the routing of water from the upper basin to the lower basin. It dominates the process of erosion and transport by transferring the location of depocenter (i.e., the lowest elevation in each basin), and positions the local baselevel. When the opening rate is high, the depocenter moves away faster and the water in the upper basin is unable to breach the AZ dam, therefore no IB occurs. The duration of basin opening controls the shape of the landscape by designating the maximum area (or width) of rift basins. However, continued extension of crust also translates the depocenter of each basin, resulting as separation of rift basins, disconnecting the pre-existing IB (Figure 6). The magnitude of initial slope also affects overall connectivity (see Supplementary Figure S1 and Supplementary material S4). If the slope is high, rift basins tend to remain disconnected and essentially exorheic, but when the slope is low, rift basins remain endorheic and eventually develop IB. Accommodation widths also control the occurrence of IB, and the models do not exhibit IB with accommodation zone width >15 *km* (Supplementary Figure S3). Initial drainage imprinting duration (spin-up) seems to have limited impact on syn-rift drainage reorganization, but further investigation with additional test cases is necessary for confirmation.

4 Discussion

4.1 Hydrologic evolution of a rift system

Rift extension promotes the development of integrated and connected drainage patterns, primarily by funneling water into rift basins. These basins serve as focal points for flow accumulation and, in conjunction with interbasin breakthrough (IB), contribute to the formation of a large, connected watershed (Figure 6A). Therefore, SHC increases during rift extension (cf. the drainage patterns of Figures 4A, 6A, 8A). The number of watersheds decrease, and contributing area of both rift basins increase over time.

This process results in both fragmentation and instances of stream or watershed capture. As the rift system extends, it significantly alters drainage networks, leading to a distinct east-west separation in the surface drainage network. The drainage west of the upper basin becomes disconnected from the east (cf. Figures 4A, 6A). A notable disconnection occurs with the longest river, which initially flowed from northwest to southeast (Figure 4A) but later redirected into the lower basin after IB formation. The northwest and southwest quadrants predominantly drain into the lower basin, with the northwest quadrant also partially contributing to the upper basin. Without an IB, the flows in the northwest and southwest quadrants remain separate until converging in the southeast corner.

The formation of an IB is dependent on the overlap of lakes within each basin. This overlap causes spillover of the northern

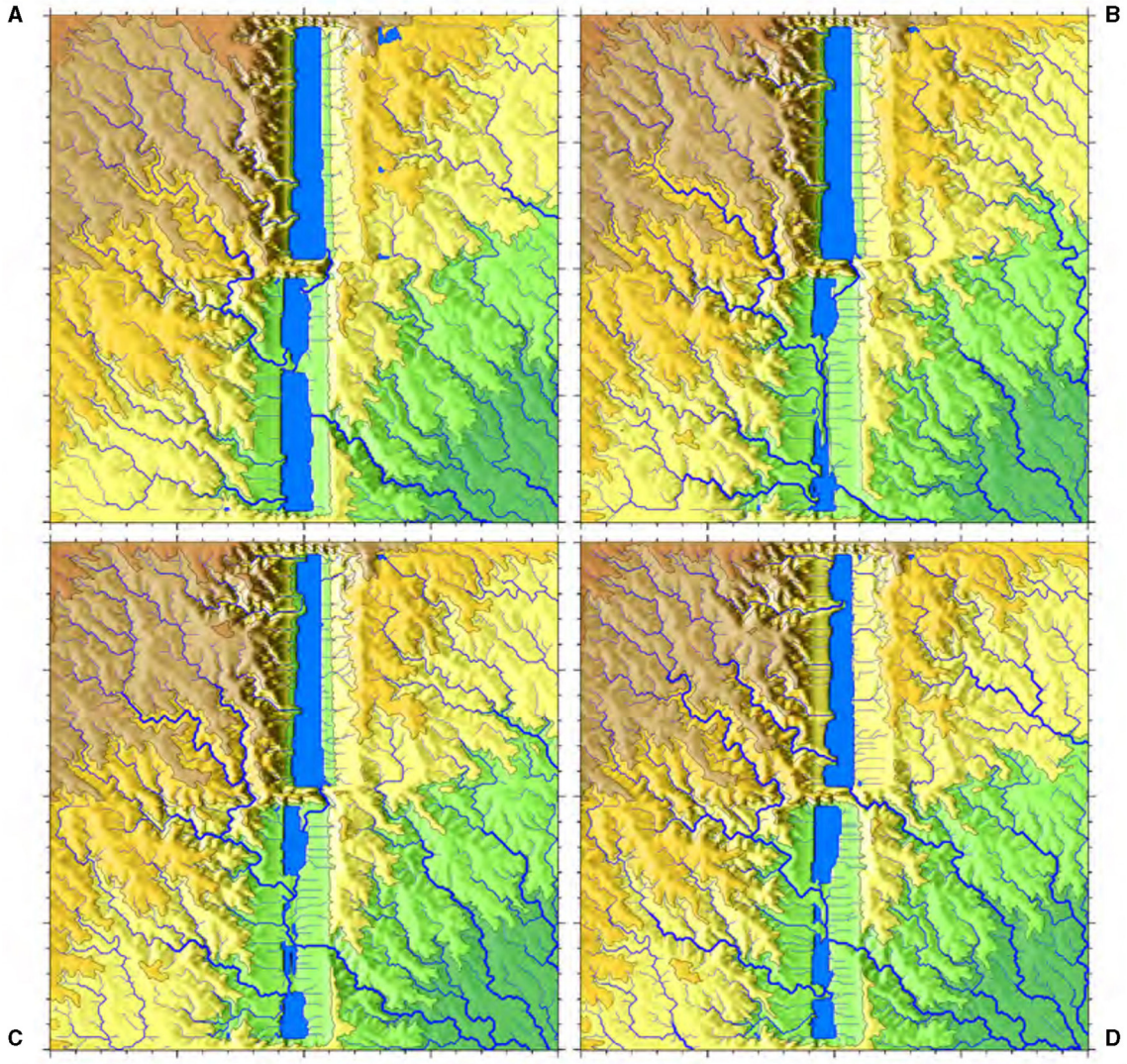

FIGURE 10
Snapshots illustrating the simulation results during the syn-rift stage at 5 *Myrs*, under different constant *MAP* conditions. They display the topography and drainage patterns corresponding to **(A)** 500 *mm/year*; **(B)** 750 *mm/year*; **(C)** 1,000 *mm/year*, which is the base-case scenario; and **(D)** 1,250 *mm/year*.

lake, amplifying the stream power on the pre-existing drainage pattern of the accommodation zone (AZ), paving the way for the IB's inception. However, as tectonic extension continues and sediment accumulates in both basins, the depocenters gradually shift apart, increasing the distance between the lakes in each basin. Lake stages significantly influence the occurrence of IB. When a basin has a high rate of opening, the lake stage tends to decrease. As a consequence, each rift basin tends to drain over the rift flanks instead of flowing into other basins, leading to the formation of non-connected basins. In the case of a basin draining outside (i.e., exorheic basin), the lake stage remains below the elevation of the spillover point on AZ where the lake would potentially drain out through IB.

The results indicate that the transition from endorheic to exorheic conditions in each rift basin is controlled by initial conditions and physical parameters. Factors such as antecedent drainage patterns before rift opening and the rate of tectonic extension applied to each basin are key determinants of SHC. Once established, the imprinted drainage patterns persist over time, enduring through IB and significant drainage reorganizations that affect the shrinkage and expansion of contributing areas. Therefore, in terms of understanding the current hydrologic condition of the Rio Grande Rift, perhaps there was an acceptable rate of extension in each individual rift basin that maintained the IBs among basins, along with accommodation zones that were not too wide, thus facilitating the generation of IBs.

4.2 Tectonics vs. climate

The syn-rift hydrologic evolution in this study indicates that the tectonic forcing drives the fragmentation of surface hydrology. Rifting-induced crustal extension reorganizes existing drainage patterns, creating a rift-basin-centered surface flow regime and

shaping the landscape, setting the stage for subsequent climate-driven hydrologic changes. The simulation results, barring non-IB cases, show that IB connections form relatively easily under specific conditions, leading to increased SHC across the entire model domain.

In the part of this study focusing solely on post-rift climate changes, the impact of climate on landscape and drainage patterns is less pronounced, primarily affecting the number of knickpoints. The findings suggest that IB connections are primarily driven by tectonic movements, whereas intra-basin hydrologic connections are influenced by post-rift climate changes. The number of knickpoints, impeding upstream species migration, emerges as a crucial factor in explaining intra-basin SHC. However, the rate of reduction in knickpoints doesn't fully capture the spatial redistribution, as they tend to migrate toward headwater areas over time (cf. Figures 7A, D), enhancing SHC in lower elevations but isolating headwater areas.

The study reveals that higher mean annual precipitation (*MAP*) does not necessarily control connections between rift basins in terms of IB and SHC. Increased MAP can lead to non-connected rift basins due to concentrated exorheic spillage (Figure 10), and post-rift climate changes primarily affect local hydrologic connections, particularly in headwater areas (Figure 11). Elevation-dependent precipitation, which varies both spatially and temporally, was not included in the study. The inclusion of time-varying climate conditions is expected to further disconnect intra- and inter-basin flow paths due to spatial precipitation differentiation, leading to increased watershed fragmentation.

4.3 Connectivity and aquatic species evolution

The major driver in aquatic species evolution is geographical separation or isolation (e.g., Rüber et al., 1999; Burridge et al., 2008). The separation processes occur through the loss of hydrologic connectivity, as aquatic species are unable to move freely in the absence of water and its flow. The presence of knickpoints elucidates the extent of vertical separation within the surface hydrologic system, specifically the connection between mountain watersheds and downstream rift basins (intra-basin), and vice versa. A higher abundance of knickpoints poses greater challenges for the upstream migration of aquatic species (e.g., May et al., 2017). The simulated knickpoints reach their maximum number ~5 *Myrs* after the initiation of rift extension, followed by a gradual decline.

Based on the time-series for various metrics (e.g., Figure 8), it becomes evident that the initial millions of years of tectonic activity play a crucial role in geographical separation. This is supported by the fact that post-rift and syn-rift climate changes have minimal impact on the metrics that reveal SHC. Therefore, to address the question of when species evolution is most impacted by climate and tectonics, the early stage of tectonic evolution should be the focal point. However, it is important to acknowledge a potential bias in this analysis, as the majority of species of interest found in the present day have evolved relatively recently, long after the most

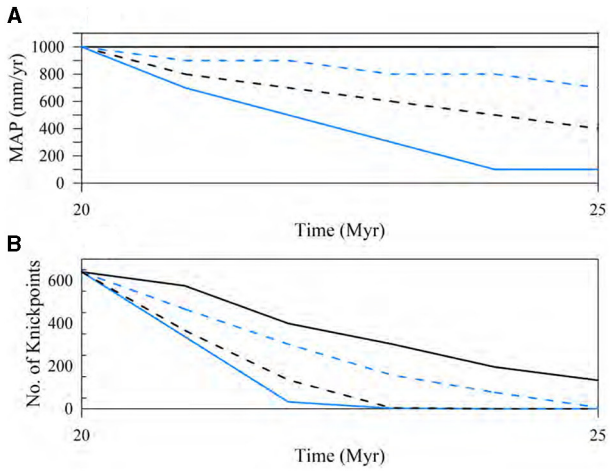

FIGURE 11
Time series plots depicting the effects of **(A)** post-rift climate change scenarios with varying decreases in *MAP*, alongside **(B)** the corresponding number of knickpoints represented by lines of the same color and style. The black solid lines in each plot represent the base-case without any post-rift climate change. The plotting interval is 0.5 *Myrs*.

active period for speciation suggested by the SHC metrics. Even if high SHC was established during the early stages of rift extension, there is a suspicion that later climate change played a significant role in driving the majority of surviving and observable endemism (i.e., the ecological state of a species being unique to a geographic location).

The topographic characteristics of rift basins prevent free migration of aquatic species upstream due to increase in knickpoints. Due to these and other topographic barriers, once they are confined within rift basins it becomes difficult for water and aquatics species to escape due to the limited availability of exorheic spillage locations. A component of SHC that changes proportional to the rift opening is intra-basin watershed connections. When extension takes longer (wider basins), surface processes on the rift flanks are promoted, resulting in a high degree of knickpoint migration and smoothing.

This study highlights key temporal and spatial points for examining SHC in continuously changing landscapes. For instance, the location of knickpoints can signal where significant hydrologic disconnections occurred, and the onset and cessation of IB can reveal the timings of abrupt connections and disconnections that impacted species migration. The results can be applied to estimate species divergence times or to make comparisons with existing species cladograms, thereby helping to elucidate the history of aquatic species evolution. This research paves the way for more advanced models of SHC aimed at helping to determine the degree to which SHC controls the divergence timings of aquatic species.

4.4 In search of comprehensive SHC metrics

Figures 8, 9 demonstrate how scalar metrics respond to 30 *Myrs* of hypothetical rift evolution, highlighting the response of

the system to rift opening. The integration of watersheds into a unified hydrologic system through IB enhances domain-wide SHC, potentially aiding aquatic species migration. Metrics indicating the beginning and end of IB are particularly vital. Additionally, knickpoints are effective indicators of functional SHC that facilitate species movement (e.g., Kollaus and Bonner, 2012; Ruppel et al., 2020). Many metrics, sensitive to the initiation and cessation of rift extension, watershed or stream capture, and IB, are useful in reconstructing paleo-hydrologic histories. Thus, the number of watersheds, knickpoints, Terrain Ruggedness Index (TRI), Topographic Wetness Index (TWI), entropy, and flow statistics are all valuable metrics for assessing SHC.

The selected application of these metrics is suggested, depending on specific objectives. For instance, to monitor overall hydrologic system changes, the number of watersheds, TRI, and TWI emerge as appropriate metrics. If the goal is to understand intra-basin SHC alterations, employing contributing area metrics proves beneficial. To elucidate how global drainage patterns reconfigure due to external forces, scrutinizing flow rate statistics is recommended (Figure 8D). And to account for aquatic species migration, utilizing the number and spatial distribution of knickpoints as measures of SHC is appropriate. This approach involves assessing the rule-based longitudinal connectivity of whether a flowpath is passable or not, as discussed in previous studies (Cote et al., 2009; Jaeger et al., 2014).

While domain-scale metrics provide insights into SHC changes, their ability to offer clear interpretations can be limited. For example, during periods with IB, models show increased SHC, yet this is not accurately reflected in the number of basins due to the inclusion of non-rift-basin watersheds (Figure 8). This is because these metrics represent hydrologic changes across the entire model domain, leading to high SHC values even if actual inter-basin connectivity is not well represented. Discrepancies arise when comparing maximum connected river lengths (i.e., the longest reach in the domain) in scenarios with and without IB; higher lengths are observed in scenarios where two watersheds are separated (859 *km*) compared to connected rift basins with IB (732 *km*), though this is not visually depicted (Figures 10C, D).

The autocorrelation inherent in flow data, such as flow accumulation downstream and bifurcation and confluence, complicates many statistical analyses that typically require independent observations. Comparing flow distributions over time indicates hydrologic changes due to tectonic and climatic shifts. Observing higher flow rate percentiles (95th and 99th) highlights areas of extreme discharge important for species migration and drainage reorganization. An increase in these percentiles over time indicates a trend toward more extreme flows due to more integrated watersheds, with water accumulating in specific areas. Conversely, a decrease suggests less spatial variability in flow and a greater number of non-connected watersheds.

There are a number of rift-related processes and conditions that this study does not address. For example, one is that real-world rift basins can undergo sequential extensions, for example, with the upper basin opening first and the second basin opening at a later time. These processes and conditions are left to future investigators.

5 Conclusions and extensions

In this study, a conceptual framework outlining the sequence of hydrologic evolution within a rift system is proposed. The sequence can be broadly summarized in two steps: (1) Tectonic forces reorganize watersheds, converging multiple basins into a rift-centric hydrologic system; (2) In response to post-rift climate change, specifically aridification, the size and extent of these drainage patterns significantly change. The results highlight the backdrop that tectonics set for geographic separation, further shaped by climate change. The sensitivity analysis on parameters like basin opening rates and mean annual precipitation showcases that the formation of an interbasin river over the accommodation zone, effectively reestablishing past hydrologic connectivity, requires specific conditions. Also, the initial slope directions and parameters such as rift opening rates significantly influence the timing, location, and even the possibility of river breakthroughs.

The suite of SHC metrics in this study, including flow statistics and morphometrics, shed light on changes in surface hydrologic connectivity (SHC) and the evolution of aquatic species. Rifting-induced watershed fragmentation significantly alters SHC. The calculation of SHC through various flow metrics show that it is strongly influenced by the formation of interbasin rivers and the overall topographic profile. Therefore, peaks and troughs in the time-series of metrics highlight key moments impacting regional hydrologic connections, potentially leading to the fragmentation of aquatic habitats and the isolation of species. By comparing these timings and the spatial distribution of flow barriers (knickpoints) against reconstructed species divergence timelines, it is possible to determine when and where evolutionary changes occurred, and perhaps what caused them.

While all the SHC metrics effectively signal hydrologic alterations within the system, they spotlight slightly different facets of the watersheds and connectivity. For a comprehensive understanding, it is recommended that future research to include additional local and site-specific metrics. More importantly, the selection of metrics should align with the specific objectives of the study to ensure a nuanced and accurate interpretation of hydrologic changes. Also, future studies should zero in on selected locations (cells) within the model domain, exploring how well these sites connect with their upstream and downstream areas using cell-by-cell and basin-by-basin metrics.

Data availability statement

The datasets presented in this study can be found in online repositories. The names of the repository/repositories and accession number(s) can be found at: https://github.com/hanhydro/Frontiers2023.

Author contributions

KH: Conceptualization, Data curation, Formal analysis, Investigation, Methodology, Software, Supervision, Validation, Visualization, Writing – original draft, Writing – review & editing. JW: Conceptualization, Funding acquisition, Investigation,

Methodology, Project administration, Resources, Validation, Writing – original draft, Writing – review & editing.

Funding

The author(s) declare that financial support was received for the research, authorship, and/or publication of this article. This research has been supported by NSF Grant EAR-1516680, Collaborative Research: Tectonic and climatic forcing of hydrological systems in the southern Great Basin: Implications for ancient and future aquatic system resilience.

Acknowledgments

The authors would like to express their sincere appreciation to the editor and the reviewers for their valuable input and feedback. Special thanks are also extended to Fred Phillips, Jeff Knott, Angela Jayko, Marty Frisbee, and Jolante van Wijk for their contributions and support throughout the study.

Conflict of interest

The authors declare that the research was conducted in the absence of any commercial or financial relationships that could be construed as a potential conflict of interest.

Publisher's note

Supplementary material

The Supplementary Material for this article can be found online at: https://www.frontiersin.org/articles/10.3389/frwa.2024.1255883/full#supplementary-material

References

Adams, S. B., Frissell, C. A., and Rieman, B. E. (2000). Movements of nonnative brook trout in relation to stream channel slope. *Trans. Am. Fish. Soc*. 129, 623–638. doi: 10.1577/1548-8659(2000)129<0623:MONBTI>2.3.CO;2

Behlke, C. E., Kane, D. L., McLean, R. F., and Travis, M. D. (1993). *Fundamentals of Culvert Design for Passage of Weak-Swimming Fish*. Alaska Department of Transportation and Public Facilities, Report FH WA-AK-RD-90-10.

Berry, M., Van Wijk, J., Cadol, D., Emry, E., and Garcia-Castellanos, D. (2019). Endorheic-exorheic transitions of the Rio Grande and East African rifts. *Geochem. Geophys. Geosyst*. 20, 3705–3729. doi: 10.1029/2018GC008176

Beven, K. J., and Kirkby, M. J. (1979). A physically based, variable contributing area model of basin hydrology/un modèle à base physique de zone d'appel variable de l'hydrologie du bassin versant. *Hydrol. Sci. J.* 24, 43–69. doi: 10.1080/02626667909491834

Boehner, J., and Selige, T. (2006). "Spatial prediction of soil attributes using terrain analysis and climate regionalization," in *SAGA - Analysis and Modelling Applications*, eds J. Boehner, K. R. McCloy, and J. Strobl (Goettingen: Goettinger Geographische Abhandlungen), 13–28.

Bracken, L. J., Wainwright, J., Ali, G., Tetzlaff, D., Smith, M., Reaney, S., et al. (2013). Concepts of hydrological connectivity: research approaches, pathways and future agendas. *Earth-Sci. Rev*. 119, 17–34. doi: 10.1016/j.earscirev.2013.02.001

Burridge, C. P., Craw, D., Fletcher, D., and Waters, J. M. (2008). Geological dates and molecular rates: fish DNA sheds light on time dependency. *Mol. Biol. Evol*. 25, 624–633. doi: 10.1093/molbev/msm271

Carpenter, S. R., Cole, J. J., Pace, M. L., Batt, R., Brock, W. A., Cline, T., et al. (2011). Early warnings of regime shifts: a whole-ecosystem experiment. *Science* 332, 1079–1082. doi: 10.1126/science.1203672

Corti, G. (2009). Continental rift evolution: from rift initiation to incipient break-up in the main Ethiopian rift, East Africa. *Earth-Sci. Rev*. 96, 1–53. doi: 10.1016/j.earscirev.2009.06.005

Cote, D., Kehler, D. G., Bourne, C., and Wiersma, Y. F. (2009). A new measure of longitudinal connectivity for stream networks. *Landsc. Ecol*. 24, 101–113. doi: 10.1007/s10980-008-9283-y

Downing, J. A., Prairie, Y., Cole, J., Duarte, C., Tranvik, L., Striegl, R. G., et al. (2006). The global abundance and size distribution of lakes, ponds, and impoundments. *Limnol. Oceanogr*. 51, 2388–2397. doi: 10.4319/lo.2006.51.5.2388

Fullerton, A. H., Burnett, K. M., Steel, E. A., Flitcroft, R. L., Pess, G. R., Feist, B. E., et al. (2010). Hydrological connectivity for riverine fish: measurement challenges and research opportunities. *Freshw. Biol*. 55, 2215–2237. doi: 10.1111/j.1365-2427.2010.02448.x

Garcia-Castellanos, D. (2002). Interplay between lithospheric flexure and river transport in foreland basins. *Basin Res*. 14, 89–104. doi: 10.1046/j.1365-2117.2002.00174.x

Garcia-Castellanos, D., and Jimenez-Munt, I. (2015). Topographic evolution and climate aridification during continental collision: insights from computer simulations. *PLoS ONE* 10:e0132252. doi: 10.1371/journal.pone.0132252

Jaeger, K. L., Olden, J. D., and Pelland, N. A. (2014). Climate change poised to threaten hydrologic connectivity and endemic fishes in dryland streams. *Proc. Natl. Acad. Sci*. 111, 13894–13899. doi: 10.1073/pnas.1320890111

Kalb, B. W., and Caldwell, C. A. (2014). *Restoration of Rio Grande Cutthroat Trout Oncorhynchus clarkii virginalis to the Mescalero Apache Reservation*. Technical report. Falls Church, VA: US Fish and Wildlife Service.

Kellogg, K. S., Shroba, R. R., Ruleman, C. A., Bohannon, R. G., McIntosh, W. C., Premo, W. R., et al. (2017). *Geologic Map of the Upper Arkansas River Valley Region, North-Central Colorado*. Technical report, USGS Scientific Investigations Map 3382. Denver, CO: US Geological Survey. doi: 10.3133/sim3382

Kollaus, K. A., and Bonner, T. H. (2012). Habitat associations of a semi-arid fish community in a karst spring-fed stream. *J. Arid Environ*. 76, 72–79. doi: 10.1016/j.jaridenv.2011.08.013

Larsen, A., May, J.-H., Moss, P., and Hacker, J. (2016). Could alluvial knickpoint retreat rather than fire drive the loss of alluvial wet monsoon forest, tropical northern Australia? *Earth Surf. Process. Landf*. 41, 1583–1594. doi: 10.1002/esp.3933

Lyons, N. J., Val, P., Albert, J. S., Willenbring, J. K., and Gasparini, N. M. (2020). Topographic controls on divide migration, stream capture, and diversification in riverine life. *Earth Surf. Dyn*. 8, 893–912. doi: 10.5194/esurf-8-893-2020

Masek, J. G., Isacks, B. L., Fielding, E. J., and Browaeys, J. (1994). Rift flank uplift in Tibet: evidence for a viscous lower crust. *Tectonics* 13, 659–667. doi: 10.1029/94TC00452

May, C., Roering, J., Snow, K., Griswold, K., and Gresswell, R. (2017). The waterfall paradox: how knickpoints disconnect hillslope and channel processes, isolating salmonid populations in ideal habitats. *Geomorphology* 277, 228–236. doi: 10.1016/j.geomorph.2016.03.029

McKenzie, D. (1978). Some remarks on the development of sedimentary basins. *Earth Planet. Sci. Lett*. 40, 25–32. doi: 10.1016/0012-821X(78)90071-7

Molnar, P., and England, P. (1990). Late cenozoic uplift of mountain ranges and global climate change: chicken or egg? *Nature* 346, 29–34. doi: 10.1038/346029a0

Moore, I. D., Grayson, R., and Ladson, A. (1991). Digital terrain modelling: a review of hydrological, geomorphological, and biological

applications. *Hydrol. Processes* 5, 3–30. doi: 10.1002/hyp.3360050103

Muehlbauer, J. D., and Doyle, M. W. (2012). Knickpoint effects on macroinvertebrates, sediment, and discharge in urban and forested streams: urbanization outweighs microscale habitat heterogeneity. *Freshw. Sci.* 31, 282–295. doi: 10.1899/11-010.1

Powers, P. D., and Orsborn, J. F. (1985). *New Concepts In Fish Ladder Design: Analysis of Barriers to Upstream Fish Migration, Volume IV of IV, Investigation of the Physical and Biological Conditions Affecting Fish Passage Success at Culverts and Waterfalls, 1982-1984 Final Report*. Technical report. Pullman, WA: Washington State University, Albrook Hydraulics Laboratory. doi: 10.2172/917018

Pringle, C. M. (1997). Exploring how disturbance is transmitted upstream: going against the flow. *J. N. Am. Benthol. Soc.* 16, 425–438. doi: 10.2307/1468028

Repasch, M., Karlstrom, K., Heizler, M., and Pecha, M. (2017). Birth and evolution of the Rio Grande fluvial system in the past 8 ma: progressive downward integration and the influence of tectonics, volcanism, and climate. *Earth-Sci. Rev.* 168, 113–164. doi: 10.1016/j.earscirev.2017.03.003

Rice, S. P., Greenwood, M. T., and Joyce, C. (2001). Tributaries, sediment sources, and the longitudinal organisation of macroinvertebrate fauna along river systems. *Can. J. Fish. Aquat. Sci.* 58, 824–840. doi: 10.1139/f01-022

Riley, S. J., De Gloria, S. D., and Elliot, R. (1999). Terrain ruggedness index that quantifies topographic heterogeneity. *Int. J. Sci.* 5, 23–27.

Rodriguez-Iturbe, I., and Rinaldo, A. (1997). *Fractal River Basins: Chance and Self-Organization*. Cambridge, MA: Cambridge University Press. doi: 10.1063/1.882305

Rüber, L., Verheyen, E., and Meyer, A. (1999). Replicated evolution of trophic specializations in an endemic cichlid fish lineage from Lake Tanganyika. *Proc. Natl. Acad. Sci.* 96, 10230–10235. doi: 10.1073/pnas.96.18.10230

Ruppel, D. S., Sotola, V. A., Craig, C. A., Martin, N. H., and Bonner, T. H. (2020). Assessing functions of movement in a great plains endemic fish. *Environ. Biol. Fishes* 103, 795–814. doi: 10.1007/s10641-020-00983-8

Strahler, A. N. (1957). Quantitative analysis of watershed geomorphology. *Eos Trans. Am. Geophys. Union* 38, 913–920. doi: 10.1029/TR038i006p00913

Van Balen, R., Van der Beek, P., and Cloetingh, S. (1995). The effect of rift shoulder erosion on stratal patterns at passive margins: implications for sequence stratigraphy. *Earth Planet. Sci. Lett.* 134, 527–544. doi: 10.1016/0012-821X(95)98955-L

van Wijk, J., Koning, D., Axen, G., Coblentz, D., Gragg, E., Sion, B., et al. (2018). Tectonic subsidence, geoid analysis, and the Miocene-Pliocene unconformity in the Rio Grande rift, southwestern united states: implications for mantle upwelling as a driving force for rift opening. *Geosphere* 14, 684–709. doi: 10.1130/GES01522.1

Whipple, K. X. (2009). The influence of climate on the tectonic evolution of mountain belts. *Nat. Geosci.* 2, 97–104. doi: 10.1038/ngeo413

Whipple, K. X., and Tucker, G. E. (1999). Dynamics of the stream-power river incision model: implications for height limits of mountain ranges, landscape response timescales, and research needs. *J. Geophys. Res. Solid Earth* 104, 17661–17674. doi: 10.1029/1999JB900120

Willett, S. D., McCoy, S. W., Perron, J. T., Goren, L., and Chen, C.-Y. (2014). Dynamic reorganization of river basins. *Science* 343:1248765. doi: 10.1126/science.1248765

Willgoose, G. (2018). *Principles of Soilscape and Landscape Evolution*. Cambridge, MA: Cambridge University Press. doi: 10.1017/9781139029339

frontiers | Frontiers in Water

TYPE Mini Review
PUBLISHED 31 March 2025
DOI 10.3389/frwa.2025.1496199

OPEN ACCESS

EDITED BY
Timothy O. Randhir,
University of Massachusetts Amherst,
United States

REVIEWED BY
Tianfang Xu,
Arizona State University, United States
Gianluca Botter,
University of Padua, Italy

*CORRESPONDENCE
Dipankar Dwivedi
✉ DDwivedi@lbl.gov

RECEIVED 13 September 2024
ACCEPTED 04 March 2025
PUBLISHED 31 March 2025

CITATION
Dwivedi D, Poeppl RE and Wohl E (2025) Hydrological connectivity: a review and emerging strategies for integrating measurement, modeling, and management. *Front. Water* 7:1496199.
doi: 10.3389/frwa.2025.1496199

Hydrological connectivity: a review and emerging strategies for integrating measurement, modeling, and management

Dipankar Dwivedi[1]*, Ronald E. Poeppl[2] and Ellen Wohl[3]

[1]Earth and Environmental Sciences, Lawrence Berkeley National Laboratory, Berkeley, CA, United States, [2]Institute of Hydrobiology and Aquatic Ecosystem Management, BOKU University Vienna, Vienna, Austria, [3]Department of Geosciences, Colorado State University, Fort Collins, CO, United States

This review synthesizes methods for measuring, modeling, and managing hydrologic connectivity, offering pathways to improve practices and address environmental challenges (e.g., climate change) and sustainability. As a key driver of water movement and nutrient cycling, hydrologic connectivity influences flood mitigation, water quality regulation, and biodiversity conservation. However, traditional field-based methods (e.g., dye tracing), indirect measurements (e.g., runoff analysis), and remote sensing techniques (e.g., InSAR) often struggle to capture the complexity of catchment-scale interactions. Similarly, modeling approaches—including process-based and percolation theory-based models, graph theory, and entropy-based metrics—face limitations in fully representing these interconnected processes. Both modeling and measurement techniques are constrained by inadequate spatial and temporal coverage, high data demands, computational complexity, and difficulties in representing subsurface connectivity. Subsequently, we critique current management practices that prioritize isolated variables (e.g., streamflow, sediment transport) over system-wide strategies and emphasize the need for adaptive, connectivity-based approaches in water resource planning and restoration. Moving forward, we highlight the importance of interdisciplinary collaboration, technological innovations (e.g., AI-driven modeling, real-time monitoring), and integrated frameworks to improve connectivity measurement, modeling, and adaptive management to restore fragmented hydrologic networks. This integrated approach sets the stage for transformative water resource management, fostering proactive policy development and stakeholder engagement.

KEYWORDS

hydrologic connectivity, interdisciplinary collaboration, catchment dynamics, climate change adaptation, geomorphological processes, ecohydrological models, environmental sustainability, ecosystem resilience

1 Introduction

Hydrologic connectivity is defined as the water-mediated transfer of matter, energy, and organisms within or between elements of the hydrologic cycle (Pringle, 2001). It is a cornerstone of catchment science, governing the movement of water, nutrients, and organisms across subsurface areas, surface layers, river streams, and wetlands (Bracken et al., 2013; Zhang et al., 2021). As an emergent property shaped by complex ecological interactions—including hydrological, biogeochemical, and geomorphological processes—connectivity facilitates critical exchanges within and between ecosystems (Lehmann et al., 2007; Wohl et al., 2018; Harvey and Gooseff, 2015). Understanding hydrologic connectivity is essential for predicting water movement in response to climate variability, land-use changes, and increasing anthropogenic pressures on water resources. It plays an indispensable role in water resource management, directly influencing flood and drought mitigation (Maxwell et al., 2021), regulating water quality (Harvey et al., 2019; Fox et al., 2022), and maintaining vital biological habitats (Pringle, 2001). Hydrologic connectivity enhances system resilience by regulating water flow, reducing erosion, and supporting habitat restoration (Fortuna et al., 2006; Rains et al., 2016). It also sustains natural purification processes by enabling wetlands to filter pollutants through sediment trapping and microbial breakdown, mitigating the impacts of urbanization and deforestation (Haarstad et al., 2012; Lane et al., 2018; Bertassello et al., 2022; Fang et al., 2024).

To better understand hydrologic connectivity and its role in catchment dynamics, it is categorized in two ways: by spatial domains (system perspective) and by connectivity dimensions (connectivity types). The system perspective categorizes hydrologic connectivity based on spatial domains—surface, surface-subsurface, and subsurface—highlighting where exchanges occur. Surface connectivity governs the movement of water, sediments, and nutrients across landscapes via rivers, streams, and overland flow. Surface-subsurface connectivity represents interactions between surface water and groundwater, such as infiltration, percolation, and hyporheic exchange, which regulate groundwater recharge and solute transport. Subsurface connectivity describes water and solute flow within soil and groundwater, influencing aquifer recharge and groundwater-surface exchanges (Covino, 2017). These categories are not mutually exclusive, as interactions between surface and sub-surface processes regulate catchment responses across spatial scales.

In contrast, hydrologic connectivity types are classified based on the connectivity dimensions that characterize water movement within and between systems—including longitudinal, lateral, and vertical connectivity—each of which uniquely shapes catchment dynamics. These connectivity types influence functional processes; for example, longitudinal connectivity facilitates the downstream transport of water, organisms, sediments, and nutrients, ensuring both hydrological and ecological continuity along river networks (Buddendorf et al., 2017; Lee S. et al., 2023). Lateral connectivity links rivers to adjacent floodplains, wetlands, and groundwater zones, facilitating nutrient cycling, habitat exchange, and floodplain dynamics (Leibowitz et al., 2018). Vertical connectivity governs surface–sub-surface water and solute exchanges, regulating groundwater recharge and biogeochemical processes.

Within surface and subsurface systems (i.e., the system perspective), hydrologic connectivity is shaped by structural and functional drivers (Turnbull et al., 2008). Structural drivers, such as topography and vegetation patterns, remain relatively static over short timescales, while functional drivers involve transient hydrologic processes, such as overland flow dynamics or storm-driven flow path formation. These structural and functional drivers regulate hydrologic exchanges across spatial domains, influencing the movement of water, solutes, and sediments throughout the catchment.

To capture the influence of transient hydrologic processes, some studies also consider temporal connectivity, which describes fluctuations in water movement driven by seasonal variations, precipitation events, and disturbances. These changes influence surface, subsurface, and vertical exchanges, shaping river discharge, sediment transport, and wetland hydrodynamics (Pringle, 2001; Lane et al., 2018; Lee E. et al., 2023; Wu et al., 2023). Recognizing the role of time in shaping hydrological connectivity, Ward (1989) introduced the four-dimensional perspective of lotic ecosystems, which conceptualizes their dynamic and hierarchical nature through longitudinal (upstream-downstream), lateral (channel-floodplain), and vertical (channel-groundwater) interactions, with time as the fourth dimension providing the temporal scale that governs ecosystem responses to disturbances.

Seminal works have shaped the understanding of various aspects of hydrologic connectivity (for a detailed list, see Pöppl et al., 2024). Key contributions by Schumm (1965), Taylor et al. (1993), Fryirs et al. (2007), Bracken and Croke (2007), Poeppl et al. (2017), and Wohl et al. (2019) have established connectivity as a driver of energy and material transfer, influencing sediment transport, landscape evolution, and hydrological regulation. For instance, Poeppl et al. (2017) proposed a framework integrating human impacts on fluvial systems, highlighting feedback loops between social and geomorphic systems. Similarly, Taylor et al. (1993) pioneered the concept of landscape connectivity, demonstrating its role in species dispersal and source-sink dynamics and urging planners to consider animal movement in conservation strategies. Despite these advancements, significant gaps remain in understanding and managing hydrologic connectivity, particularly in *foundational knowledge*, *methodological development*, and *management applications*.

Effective resource management and predictive modeling depend on a robust understanding of hydrologic connectivity, which requires bridging knowledge gaps in process interactions. Studies highlight the challenges posed by spatial and temporal scale variations, as hydrologic systems exhibit nonlinear behaviors and complex flow pathways (Lehmann et al., 2007; Wohl et al., 2018). Moreover, hydrologic connectivity is deeply intertwined with ecological systems, yet many studies fail to consider these linkages, emphasizing the need for interdisciplinary approaches integrating hydrology, ecology, geomorphology, and biogeochemistry (Bracken et al., 2013; Covino, 2017; Yu et al., 2023).

Accurate assessments of hydrologic connectivity require standardized methodologies to ensure consistent evaluations across spatial and temporal scales (Turnbull et al., 2018). Traditional techniques often fail to capture subsurface and dynamic flow complexities, while graph theory and entropy-based metrics offer

novel solutions (Zuecco et al., 2019; Tejedor et al., 2015). Existing models frequently over-rely on static metrics, neglecting the real-time dynamic behaviors essential for managing subsurface flow and transport (Renard and Allard, 2013). Furthermore, the absence of standardized metrics has hindered collaboration and integration across research disciplines (Zhang et al., 2021; Bracken et al., 2013).

Many management applications need to adopt adaptive, connectivity-based approaches, resulting in significant gaps in managing hydrological systems and ensuring ecosystem resilience amid climate variability and human-induced changes (Poeppl et al., 2017; Keesstra et al., 2018; Poeppl et al., 2020; Aho et al., 2020; Roy, 2023; Herzog et al., 2024). Although the importance of such strategies is well-recognized, Lexartza-Artza and Wainwright (2009, 2011) emphasize the need for adaptive methods to manage sediment and water interactions whereas Wainwright et al. (2011) highlight the complex interplay of environmental regimes across spatial and temporal scales. Incorporating hydrologic connectivity is vital for global water resource management and climate adaptation. The absence of such approaches weakens flood mitigation, groundwater recharge management, and ecosystem conservation efforts, leading to increased risks of habitat loss and water quality degradation (Good et al., 2015; Tejedor et al., 2015; Maxwell et al., 2021; Chen et al., 2021; Li et al., 2024).

Given hydrologic connectivity's complexities and interdisciplinary nature, this mini-review synthesizes current knowledge on its spatial and temporal dynamics, methodological advancements, and implications for catchment dynamics, connectivity restoration, and water resource management amid climate change and human activities. While analyzing connectivity by system, type, or temporal scale provides a structured approach, its full impact on catchment dynamics emerges only when considered holistically. Therefore, this review examines how an integrated approach can enhance measurement, modeling, and management strategies (Figure 1).

2 Measurement and modeling approaches for hydrologic connectivity

This section explores measurement techniques and modeling approaches, evaluates their strengths and limitations, and highlights the need for further advancements. We organize the following section around system perspective because it provides a tangible framework for measuring connectivity by integrating spatial and temporal scales and capturing multiple types (e.g., longitudinal, lateral, and vertical) across surface and subsurface systems. Below, we explore measurement techniques tailored to different systems, evaluating their strengths and limitations.

2.1 Techniques for measuring hydrologic connectivity

Hydrologic connectivity measurement techniques fall into field-based methods, proxies, and remote sensing techniques (Figure 1). While field-based methods and proxies can characterize connectivity in surface and subsurface systems, remote sensing techniques primarily assess surface connectivity, though some applications can indirectly infer subsurface changes.

2.1.1 Field-based methods

Among these approaches, field-based methods provide direct, high-resolution measurements of water movement, making them essential for understanding localized connectivity dynamics (e.g., Zimmer et al., 2020). For instance, dye tracing involves introducing a tracer dye into a water source to track flow pathways and residence times. This approach provides detailed insights into water movement and surface-subsurface interactions, particularly in wetlands and rivers (Zhang et al., 2022). Although highly precise, these methods are labor-intensive, temporally limited, and constrained in spatial coverage. These limitations reduce their effectiveness for large-scale assessments.

2.1.2 Indirect measurement through proxies

Proxies offer valuable tools for inferring hydrological connectivity by measuring environmental variables (Zhang et al., 2022). In surface systems, runoff patterns provide critical insights into hydrologic connectivity (Bracken and Croke, 2007). In sub-surface systems, soil moisture and plant distribution are key factors in assessing subsurface hydrologic connectivity (Yang et al., 2023). Beyond subsurface flow, they also regulate surface runoff, modifying surface connectivity (Liu et al., 2019). This interdependence reinforces that surface and sub-surface systems are not mutually exclusive but dynamically linked.

Sediment connectivity provides a more integrated perspective by linking sediment transport and retention across surface and sub-surface systems (Drummond et al., 2014; Olliver et al., 2020). Surface connectivity is assessed by measuring sediment transport through runoff, river channels, and overland flow (Julien and Simons, 1985; Prosser et al., 1995). For example, Bracken and Croke (2007) highlight hydrological connectivity in runoff-dominated systems, showing its influence on erosion and sedimentation. Building on this, Borselli et al. (2008) demonstrate using Geographic Information System (GIS) and field assessments to explore sediment and flow connectivity. GIS-based approaches, particularly those utilizing digital elevation models (DEMs), calculate connectivity indices that quantify flow pathways and identify areas of high and low connectivity based on topographic features (Borselli et al., 2008; Heckmann et al., 2018). Subsequently, Bracken et al. (2015) propose a sediment connectivity framework to understand sediment transfer across scales, directly influencing landscape stability. In contrast, subsurface connectivity is evaluated by examining sediment movement within soils, hyporheic zones, and groundwater pathways, emphasizing the complex interactions between surface and subsurface processes (Harvey et al., 2012; Lewandowski et al., 2015; Somers et al., 2016).

2.1.3 Remote sensing techniques

Complementing these approaches, remote sensing techniques, such as InSAR, provide large-scale, high-resolution monitoring

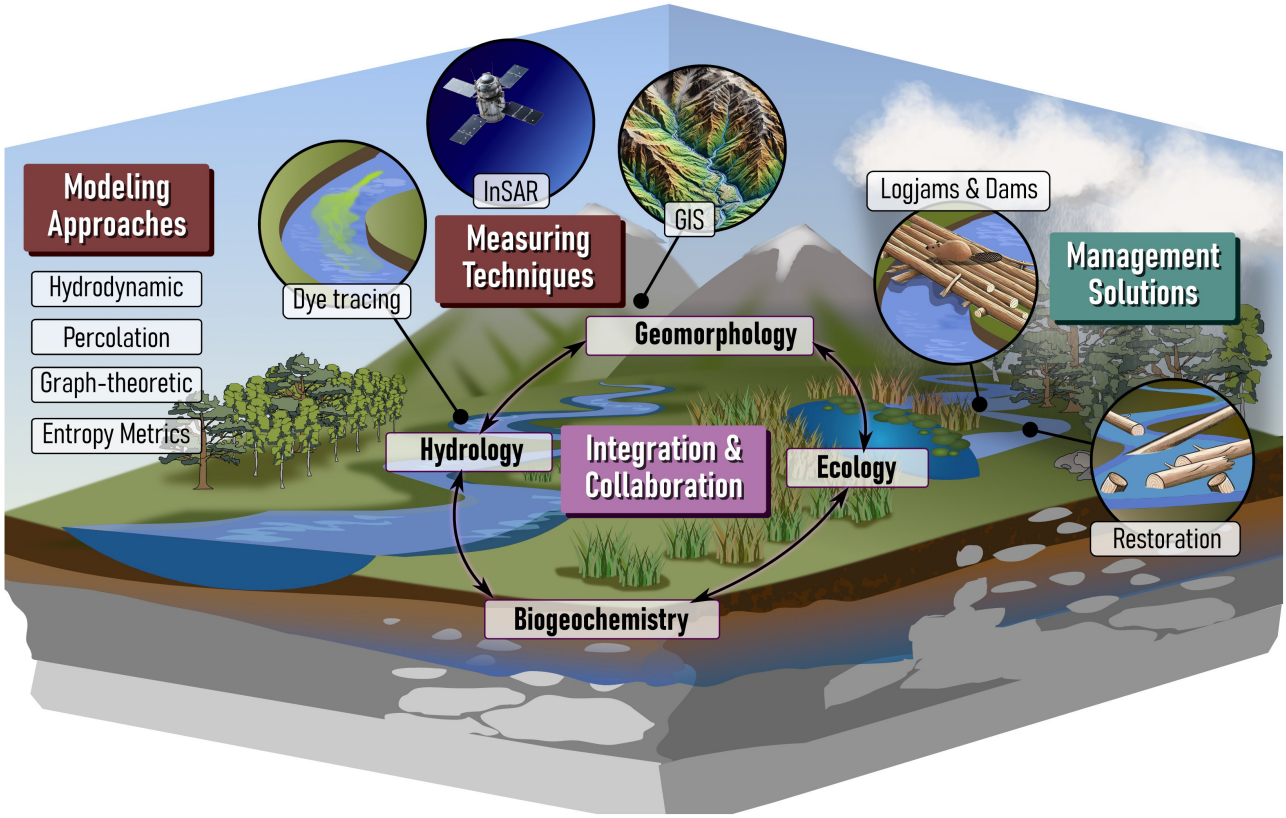

FIGURE 1
Hydrologic connectivity: advancing measurement techniques, interdisciplinary integration, and management strategies to deepen understanding and optimize water-mediated transfers in the hydrologic cycle, which are vital for river ecosystem health and critical for ensuring the sustainability and resilience of water resources in the face of environmental change.

of surface water connectivity, making them particularly useful for assessing fragmented landscapes (Liu D. et al., 2020). InSAR relies on satellite-based radar to detect surface elevation changes, enabling broad-scale monitoring of water movement and identifying fragmented or connected areas in river networks. While remote sensing methods primarily capture surface connectivity, some techniques (e.g., gravity-based satellite data like GRACE) can infer subsurface storage changes (Tapley et al., 2004). Optical imagery and LiDAR complement these approaches by detecting land cover changes, vegetation dynamics, and erosion patterns, indirectly influencing connectivity. However, remote sensing methods typically provide surface-level snapshots and often lack the resolution needed to represent subsurface dynamics accurately (Ameli and Creed, 2017).

2.2 Modeling approaches for hydrologic connectivity

Modeling approaches for hydrologic connectivity can be categorized into process-based models (for either surface or subsurface systems), network and graph-based models, and integrated models (Figure 1). While all these approaches can characterize surface and sub-surface connectivity, integrated models uniquely link surface and sub-surface processes, explicitly capturing feedback mechanisms at their interface.

2.2.1 Process-based models

Process-based models, such as hydrodynamic models (Liu Y. et al., 2020; Yang et al., 2021) and percolation theory (Lehmann et al., 2007), simulate physical flow processes and water quality across different spatial and temporal scales. Hydrodynamic models provide detailed simulations of water movement, including flow velocities, flood dynamics, and water quality, making them valuable for localized analyses of both surface and subsurface systems (e.g., Baram et al., 2013; Siqueira et al., 2018). However, they are highly data-intensive, sensitive to parameter errors, and often limited in scalability to larger systems (e.g., Rimon et al., 2011; Siqueira et al., 2018).

Percolation models focus on flow pathways and connectivity thresholds in porous media, primarily addressing subsurface systems (e.g., Lehmann et al., 2007; Rimon et al., 2011). They can be applied probabilistically to analyze runoff thresholds or identify key flow characteristics statistically. While effective for modeling nonlinear flow behaviors in hillslope hydrology and identifying significant runoff thresholds, percolation theory often oversimplifies hydrological systems by neglecting biogeochemical

interactions critical for ecosystem management (Lehmann et al., 2007; Dahan et al., 2009).

2.2.2 Network and graph-based models

Network and graph-based models, including graph-theoretic models (Tejedor et al., 2015) and entropy-based metrics (Tejedor et al., 2015), represent hydrologic systems as networks, where nodes and edges depict connected water bodies. This enables clear visualization and quantification of connectivity across river basins and delta channels (Passalacqua, 2017; Garbin et al., 2019). These models effectively assess structural connectivity (Bertassello et al., 2020; Xingyuan et al., 2023; Huang et al., 2024) but require extensive input data and primarily focus on static representations (Durighetto et al., 2023), often overlooking dynamic hydrological behaviors, particularly during extreme events (Beven, 2012).

Entropy-based metrics integrate both topological and dynamic complexity, making them valuable for evaluating system vulnerabilities and resilience. They quantify system disorder and assess dynamic connectivity under varying hydrological conditions, such as flood pulses or droughts, and have been widely applied in hydrologic connectivity and environmental sciences (e.g., Dwivedi and Mohanty, 2016; Arora et al., 2019; Bennett et al., 2019). While these methods can characterize subsurface connectivity, they are more suited for surface connectivity due to the natural network structure of river streams and the greater availability of surface data. However, subsurface connectivity can be analyzed using fracture networks or model outputs with sufficient data. Nonetheless, their computational complexity and lack of standardized metrics limit their broader applicability across diverse landscapes.

2.2.3 Integrated models

Integrated models couple sub-surface and surface hydrology while incorporating land surface processes (e.g., energy fluxes, soil moisture, runoff) and ecohydrology (e.g., plant-water interactions, ecological responses) (e.g., Coon and Shuai, 2022; Xu et al., 2022; Shuai et al., 2022; Ackerer et al., 2023). By simulating hydrological, climatic, and ecological interactions, these models provide a comprehensive understanding of water dynamics, energy exchange, and biogeochemical cycles across scales. These models capture hydrologic connectivity across surface, subsurface, and interface domains, distinguishing longitudinal, vertical, and lateral connectivity (Mikkelson et al., 2013; Camporese et al., 2019). Their ability to simulate biogeochemical processes aids in understanding catchment dynamics and tracing solute sources, differentiating biogenic and geogenic contributions in river systems (Dwivedi et al., 2018b; Arora et al., 2016; Godsey et al., 2019). They are also valuable for managing flood flows and enhancing ecosystem resilience, especially in sensitive regions like drylands (Şensoy et al., 2018).

Their ability to integrate ecohydrological interactions makes them highly relevant for interdisciplinary applications. They can leverage modular studies, such as ecohydrological frameworks (Maxwell et al., 2021; Van Meerveld et al., 2021) and dimensionless river connectivity metrics (Harvey et al., 2019), to predict outcomes like habitat connectivity and species distribution based on water availability and flow patterns.

These data-intensive models struggle to represent complex ecological-hydrological relationships due to the need for distributed parameters (Chen et al., 2021). Their computational demands limit global applicability and often lack adaptive management integration, reducing flexibility in changing environmental conditions.

2.3 Comparative strengths and limitations of measurement and modeling approaches

A comprehensive understanding of hydrologic connectivity requires integrating field-based methods, relevant state variables (proxies), remote sensing, and advanced modeling approaches. As discussed above, field methods are accurate but labor-intensive, while remote sensing offers broad coverage but lacks subsurface insights. Modeling translates these measurements into predictions: process-based models provide detailed simulations but demand extensive data and computing power; network models capture structure but struggle with dynamics and subsurface flow; integrated models offer the most comprehensive view but are data-intensive and computationally demanding. Advancing hydrologic connectivity assessments in the future requires improving data availability, scalability, dynamic modeling, and interdisciplinary integration.

3 Role of interdisciplinary approaches in enhancing hydrologic connectivity understanding

3.1 Need to integrate knowledge from multiple disciplines

Catchment systems are shaped by a complex interplay of processes (Figure 1), making interdisciplinary integration—across hydrology, ecology, biogeochemistry, and geomorphology—essential for both understanding hydrologic connectivity and developing effective restoration strategies that enhance ecosystem functioning (e.g., Hubbard et al., 2018). This approach provides deeper insights into how water movement affects key biogeochemical cycles, such as carbon and nitrogen cycling, which are vital for sustaining ecosystem health. For example, integrating geomorphological insights accounts for terrain evolution and sediment dynamics while incorporating biogeochemical processes captures feedback between water flow and nutrient availability (Liu D. et al., 2020). Appling et al. (2014) demonstrate the critical role of integrating geomorphology and hydrology, showing how the geomorphic history of floodplains influences nutrient movement and transformation through landscape structure and flow paths. The interaction between hydrologic flow and geomorphic configuration plays a crucial role in shaping water residence times and flow pathways (Helton et al., 2014). Integrating hydrology and biogeochemistry further enhances our understanding of nutrient cycling in river systems (Liu D. et al., 2020).

In the context of ecology, hydrologic connectivity plays a vital role in shaping biodiversity and ecosystem resilience. Ecological dynamics, such as species migration and habitat access, further refine spatial and temporal scales of connectivity, identifying critical thresholds for habitat connectivity in floodplain systems (Stoffers et al., 2022). Stoffers et al. (2022) underscore how fish populations in floodplain rivers depend on habitat connectivity, facilitating migration and access to critical habitats. Likewise, Uno et al. (2022) show that aquatic communities in floodplains reflect varying degrees of hydrological connectivity, highlighting the importance of integrating ecological and hydrological research to understand species' distributions and community structure. These studies highlight the need for interdisciplinary approaches to accurately model hydrological and biogeochemical interactions, improving calibration and predictions of nutrient transport and biodiversity responses to climate-driven hydrologic connectivity changes.

3.2 Interdisciplinary collaborations driving scientific progress

Successful interdisciplinary collaborations have led to significant breakthroughs in understanding hydrologic connectivity (Turnbull et al., 2018; iConn Network, 2024). For instance, the collaboration between hydrologists and biogeochemists has helped address the "old water paradox" in hydrology (Kirchner, 2003), where streamflow is often found to contain a significant proportion of older water. Using geochemical tracers, as Cartwright and Morgenstern (2012) describe, has enabled researchers to unravel the sources of this older water, which is critical for understanding the dynamics between surface and subsurface hydrological systems. Similarly, collaboration between geomorphologists and hydrologists has advanced deltaic stability and sustainability knowledge (Figure 1). Passalacqua et al. (2021) emphasize that delta sustainability requires understanding the spatial scale of sediment transport and hydrodynamic processes, which are best assessed through interdisciplinary methods. Overall, these interdisciplinary collaborations—resolving the old water paradox and advancing delta sustainability—highlight how integrating expertise improves hydrologic understanding, modeling accuracy, and restoration strategies.

4 Management implications and opportunities

Effective management requires not only modeling hydrologic connectivity but also implementing restoration strategies, such as floodplain reconnection, wetland rehabilitation, and riparian corridor restoration (Stoffers et al., 2022), to enhance water and nutrient flow across landscapes (Figure 1). As demonstrated, current approaches often fail to consider how multiple ecological, hydrological, and geomorphological variables interact within an ecosystem. This is an especially problematic oversight when accounting for thresholds, feedback loops, and interactions vital to ecosystem health. Consequently, management efforts often focus on individual variables (e.g., streamflow regulation, sediment transport, or nutrient cycling) in isolation rather than adopting a holistic framework that accounts for system-wide interactions (Zhang et al., 2021). The underutilization of predictive capabilities hampers effective nutrient management, habitat restoration, and flood mitigation. For example, although engineered structures like logjams and beaver dam analogs are increasingly implemented to enhance nitrate removal in headwater streams (e.g., Krause et al., 2024; Wade et al., 2020; Dewey et al., 2022), no reliable method exists to predict the optimal number or placement of these obstructions for achieving desired outcomes (Covino, 2017).

Moreover, current management approaches often need to pay more attention to the complexity of hydrologic connectivity in areas like habitat restoration and flood control (Poeppl et al., 2017, 2020). Restoration projects that reestablish natural water flow—including levee setbacks, wetland rehydration, and beaver dam analogs—are typically based on incomplete models that need to account for hydrological impacts on species migration or vegetation growth. Similarly, flood mitigation strategies often neglect the significance of river corridors and floodplain connectivity, which are critical for water storage and nutrient filtering during high-water events (Wohl et al., 2018; Harvey et al., 2019).

5 Discussion

We evaluated the strengths and limitations of current measurement and modeling techniques, emphasizing the need to integrate hydrologic connectivity restoration efforts into management strategies. We highlighted the importance of predictive modeling, interdisciplinary collaboration, and system-wide approaches to enhance hydrologic resilience and inform adaptive water management. We noted that an integrated and interdisciplinary perspective on hydrologic connectivity is key to effective management, drawing from hydrology, biogeochemistry, geomorphology, and ecology to address system-wide complexities. The discussion in the following subsections underscores the need for future research to develop integrated frameworks that combine hydrological, ecological, and biogeochemical processes to tackle pressing environmental challenges like climate change.

5.1 Challenges and solutions in measurement and modeling techniques

Despite advancements in measuring and modeling hydrologic connectivity, several challenges have remained. For instance, traditional field-based methods (e.g., dye tracing) provide high-resolution data but lack broad spatial coverage (see Section 2.1), while remote sensing offers wide spatial coverage but limited temporal resolution (see Section 2.2). Models are limited by high data requirements (e.g., process-based models), computational complexity (e.g., integrated models), and oversimplified representations (e.g., percolation theory-based models), all of which reduce accuracy. Additionally, they often struggle with inadequate subsurface characterization. Addressing these challenges requires improved spatial and temporal coverage for a more comprehensive understanding of hydrologic connectivity. Researchers increasingly rely on

remote sensing and predictive modeling to bridge this gap and complement traditional measurement approaches.

Researchers have increasingly integrated automated sensors and drones into field-based methods to enhance spatial coverage, reduce labor costs, and provide consistent real-time data collection (Hubbard et al., 2018; Chen et al., 2021). Advancements in visual surveys and high-temporal-resolution camera-based approaches offer promising solutions for reconstructing stream network dynamics (Noto et al., 2024; Manfreda et al., 2024). Efforts should focus on expanding visual surveys, developing machine learning (ML) tools for image analysis, and integrating high-resolution data into models to improve hydrological predictions. To improve subsurface characterization, Wireless Underground Sensor Networks (WUSN) capable of providing subsurface properties should be leveraged (e.g., Barnhart et al., 2010; Ajo-Franklin et al., 2018).

Although automated sensors, drones, visual surveys, high-temporal-resolution cameras, and WUSN offer deeper insights into localized hydrological processes, their full potential can only be realized through scaling and broader application. Remote sensing advancements improve temporal resolution, such as increased satellite monitoring frequency and combining multiple data types (optical, thermal, radar). Incorporating subsurface sensing technologies will further enrich our understanding of surface and subsurface dynamics.

Artificial Intelligence (AI) and ML are already being used to enhance hydrodynamic models by optimizing calibration and reducing dependence on large datasets (Shen et al., 2023). To achieve global applicability, these models require ongoing refinement to address scalability. Incorporating biogeochemical fluxes into percolation theory would make these models more ecologically relevant; meanwhile, integrating real-time monitoring into graph-theoretic models would capture adaptive changes in connectivity. Although graph-theoretic models often use a fixed structure to represent connections, they can be adapted dynamically by integrating real-time monitoring data (Durighetto et al., 2022; Bertassello et al., 2022). For instance, real-time measurements of flow conditions, water levels, or seasonal variations can update edge weights or node attributes, allowing the graph to reflect temporal changes in connectivity, such as flow interruptions or restored connectivity after precipitation events (Himmel et al., 2017; Casteigts et al., 2021). Integrating this real-time monitoring would enhance the models' ability to capture adaptive changes in connectivity (Casteigts et al., 2021). Similarly, ongoing efforts to simplify entropy-based metrics and embed them into flexible frameworks are progressing, yet further refinement is urgently needed to make them more accessible across various ecosystems (Bennett et al., 2019). Similarly, adaptive river connectivity metrics that factor in real-time environmental changes will enhance assessment precision, provided they are consistently implemented across diverse settings (Godsey and Kirchner, 2014).

Significant strides have been made in developing globally applicable ecohydrological models that account for regional ecological dynamics (e.g., Xu et al., 2022; Shuai et al., 2022), yet further efforts are needed to ensure their consistency and broader applicability. Developing integrated frameworks that combine remote sensing, field methods, and modeling will improve assessments and predictive capabilities and enhance adaptive management of hydrologic connectivity by addressing scale, complexity, and metric standardization gaps. However, achieving these advancements requires not only technical innovations but also interdisciplinary collaboration. Hydrologists, ecologists, and data scientists must work together to integrate diverse methodologies and ensure that emerging tools are effectively implemented across various ecosystems.

5.2 Challenges and solutions in interdisciplinary research and management

Despite the clear benefits of interdisciplinary approaches, several challenges remain (e.g., Hubbard et al., 2020). A major issue is the lack of data standardization across fields (Varadharajan et al., 2019; Faybishenko et al., 2022; Simmonds et al., 2022; Arora et al., 2023), as researchers employ diverse data collection and analysis methods, leading to inconsistencies that hinder integration. For example, hydrologists use high-frequency sensor networks to measure water fluxes at 5-min intervals, whereas geochemists rely on seasonal field sampling to analyze water chemistry (Faybishenko et al., 2022). Similarly, in overland flow connectivity studies, hydrologists focus on processes like infiltration and runoff. At the same time, geomorphologists examine structural factors such as slope and gradient—both essential for understanding hydrologic connectivity (Reaney et al., 2014). Maximizing the impact of interdisciplinary collaboration to advance hydrologic connectivity research requires standardized measurement strategies, particularly in data frequency and spatial distribution, to improve research integration and applicability.

In addition, data availability and accessibility remain challenges, as many datasets are fragmented, discipline-specific, or lack open access. Expanding data-sharing platforms and cross-institutional collaborations can help bridge these gaps. Initiatives like the Department of Energy's Environmental System Science Data Infrastructure for a Virtual Ecosystem (ESS-DIVE), United States Geological Survey (USGS) data repositories, and journal-driven open-access mandates aim to improve data accessibility and support interdisciplinary research (Clark et al., 1993; Varadharajan et al., 2019; Simmonds et al., 2022; Lightsom et al., 2022).

Communication barriers further complicate interdisciplinary research, including hydrologic connectivity studies. Scientists from different fields often use distinct terminologies (e.g., runoff in hydrology vs. overland flow in ecology for the same process) and different measurement frameworks (e.g., infiltration measured using infiltrometers in hydrology vs. soil water recharge assessed in ecology through plant water potential), making collaboration difficult. Addressing these challenges requires fostering a culture of interdisciplinary thinking through education and training. Several studies have advocated for educational frameworks that equip scientists with the skills to work across disciplines, enabling them to understand better complex Earth system interactions (e.g., Arora et al., 2022; Dwivedi et al., 2022; Arora et al., 2024).

Hydrologic connectivity research must develop quantifiable metrics and standardized frameworks through interdisciplinary research and collaboration to enable comparisons across space and

time. These tools will enable managers to assess connectivity across diverse regions and time periods, plan accordingly, and simulate future scenarios under changing climate conditions. However, more empirical research is needed to quantify the relationships between hydrologic connectivity and ecological diversity, including habitat heterogeneity and biodiversity (Liu D. et al., 2020; Stoffers et al., 2022).

5.3 Hydrologic connectivity: processes, disruptions, and strategies for management, policy, and practical applications

As discussed in this review, Hydrologic connectivity, encompassing the interplay of hydrological, biogeochemical, ecological, and geomorphological processes, plays a fundamental role in shaping catchment dynamics and resilience. However, both natural processes—such as drought, flooding, and sediment deposition—and human interventions—such as dam removal, fish passage installations, levee setbacks, floodplain reconnection, beaver reintroduction, and wetland rehabilitation—can alter these networks, potentially impacting catchment functionality. Effectively managing these changes requires an integrated approach that combines scientific research with practical applications.

Many field-based studies—such as wetland monitoring (e.g., Ury et al., 2023), river corridor assessments (e.g., Dwivedi et al., 2018a), and beaver dam analog (e.g., Dewey et al., 2022) studies—do not always explicitly assess hydrologic connectivity but still provide valuable insights into its dynamics. These studies can supplement hydrologic connectivity measurements and be used to evaluate restoration interventions by tracking changes in water flow, sediment transport, groundwater levels, and floodplain inundation.

Enhancing or restoring hydrologic connectivity is essential for sustaining water flow regulation, ecosystem resilience, and water quality. Restoring connectivity—reestablishing natural flows within a catchment by removing physical barriers, enhancing natural storage, and improving hydrologic linkages—is a key strategy for effective catchment management and climate adaptation (Jacobson et al., 2022). Key techniques for restoring hydrologic connectivity include longitudinal connectivity restoration, dam removal, fish passage installations, culvert replacement, and sediment transport restoration to improve water, sediment, and organism movement along rivers and streams (Heckmann et al., 2018; Rogosch et al., 2024). Lateral connectivity restoration focuses on reconnecting floodplains through levee setbacks, wetland restoration, and riparian buffer establishment to enhance flood storage and infiltration (Covino, 2017; Ameli and Creed, 2017). Vertical connectivity improvements aim to restore surface-subsurface interactions through soil conservation, permeable urban surfaces, and groundwater flow path restoration to support infiltration and water retention. Ecological connectivity enhances habitat continuity by reintroducing beavers, creating side channels, and managing invasive species to restore natural hydrologic dynamics (Zimmer and McGlynn, 2018; Walker and Hassall, 2021).

While policy measures—such as wetland protection laws, river corridor zoning—and financial incentives for floodplain restoration, and ecological interventions—such as dam removal, riparian buffer restoration, and reintroducing beavers—can help restore hydrologic connectivity, successful implementation depends on a robust understanding of the complex interactions among water, sediment, and ecosystems across landscapes (Magilligan et al., 2016; Kendall, 2023; Brown et al., 2024). Because these interactions are complex and abstract, analogies—such as social networks, ecological corridors, and fluid flow—help visualize connectivity patterns (Masselink et al., 2017; Rinaldo et al., 2018; Gooseff et al., 2017). Similarly, hydrologic connectivity can be likened to an electric circuit, where water flow resembles electrical current, obstacles such as vegetation and rocky outcrops act as resistors, and wetlands function as capacitors, temporarily storing and regulating water (Al-Sayouri et al., 2018; Hasanah et al., 2022). These interdisciplinary frameworks provide valuable tools for research and management, though further refinement is needed for effective real-world application.

6 Concluding insights

This review synthesizes current approaches to measuring, modeling, and managing hydrologic connectivity, focusing on the importance of interdisciplinary collaboration (e.g., between hydrologists and ecologists) and the potential of emerging technologies such as drones and imagery. Traditional measurement and modeling approaches for hydrologic connectivity struggle to capture complex catchment interactions, constrained by spatial, temporal, and computational limitations, as well as the inherent difficulty of integrating subsurface processes with surface hydrology. Other challenges are posed by fragmented datasets, limited open-access data, and communication barriers across disciplines. Without broader implementation and comparability across different regions and scales, the true potential of hydrologic connectivity in water resource management cannot be realized, yet the absence of standardized connectivity metrics and methodologies hampers progress. All of these issues require urgent attention.

A comprehensive approach to hydrologic connectivity should integrate emerging technologies—including camera imagery, drones, AI, and WUSN—to enhance data collection and improve spatial and temporal coverage. Expanding standardization efforts, including open-access data platforms (e.g., ESS-DIVE, USGS repositories) and unified measurement strategies, will facilitate interdisciplinary collaboration and improve data integration. A unified framework is required to facilitate interdisciplinary collaboration and enhance science-based decision-making in water resource management. Conceptual simplifications, such as the electric circuit analogy, can provide such a framework by illustrating hydrologic connectivity holistically within a catchment and fostering a shared perspective, common language, and integrated approach across disciplines. Future research should prioritize high-resolution and long-term monitoring as well as adaptive management to restore hydrologic connectivity in fragmented landscapes. Management strategies must integrate predictive modeling to account for

system-wide connectivity, anticipate climate-driven shifts, and enhance ecosystem resilience. Ultimately, this review inspires the catchment science community to transform hydrologic connectivity research into practical management tools that guide policy decisions and promote adaptive, resilient water resource strategies.

Author contributions

DD: Conceptualization, Methodology, Writing – original draft, Writing – review & editing. RP: Conceptualization, Writing – review & editing. EW: Conceptualization, Writing – review & editing.

Funding

The author(s) declare that financial support was received for the research and/or publication of this article. DDs work was supported by the Watershed Function Scientific Focus Area at Lawrence Berkeley National Laboratory, funded by the U.S. Department of Energy, Office of Science, Office of Biological and Environmental Research, under Award No. DE-AC02-05CH11231.

Acknowledgments

Graphics support provided by Susana Roque-Malo from Convey Scientific Graphics and Ella Maru Studio.

Conflict of interest

The authors declare that the research was conducted in the absence of any commercial or financial relationships that could be construed as a potential conflict of interest.

The author(s) declared that they were an editorial board member of Frontiers, at the time of submission. This had no impact on the peer review process and the final decision.

Publisher's note

References

Ackerer, J., Kuppel, S., Braud, I., Pasquet, S., Fovet, O., Probst, A., et al. (2023). Exploring the critical zone heterogeneity and the hydrological diversity using an integrated ecohydrological model in three contrasted long-term observatories. *Water Resour. Res.* 59:e2023WR035672. doi: 10.1029/2023WR035672

Aho, K. B., Flotemersch, J. E., Leibowitz, S. G., LaCroix, M. A., and Weber, M. H. (2020). Applying the index of watershed integrity to the matanuska-susitna basin. *Arct. Antarct. Alp. Res.* 52, 435–449. doi: 10.1080/15230430.2020.1800219

Ajo-Franklin, J., Dou, S., Lindsey, N., Monga, I., Tracy, C., Robertson, M., et al. (2018). Using dark fiber and distributed acoustic sensing for near-surface characterization and broadband seismic event detection. *Sci. Rep*. 9:1328. doi: 10.31223/OSF.IO/KXQB2

Al-Sayouri, S. A., Koutra, D., Papalexakis, E. E., and Lam, S. S. (2018). Recs: robust graph embedding using connection subgraphs. *arXiv preprint arXiv:1805.01509*.

Ameli, A. A., and Creed, I. F. (2017). Quantifying hydrologic connectivity of wetlands to surface water systems. *Hydrol. Earth Syst. Sci*. 21, 1791–1808. doi: 10.5194/hess-21-1791-2017

Appling, A. P., Bernhardt, E. S., and Stanford, J. A. (2014). Floodplain biogeochemical mosaics: a multidimensional view of alluvial soils. *J. Geophys. Res*. 119, 1538–1553. doi: 10.1002/2013JG002543

Arora, B., Currin, A., Dwivedi, D., Fru, M. I., Kumar, N., McLeod, C. L., et al. (2022). Volcanology, geochemistry, and petrology perspectives on integrated, coordinated, open, networked (ICON) science. *Earth Space Sci*. 9:e2021EA002120. doi: 10.1029/2021EA002120

Arora, B., Kuppel, S., Wellen, C., Oswald, C., Groh, J., Payandi-Rolland, D., et al. (2023). Building cross-site and cross-network collaborations in critical zone science. *J. Hydrol.* 618:129248. doi: 10.1016/j.jhydrol.2023.129248

Arora, B., Seybold, E., and Jin, L. (2024). Women in critical zone science. *Front. Water* 6:1404317. doi: 10.3389/frwa.2024.1404317

Arora, B., Spycher, N. F., Steefel, C. I., Molins, S., Bill, M., Conrad, M. E., et al. (2016). Influence of hydrological, biogeochemical and temperature transients on subsurface carbon fluxes in a flood plain environment. *Biogeochemistry* 127, 367–396. doi: 10.1007/s10533-016-0186-8

Arora, B., Wainwright, H. M., Dwivedi, D., Vaughn, L. J., Curtis, J. B., Torn, M. S., et al. (2019). Evaluating temporal controls on greenhouse gas (ghg) fluxes in an arctic tundra environment: an entropy-based approach. *Sci. Total Environ*. 649, 284–299. doi: 10.1016/j.scitotenv.2018.08.251

Baram, S., Ronen, Z., Kurtzman, D., Külls, C., and Dahan, O. (2013). Desiccation-crack-induced salinization in deep clay sediment. *Hydrol. Earth Syst. Sci*. 17, 1533–1545. doi: 10.5194/hess-17-1533-2013

Barnhart, K., Urteaga, I., Han, Q., Jayasumana, A., and Illangasekare, T. (2010). On integrating groundwater transport models with wireless sensor networks. *Groundwater* 48, 771–780. doi: 10.1111/j.1745-6584.2010.00684.x

Bennett, A., Nijssen, B., Ou, G., Clark, M., and Nearing, G. (2019). Quantifying process connectivity with transfer entropy in hydrologic models. *Water Resour. Res*. 55, 4613–4629. doi: 10.1029/2018WR024555

Bertassello, L. E., Durighetto, N., and Botter, G. (2022). Eco-hydrological modelling of channel network dynamics part 2: application to metapopulation dynamics. *R. Soc. Open Sci*. 9:220945. doi: 10.1098/rsos.220945

Bertassello, L. E., Rao, P. S. C., Jawitz, J. W., Aubeneau, A. F., and Botter, G. (2020). Wetlandscape hydrologic dynamics driven by shallow groundwater and landscape topography. *Hydrol. Process*. 34, 1460–1474. doi: 10.1002/hyp.13661

Beven, K. J. (2012). *Rainfall-Runoff Modelling: the Primer*. New York: John Wiley Sons. doi: 10.1002/9781119951001

Borselli, L., Cassi, P., and Torri, D. (2008). Prolegomena to sediment and flow connectivity in the landscape: a gis and field numerical assessment. *Catena* 75, 268–277. doi: 10.1016/j.catena.2008.07.006

Bracken, L. J., and Croke, J. (2007). The concept of hydrological connectivity and its contribution to understanding runoff-dominated geomorphic systems. *Hydrol. Proc*. 21, 1749–1763. doi: 10.1002/hyp.6313

Bracken, L. J., Turnbull, L., Wainwright, J., and Bogaart, P. (2015). Sediment connectivity: a framework for understanding sediment transfer at multiple scales. *Earth Surf. Proc. Landf*. 40, 177–188. doi: 10.1002/esp.3635

Bracken, L. J., Wainwright, J., Ali, G., Tetzlaff, D., Smith, M., Reaney, S., et al. (2013). Concepts of hydrological connectivity: research approaches, pathways and future agendas. *Earth-Sci. Rev*. 119, 17–34. doi: 10.1016/j.earscirev.2013.02.001

Brown, R. L., Charles, D., Horwitz, R. J., Pizzuto, J. E., Skalak, K., Velinsky, D. J., et al. (2024). Size-dependent effects of dams on river ecosystems and implications for dam removal outcomes. *Ecol. Applic*. 34:e3016. doi: 10.1002/eap.3016

Buddendorf, W., Malcolm, I., Geris, J., Fabris, L., Millidine, K., Wilkinson, M., et al. (2017). Spatio-temporal effects of river regulation on habitat quality for atlantic salmon fry. *Ecol. Indic*. 83, 292–302. doi: 10.1016/j.ecolind.2017.08.006

Camporese, M., Paniconi, C., Putti, M., and McDonnell, J. J. (2019). Fill and spill hillslope runoff representation with a richards equation-based model. *Water Resour. Res.* 55, 8445–8462. doi: 10.1029/2019WR025726

Cartwright, I., and Morgenstern, U. (2012). Constraining groundwater recharge and the rate of geochemical processes using tritium and major ion geochemistry: ovens catchment, southeast australia. *J. Hydrol.* 475, 137–149. doi: 10.1016/j.jhydrol.2012.09.037

Casteigts, A., Peters, J. G., and Schoeters, J. (2021). Temporal cliques admit sparse spanners. *J. Comput. Syst. Sci.* 121, 1–17. doi: 10.1016/j.jcss.2021.04.004

Chen, X., Lee, R. M., Dwivedi, D., Son, K., Fang, Y., Zhang, X., et al. (2021). Integrating field observations and process-based modeling to predict watershed water quality under environmental perturbations. *J. Hydrol.* 602:125762. doi: 10.1016/j.jhydrol.2020.125762

Clark, R. N., Swayze, G. A., Gallagher, A. J., King, T. V., and Calvin, W. M. (1993). *The us geological survey, digital spectral library: version 1 (0.2 to 3.0 um)*. Technical report, Geological Survey (US). doi: 10.3133/ofr93592

Coon, E. T., and Shuai, P. (2022). Watershed workflow: a toolset for parameterizing data-intensive, integrated hydrologic models. *Environ. Model. Softw.* 157:105502. doi: 10.1016/j.envsoft.2022.105502

Covino, T. (2017). Hydrologic connectivity as a framework for understanding biogeochemical flux through watersheds and along fluvial networks. *Geomorphology* 277, 133–144. doi: 10.1016/j.geomorph.2016.09.030

Dahan, O., Talby, R., Yechieli, Y., Adar, E., Lazarovitch, N., and Enzel, Y. (2009). *In situ* monitoring of water percolation and solute transport using a vadose zone monitoring system. *Vadose Zone J.* 8, 916–925. doi: 10.2136/vzj2008.0134

Dewey, C., Fox, P. M., Bouskill, N. J., Dwivedi, D., Nico, P., and Fendorf, S. (2022). Beaver dams overshadow climate extremes in controlling riparian hydrology and water quality. *Nat. Commun.* 13:6509. doi: 10.1038/s41467-022-34022-0

Drummond, J., Aubeneau, A., and Packman, A. (2014). Stochastic modeling of fine particulate organic carbon dynamics in rivers. *Water Resour. Res.* 50, 4341–4356. doi: 10.1002/2013WR014665

Durighetto, N., Mariotto, V., Zanetti, F., McGuire, K. J., Mendicino, G., Senatore, A., et al. (2022). Probabilistic description of streamflow and active length regimes in rivers. *Water Resour. Res.* 58:e2021WR031344. doi: 10.1029/2021WR031344

Durighetto, N., Noto, S., Tauro, F., Grimaldi, S., and Botter, G. (2023). Integrating spatially-and temporally-heterogeneous data on river network dynamics using graph theory. *Iscience* 26:107417. doi: 10.1016/j.isci.2023.107417

Dwivedi, D., Arora, B., Steefel, C. I., Dafflon, B., and Versteeg, R. (2018a). Hot spots and hot moments of nitrogen in a riparian corridor. *Water Resour. Res.* 54, 205–222. doi: 10.1002/2017WR022346

Dwivedi, D., and Mohanty, B. P. (2016). Hot spots and persistence of nitrate in aquifers across scales. *Entropy* 18:25. doi: 10.3390/e18010025

Dwivedi, D., Santos, A., Barnard, M. A., Crimmins, T. M., Malhotra, A., Rod, K. A., et al. (2022). Biogeosciences perspectives on integrated, coordinated, open, networked (ICON) science. *Earth Space Sci.* 9:e2021EA002119. doi: 10.1029/2021EA002119

Dwivedi, D., Steefel, C. I., Arora, B., Newcomer, M., Moulton, J. D., Dafflon, B., et al. (2018b). Geochemical exports to river from the intrameander hyporheic zone under transient hydrologic conditions: east river mountainous watershed, colorado. *Water Resour. Res.* 54, 8456–8477. doi: 10.1029/2018WR023377

Fang, S., Chen, M., Li, J., Zhang, L., Zhang, Y., Yang, C., et al. (2024). Evaluation and optimization of urban hydrological connectivity based on graph theory: a case study in chengdu, China. *Ecol. Inform.* 82:102749. doi: 10.1016/j.ecoinf.2024.102749

Faybishenko, B., Versteeg, R., Pastorello, G., Dwivedi, D., Varadharajan, C., and Agarwal, D. (2022). Challenging problems of quality assurance and quality control (QA/QC) of meteorological time series data. *Stoch. Environ. Res. Risk Assess.* 36, 1049–1062. doi: 10.1007/s00477-021-02106-w

Fortuna, M. A., Gómez-Rodríguez, C., and Bascompte, J. (2006). Spatial network structure and amphibian persistence in stochastic environments. *Proc. R. Soc. B Biol. Sci.* 273, 1429–1434. doi: 10.1098/rspb.2005.3448

Fox, P. M., Carrero, S., Anderson, C., Dewey, C., Keiluweit, M., Conrad, M., et al. (2022). Sulfur biogeochemical cycling and redox dynamics in a shale-dominated mountainous watershed. *J. Geophys. Res.* 127:e2021JG006769. doi: 10.1029/2021JG006769

Fryirs, K. A., Brierley, G. J., Preston, N. J., and Kasai, M. (2007). Buffers, barriers and blankets: The (dis) connectivity of catchment-scale sediment cascades. *Catena* 70, 49–67. doi: 10.1016/j.catena.2006.07.007

Garbin, S., Celegon, E. A., Fanton, P., and Botter, G. (2019). Hydrological controls on river network connectivity. *R. Soc. Open Sci.* 6:181428. doi: 10.1098/rsos.181428

Godsey, S., and Kirchner, J. W. (2014). Dynamic, discontinuous stream networks: hydrologically driven variations in active drainage density, flowing channels and stream order. *Hydrol. Process.* 28, 5791–5803. doi: 10.1002/hyp.10310

Godsey, S. E., Hartmann, J., and Kirchner, J. W. (2019). Catchment chemostasis revisited: water quality responds differently to variations in weather and climate. *Hydrol. Process.* 33, 3056–3069. doi: 10.1002/hyp.13554

Good, S. P., Noone, D., and Bowen, G. (2015). Hydrologic connectivity constrains partitioning of global terrestrial water fluxes. *Science* 349, 175–177. doi: 10.1126/science.aaa5931

Gooseff, M. N., Wlostowski, A., McKnight, D. M., and Jaros, C. (2017). Hydrologic connectivity and implications for ecosystem processes-lessons from naked watersheds. *Geomorphology* 277, 63–71. doi: 10.1016/j.geomorph.2016.04.024

Haarstad, K., Bavor, H., and Mæhlum, T. (2012). Organic and metallic pollutants in water treatment and natural wetlands: a review. *Water Sci. Technol.* 65, 76–99. doi: 10.2166/wst.2011.831

Harvey, J., Gomez-Velez, J., Schmadel, N., Scott, D., Boyer, E., Alexander, R., et al. (2019). How hydrologic connectivity regulates water quality in river corridors. *JAWRA J. Am. Water Resour. Assoc.* 55, 369–381. doi: 10.1111/1752-1688.12691

Harvey, J., and Gooseff, M. (2015). River corridor science: hydrologic exchange and ecological consequences from bedforms to basins. *Water Resour. Res.* 51, 6893–6922. doi: 10.1002/2015WR017617

Harvey, J. W., Drummond, J. D., Martin, R. L., McPhillips, L. E., Packman, A. I., Jerolmack, D., et al. (2012). Hydrogeomorphology of the hyporheic zone: stream solute and fine particle interactions with a dynamic streambed. *J. Geophys. Res.* 117:2043. doi: 10.1029/2012JG002043

Hasanah, A., Sunarya, A., and Viridi, S. (2022). "Charge and discharge of capasitors: revisiting the analogy with water in connected containers, in *Journal of Physics: Conference Series* (IOP Publishing), 012073. doi: 10.1088/1742-6596/2243/1/012073

Heckmann, T., Cavalli, M., Cerdan, O., Foerster, S., Javaux, M., Lode, E., et al. (2018). Indices of sediment connectivity: opportunities, challenges and limitations. *Earth-Sci. Rev.* 187, 77–108. doi: 10.1016/j.earscirev.2018.08.004

Helton, A. M., Poole, G. C., Payn, R. A., Izurieta, C., and Stanford, J. A. (2014). Relative influences of the river channel, floodplain surface, and alluvial aquifer on simulated hydrologic residence time in a montane river floodplain. *Geomorphology* 205, 17–26. doi: 10.1016/j.geomorph.2012.01.004

Herzog, A., Hellwig, J., and Stahl, K. (2024). An investigation of anthropogenic influences on hydrologic connectivity using model stress tests. *Hydrol. Earth Syst. Sci.* 28, 4065–4083. doi: 10.5194/hess-28-4065-2024

Himmel, A.-S., Molter, H., Niedermeier, R., and Sorge, M. (2017). Adapting the bron-kerbosch algorithm for enumerating maximal cliques in temporal graphs. *Soc. Netw. Anal. Mining* 7, 1–16. doi: 10.1007/s13278-017-0455-0

Huang, S., Wang, P., Hua, Z., Dong, Y., and Shi, J. (2024). Structural characteristics and spatiotemporal changes of a reticular river network based on complex network theory. *J. Hydrol.* 638:131577. doi: 10.1016/j.jhydrol.2024.131577

Hubbard, S. S., Varadharajan, C., Wu, Y., Wainwright, H., and Dwivedi, D. (2020). Emerging technologies and radical collaboration to advance predictive understanding of watershed hydrobiogeochemistry. *Hydrol. Process.* 34, 3175–3182. doi: 10.1002/hyp.13807

Hubbard, S. S., Williams, K. H., Agarwal, D., Banfield, J., Beller, H., Bouskill, N., et al. (2018). The east river, colorado, watershed: a mountainous community testbed for improving predictive understanding of multiscale hydrological-biogeochemical dynamics. *Vadose Zone J.* 17, 1–25. doi: 10.2136/vzj2018.03.0061

iConn Network (2024). *Useful papers*. Available online at: https://iconn.network/network-resources/useful-papers/ (accessed December 20, 2024).

Jacobson, R. B., Bouska, K. L., Bulliner, E. A., Lindner, G. A., and Paukert, C. P. (2022). Geomorphic controls on floodplain connectivity, ecosystem services, and sensitivity to climate change: an example from the lower missouri river. *Water Resour. Res.* 58:e2021WR031204. doi: 10.1029/2021WR031204

Julien, P., and Simons, D. (1985). Sediment transport capacity of overland flow. *Trans. ASAE* 28, 755–0762. doi: 10.13031/2013.32333

Keesstra, S., Nunes, J. P., Saco, P., Parsons, T., Poeppl, R., Masselink, R., et al. (2018). The way forward: can connectivity be useful to design better measuring and modelling schemes for water and sediment dynamics? *Sci. Total Environ.* 644, 1557–1572. doi: 10.1016/j.scitotenv.2018.06.342

Kendall, M. (2023). *From Wastelands to Wetlands: The Story of Coastal Wetlands in the United States*. PhD thesis, Duke University.

Kirchner, J. W. (2003). A double paradox in catchment hydrology and geochemistry. *Hydrol. Process.* 17, 871–874. doi: 10.1002/hyp.5108

Krause, S., Lewandowski, J., Grimm, N. B., Hannah, D. M., Pinay, G., McDonald, K., et al. (2024). Ecohydrological interfaces as hotspots of ecosystem processes. *Ecohydrol. Interf.* 56, 1–28. doi: 10.1002/9781119489702.ch1

Lane, C. R., Leibowitz, S. G., Autrey, B. C., LeDuc, S. D., and Alexander, L. C. (2018). Hydrological, physical, and chemical functions and connectivity of non-floodplain wetlands to downstream waters: a review. *JAWRA* 54, 346–371. doi: 10.1111/1752-1688.12633

Lee, E., Epstein, J. M., and Cohen, M. J. (2023). Patterns of wetland hydrologic connectivity across coastal-plain wetlandscapes. *Water Resour. Res.* 59:e2023WR034553. doi: 10.1029/2023WR034553

Lee, S., Lee, B., Lee, J., Song, J., and McCarty, G. W. (2023). Detecting causal relationship of non-floodplain wetland hydrologic connectivity using convergent cross mapping. *Sci. Rep*. 13:17220. doi: 10.1038/s41598-023-44071-0

Lehmann, P., Hinz, C., McGrath, G., Tromp-van Meerveld, H., and McDonnell, J. J. (2007). Rainfall threshold for hillslope outflow: an emergent property of flow pathway connectivity. *Hydrol. Earth Syst. Sci*. 11, 1047–1063. doi: 10.5194/hess-11-1047-2007

Leibowitz, S. G., Wigington Jr, P. J., Schofield, K. A., Alexander, L. C., Vanderhoof, M. K., and Golden, H. E. (2018). Connectivity of streams and wetlands to downstream waters: an integrated systems framework. *JAWRA* 54, 298–322. doi: 10.1111/1752-1688.12631

Lewandowski, J., Meinikmann, K., Nützmann, G., and Rosenberry, D. O. (2015). Groundwater-the disregarded component in lake water and nutrient budgets. part 2: effects of groundwater on nutrients. *Hydrol. Proc*. 29, 2922–2955. doi: 10.1002/hyp.10384

Lexartza-Artza, I., and Wainwright, J. (2009). Hydrological connectivity: Linking concepts with practical implications. *Catena* 79, 146–152. doi: 10.1016/j.catena.2009.07.001

Lexartza-Artza, I., and Wainwright, J. (2011). Making connections: changing sediment sources and sinks in an upland catchment. *Earth Surf. Proc. Landforms* 36, 1090–1104. doi: 10.1002/esp.2134

Li, L., Knapp, J. L., Lintern, A., Ng, G.-H. C., Perdrial, J., Sullivan, P. L., et al. (2024). River water quality shaped by land-river connectivity in a changing climate. *Nat. Clim. Chang*. 14, 225–237. doi: 10.1038/s41558-023-01923-x

Lightsom, F. L., Hutchison, V. B., Bishop, B., Debrewer, L. M., Govoni, D. L., Latysh, N., et al. (2022). *Opportunities to improve alignment with the fair principles for us geological survey data*. Technical report, US Geological Survey. doi: 10.3133/ofr20221043

Liu, D., Wang, X., Aminjafari, S., Yang, W., Cui, B., Yan, S., et al. (2020). Using insar to identify hydrological connectivity and barriers in a highly fragmented wetland. *Hydrol. Process*. 34, 4417–4430. doi: 10.1002/hyp.13899

Liu, J., Engel, B. A., Wang, Y., Wu, Y., Zhang, Z., and Zhang, M. (2019). Runoff response to soil moisture and micro-topographic structure on the plot scale. *Sci. Rep*. 9:2532. doi: 10.1038/s41598-019-39409-6

Liu, Y., Wallace, C. D., Zhou, Y., Ershadnia, R., Behzadi, F., Dwivedi, D., et al. (2020). Influence of streambed heterogeneity on hyporheic flow and sorptive solute transport. *Water* 12:1547. doi: 10.3390/w12061547

Magilligan, F. J., Graber, B. E., Nislow, K. H., Chipman, J. W., Sneddon, C. S., and Fox, C. A. (2016). River restoration by dam removal: enhancing connectivity at watershed scales. *Elementa* 4:000108. doi: 10.12952/journal.elementa.000108

Manfreda, S., Miglino, D., Saddi, K. C., Jomaa, S., Eltner, A., Perks, M., et al. (2024). Advancing river monitoring using image-based techniques: challenges and opportunities. *Hydrol. Sci. J*. 69, 657–677. doi: 10.1080/02626667.2024.2333846

Masselink, R. J., Heckmann, T., Temme, A. J., Anders, N. S., Gooren, H. P., and Keesstra, S. D. (2017). A network theory approach for a better understanding of overland flow connectivity. *Hydrol. Process*. 31, 207–220. doi: 10.1002/hyp.10993

Maxwell, C. M., Fernald, A. G., Cadol, D., Faist, A. M., and King, J. P. (2021). Managing flood flow connectivity to landscapes to build buffering capacity to disturbances: an ecohydrologic modeling framework for drylands. *J. Environ. Manage*. 278:111486. doi: 10.1016/j.jenvman.2020.111486

Mikkelson, K., Maxwell, R., Ferguson, I., Stednick, J., McCray, J., and Sharp, J. (2013). Mountain pine beetle infestation impacts: modeling water and energy budgets at the hill-slope scale. *Ecohydrology* 6, 64–72. doi: 10.1002/eco.278

Noto, S., Durighetto, N., Tauro, F., Grimaldi, S., and Botter, G. (2024). Characterizing space-time channel network dynamics in a mediterranean intermittent catchment of central Italy combining visual surveys and cameras. *Water Resour. Res*. 60:e2023WR034682. doi: 10.1029/2023WR034682

Olliver, E. A., Edmonds, D., and Shaw, J. B. (2020). Influence of floods, tides, and vegetation on sediment retention in wax Lake Delta, Louisiana, USA. *J. Geophys. Res*. 125:e2019JF005316. doi: 10.1029/2019JF005316

Passalacqua, P. (2017). The delta connectome: a network-based framework for studying connectivity in river deltas. *Geomorphology* 277, 50–62. doi: 10.1016/j.geomorph.2016.04.001

Passalacqua, P., Giosan, L., Goodbred, S., and Overeem, I. (2021). Stable≠ sustainable: delta dynamics versus the human need for stability. *Earth's Future* 9:e2021EF002121. doi: 10.1029/2021EF002121

Poeppl, R. E., Fryirs, K. A., Tunnicliffe, J., and Brierley, G. J. (2020). Managing sediment (dis) connectivity in fluvial systems. *Sci. Total Environ*. 736:139627. doi: 10.1016/j.scitotenv.2020.139627

Poeppl, R. E., Keesstra, S. D., and Maroulis, J. (2017). A conceptual connectivity framework for understanding geomorphic change in human-impacted fluvial systems. *Geomorphology* 277, 237–250. doi: 10.1016/j.geomorph.2016.07.033

Pöppl, R. E., Parsons, A. J., and Keesstra, S. D. (2024). "Connectivity in geomorphology, in *Connectivity in Geomorphology*, eds. R. E. Pöppl, A. J. Parsons, and S. D. Keesstra (Cambridge: Cambridge University Press).

Pringle, C. M. (2001). Hydrologic connectivity and the management of biological reserves: a global perspective. *Ecol. Applic*. 11, 981–998. doi: 10.1890/1051-0761(2001)011[0981:HCATMO]2.0.CO;2

Prosser, I. P., Dietrich, W. E., and Stevenson, J. (1995). Flow resistance and sediment transport by concentrated overland flow in a grassland valley. *Geomorphology* 13, 71–86. doi: 10.1016/0169-555X(95)00020-6

Rains, M., Leibowitz, S., Cohen, M., Creed, I., Golden, H., Jawitz, J., et al. (2016). Geographically isolated wetlands are part of the hydrological landscape. *Hydrol. Process*. 30, 153–160. doi: 10.1002/hyp.10610

Reaney, S., Bracken, L. J., and Kirkby, M. (2014). The importance of surface controls on overland flow connectivity in semi-arid environments: results from a numerical experimental approach. *Hydrol. Process*. 28, 2116–2128. doi: 10.1002/hyp.9769

Renard, P., and Allard, D. (2013). Connectivity metrics for subsurface flow and transport. *Adv. Water Resour*. 51, 168–196. doi: 10.1016/j.advwatres.2011.12.001

Rimon, Y., Nativ, R., and Dahan, O. (2011). Physical and chemical evidence for pore-scale dual-domain flow in the vadose zone. *Vadose Zone J*. 10, 322–331. doi: 10.2136/vzj2009.0113

Rinaldo, A., Gatto, M., and Rodriguez-Iturbe, I. (2018). River networks as ecological corridors: a coherent ecohydrological perspective. *Adv. Water Resour*. 112, 27–58. doi: 10.1016/j.advwatres.2017.10.005

Rogosch, J. S., Boehm, H. I., Tingley III, R. W., Wright, K. D., Webb, E. B., Paukert, C. P. (2024). Evaluating effectiveness of restoration to address current stressors to riverine fish. *Freshw. Biol*. 69, 607–622. doi: 10.1111/fwb.14232

Roy, S. (2023). "Identification of potential anthropogenic barriers to fluvial connectivity in the lower gangetic basin of India", in *Environmental Management and Sustainability in India: Case Studies from West Bengal* (Springer), 35–55. doi: 10.1007/978-3-031-31399-8_3

Schumm, S. A. (1965). *Quaternary Paleohydrology. The Quaternary of the U.S.* Princeton: Princeton University Press, 783–794. doi: 10.1515/9781400876525-050

Şensoy, A., Uysal, G., and Şorman, A. (2018). Developing a decision support framework for real-time flood management using integrated models. *J. Flood Risk Manag*. 11, S866–S883. doi: 10.1111/jfr3.12280

Shen, C., Appling, A. P., Gentine, P., Bandai, T., Gupta, H., Tartakovsky, A., et al. (2023). Differentiable modelling to unify machine learning and physical models for geosciences. *Nat. Rev. Earth Environ*. 4, 552–567. doi: 10.1038/s43017-023-00450-9

Shuai, P., Chen, X., Mital, U., Coon, E. T., and Dwivedi, D. (2022). The effects of spatial and temporal resolution of gridded meteorological forcing on watershed hydrological responses. *Hydrol. Earth Syst. Sci*. 26, 2245–2276. doi: 10.5194/hess-26-2245-2022

Simmonds, M. B., Riley, W. J., Agarwal, D. A., Chen, X., Cholia, S., Crystal-Ornelas, R., et al. (2022). Guidelines for publicly archiving terrestrial model data to enhance usability, intercomparison, and synthesis. *Data Sci. J*. 21:3. doi: 10.5334/dsj-2022-003

Siqueira, V. A., Paiva, R. C., Fleischmann, A. S., Fan, F. M., Ruhoff, A. L., Pontes, P. R., et al. (2018). Toward continental hydrologic-hydrodynamic modeling in South America. *Hydrol. Earth Syst. Sci*. 22, 4815–4842. doi: 10.5194/hess-22-4815-2018

Somers, L. D., Gordon, R. P., McKenzie, J. M., Lautz, L. K., Wigmore, O., Glose, A., et al. (2016). Quantifying groundwater-surface water interactions in a proglacial Valley, Cordillera Blanca, Peru. *Hydrol. Process*. 30, 2915–2929. doi: 10.1002/hyp.10912

Stoffers, T., Buijse, A., Geerling, G., Jans, L., Schoor, M., Poos, J., et al. (2022). Freshwater fish biodiversity restoration in floodplain rivers requires connectivity and habitat heterogeneity at multiple spatial scales. *Sci. Total Environ*. 838:156509. doi: 10.1016/j.scitotenv.2022.156509

Tapley, B. D., Bettadpur, S., Ries, J. C., Thompson, P. F., and Watkins, M. M. (2004). Grace measurements of mass variability in the earth system. *Science* 305, 503–505. doi: 10.1126/science.1099192

Taylor, P. D., Fahrig, L., Henein, K., and Merriam, G. (1993). Connectivity is a vital element of landscape structure. *Oikos* 68, 571–573. doi: 10.2307/3544927

Tejedor, A., Longjas, A., Zaliapin, I., and Foufoula-Georgiou, E. (2015). Delta channel networks: 2. metrics of topologic and dynamic complexity for delta comparison, physical inference, and vulnerability assessment *Water Resour. Res*. 51, 4019–4045. doi: 10.1002/2014WR016604

Turnbull, L., Hütt, M.-T., Ioannides, A. A., Kininmonth, S., Poeppl, R., Tockner, K., et al. (2018). Connectivity and complex systems: learning from a multi-disciplinary perspective. *Appl. Netw. Sci*. 3, 1–49. doi: 10.1007/s41109-018-0067-2

Turnbull, L., Wainwright, J., and Brazier, R. E. (2008). A conceptual framework for understanding semi-arid land degradation: ecohydrological interactions across multiple-space and time scales. *Ecohydrology* 1, 23–34. doi: 10.1002/eco.4

Uno, H., Yokoi, M., Fukushima, K., Kanno, Y., Kishida, O., Mamiya, W., et al. (2022). Spatially variable hydrological and biological processes shape diverse post-flood aquatic communities. *Freshw. Biol*. 67, 549–563. doi: 10.1111/fwb.13862

Ury, E. A., Arrumugam, P., Herbert, E. R., Badiou, P., Page, B., and Basu, N. B. (2023). Source or sink? Meta-analysis reveals diverging controls of phosphorus retention and release in restored and constructed wetlands. *Environ. Res. Lett*. 18:083002. doi: 10.1088/1748-9326/ace6bf

Van Meerveld, H., Jones, J. P., Ghimire, C. P., Zwartendijk, B. W., Lahitiana, J., Ravelona, M., et al. (2021). Forest regeneration can positively contribute to local hydrological ecosystem services: implications for forest landscape restoration. *J. Appl. Ecol.* 58, 755–765. doi: 10.1111/1365-2664.13836

Varadharajan, C., Agarwal, D. A., Brown, W., Burrus, M., Carroll, R. W., Christianson, D. S., et al. (2019). Challenges in building an end-to-end system for acquisition, management, and integration of diverse data from sensor networks in watersheds: lessons from a mountainous community observatory in east river, colorado. *IEEE Access* 7, 182796–182813. doi: 10.1109/ACCESS.2019.2957793

Wade, J., Lautz, L., Kelleher, C., Vidon, P., Davis, J., Beltran, J., et al. (2020). Beaver dam analogues drive heterogeneous groundwater-surface water interactions. *Hydrol. Process.* 34, 5340–5353. doi: 10.1002/hyp.13947

Wainwright, J., Turnbull, L., Ibrahim, T. G., Lexartza-Artza, I., Thornton, S. F., and Brazier, R. E. (2011). Linking environmental regimes, space and time: interpretations of structural and functional connectivity. *Geomorphology* 126, 387–404. doi: 10.1016/j.geomorph.2010.07.027

Walker, J. R., and Hassall, C. (2021). The effects of water chemistry and lock-mediated connectivity on macroinvertebrate diversity and community structure in a canal in northern england. *Urban Ecosyst.* 24, 491–500. doi: 10.1007/s11252-020-01053-8

Ward, J. (1989). The four-dimensional nature of lotic ecosystems. *J. North Am. Benthol. Soc.* 8, 2–8. doi: 10.2307/1467397

Wohl, E., Brierley, G., Cadol, D., Coulthard, T. J., Covino, T., Fryirs, K. A., et al. (2019). Connectivity as an emergent property of geomorphic systems. *Earth Surf. Proc. Landforms* 44, 4–26. doi: 10.1002/esp.4434

Wohl, E., Lininger, K. B., and Scott, D. N. (2018). River beads as a conceptual framework for building carbon storage and resilience to extreme climate events into river management. *Biogeochemistry* 141, 365–383. doi: 10.1007/s10533-017-0397-7

Wu, L., Zhang, M., Xie, X., Lv, J., Zhou, X., and Shen, N. (2023). Effect of wetland hydrological connectivity on runoff based on a basin comparison. *J. Hydrol.* 619:129348. doi: 10.1016/j.jhydrol.2023.129348

Xingyuan, Z., Fawen, L., and Yong, Z. (2023). Impact of changes in river network structure on hydrological connectivity of watersheds. *Ecol. Indic.* 146:109848. doi: 10.1016/j.ecolind.2022.109848

Xu, Z., Molins, S., Özgen-Xian, I., Dwivedi, D., Svyatsky, D., Moulton, J. D., et al. (2022). Understanding the hydrogeochemical response of a mountainous watershed using integrated surface-subsurface flow and reactive transport modeling. *Water Resour. Res.* 58:e2022WR032075. doi: 10.1029/2022WR032075

Yang, Q., Hu, P., Wang, J., Zeng, Q., Yang, Z., Liu, H., et al. (2021). The stereoscopic spatial connectivity of wetland ecosystems: evaluation method and regulation measures. *Hydrol. Process.* 35:e14074. doi: 10.1002/hyp.14074

Yang, Q., Zhang, C., Liu, X., Yao, S., and Huang, R. (2023). Assessment of hydrological connectivity characteristics of riparian zones and their correlation with root-soil composites at different bank heights of a first-class river in China. *Front. Ecol. Evol.* 11:1205697. doi: 10.3389/fevo.2023.1205697

Yu, Y., Feng, J., Liu, H., Wu, C., Zhang, J., Wang, Z., et al. (2023). Linking hydrological connectivity to sustainable watershed management in the loess plateau of China. *Curr. Opin. Environ. Sci. Health* 35:100493. doi: 10.1016/j.coesh.2023.100493

Zhang, Y., Huang, C., Zhang, W., Chen, J., and Wang, L. (2021). The concept, approach, and future research of hydrological connectivity and its assessment at multiscales. *Environ. Sci. Pollut. Res.* 28, 52724–52743. doi: 10.1007/s11356-021-16148-8

Zhang, Y., Jiang, J., Zhang, J., Zhang, Z., and Zhang, M. (2022). Effects of roots systems on hydrological connectivity below the soil surface in the yellow river delta Wetland. *Ecohydrology* 15:e2393. doi: 10.1002/eco.2393

Zimmer, M. A., Kaiser, K. E., Blaszczak, J. R., Zipper, S. C., Hammond, J. C., Fritz, K. M., et al. (2020). Zero or not? Causes and consequences of zero-flow stream gage readings. *Water* 7:e1436. doi: 10.1002/wat2.1436

Zimmer, M. A., and McGlynn, B. L. (2018). Lateral, vertical, and longitudinal source area connectivity drive runoff and carbon export across watershed scales. *Water Resour. Res.* 54, 1576–1598. doi: 10.1002/2017WR021718

Zuecco, G., Rinderer, M., Penna, D., Borga, M., and Van Meerveld, H. (2019). Quantification of subsurface hydrologic connectivity in four headwater catchments using graph theory. *Sci. Total Environ.* 646, 1265–1280. doi: 10.1016/j.scitotenv.2018.07.269

Frontiers in Water

Transforming our approach to water research and its applications

A journal dedicated to exploring challenges facing freshwater systems, including demand and supply of water resources, extreme weather events and climate change.

Discover the latest Research Topics

See more →

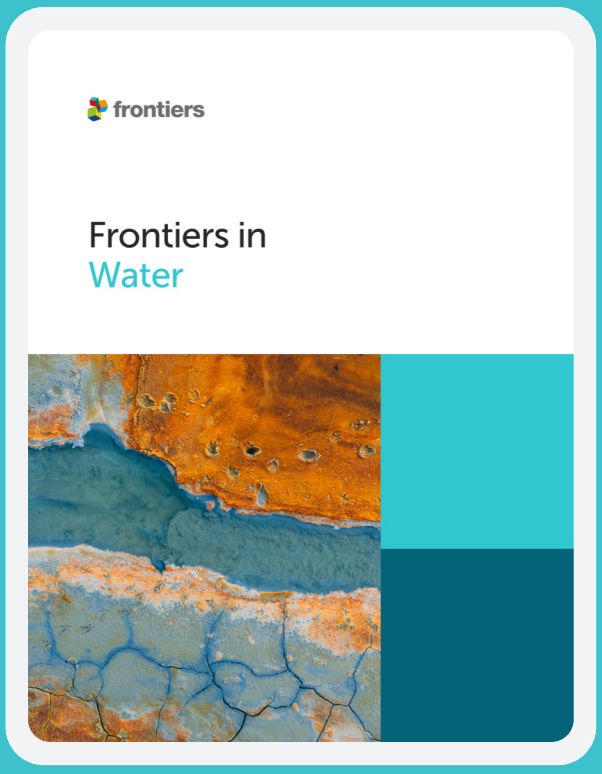

Frontiers

Avenue du Tribunal-Fédéral 34
1005 Lausanne, Switzerland
frontiersin.org

Contact us

+41 (0)21 510 17 00
frontiersin.org/about/contact